



UNIVERSITÀ  
DEGLI STUDI  
DI PADOVA

**University of Padova**

Department of Management and Engineering

PhD School in Mechatronics and Product Innovation Engineering

Programme: Mechanics of Materials

Cycle XXVIII

**LOCAL APPROACHES FOR THE FATIGUE  
DESIGN OF COMPONENTS SUBJECTED TO  
HIGH TEMPERATURE**

**School Director:** Ch.mo Prof. Alessandro Persona

**Supervisor:** Ch.mo Prof. Filippo Berto

**Ph.D. Candidate:** Pasquale Gallo





UNIVERSITÀ  
DEGLI STUDI  
DI PADOVA

**Università degli Studi di Padova**

Dipartimento di Tecnica e Gestione dei Sistemi Industriali

Scuola di Dottorato di Ricerca in Ingegneria Meccatronica e  
dell'Innovazione Meccanica del Prodotto

Curriculum: Meccanica dei Materiali

Ciclo XXVIII

**APPROCCI LOCALI PER LA PREVISIONE  
DELLA RESISTENZA A FATICA AD ALTA  
TEMPERATURA DI COMPONENTI INTAGLIATI**

**Direttore della Scuola:** Ch.mo Prof. Alessandro Persona

**Supervisore:** Ch.mo Prof. Filippo Berto

**Dottorando:** Pasquale Gallo



## Summary

The present document summarized the aims and the results obtained by the candidate, during the Ph.D. programme. The research activity consisted in the investigation of the high temperature fatigue behavior, considering the effect of the temperature combined with creep. After a preliminary analysis, the investigation of different notches reproducing the geometry of real components was considered a key topic in the present research activity. These geometries, indeed, are completely neglected in the past and recent literature, despite their important role played in industrial applications. Moreover, the interaction between creep and fatigue is still not well understood and the available design tools are not effective.

Considering a topic so wide and complex, it was essential to approach and face the problems from different viewpoints strictly related one another:

- from the experimental point of view: the aim was the characterization of the high temperature fatigue behavior of different innovative materials, considering a large number of notch geometries, in order to obtain a robust experimental set of new data;
- from analytical/theoretical point of view: with the aim to develop and/or extend methods based on energy approaches to high temperature phenomena, to analyze the elastic-plastic behavior of the material and try to give robust and reliable tool for the design against creep.

Attention was first paid to Cu–Be alloys that surely stand out and fall within the most interesting materials for high temperature applications, thanks to their excellent compromise between thermal conductivity and mechanical properties over a wide range of temperatures. For this reason, a large bulk of uniaxial fatigue tests at 650°C have been conducted on plates with a central hole and smooth specimens. The new data from un-notched and notched specimens were first summarized in the corresponding fatigue curves and later in terms of the mean value of the Strain Energy Density (SED). The approach, successfully used to summarize fatigue data from notched specimens tested at room temperature, was extended for the first time to high-temperature fatigue. A value of the radius equal to 0.6 mm resulted to be appropriate to summarize all fatigue data in a quite narrow scatter band, giving an easy and fast tool to design against fatigue, regardless of the specimens geometry.

Subsequently, high temperature fatigue tests at 500°C were conducted on specimens made of Titanium Grade 2. Semi-circular notches and plates weakened by symmetric V-notches were considered. Since the preliminary good results obtained by the Cu-Be alloy analyzed previously, the fatigue data were reanalyzed in terms of the Strain Energy Density (SED) averaged over a control volume. Also in this case, a useful control radius was derived and a master curve at high temperature was provided.

A third experimental campaign was conducted considering 40CrMoV13.9 steel. This steel is commonly employed in numerous high temperature applications, such as hot-rolling of metals and other alloys. A wide range of temperature was considered, from room temperature to 650°C, in order to completely characterize the high temperature behavior. Two geometries were analysed: plates weakened by lateral symmetric V-notches and smooth specimens. The results were first summarized in the common Wöhler curves, and later by means of the SED averaged over a control volume. In this case, a new approach compared to previous tests was developed: the SED formulation was modified in order to include some important parameters related to high temperature, and a notch sensitivity function (depending on the temperature) was introduced. Thanks to this new formulation, the data were summarized in a single narrow scatter band, regardless of the specimens geometries, but employing the same control radius proposed at room temperature. Moreover, a limit temperature (500°C) was defined: below that temperature, the specimens fatigue strength is still comparable to that detected at room temperature; above 500 °C, a significant reduction in the fatigue strength is shown both for plain and V-notched specimens. It must be pointed out that the percentage fatigue strength reduction for the notched components was found to be lower than that characterizing the plain specimens.

On the same steel, an investigation on the crack initiation from notches and on the influence of surface roughness was accurately conducted. Uniaxial-tension load controlled fatigue tests were conducted on plates with central holes at a service temperature of 650°C, varying the surface roughness. Two objectives were set and achieved: first, clarify if at high temperature most of the specimen life is spent for crack initiation; second, clarify the influence of the surface roughness on the crack initiation and consequently on the total fatigue life of the components. The results showed that an improvement of the surface roughness returns an enhancement of the fatigue life that can reach an increment in terms of strength equal to 44%.

Because of the good results obtained with the SED approach, it was investigated the accuracy of the averaged SED considering a large bulk of high temperature fatigue data taken from literature. Notched components made of different C45 carbon steel at 250°C, Inconel 718 at 500°C and directionally solidified superalloy DZ125 at 850°C were considered. The control volume was derived for each material through the analytical relation within El Haddad-Smith-Topper parameter and the material characteristic length defined by the Theory of Critical Distances. SED based curves were obtained and allowed proving that the proposed approach can be a reliable design tool in practical applications when dealing with high temperature.

As briefly stated at the beginning, the high temperature environment induces time and temperature dependent deformations resulting in a nonlinear stress-strain response such as creep (visco-plasticity), that are very critical in the design of notched components. When the creep effects are localized in a small region near the notch root, they can be considered as localized-creep cases. However, creep strains (although low) can also occur away from the notch tip, resulting in a non-localized creep. Numerous components in different applications are subjected to non-localized creep, such as power plant, gas turbine and nuclear pressure vessel industry. Because of the analytical complexity of the problem, only a limited number of solutions concerning localized and non-localized time-dependent creep-plasticity problems are available in literature, although the industrial relevance. For this reason, it has been developed a useful numerical tool allowing assessing the stress relaxation and the strain evolution against time, at the tip of blunt V-notches. In detail, starting from Neuber's rule extended to time-dependent problems and assuming Lazzarin-Tovo equations to describe the early elastic state of the system, a set of new differential equations to be solved numerically has been derived in order to predict the evolution of stresses and strains for a material obeying a Norton power law. Subsequently, the method has been implemented and solved in the MatLab code. The new approach showed a good agreement with a set of validation data obtained from detailed finite element analyses considering blunt V-notches with different notch opening angles, notch depths, notch tip radii and the mechanical properties related to creep. All the stresses and strains as a function of time have been predicted with acceptable and limited errors. In some few cases, the strain presented a maximum discrepancy of 20%. This error is mostly due to different approximations introduced in the

theoretical formulation, such as the assumption of the elastic-perfectly plastic behavior of the material inside the plastic zone and the employment of the Irwin's method to estimate the plastic radius. Enhancement in the estimation of the plastic zone and of the elastic-plastic state substituting the Neuber's rule with other more appropriate rules (e.g. with the Glinka's Equivalent Strain Energy Method), can lead to a major improvement of the strain results. However it must be underlined that other researchers have found bigger discrepancy within finite element results and theoretical prediction when dealing with notches strains under creep condition, but all the parameters related to the stress state (and also the minimum creep strain rate) were in good agreement comparing numerical/theoretical and experimental results. Moreover, the proposed solution, is valid for U-notches also, and can be easily extended to the fatigue design against multiaxial loading. In addition, the localized creep solution can be easily obtained neglecting the far field contribution. The main advantage of the proposed method is that it permits a fast evaluation of the stresses and strains at notches under non-localized creeping condition, without the use of complex and time-consuming FE non-linear analyses. The so obtained stresses and strains can be used as input parameters for life prediction creep models and design method based on local approaches. However, as well known, local approaches based on notch tip stresses and strains failed when the stress fields tends toward infinity (such as for crack or sharp notches). Different methods are available in literature dealing with this matter, for example the theory of critical distances, or based energy approaches such as Strain Energy Density averaged over a control volume. To better investigate this point, the SED under creeping conditions have been evaluated thanks to some preliminary non-linear finite element analysis. From analytical viewpoint, different aspects remain opened: evolution from an elastic SED to a plastic SED with time; consideration of time dependent eigenvalues; SED formulation under creeping conditions.

Other energetic approaches, developed for elastic-plastic problems, have been also considered for further applications to high temperature and creep. Among the local approaches available for non-linear analyses, the contour J-Integral has received an excellent feedback as a fracture parameter characterizing nonlinear materials under different loading conditions, considering also thermo-mechanical fatigue and creep. The application of the method was investigated considering cracked components.



The influence of the chosen material law on the results in terms of stress field was investigated and a number of nonlinear FE analyses were provided to support the conclusions. In particular, Ramberg-Osgood law and Power Law have been considered for modelling the material behavior. Numerous interesting results were achieved showing pros and cons of such method, e.g. a clear definition of parameters necessary for the calculation of J, formulation of useful formulas and guidelines for parameter evaluation. Especially, it emerges that, also if non-linear phenomena are taking place, the superposition principle still be applicable in the J calculation.

In general, the research activity was intense. Different aspects of a wide and complex topic have been considered and the results accomplished were synthesized in a large number of international publications as well as presented in important international and national conferences, with an excellent feedback. The activity also led to several international fruitful collaborations and solid bases for interesting future developments.



## Sommario

L'obiettivo del Dottorato di Ricerca era lo studio del comportamento a fatica di materiali metallici ad alta temperatura, indagando in modo particolare il fenomeno del *creep*, che diventa non trascurabile in determinate condizioni di carico e interagisce con la resistenza a fatica stessa. È stata ritenuta interessante soprattutto l'analisi di componenti in presenza di intagli e/o di geometrie complesse che rappresentassero in qualche modo la geometria di componenti effettivamente utilizzati nelle applicazioni industriali.

Da un'iniziale e approfondita analisi bibliografica è emerso come in letteratura si trascurino la fatica ad alta temperatura ad alto numero di cicli e in particolar modo le applicazioni relative a componenti intagliati. Inoltre, l'interazione fra fatica e creep si presenta come un evento ancora poco chiaro e trattato con strumenti poco efficienti.

Considerando fenomeni molto complessi e un tema così ampio, è stato indispensabile affrontare l'oggetto del presente dottorato di ricerca da diversi punti di vista ma strettamente interconnessi:

-quello sperimentale: caratterizzando il comportamento a fatica ad alta temperatura di diversi materiali innovativi e multifunzionali d'interesse industriale, considerando varie geometrie d'intaglio, in modo tale da fornire un consistente numero di dati sperimentali di partenza;

-quello analitico/teorico: cercando di sviluppare e/o estendere approcci energetici ad alta temperatura, analizzando il comportamento elasto-plastico, gli strumenti a disposizione e cercando, infine, di fornire strumenti efficaci per la progettazione in presenza di creep.

Tra i materiali disponibili per applicazioni a elevata temperatura, sono state considerate particolarmente interessanti le leghe di rame-cobalto-berillio, caratterizzate da ottime proprietà meccaniche e termiche su un ampio range di temperatura. Tali famiglie di leghe sono impiegate in diversi settori di rilievo industriale e, fra questi, il settore aerospaziale, militare e nucleare. È stata quindi condotta una campagna sperimentale al fine di caratterizzare il comportamento a fatica ad alta temperatura della lega considerata. Sono stati analizzati provini lisci e piastre forate alla temperatura di 650°C. I dati ottenuti sono stati sintetizzati dapprima in termini di tensioni nominali, ottenendo le classiche curve di Wöhler, e in

seguito mediante la Strain Energy Density. In particolare è stato determinato e proposto un raggio critico di controllo per la lega considerata che ha permesso una sintesi delle due geometrie in un'unica banda di fatica. È stato così fornito uno strumento utile per la progettazione di componenti intagliati alla temperatura in esame, e valido indipendentemente dalla geometria considerata.

In seguito, sono state condotte prove di fatica uniassiali su provini intagliati in Titanio Grado 2 alla temperatura di 500°C. Sono state considerate due geometrie: provini indeboliti da intagli semi-circolari e da intagli a V. Visti i promettenti risultati preliminari ottenuti, i dati sono stati sintetizzati mediante l'approccio energetico del SED esteso all'alta temperatura, fornendo ancora una volta una master-curve basata sull'energia locale di deformazione utile per la progettazione a fatica ad alta temperatura.

Una terza campagna sperimentale è stata condotta al fine di caratterizzare il comportamento a fatica, ad alta temperatura, dell'acciaio 40CrMoV13.9. Questo tipo di acciaio è utilizzato in diverse applicazioni industriali, tra cui la fabbricazione di rulli per la laminazione a caldo di leghe leggere, applicazione in cui carichi ciclici si combinano all'alta temperatura. Le prove sono state condotte considerando un ampio range di temperatura, partendo da quella ambiente fino a quella massima di 650°C, in modo tale da caratterizzare gradualmente il comportamento a fatica del materiale considerato. Sono state realizzate due geometrie: provini indeboliti da intagli a V con raccordo severo, e provini lisci. I risultati ottenuti sono stati prima sintetizzati nelle classiche curve di Wöhler, e in seguito mediante la densità di energia di deformazione mediata su un volume di controllo di appropriate dimensioni. A differenza della lega di Cu-Co-Be, in questo caso, visti i dati a disposizione, è stata introdotta una particolare funzione nella formulazione del SED che ha permesso di considerare la diversa sensibilità all'intaglio mostrata dal materiale alle alte temperature, permettendo di mantenere lo stesso raggio critico del volume di controllo utilizzato a temperatura ambiente. Questa innovativa estensione del metodo SED ad alta temperatura ha portato a una sintesi unificata dei dati sperimentali delle diverse geometrie in esame. È stato inoltre possibile determinare una temperatura di riferimento (500°C) al di sotto della quale il comportamento del materiale continua a restare identico a quello osservabile a temperatura ambiente. Sopra tale temperatura, invece, si registra una notevole riduzione della vita a fatica per entrambe le

geometrie che però è, in termini percentuali, minore per intagli severi rispetto a quella dei provini lisci.

Sempre considerando lo stesso acciaio, è stata condotta un'analisi sull'innescò di cricche a bordo foro, ad alta temperatura, valutando l'influenza della rugosità superficiale. L'obiettivo era duplice: innanzi tutto verificare che, anche ad alta temperatura, la maggior parte della vita a fatica fosse spesa per la fase d'innescò delle cricche; valutare l'influenza della finitura superficiale sull'innescò e quindi vedere l'impatto sulla vita a fatica totale. Per questo motivo sono state analizzate sperimentalmente delle piastre forate, alla temperatura di 650°C. I risultati ottenuti hanno evidenziato come, anche alla temperatura di 650°C, il rapporto tra numero di cicli necessari all'innescò delle cricche e cicli a rottura fosse sempre superiore al valore di 0.8. Da osservazioni anche pratiche e d'interesse industriale, è stata quindi valutata successivamente l'influenza della rugosità superficiale sulla resistenza a fatica. A un miglioramento della finitura superficiale è stato registrato un netto miglioramento del numero di cicli a innescò e quindi totali, a parità di range di tensione applicato sul componente. Il limite di fatica ha registrato un incremento del 44% per il valore minimo di rugosità.

Visti i positivi riscontri ottenuti con la sintesi in energia dei dati sperimentali, la potenzialità del metodo è stata ulteriormente verificata considerando nuovi materiali e geometrie presenti in letteratura. Sono state prese in esame prove a fatica condotte su un acciaio C45 a 250°C, Inconel 718 a 500°C e sulla superlega DZ125 a 850°C. I dati, originariamente sintetizzati attraverso la Teoria delle Distanze Critiche, sono stati ripresentati con successo in termini di densità di energia di deformazione mediata su un volume di controllo. Il raggio di controllo per ogni materiale è stato determinato attraverso la relazione che lega il raggio stesso con il parametro di El Haddad-Smith-Topper e la distanza critica caratteristica del materiale.

Come già accennato in precedenza, l'alta temperatura induce, in alcuni casi, un comportamento non-lineare e fenomeni visco-plastici dipendenti dal tempo non trascurabili, tra i quali il creep. Questo può essere particolarmente gravoso in componenti intagliati, a causa degli effetti di concentrazione delle tensioni. Quando il creep è localizzato, o comunque concentrato, in una piccola regione in prossimità dell'intaglio, esso è definito "creep localizzato". Quando invece le deformazioni dovute a creep si manifestano anche lontano dall'intaglio, si parla di "creep non

localizzato” (situazione tipica per componenti che operano ad alta temperatura sottoposti a carichi costanti nel tempo). In letteratura sono pochi i lavori che considerano il creep localizzato, e quasi tutti trascurano quello non-localizzato per la difficoltà nella trattazione del problema. È stato quindi con successo fornito uno strumento numerico capace di prevedere il rilassamento delle tensioni e l’evoluzione delle deformazioni nel tempo, all’apice d’intagli a V raccordati. In dettaglio, partendo dall’estensione della regola di Neuber a problemi dipendenti dal tempo, e utilizzando le equazioni di Lazzarin-Tovo al fine di descrivere lo stato elastico iniziale del problema, è stato poi ricavato un set di equazioni differenziali da risolvere in modo iterativo/numerico al fine di valutare tensioni e deformazioni nel tempo, assumendo la legge di Norton per la rappresentazione del fenomeno del creep. Il metodo è stato poi implementato in MatLab e utilizzato per ricavare l’evoluzione delle tensioni e delle deformazioni nel tempo per diverse proprietà meccaniche e varie geometrie, variando la profondità d’intaglio, l’angolo di apertura e il raggio di raccordo. Al fine di validare il metodo, i risultati ottenuti sono stati confrontati con quelli ricavati da accurate analisi agli elementi finiti, ottenendo un buon accordo. Tutte le tensioni sono state previste con errori trascurabili, mentre in alcuni e limitati casi, le deformazioni hanno mostrato un errore percentuale leggermente più elevato ma comunque inferiore al 20%. Quest’ultimo è stato attribuito ad alcune approssimazioni introdotte nella trattazione, come ad esempio l’utilizzo della regola di Neuber per la determinazione dello stato tensionale elastoplastico, o l’utilizzo dell’approccio suggerito da Irwin nella stima del raggio plastico. L’adozione di una procedura più efficiente nel calcolo di questi due parametri (e.g. Equivalent Strain Energy Density method), può sicuramente portare ad un netto calo dell’errore nei casi in cui è stata riscontrata la deviazione massima. Il metodo sviluppato fornisce l’evoluzione delle tensioni e delle deformazioni del tempo per intagli a V raccordati, anche per intagli a U. Esso trova una notevole utilità se combinato con metodi e/o approcci locali basati sullo stato tensionale per progettazione in presenza di creep. Inoltre può essere potenzialmente esteso al campo della fatica ed a sollecitazioni multiassiali, nonché al creep localizzato. Un problema comunque aperto è quello degli intagli acuti. Una possibile soluzione è l’adozione di approcci di tipo energetico, come la Strain Energy Density mediata su un volume di controllo. A tal proposito, sono state condotte delle analisi preliminari agli elementi

finiti al fine di esplorare il comportamento del SED in presenza di creep, risultando anch'esso tempo-variante ma tendente ad un valore di plateau. Da un punto di vista analitico restano invece aperti i seguenti temi: come trattare il passaggio da una SED elastica a una progressivamente plastica; la valutazione dei gradi di singolarità che risultano anch'essi dipendenti dal tempo; e più in generale come riformulare il SED in campo elasto-plastico e/o plastico per il creep.

Sono stati inoltre considerati approcci energetici alternativi utilizzati nella caratterizzazione dei fenomeni elasto-plastici che possono essere presenti alle alte temperature. In particolare, tra le varie metodologie presenti in letteratura, è stato considerato il J-Integral. Il metodo è stato applicato a componenti in presenza di difetti, ed è stato operato un confronto tra risultati analitici e numerici ottenuti al calcolatore, considerando due modelli costitutivi del materiale: Power Law e Ramberg-Osgood. Dalle analisi sono emersi interessanti risultati che hanno reso evidenti limiti e vantaggi di quest'approccio, fornendo interessanti linee guida nel trattare le due leggi e nella determinazione di alcuni parametri necessari all'applicazione del metodo. Inoltre è emerso come, nonostante la presenza di fenomeni non lineari, il principio di sovrapposizione degli effetti possa essere ancora applicato con successo.

In generale, l'attività di ricerca è stata intensa, ed ha toccato vari aspetti di un tema molto ampio e complesso. I risultati conseguiti sono stati sintetizzati in un elevato numero di pubblicazioni scientifiche su riviste internazionali di prestigio e sono stati presentati in numerosi importanti convegni internazionali e nazionali. Sono state inoltre condotte importanti collaborazioni internazionali con esperti del settore. L'attività lascia infine interessanti possibili sviluppi futuri di ricerca che possono portare a un approccio unificato per progettazione a fatica in presenza di creep e di forte interazione creep-fatica.





# Table of Content

<b>Summary .....</b>	<b>i</b>
<b>Sommario .....</b>	<b>vii</b>
<b>1. Introduction .....</b>	<b>1</b>
1.1 Background and motivations .....	1
1.2 Thesis structure .....	5
<b>2. High-temperature fatigue strength of a copper-cobalt-beryllium alloy.....</b>	<b>7</b>
2.1 Introduction.....	9
2.2 Experimental procedure .....	11
2.2.1 Material .....	11
2.2.2 Fatigue tests.....	18
2.3 Results and discussion .....	21
2.3.1 Fatigue test results.....	21
2.3.2 Microstructure after fatigue test.....	25
2.4 A synthesis in terms of linear elastic SED averaged over a control volume ...	26
2.5 Conclusions .....	30
References .....	32
<b>3. High temperature fatigue tests of notched specimens made of titanium Grade 2 .....</b>	<b>35</b>
3.1 Introduction.....	37
3.2 Material properties and experimental procedures .....	39
3.2.1 Titanium Grade 2 and specimen geometries.....	39
3.2.2 Fatigue testing equipment and procedures.....	41
3.3 Fatigue tests results and discussion.....	43
3.3.1 Fatigue curves .....	43
3.3.2 Microstructural analyses .....	46
3.4 A synthesis in terms of linear elastic SED averaged over a control volume ...	48
3.4.1 Room temperature data by means of SED approach .....	49
3.4.2 High temperature data by means of SED approach .....	50
3.5 Conclusions .....	53
References .....	55

<b>4. High temperature fatigue of 40CrMoV13.9 steel and influence of surface roughness .....</b>	<b>59</b>
4.1 Introduction .....	61
4.2 Material properties and specimens geometry .....	65
4.2.1 Material .....	65
4.2.2 Specimen geometry .....	67
4.3 Fatigue testing equipment and testing procedures .....	68
4.4. Results and discussion.....	69
4.4.1 Fatigue curves .....	69
4.4.2 Notch sensitivity.....	72
4.4.3 Fracture surfaces by Scanning Electron Microscopy .....	72
4.4.4 Influence of surface roughness on high temperature fatigue and crack initiation .....	77
4.5 A synthesis in terms of linear elastic SED averaged over a control volume ...	80
4.5.1 Strain energy density as a design parameter .....	80
4.5.2 A synthesis in terms of linear elastic SED of room and high temperature data .....	83
4.6 Conclusions .....	87
References .....	89
<b>5. High temperature fatigue assessment by local Strain Energy Density of C45, Inconel 718 and DZ125 superalloy .....</b>	<b>93</b>
5.1 Introduction .....	95
5.2 Fundamentals of the Strain Energy Density averaged over a control volume .	97
5.3 Validation of Strain Energy Approach applied to high temperature fatigue..	101
5.4 Discussion .....	107
5.5 Conclusion.....	108
References .....	109
<b>6. Estimation of strains and stresses at blunt V-notches under creeping condition .....</b>	<b>113</b>
6.1 Introduction .....	115
6.2 Nuñez and Glinka method for the evaluation of stresses and strains under non-localized creep.....	117
6.3 Extension of Nuñez-Glinka Method to blunt V-Notches.....	124

6.3.1 Examples of Nuñez-Glinka method applied to U-notches: considerations and comparison between numerical and FEM analysis .....	129
6.4 Examples of the new method applied to blunt V-notches: considerations and comparison between numerical and FE analysis .....	133
6.5 Discussion .....	142
6.6 Conclusions .....	143
References .....	146
<b>7. Strain Energy Density under creeping conditions: preliminary analysis and considerations .....</b>	<b>149</b>
7.1 Introduction .....	151
7.2 Evaluation of Strain Energy Density under creep conditions .....	155
7.3 Effect of mesh refinement on the SED evaluation under creeping condition .....	159
7.4. Discussion of the results: SED as a creep characterizing parameter .....	161
7.5. Conclusions .....	163
References .....	165
<b>8. Some considerations on the J-Integral under high temperature elastic-plastic conditions .....</b>	<b>169</b>
8.1 Introduction .....	171
8.2 Material models .....	173
8.2.1 Geometry and mechanical properties .....	173
8.2.2 Ramberg Osgood and power law .....	174
8.3 J-Integral evaluation .....	175
8.3.1 The J contour integral .....	175
8.3.2 Parameters $\alpha$ , $P_0$ and $h_1$ .....	177
8.4 Numerical analyses .....	179
8.4.1 Power-Law convergence problem .....	180
8.5 Results .....	182
8.5.1 Assuming negligible elastic contribution of the Ramberg-Osgood law. .....	182
8.5.2 Unified assessment of elastic and plastic contribution .....	183
8.5.3 Evaluation of J through superposition principle .....	183
8.6 Conclusions .....	184
Appendix .....	186
References .....	188

<b>9. Concluding remarks.....</b>	<b>191</b>
<b>List of publications .....</b>	<b>193</b>
<b>Acknowledgments.....</b>	<b>195</b>

# 1. Introduction

## 1.1 Background and motivations

In last decades, the interest on fatigue assessment of steels and different alloys at high temperature has increased continuously. In fact, high-temperature applications have become ever more important in different engineering fields, e.g. turbine blades of jet engine, nuclear power plant, molds for the continuous casting of steel, hot rolling of metals. The primary role of this topic in the engineering field is also well supported by the recent literature that is devoting more and more effort in the investigation of high temperature fatigue. In particular, the interaction within fatigue and creep seems to be the main attractive issue to be addressed near future.

First studies on high temperature fatigue were conducted by Coffin in 1954 (*L.F. Coffin, A study of the effects of cyclic thermal stress in a ductile metal, Trans. ASME 76.931, 1954*). During his activity, related to the development of nuclear power plants, he faced some problems completely ignored in the past: how to deal with components working at high temperature, and how to quantify the damages due to thermal cycles. In fact, in those components, in addition to the phenomena related to usual room temperature fatigue and to elastic stress and strain field, plastic phenomena due to high temperature arose. The belief of the elastic-plastic effects derived from very simple observations: when subjected to high temperature, the components showed a considerable reduction of the fatigue strength with respect to the room temperature one. Sure of these findings, Coffin programmed a large bulk of high temperature experimental tests on pipe specimens, made of AISI 347: this work inspired the first studies on high temperature fatigue and led to well-known Manson-Coffin laws.

Nowadays, several new solutions have been obtained on this topic, and new high performance alloys have been developed.

Usually, the high temperature fatigue can be classified as follows:

- ❖ High number of cycles fatigue (HCF): that is the classic fatigue phenomenon but at high temperature;
- ❖ Thermal fatigue: thermal cycles induce cyclic stress, without the applications of any other external load;

- ❖ Thermal mechanical fatigue: in which thermal cycles and cyclic loads are combined together. They can be in-phase as well as out-of-phase;
- ❖ High temperature low cycle fatigue (LCF): strain-controlled fatigue at low number of cycles and high temperature.

The statement “high temperature induces elastic-plastic phenomena” is really simplistic. Usually, the effects of the high temperature are numerous and diversified, involving metallurgical and environmental considerations. Among them, creep and oxidation are the most relevant phenomena. Considering the creep, it is defined as the tendency of a solid material to deform permanently under the influence of mechanical constant stresses. In high temperature applications, creep interacts with the fatigue through two ways:

- ❖ The first one involves two deformation processes: a monotonic creep strain superimposed on a more rapid deformations cycle. In this case, the damage due to creep (void formations at grain boundaries) interacts with the fatigue damage (e.g. cracks initiation and propagation). This situation induces a strong interaction within fatigue and creep and generates a failure process that is very different respect to the individual creep damage and individual fatigue damage.
- ❖ The second way is due to a very slow cyclic strain that can be interpreted as a cyclic-creep. Hold-time periods may occur as well.

In this background, new methodologies, able to take into account both effects (fatigue and creep) are nowadays essential for the high temperature fatigue assessment of components working at elevated temperature.

The existing methods that are not presented in details here for the sake of brevity are classified as follows:

- ❖ Linear Summation Methods (LSM): the simplest damage summation methods are based on a linear summation of the separate effects of time-dependent fatigue and time-dependent creep (the life fraction rule):

$$\frac{n}{N_f} + \frac{t}{t_R} = D$$

- ❖ Frequency-Modified Strain Range Methods: the basic Manson-Coffin equation is adapted to take into account creep or environmental effects during

slow cycling tests at elevated temperature, by including a frequency factor, giving the well-known frequency-modified Manson-Coffin equation:

$$\Delta\varepsilon_p = C(N_f v^{k-1})^{-\beta}$$

The equation has been later rewritten and modified in a very large number of forms.

- ❖ **Strain Range Partitioning Methods:** the strain range partitioning methods separate damage into time-dependent and time-independent components of the strain range, but unlike the damage summation methods they also take into account the reversed deformation associated with each process.

Although the listed methods are not addressed in detail in the present work, it must be underlined that they present common weak points:

- ❖ They are continuously modified and adapted to the considered materials;
- ❖ Mostly based on experimental tests that implies a low applicability to different boundary conditions;
- ❖ They failed when a strong interaction within fatigue and creep takes place;
- ❖ They try to evaluate separately two phenomena that are strongly interacting each other;
- ❖ Mostly they are focused on low cycle fatigue and strain controlled tests.

From a deep bibliographic research on these topics, more interest considerations emerge:

- ❖ There is a lack of data regarding high cycle fatigue, the high temperature fatigue is mainly considered at low number of cycle, and so through approaches based on strain. Despite that, most of the real components work under high cycle fatigue;
- ❖ Even if the real components present complex shapes, only a limited number of works considered the notched geometries;
- ❖ The available tools to deal with creep, fatigue, and creep fatigue interaction are not effective and different points are un-clear.

On the basis of the considerations presented before, the undersigned strongly believe on the necessity to explore new and innovative methodologies, taking into account notched geometries.

Among several methods to deal with notches, the idea of the author is that an energy criterion can lead to several advantages and to better results also in case of high temperature, and the present thesis tries exactly to give solid experimental results and a preliminary answer to these needs.

Because of the complexity of the topic, it was essential to pursue simultaneously two directions (see Fig. 1):

- ❖ Experimental viewpoint: conducting a large number of experimental tests on notched geometries, considering high number of cycles and different materials for high temperature applications.

The final aim was to obtain a robust set of new data, because of the lack of the recent literature on this point, as we saw previously.

- ❖ On the other side, we faced the topic from theoretical viewpoint: considering elastic-plastic behavior of the material, we focused especially on creep of notches; we evaluated the applicability at high temperature of energy based methods and especially of the Strain Energy Density.

The final aim was to give a powerful and easy to deal to deal with high temperature fatigue and creep because.

The investigation and extension of the SED to high temperature, and the results obtained in the present work, can lead in the near future to a unified approach for fatigue-creep interaction at high temperature.

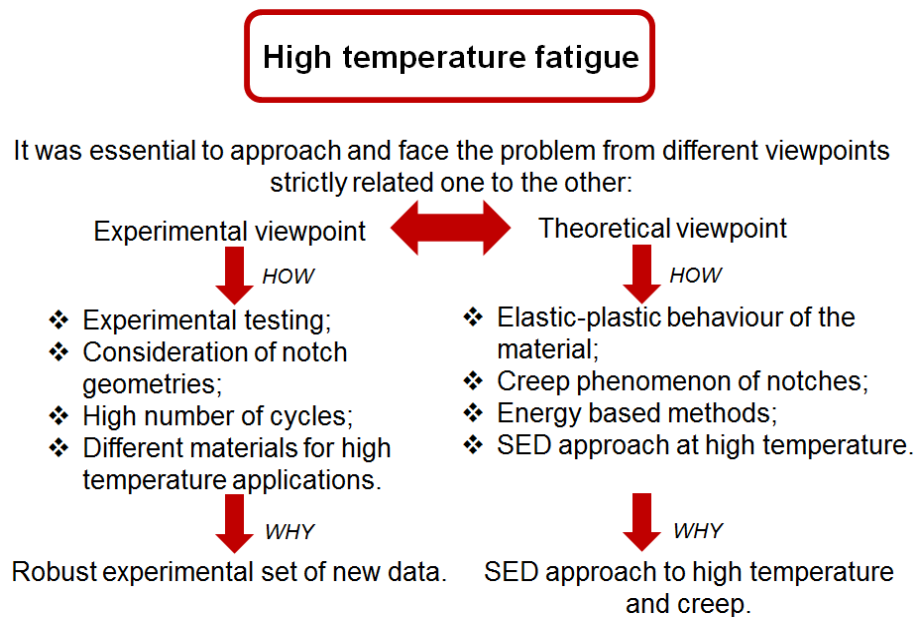


**Fig. 1:** logical flow of the conducted activities



## 1.2 Thesis structure

This section is an overview on the structure of the present thesis. Because of the large and complex considered topic, this section provides a useful tool that helps the reader to pick his way through the entire document.

In general, the chapters are briefly introduced by some *Highlights* that provide a brief summary of the aims, methods and results presented in the chapter. Subsequently, an extensive introduction to be considered as a state of the art on that specific topic is given. At the end, the most significant results are summarized in the *Conclusions* and the related *References* are listed for each chapter.

The topics are structured as follows:

- **§Chapter 1** presents a brief and general introduction on high temperature fatigue. A brief state of the art on the topic and some comments on the methods available to design against fatigue at high temperature are given. The motivations of the present work and the structure of the thesis are also presented. Extensive state of the art is not provided since already given for each chapter.
- **§Chapter 2** presents experimental results from high temperature fatigue tests of Cu-Co-Be alloy and a synthesis in terms of Strain Energy Density of the high temperature data. Highlights and state of the art related to this specific topic are provided at the beginning.
- **§Chapter 3** shows high temperature fatigue tests conducted on notched components made of Titanium Grade 2. A synthesis in terms of Strain Energy Density is also proposed.
- **§Chapter 4** presents high temperature fatigue tests conducted on notched components made of 40CrMoV13.9 steel. A study on the influence of surface roughness on high temperature fatigue strength and cracks initiation on notches is also presented. At the end, specific master curves in terms of SED are given.
- **§Chapter 5** is focused on the extension of the Strain Energy Density to high temperature fatigue re-analysing experimental data taken from the literature. Thanks to the link within the theory of critical distances and SED method, high temperature master curves are provided for C45 steel, Inconel 718 and

DZ125 superalloy. Fundamentals of the Strain Energy Density are also shown.

- **§Chapter 6** presents a generalized approach to estimation of strains and stresses at blunt V notches under non-localized creep. The most important theoretical concepts are defined and the analytical frame is given. At the end the results are presented and commented.
- **§Chapter 7** comments a possible extension of the Strain Energy Density under creeping conditions of notches. To this end, preliminary analysis on the estimation of the strain energy density under creeping condition is presented for sharp V-notches. This chapter is intended primarily to emphasize SED behaviour in case of creep and the limits to be overcome in the near future in order to extend this approach to creep.
- **§Chapter 8** discusses how the J-Integral evaluation can be performed for elastic-plastic cracked components, in view of a possible assumption of this parameter for the development/improvement of energy methods for creep and high temperature assessment.
- **§Chapter 9** presents concluding remarks on the work in order to discuss the main results and the future developments.

The *List of publications* of the candidate is given at the end.

## 2. High-temperature fatigue strength of a copper-cobalt-beryllium alloy

*F. Berto, P. Lazzarin, P. Gallo, High-temperature fatigue strength of a copper-cobalt-beryllium alloy, J. Strain Analysis 49(4) (2014) 244-256.*

### Highlights

This chapter summarizes the results from uniaxial-tension load-controlled fatigue tests performed at 650°C on Cu-Be specimens. Two geometries are considered: hourglass shaped specimens and plates weakened by a central hole.

Despite the numerous industrial applications of the considered alloy, only a limited number of works on copper alloys under high-temperature fatigue are available in the literature and no results from these alloys deal with notched components. In the present chapter, after a brief review of the recent literature, material properties and experimental procedure are described. The new data from un-notched and notched specimens are summarized in the corresponding fatigue curves. By analyzing the fatigue behavior of the plates weakened by central holes, it can be noted a reduction of the fatigue strength about equal to 40% at two million cycles, whereas the inverse slope,  $k$ , is very close to that of un-notched specimens.

All fatigue data from un-notched and notched specimens are re-analysed here in terms of the mean value of the Strain Energy Density (SED). The approach, successfully used in the past to summarise fatigue data from notched specimens made of different materials tested at room temperature, is extended here for the first time to high-temperature fatigue. In the plates with central holes the SED is evaluated over a finite size control volume surrounding the highly stressed zone at the hole edge. A value of the radius equal to 0.6 mm seems to be appropriate to summarize all fatigue data in a quite narrow scatterband. The scatter index,  $T_{\Delta w} = 1.80$ , is obtained from the synthesis in terms of SED with reference to probabilities of survival equal to 10-90 percent. It becomes equal to 1.34 when reconverted in terms of equivalent stress range.



## 2.1 Introduction

In recent years, the interest on fatigue assessment of steels and different alloys at high temperature has increased continuously. In fact, high-temperature applications have become ever more important in different engineering fields, e.g. turbine blades of jet engine, nuclear power plant, molds for the continuous casting of steel, hot rolling of metals. In parallel, in order to bear mechanical loadings combined with critical conditions at high temperature, the development and testing of innovative materials has progressed substantially [1]. Among the traditional alloys available for this kind of applications, Cu-Be alloys surely stand out and fall within the most interesting materials suitable not only for high-temperature applications. In fact, they are also commonly adopted for magnet applications, thanks to their excellent compromise between thermal conductivity and mechanical properties over a wide range of temperatures [2–7]. In the above mentioned usages, cyclic mechanical loadings are usually combined with extreme heat flux, leading to the well-known conditions of high-temperature fatigue.

Despite that the required mechanical properties of Cu alloys have been gradually increased, at the current state of the art relatively few papers are available in the literature dealing with the role played by a small amount of Cu on static properties of different steels [8–12]. On the other hand, the number of scientific works on the fatigue strength of copper alloys (both at room and high-temperature) reduces drastically. Worth mentioning is contribution by Li, Singh and Stubbins [13], who reviewed some expressions able to quantify the thermal creep and fatigue life time of various copper alloys, including Cu-Ni-Be alloy. Fatigue experiments on bimetallic copper/stainless steel plates up to 500°C were performed in order to simulate the behavior of the first wall of the ITER (International Thermonuclear Experimental Reactor) [13,14]. The fatigue lifetime was given in terms of total strain amplitude and the specimens were designed for the specific application.

In another newsworthy paper [15], the cyclic creep behavior of copper, which usually accompanies low cycle fatigue under tensile mean stress, was investigated. Starting from a previously proposed exponential mean-stress function that accounts for the effect of the mean stress on cyclic loading behavior at room temperature, an empirical relationship was proposed for cyclic creep as an extension to high-

temperature applications. The relationship involves the imposed stress amplitude and the mean stress value [15].

Other authors analyzed the fatigue-creep behavior of single crystals and bicrystals copper under fatigue at elevated and room temperature, paying attention to microstructural aspects. For example, in [16], the temperature dependence on the cyclic creep behavior of Cu–SiO<sub>2</sub> bi-crystals of different but controlled misorientation angles was investigated at 400°C.

In [17] the deformation and dislocation microstructure of a [0 1 3] double-slip-oriented copper single crystal, under a symmetric tension–compression cyclic load, was studied at room temperature, in open-air and in a neutral 0.5M NaCl aqueous solution, respectively.

Hot compression tests were carried out in [18] to study the static properties and microstructure of dispersion strengthened copper alloy deformed at high temperatures. With reference to the static properties, a new method of carrying out high-strain-rate tests at elevated temperatures on beryllium copper was proposed in [19]. In this work some equations correlating the ultimate tensile strength to the strain rate and the temperature were provided as well as some relationships linking elongation at fracture and strain rate [19].

While the fatigue strength problem at high temperature has been investigated in a number of papers and books [20–22] (see also References reported therein) as well as the modeling of materials subjected to high temperature inelastic behavior has been studied in recent contributions [23,24], the number of works dealing with copper alloys is limited and, in particular, no papers discuss the fatigue behavior at elevated temperature of notched specimens made of Cu-Be alloys.

The aim of this chapter is to present a set of new results from high-temperature fatigue tests performed on Cu-Be un-notched and notched specimens in the medium and high cycle regime ( $10^5$ - $10^6$  cycles). The tests have been performed under uniaxial-tension and load-controlled conditions in agreement with [25]. The notched specimens are characterized by a central hole. The experimental procedure adopted during the tests and the microstructural aspects before and after the high-temperature fatigue loading (650°C) is described. The obtained fatigue curves, both for plain and notched specimens, are discussed with emphasis on the reduction of stress concentration effects. Finally, the fatigue data are re-analyzed in terms of the

averaged Strain Energy Density approach [26,27] applied to a control volume surrounding the most stressed region at the notch edge. The main objective is to present a complete characterization of the high-cycle fatigue behavior at elevated temperature of the considered alloy, providing a basic design tool for lifetime prediction. In that range of cycles the plastic strain amplitude as well as the phenomena tied to ratchetting are negligible [25].

## **2.2 Experimental procedure**

### **2.2.1 Material**

Beryllium copper alloys are commonly classified in two general categories: high strength and high conductivity alloys. The Cu-Be alloy under investigation belongs to high conductivity class usually used for production of shells for hot rolling. Rolling is classified according to the temperature of the metal rolled. If the temperature of the metal is above its recrystallization temperature, then the process is termed as hot rolling.

The spark emission spectroscopy analysis gave the composition reported in Table 1 and was carried out on the specimen shown in Fig. 1. A small concentration of beryllium (about 0.2%) and a greater amount of cobalt, about 0.9%, has been detected in the considered alloy. Moreover, the presence of Zr has been registered, while Fe and Si are negligible. In Table 1, a comparison between the present alloy and the copper alloy UNS Number C17410 is carried out. This is a specific alloy belonging to the above mentioned high conductivity class but characterized by a very low concentration of alloying elements: 0.15-0.50 % of beryllium and 0.35-0.60 % of cobalt. However it is the most close to the material under investigation in the present paper.

Some general comments are usually true for this kind of copper-cobalt-beryllium alloys. The influence of the beryllium on the thermal properties is very notable and its low concentration is easily justified: the lower is the concentration of Be, the higher is the thermal conductivity [4]. The addition of cobalt, instead, promotes fine grain size in the cast form, lessens grain growth during annealing and reduces the rapid softening of the alloy due to the overaging. Despite the low concentration of beryllium, these materials may be dangerous for health if excessive quantities of dust, mist, or fumes containing small particle of alloy are inhaled [28]. However,

special precautions are not required for metallographic characterization if no dry alloy particles are produced.

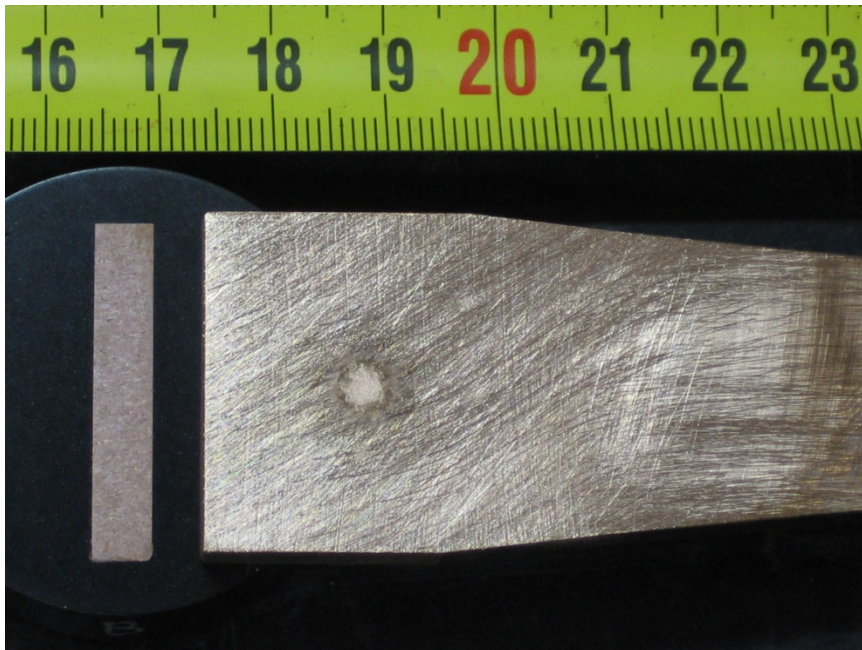


**Fig. 1:** Specimen prepared for metallographic analysis

Figure 2 shows the microstructure of the specimen along the thickness after metallographic preparation and etching treatment. It is evident that the microstructure is homogenous and almost the same, exhibiting equiaxed grain growth. For the sake of completeness, the etchant is an ammonium persulfate with distilled water, which is a general purpose etchant for beryllium-copper alloys. The grain structure is well visible in Fig. 3, where different optical micrographs are presented at different magnification values: it is clear the common grain morphology of annealed Cu alloys, with the presence of twinning and blue-grey particles. These precipitates are more evident in the micrographs of Fig. 4 taken before etching procedures: the particles have a rod-like morphology and are equal distributed in the  $\alpha$ -phase with preferred crystallographic orientation with the matrix. In order to better understand the composition of the precipitates, the EDS spectrum is shown in Fig. 5 carried out on the particle shown in the secondary electron SEM micrograph of Fig. 6. The results are clear: cobalt and zirconium are the main elements while beryllium is not registered because its small amount in the alloy does not generate precipitates, so the particles can be identified as cobalt rich beryllides [28].



The tensile properties of the material at 650°C, obtained through tensile tests on un-notched specimens, are listed Table 2. Young’s modulus  $E$  and Poisson’s ratio  $\nu$  are equal to 133000 MPa and 0.3, respectively. Three typical force-displacements curves at 650°C are shown in Fig. 7. Some hardness tests have been also carried out since the material hardness may play an important role in hot-rolling processes. The results are given in Table 3 and appear very well aligned with the Brinell hardness values reported for the C17410 high conductivity alloy.

**Table 1:** Chemical composition of the material, %

Copper Alloy	Cu	Co	Be	Ni	Fe	Zr	Si	Al
UNS No.								
C17410	99.5 min	0.35-0.6	0.15-0.50	/	0.20 max	/	0.20	0.20
Specimen	98.6	0.88	0.215	0.0052	0.0197	>0.12	0.0019	/

**Table 2:** Static properties of the investigated Cu-Be alloy at 650°

Test No.	Ultimate stress (MPa)	Yield stress (MPa)	Percentage elongation (%)
1	673	410	15.6
2	676	413	18.3
3	660	403	20.1

**Table 3:** Brinell and equivalent Rockwell hardness of the specimens

Test No.	HB/62,5/2,5	HRB
1	197	
2	193	
3	197	92
4	197	
5	193	
Average	195	92
C17410		89-98

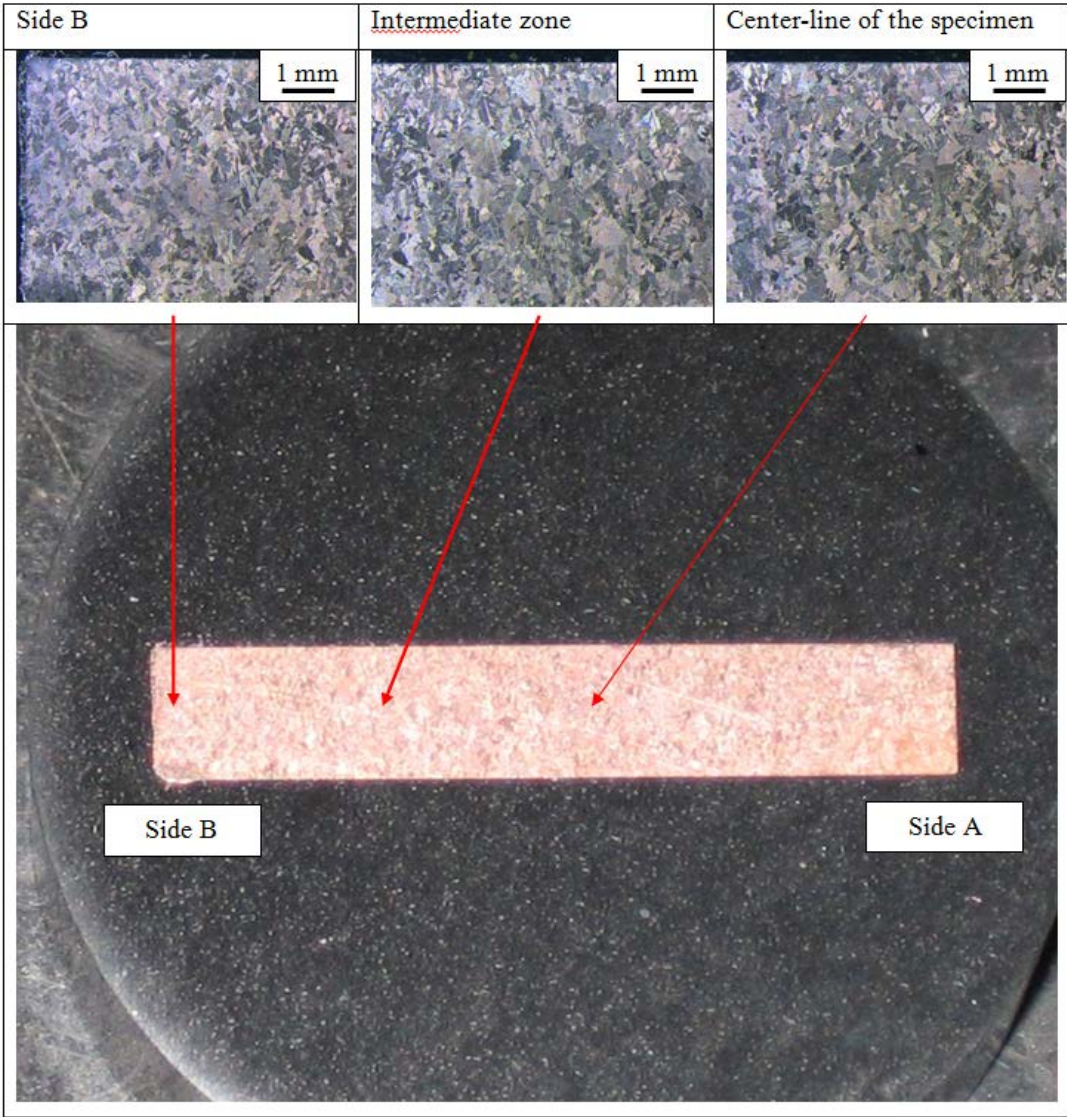


**Fig. 2:** Macrographs of the microstructure along the thickness

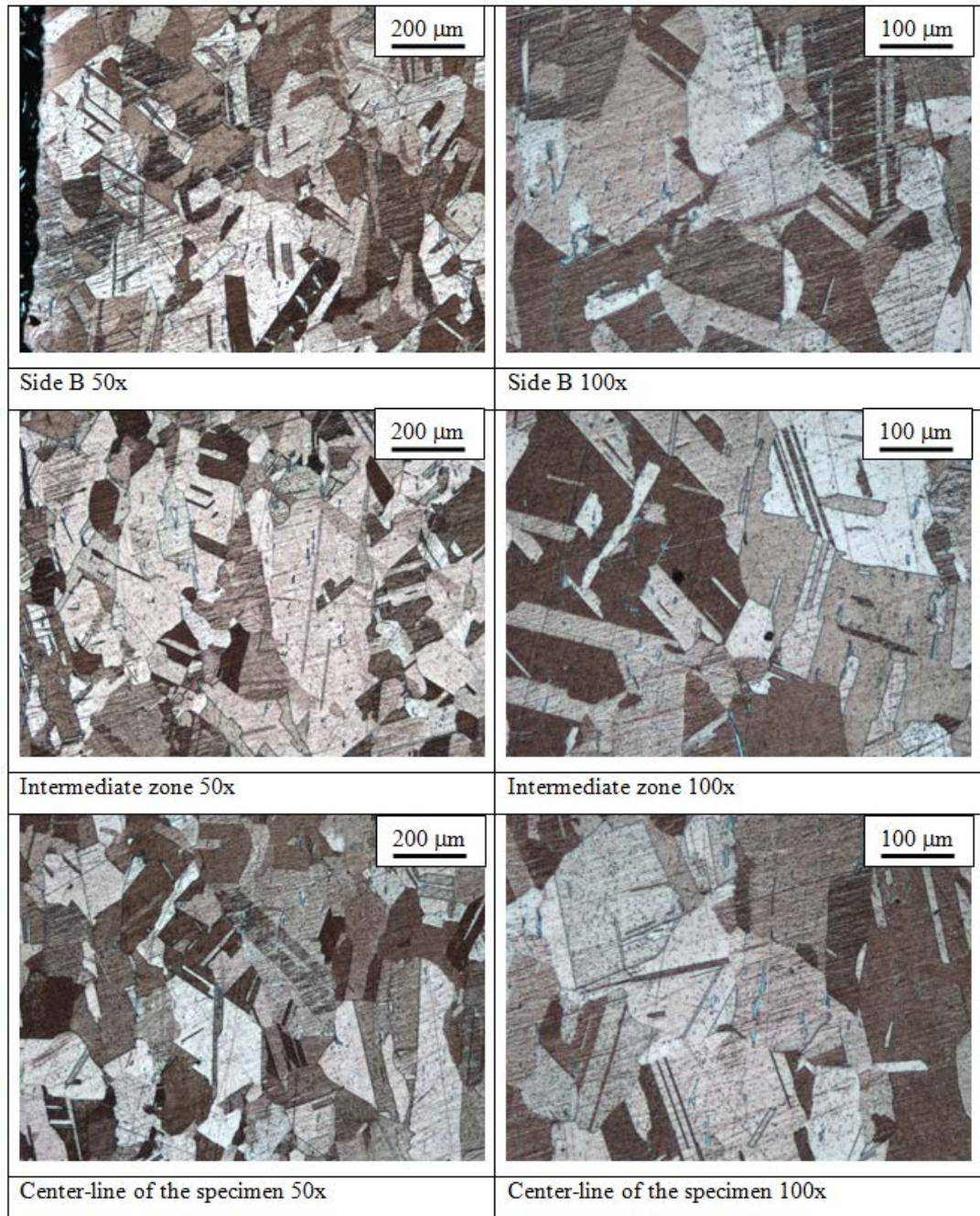


**Fig. 3:** Optical micrographs of the alloy at different magnification values

2.2 Experimental procedure

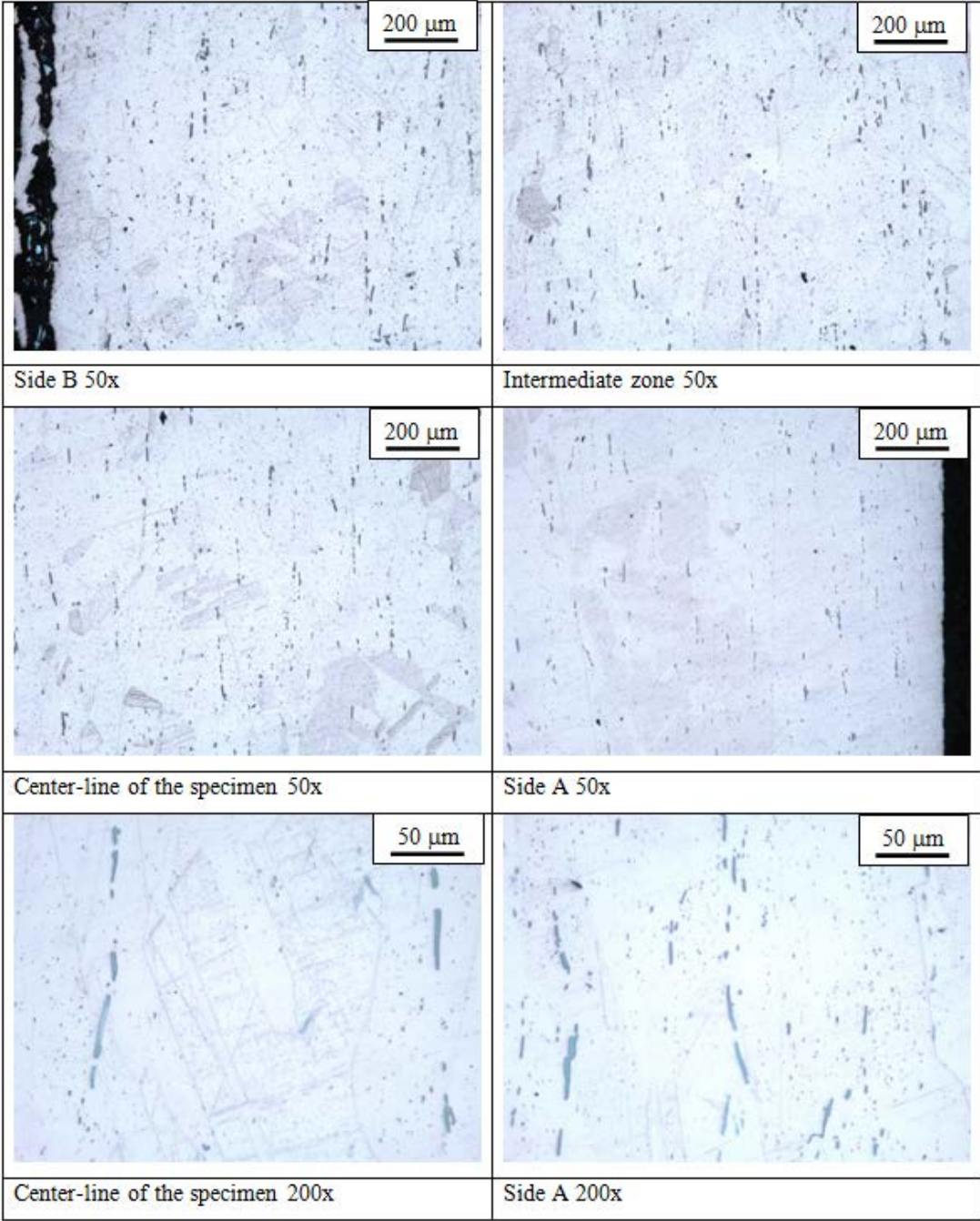


**Fig. 4:** Micrographs of the microstructure at different magnification values before the etching procedures

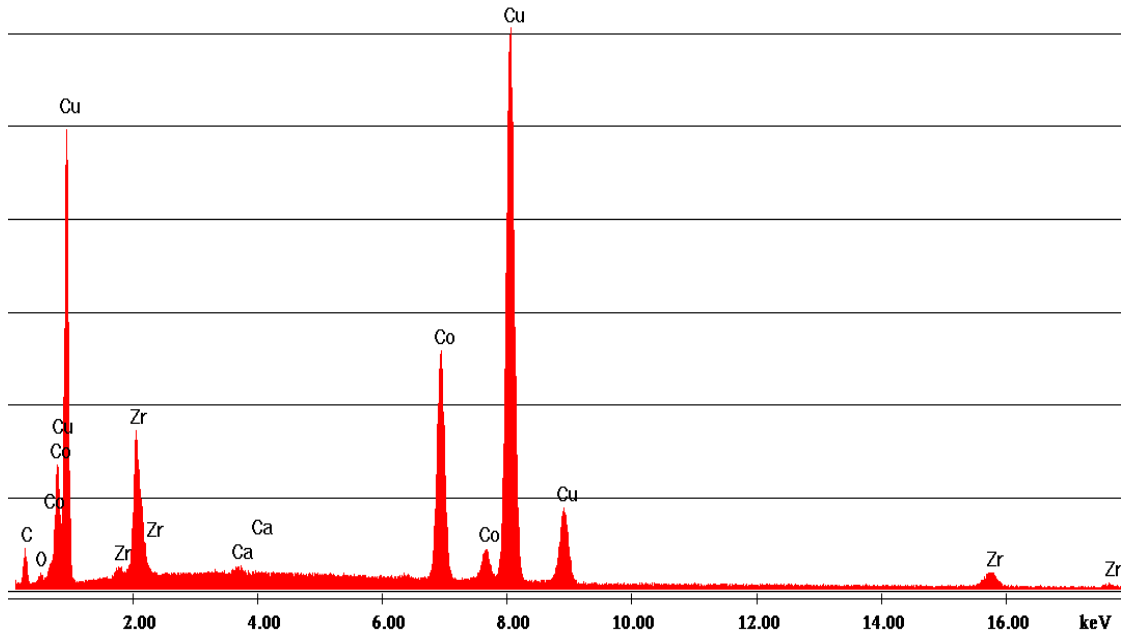


Fig. 5: EDS spectrum of the precipitate shown in Fig.6

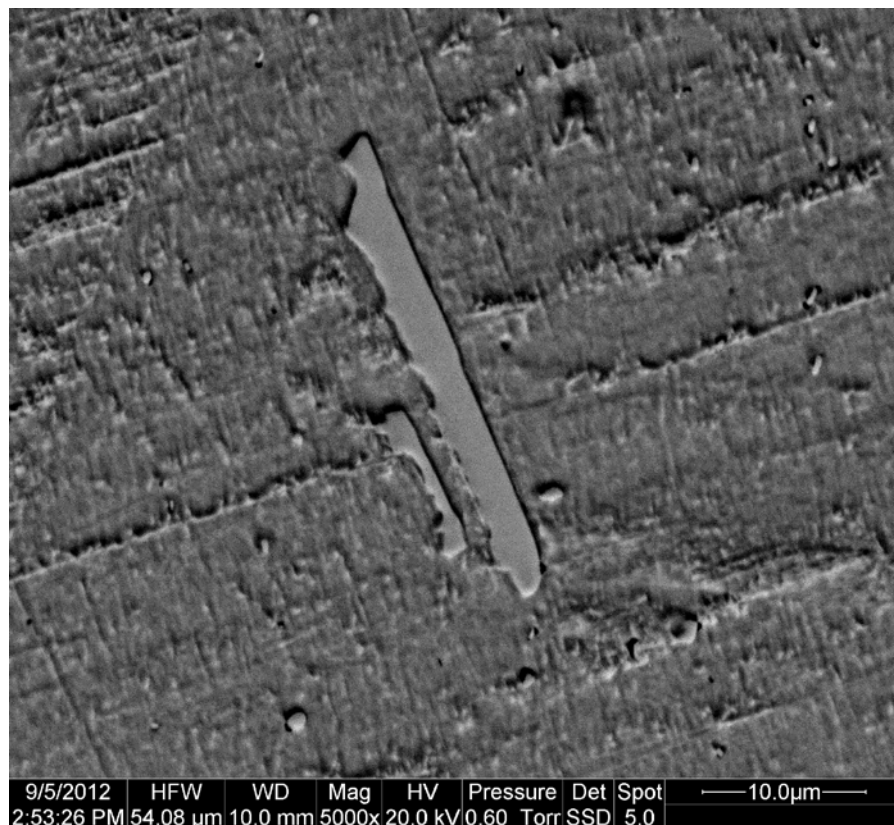
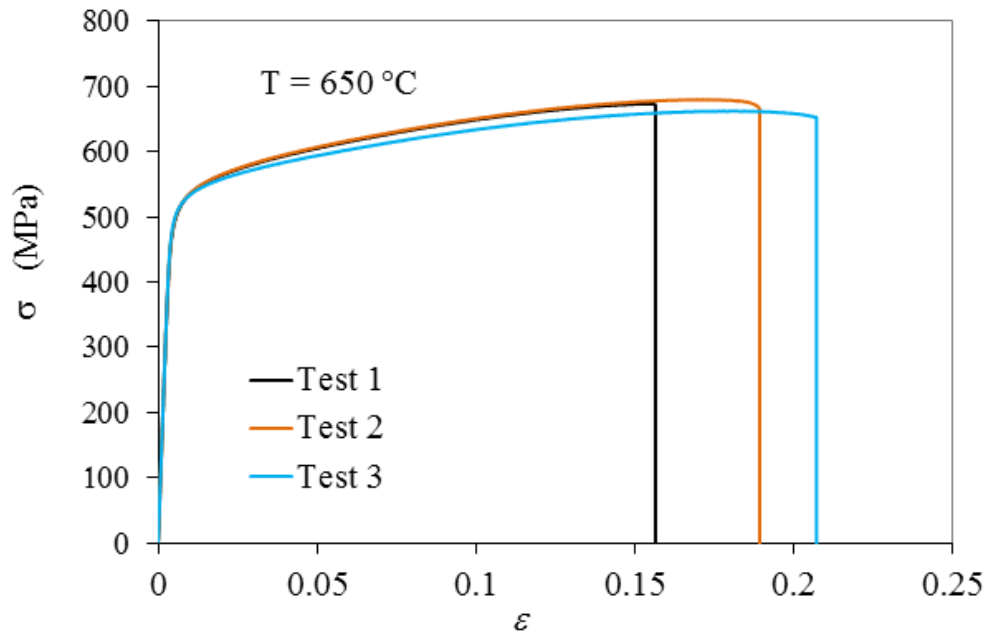


Fig. 6: Secondary electron SEM micrograph of a precipitate



**Fig. 7:** Stress-strain curves of the considered Cu-Be alloy

### 2.2.2 Fatigue tests

The fatigue tests are conducted on a servo-hydraulic MTS 810 test system with a load cell capacity of 250 kN. The system is provided with a MTS Model 653 High Temperature Furnace as shown in Fig. 8. It is ideal for a wide variety of high-temperature tests, including tension, compression, bending and fatigue testing of different materials, metallic and so on. It has a center-split design that enables easy access to both grippers and specimens. The furnace includes the MTS digital PID Temperature Control System and is configured for two heating zones which can be independently temperature-controlled through high precision thermocouples. The heating elements are made of silicon carbide. An insulation plate situated between the upper and lower elements helps ensure reliable zone separation and pre-cut insulation reduces heat loss. This furnace is particularly well-suited for applications that require a lower thermal gradient on a fatigue (or tensile) specimen. The nominal temperature for this furnace ranges from 100°C to 1400°C and the control point stability is about  $\pm 1^\circ\text{C}$ . Since the wedge grips are affected by the heat of the furnace, they are equipped with a cooling system that keeps the temperature low enough in order to not provoke any damage to the test-instruments.

The concerned load-controlled fatigue tests were carried out at 650 °C: the specimen was heated to reach the desired temperature and after a short waiting period (20

minutes) necessary to assure a uniform temperature, the test was started. The temperature was maintained constant until specimen failures thank to the PID temperature control system. The uniaxial tensile fatigue tests were carried out over a range of cyclic stresses at 5 Hz on the MTS servo-hydraulic device described above; the load ratio  $R$  was kept constant and equal to 0.01.

Two specimen geometries were considered:

- Hourglass shaped (smooth) specimens with the stress concentration factor close to 1.0;
- Plates with a central hole, with a cross section of  $30 \text{ mm} \times 5 \text{ mm}$  and a total length of 300 mm; the hole radius is 5 mm, which results in a theoretical stress concentration factor  $K_t=2.3$  (on the net transverse area).

The specimens were designed to avoid an increase of temperature near the grippers and the length of 300 mm, which is higher than the length usually adopted at room temperature, was chosen for this reason. Figure 9 shows an image of the tested specimens while Figs. 10 and 11 give all the geometrical parameters. Twenty-six specimens were tested; fifteen un-notched specimens and eleven notched plates, in order to obtain a database sufficient to draw reliable fatigue curves.

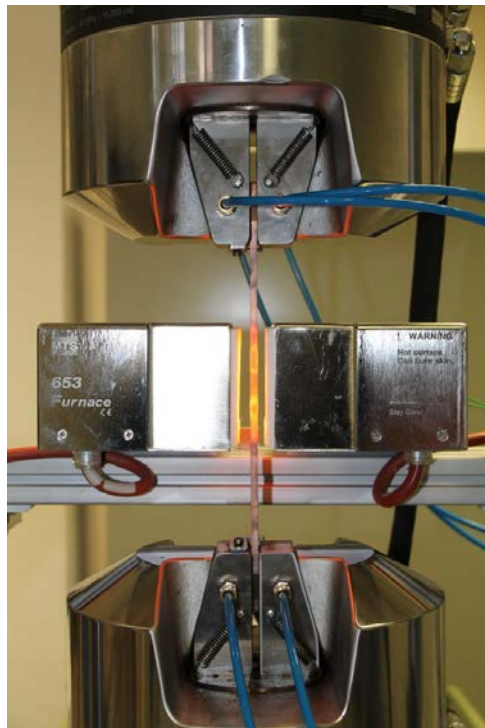


**Fig. 8:** Servo-hydraulic test system and high temperature furnace



**Fig. 9:** Hour-glass shaped specimen and notched specimen

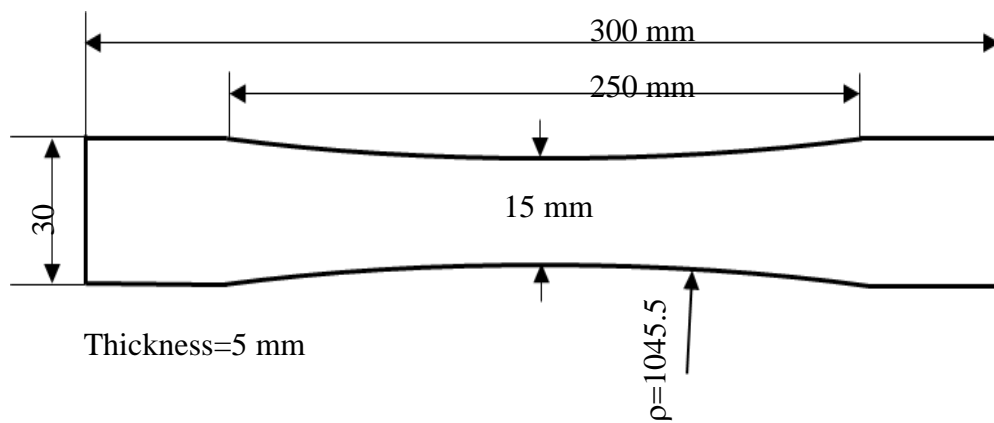


**Fig. 10:** Hour-glass shaped specimen geometry

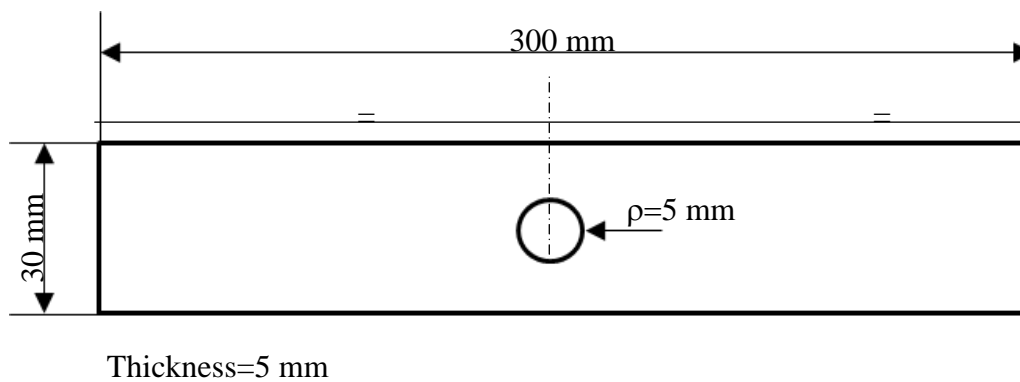


**Fig. 11:** Plate specimen with central hole



## 2.3 Results and discussion

### 2.3.1 Fatigue test results

The fatigue data were statistically elaborated by using a log-normal distribution and are plotted here in a double log scale. All stress ranges are referred to the net area.

Figures 12 and 13 show the fatigue data of the hourglass specimens and plates weakened by central holes, respectively, the mean Wöhler curve (probability of survival  $P_s = 50\%$ ) and the Haibach scatter band referred to 10% and 90% of probabilities of survival (for confidence level equal to 95%). The run-out samples, over two million cycles, were not included in the statistical analysis and are marked with a horizontal arrow. A vertical line indicates the values corresponding to two million cycles. For the sake of completeness the values of the inverse slope  $k$  and the scatter index  $T_\sigma$  are also shown.

By comparing the results from notched and un-notched specimens, a reduction of 40% of the mean value of the stress range at two million cycles can be observed (see Figure 14). It decreases from 241 MPa (for plain specimens) to 145 MPa (for notched specimens).

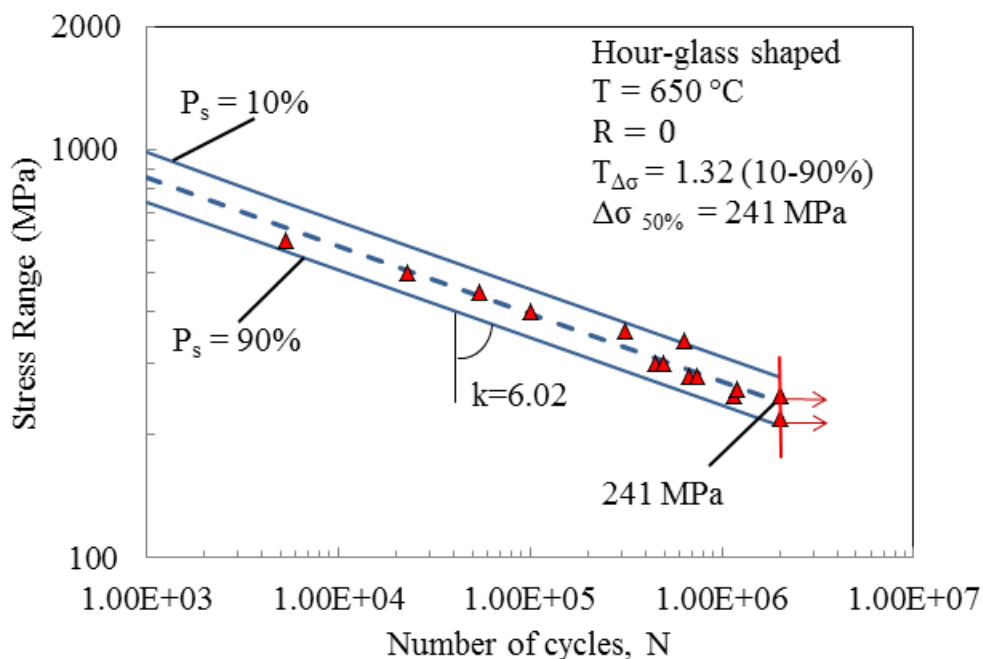


**Fig. 12:**  $S$ - $N$  fatigue data from the hourglass shaped specimens

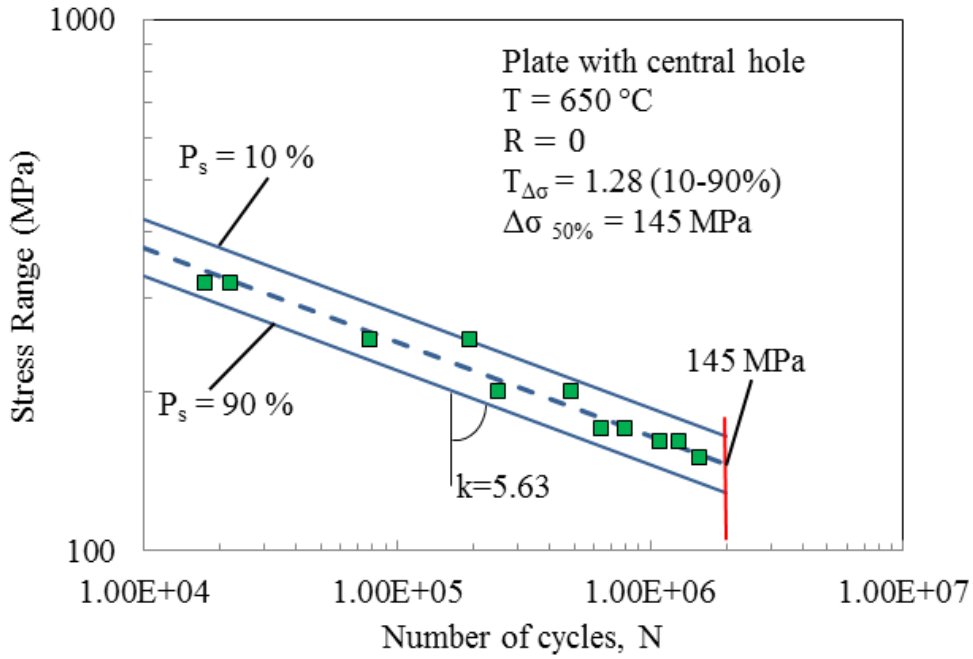


**Fig. 13:** *S-N* fatigue data from notched specimens

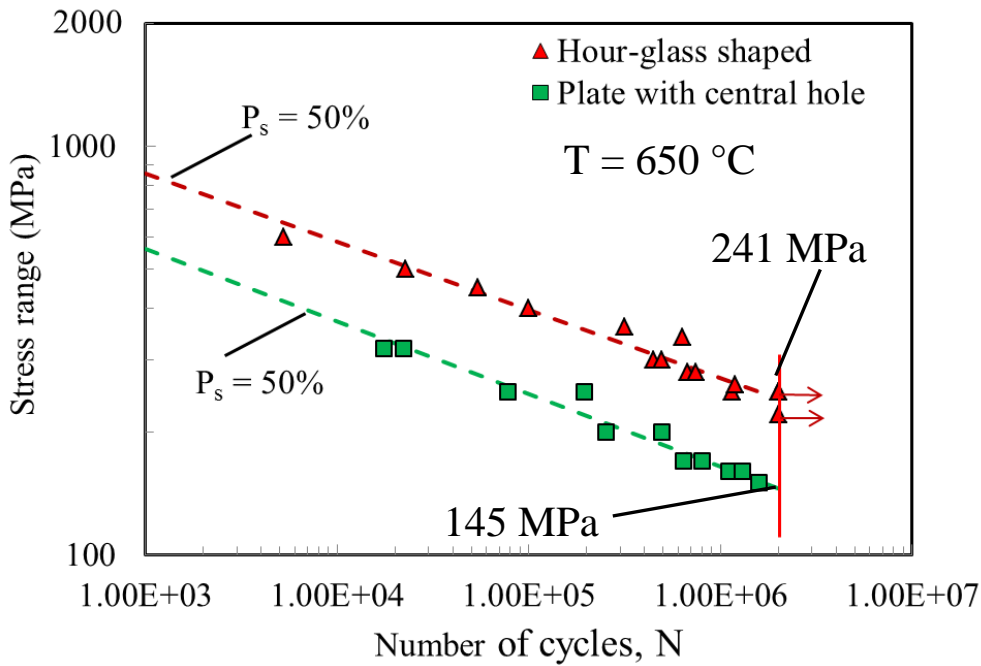


**Fig. 14:** *S-N* curves ( $P_s = 50\%$ )

The inverse slope of the two curves is very close:  $k=6.02$  for hourglass specimens and  $k=5.63$  for plates with central holes. In both cases the scatter index is limited, with  $T_{\Delta\sigma}=1.32$  for smooth specimens and  $T_{\Delta\sigma}=1.28$  for notched specimens. The reduction in fatigue strength is almost the same at low cycle fatigue regime and this

effect is due to the stress concentration combined with the high temperature effect. During the tests, both for un-notched and notched specimens no signs of plasticity were detected. Due to the large radius of the hole (5 mm), it was natural to think that the fatigue strength reduction factor  $K_f$  could assume a value equal to the theoretical stress concentration factor  $K_t$ , which is 2.30 (with reference to the net area). This value, obtained by means of a numerical analysis performed by using the software Ansys (release 12.0), is in agreement with Peterson's handbook. By assuming *a priori*  $K_f$  numerically equal to  $K_t$ , i.e. by considering a full notch sensitivity, one might calculate the expected maximum stress range at two million cycles for the plate with central holes. Comparing this value with the experimental data, it is evident that the temperature has reduced the notch sensitivity of the material, which is not full, as expected, but less than unity. As a matter of fact the actual  $K_f$  is equal to 1.66 whereas the expected value was 2.3. The experimental maximum stress at two million cycles of the plate with the hole is 145 MPa whereas, the value estimated by means of  $K_t$  would be much lower, 105 MPa.

All fatigue test data are listed in Tables 4 and 5; the results from the statistical analyses are provided in Tables 6 and 7 for the two series.

**Table 4:** Fatigue data of hourglass shaped specimens, load ratio R=0, T=650°C

Specimen	Cross Section (net) (mm <sup>2</sup> )	$\sigma_{\max}$ (MPa)	$\sigma_{\min}$ (MPa)	Cycles	Notes
1	75	250	5	2000000	Run out
2	75	250	5	2000000	Run out
3	75	600	12	5270	
4	75	500	10	22871.5	
5	75	400	8	99990.5	
6	75	340	6.8	629416.5	
7	75	360	7.2	315017.5	
8	75	450	9	54376	
9	75	300	6	445575	
10	75	300	6	495000	
11	75	280	5.6	675000	
12	75	280	5.6	743000	
13	75	250	5	1150000	
14	75	250	5	2000000	Run out
15	75	260	5.2	1197878	

**Table 5:** Fatigue data of plate with a central hole specimens, load ratio  $R=0$ ,  $T=650^{\circ}\text{C}$

Specimen	Cross Section (net) (mm <sup>2</sup> )	$\sigma_{\max}$ (MPa)	$\sigma_{\min}$ (MPa)	Cycles	Notes
1	100	250	5	193397	
2	100	160	3.2	1100500	
3	100	200	4	253122	
4	100	200	4	490500	
5	100	320	6.4	22083	
6	100	320	6.4	17412.5	
7	100	250	5	77873	
8	100	160	3.2	1300000	
9	100	150	3	1581500	
10	100	170	3.4	799910	
11	100	170	3.4	640561	

**Table 6:** Statistical analysis of smooth specimens fatigue data

P.s.	$\Delta\sigma_a$ (MPa)	N
10%	982.3	1000
50%	854.7	1000
90%	744.1	1000
10%	277.2	2000000
50%	241.3	2000000
90%	210.6	2000000
$T_{\Delta\sigma} = 1.32$		

**Table 7:** Statistical analysis of plate with a central hole specimens fatigue data

P.s.	$\Delta\sigma_a$ (MPa)	N
10%	635.4	1000
50%	560.5	1000
90%	494.4	1000
10%	164.7	2000000
50%	145.3	2000000
90%	128.2	2000000
$T_{\Delta\sigma} = 1.28$		

### 2.3.2 Microstructure after fatigue test

Some metallographic analyses have been conducted on fatigue tested specimens in order to compare the microstructure with the untested morphology. The micrographs are shown in Fig. 15 (after chemical etching) and in Fig. 16 (before the etching procedure). It can be noted that no changes occur although the long-time exposure at high temperature. Both figures document that the microstructure, the dispersion and morphology of the beryllides are identical to those of the untested specimens. No signs due to plasticity or other non-linear effects have been detected also analyzing the fracture surfaces after the tests. In fact at the temperature used here, which corresponds to the service condition in hot-rolling applications, these effects have to be avoided to guarantee a satisfactory quality of the laminated and a life of the shell in the range of  $10^5$ - $10^6$  cycles.

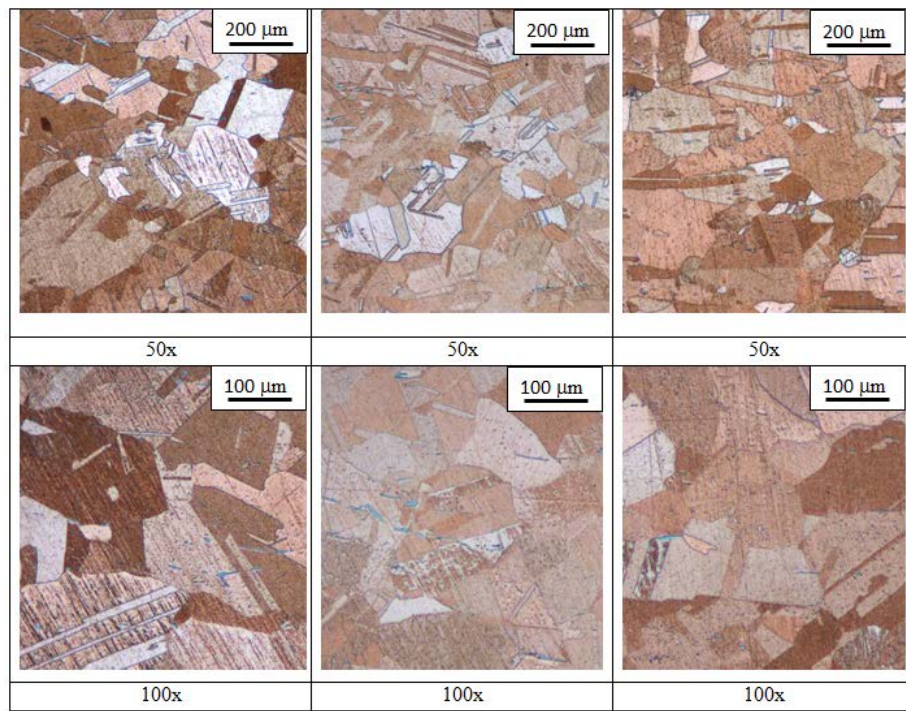


**Fig. 15:** Micrographs after etching procedures at different magnifications; comparison between microstructures before and after the fatigue test at high temperature

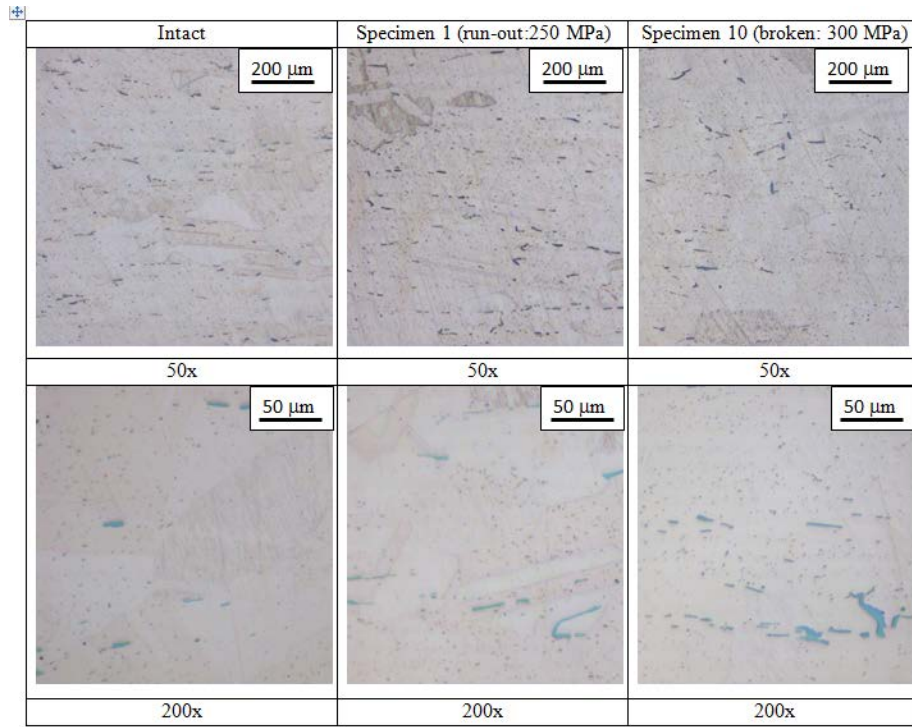


**Fig. 16:** Micrographs before etching procedures at different magnifications which compare the microstructure of the specimen before (intact) and after the fatigue test at high temperature

## 2.4 A synthesis in terms of linear elastic SED averaged over a control volume

The averaged strain energy density criterion (SED) states that brittle or quasi-brittle failure occurs when the mean value of the strain energy density over a given control volume (that becomes an area in two dimensional cases) is equal to a critical value  $W_c$ . Such a method has been extensively used in the literature and its power, especially when dealing with fatigue of notched components, has been largely proved. A review of the method has been presented in [29], where the analytical frame and the main applications of the averaged SED approach are revisited in detail. This review refers to more than eighty papers published over the last fifty years, and has conducted the present authors to formulate such a criterion for brittle and quasi-brittle materials under different loading modes.

In order to re-analyse the high temperature fatigue data in terms of strain energy density over a control volume, it is necessary to determine the critical radius  $R_c$  that defines the size of the volume (see Figure 17) and that does not depend on the

loading conditions but only on the material properties. As widely described in [29,26,27,30,31] the control radius  $R_c$  of the volume, over which the energy was averaged, depends on the ultimate tensile strength and the fracture toughness  $K_{IC}$  in the case of static loads and brittle materials. It depends also on plain specimen fatigue limit and on the threshold behavior  $\Delta K_{th}$  in the case of metallic materials under high-cycle fatigue loads. Due to the reduced dimension of  $R_c$ , no attention was paid to crack propagation direction. The energy was given in closed form as a function of the geometry-dependent Notch Stress Intensity Factors. Plane stress and plane strain conditions as well as isotropic and linear elastic material behavior were considered. Since high temperature data from the cracked material under investigation were not available (e.g.  $\Delta K_{th}$ ), the critical radius has been estimated here by equating the values of the critical SED at  $2 \times 10^6$  cycles as determined from the plain and the notched specimens.

In the high cycle fatigue regime the critical SED range for un-notched specimens can be simply evaluated by using the following expression:

$$\Delta W_c = \Delta \sigma^2 / 2E \quad (1)$$

At  $2 \times 10^6$  cycles, by using the mean value of the stress range from plain specimens (241 MPa), the SED range is  $0.22 \text{ MJ/m}^3$ . In parallel, the averaged SED for plates with central holes have been calculated by means of Ansys code modelling one-fourth of the plate and taking advantages of the double symmetry. The radius of the control volume has been varied to match the SED value previously determined from the un-notched specimens at  $2 \times 10^6$  cycles.

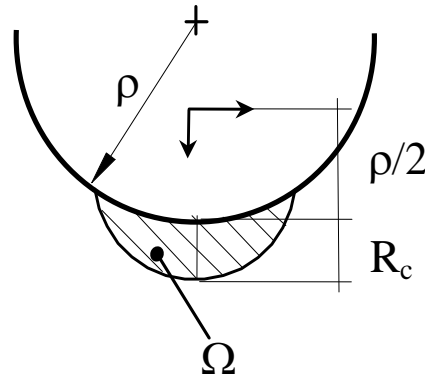


**Fig. 17:** Critical volume (area) for plate with a central hole (U-notches)

The material has been assumed isotropic and linear elastic with the Young's modulus  $E = 133000$  MPa (which is typical of CuBe alloy under investigation) and the Poisson's ratio  $\nu = 0.3$ . The 8-nodes iso-parametric element plane 82, with plane strain key-option has been selected.

The mean of the local energy density has been obtained by dividing the elastic stored strain energy (SENE command of ANSYS code) by the control area,  $\Omega$ , both related to a varying value of  $R_c$ . The simulation has been repeated for different values of  $R_c$ , ranging from 0.2 to 0.9 mm (with a step of 0.1 mm). Coarse meshes have been used because the SED value is independent of the mesh pattern as documented in previous works [31,32]. The idea of using, under mode I loading, the linear elastic SED also in case of small scale yielding conditions is well motivated in Refs [33,34]. In [34] by using the notch stress intensity factors a reformulation of the ESED approach applied no longer at the notch tip [33] but to a finite size circular sector surrounding the notch tip has been proposed. Under plane strain conditions, the value of the energy concentration due to the notch is constant and independent of the constitutive law. When small scale yielding conditions are satisfied this immediately results in the constancy of the strain energy averaged over the process volume.

For the plates with the central hole, the lower deviation with respect to the reference values ( $0.22 \text{ MJ/m}^3$ ) has been obtained considering a control radius  $R_c=0.6$  mm. For this value, in fact, the SED range has been found to be  $0.24 \text{ MJ/m}^3$ , which is very close to that of un-notched specimens.

The fatigue data are plotted in terms of averaged strain energy density range over a control volume in Figure 18, considering the aforementioned critical radius. In addition, Table 8 summarizes the statistical analysis. It is possible to observe that the scatter band is narrow, being the scatter index  $T_w=1.805$ , equal to 1.34 when reconverted to an equivalent local stress range. The inverse slope of the scatterband is equal to 2.66. Thanks to the SED approach it is possible to summarise in a single scatterband all the fatigue data, independent of the specimen geometry, estimating also the characteristic radius for the considered material. Future developments will be devoted to understand at which temperature the transition between elevate temperature and creep occurs. Another open point is the behavior of the same alloy under different loading conditions, for example prevalent mode II.



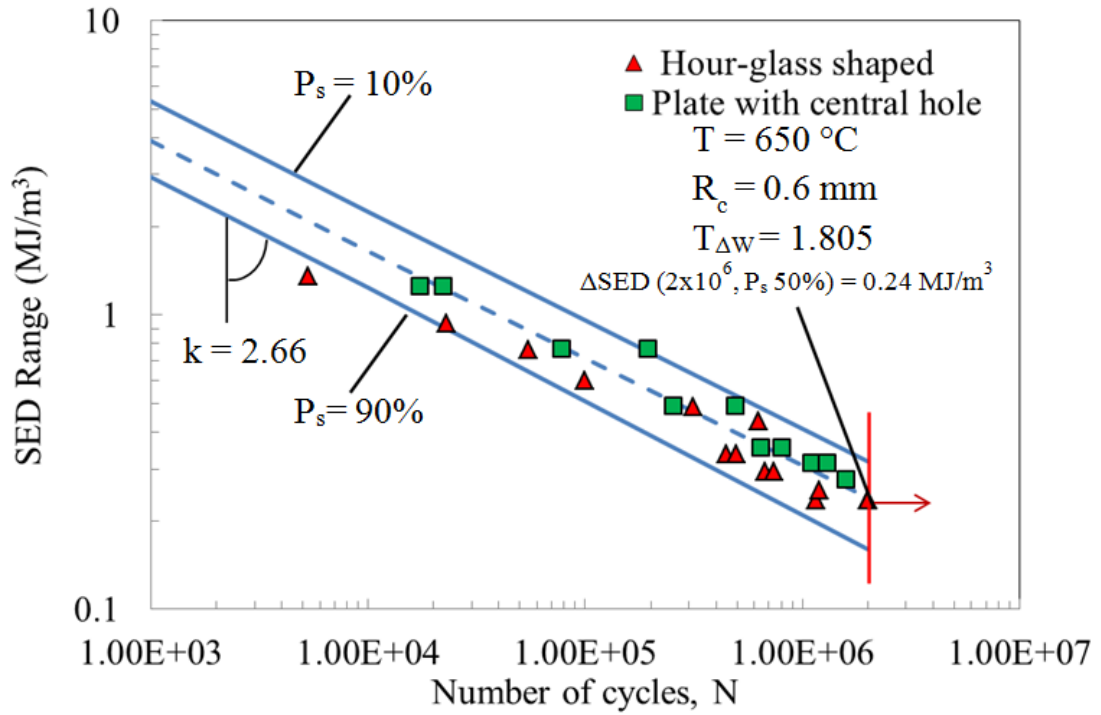


**Fig. 18:** Synthesis of fatigue data by means of local SED

**Table 8:** Statistical analysis of the fatigue data synthesis in terms of mean SED

P.s.	$\overline{\Delta W}$ (MJ/m <sup>3</sup> )	N
90%	2.95	1000
50%	3.90	1000
10%	5.32	1000
90%	1.24	10000
50%	1.64	10000
10%	2.24	10000
90%	0.16	2000000
50%	0.24	2000000
10%	0.32	2000000
$T_{\Delta W}=1.805$		

## 2.5 Conclusions

Fatigue tests and metallographic analyses were carried out on copper cobalt beryllium alloy for high temperature applications in order to investigate the fatigue strength of this material at high temperature, up to 650°C. Two specimen geometries were considered: hourglass shaped and plate with a central hole. Furthermore, a statistical analysis of fatigue data was carried out for both geometries. The data obtained were first summarized in the fatigue curves and later re-analyzed in terms of the local energy density.

The main results are summarised as follows:

- The tested alloy exhibits a good high temperature fatigue behavior.
- When the two sets of specimens are analyzed separately and compared within them, the mean value of the stress range at 2 million cycles of plate with central hole specimens decreases of about 39% with respect to the smooth ones.
- In both cases the scatter band is narrow, being the scatter index equal to 1.321 for smooth specimens and to 1.285 for the notched ones.
- The decrement of the inverse slope  $k$  is very small, it decreases from 6.02 to 5.63 for hourglass shaped and plate with central hole specimens, respectively.
- The reduction in strength is mainly due to stress concentration in presence of the hole, and it can be asserted that material is notch sensitive; despite the 39% reduction of mean stress at 2 million cycles of the plate with a central hole, the material has a very good fatigue strength.
- No changes of the microstructure occur although the long-time exposure at high temperature.
- The high temperature mitigates the stress concentration effect: the experimental value of  $K_f$  has been found to be equal to 1.66 that should be compared with the expected value 2.30 ( $K_f=K_t$ ) in the case of full notch sensitivity.
- A value of  $R_c$  equal to 0.6 mm seems to be a good choice in order to summarize the fatigue data in terms of mean SED over a control volume: a very narrow scatter band characterized by a limited value of the scatter index

has been obtained ( $T_w = 1.805$ ). It becomes equal to 1.34 if reconverted to an equivalent local stress range.

## References

- [1] A.C. Reardon, *Metallurgy for the Non-metallurgist, II*, ASM International, 2011.
- [2] J.O. Ratka, W.D. Spiegelberg, A high performance beryllium copper alloy for magnet applications, *IEEE Trans. Magn.* 30 (1994) 1859–1862.
- [3] S. Constantinescu, A. Popa, J. Groza, I. Bock, New high-temperature copper alloys, *J. Mater. Eng. Perform.* 5 (1996) 695–698.
- [4] J.R. Davis, *Copper and Copper Alloys*, ASM International, 2001.
- [5] R.N. Caron, *Copper Alloys: Properties and Applications*, *Encycl. Mater. Sci. Technol.* (2001) 1665–1668.
- [6] D.-P. Lu, J. Wang, W.-J. Zeng, Y. Liu, L. Lu, B.-D. Sun, Study on high-strength and high-conductivity Cu–Fe–P alloys, *Mater. Sci. Eng. A.* 421 (2006) 254–259.
- [7] H.T. Zhou, J.W. Zhong, X. Zhou, Z.K. Zhao, Q.B. Li, Microstructure and properties of Cu–1.0Cr–0.2Zr–0.03Fe alloy, *Mater. Sci. Eng. A.* 498 (2008) 225–230.
- [8] B.. Gonzalez, C.S.. Castro, V.T.. Buono, J.M.. Vilela, M.. Andrade, J.M.. Moraes, et al., The influence of copper addition on the formability of AISI 304 stainless steel, *Mater. Sci. Eng. A.* 343 (2003) 51–56.
- [9] A. Kar, M. Ghosh, A.K. Ray, R.N. Ghosh, Effect of copper addition on the microstructure and mechanical properties of lead free solder alloy, *Mater. Sci. Eng. A.* 459 (2007) 69–74.
- [10] B. Bose, R.J. Klassen, Effect of copper addition and heat treatment on the depth dependence of the nanoindentation creep of aluminum at 300K, *Mater. Sci. Eng. A.* 500 (2009) 164–169.
- [11] K.K. Alaneme, S.M. Hong, I. Sen, E. Fleury, U. Ramamurty, Effect of copper addition on the fracture and fatigue crack growth behavior of solution heat-treated SUS 304H austenitic steel, *Mater. Sci. Eng. A.* 527 (2010) 4600–4604.
- [12] B.C. Maji, M. Krishnan, Effect of copper addition on the microstructure and shape recovery of Fe–Mn–Si–Cr–Ni shape memory alloys, *Mater. Sci. Eng. A.* 570 (2013) 13–26.
- [13] M. Li, B.. Singh, J.. Stubbins, Room temperature creep–fatigue response of selected copper alloys for high heat flux applications, *J. Nucl. Mater.* 329–333

- (2004) 865–869.
- [14] G. Li, B. Thomas, J. Stubbins, Modeling creep and fatigue of copper alloys, *Metall. Mater. Trans. A.* 31 (2000) 2491–2502.
- [15] S. Kwofie, Cyclic creep of copper due to axial cyclic and tensile mean stresses, *Mater. Sci. Eng. A.* 427 (2006) 263–267.
- [16] H. Miura, Y. Ito, T. Sakai, M. Kato, Cyclic creep and fracture behavior of Cu–SiO<sub>2</sub> bicrystals with [011] twist boundaries, *Mater. Sci. Eng. A.* 387-389 (2004) 522–524.
- [17] J.H. Yang, X.P. Zhang, Y.-W. Mai, W.P. Jia, W. Ke, Environmental effects on deformation mechanism and dislocation microstructure in fatigued copper single crystal, *Mater. Sci. Eng. A.* 396 (2005) 403–408.
- [18] K. Shen, M.P. Wang, S.M. Li, Study on the properties and microstructure of dispersion strengthened copper alloy deformed at high temperatures, *J. Alloys Compd.* 479 (2009) 401–408.
- [19] M.F. Quinlan, M.T. Hillery, High-strain-rate testing of beryllium copper at elevated temperatures, *J. Mater. Process. Technol.* 153-154 (2004) 1051–1057.
- [20] S.J. Ko, Y.-J. Kim, High temperature fatigue behaviors of a cast ferritic stainless steel, *Mater. Sci. Eng. A.* 534 (2012) 7–12.
- [21] K. Prasad, R. Sarkar, P. Ghosal, V. Kumar, M. Sundararaman, High temperature low cycle fatigue deformation behaviour of forged IN 718 superalloy turbine disc, *Mater. Sci. Eng. A.* 568 (2013) 239–245.
- [22] J. Liu, Q. Zhang, Z. Zuo, Y. Xiong, F. Ren, A. a. Volinsky, Microstructure evolution of Al–12Si–CuNiMg alloy under high temperature low cycle fatigue, *Mater. Sci. Eng. A.* 574 (2013) 186–190.
- [23] E. Hosseini, S.R. Holdsworth, E. Mazza, Creep constitutive model considerations for high-temperature finite element numerical simulations, *J. Strain Anal. Eng. Des.* 47 (2012) 341–349.
- [24] Y. Gorash, H. Altenbach, G. Lvov, Modelling of high-temperature inelastic behaviour of the austenitic steel AISI type 316 using a continuum damage mechanics approach, *J. Strain Anal. Eng. Des.* 47 (2012) 229–243.
- [25] I. Altenberger, R.K. Nalla, Y. Sano, L. Wagner, R.O. Ritchie, On the effect of deep-rolling and laser-peening on the stress-controlled low- and high-cycle

- fatigue behavior of Ti–6Al–4V at elevated temperatures up to 550°C, *Int. J. Fatigue*. 44 (2012) 292–302.
- [26] P. Lazzarin, R. Zambardi, A finite-volume-energy based approach to predict the static and fatigue behavior of components with sharp V-shaped notches, *Int. J. Fract.* 112 (2001) 275–298.
- [27] P. Lazzarin, F. Berto, Some Expressions for the Strain Energy in a Finite Volume Surrounding the Root of Blunt V-notches, *Int. J. Fract.* 135 (2005) 161–185.
- [28] J. Harkness, A. Guha, *Metallographic Techniques For Beryllium Copper and Beryllium Nickel Alloys*, 1997.
- [29] F. Berto, P. Lazzarin, A review of the volume-based strain energy density approach applied to V-notches and welded structures, *Theor. Appl. Fract. Mech.* 52 (2009) 183–194.
- [30] F.J. Gómez, M. Elices, F. Berto, P. Lazzarin, A generalised notch stress intensity factor for U-notched components loaded under mixed mode, *Eng. Fract. Mech.* 75 (2008) 4819–4833.
- [31] P. Lazzarin, F. Berto, M. Zappalorto, Rapid calculations of notch stress intensity factors based on averaged strain energy density from coarse meshes: Theoretical bases and applications, *Int. J. Fatigue*. 32 (2010) 1559–1567.
- [32] P. Lazzarin, F. Berto, F.J. Gómez, M. Zappalorto, Some advantages derived from the use of the strain energy density over a control volume in fatigue strength assessments of welded joints, *Int. J. Fatigue*. 30 (2008) 1345–1357.
- [33] G. Glinka, Energy density approach to calculation of inelastic strain-stress near notches and cracks, *Eng. Fract. Mech.* 22 (1985) 485–508.
- [34] P. Lazzarin, R. Zambardi, The Equivalent Strain Energy Density approach reformulated and applied to sharp V-shaped notches under localized and generalized plasticity, *Fatigue Fract. Engng. Mater. Struct.* 25 (2002) 917–928.

### 3. High temperature fatigue tests of notched specimens made of titanium Grade 2

*P. Gallo, F. Berto, P. Lazzarin, High temperature fatigue tests of notched specimens made of titanium Grade 2, Theor. Appl. Fract. Mech. 76 (2015) 27-34.*

#### **Highlights**

The present chapter summarizes data from uniaxial-tension load controlled fatigue tests on notched specimens made of titanium Grade 2. The tests are performed at room temperature and 500 °C that, having regard to the properties of titanium Grade 2, can be considered as a limit temperature. Indeed, in the final application, a component can be intentionally or unintentionally pushed to the limit. Commercially Pure (CP) titanium Grade 2 is employed for high-performance applications, such as jet engine and airframe components (e.g. ductwork, brackets), or small rolls for hot-rolling of metals, and it is subjected, in service, to a combination of mechanical and moderate thermal loadings that under uncontrolled conditions can become very important. Two geometries are considered: semicircular notches and plates weakened by symmetric V-notches, with opening angle and tip radius being equal to 90 degrees and 0.75 mm, respectively. The present research activity is motivated by the fact that, at the best of authors' knowledge, no results seem to be available for notched components tested at high temperature made of titanium Grade 2.

After a brief literature review of the recent works available for titanium in general, the Grade 2 is introduced in §Section 3.2. Subsequently, the experimental procedure is described in detail and the new fatigue data are summarized in terms of stress range, at the considered temperatures. Finally, the results are re-analysed by means of the mean value of the Strain Energy Density (SED) and the advantages of the method are pointed out.





### 3.1 Introduction

In general, the titanium has been recognized for its strategic importance as a unique lightweight, high strength alloyed, structurally efficient metal for critical, high-performance applications, such as jet engine and airframe components. One of the primary attributes of these alloys is the elevated strength-to-density ratio which represents the traditional primary incentive for selection and design into aerospace engines and airframe structures and components. Moreover, very low density and the exceptional corrosion resistance make titanium alloys very attractive for high temperature applications such as hot gas turbine and automotive engine components, where more creep-resistant alloys are required for temperatures as high as 600°C. Titanium is a very well-established heat transfer material that shows a good strength and ability to fully withstand corrosion and erosion at high temperature [1–3].

The literature about titanium and its alloys is very wide and diversified. Different titanium alloys have been largely analysed in a number of papers, considering different topics and point of views, e.g. fatigue resistance in air and corrosive environment, effects of high temperature, microstructural aspects, notch sensitivity, crack propagation. Among the recent works, in [4], the crack growth behaviour in titanium alloys at high temperature was examined. A focus is made on the concept that the fracture mechanisms in these alloys are governed by the slip process taking place within the crack tip region. The effect of different parameters (load frequency, hold time period) on the damaging was also analysed. In [5], it was investigated the fatigue crack propagation behaviour in commercial pure Ti severely deformed by accumulative roll bonding (ARB) process. It was found a different mechanical behaviour between specimens and starting sheet, maybe due to crack closure phenomena related to the ARB process. In [6] it was studied the effect of notch geometry on the critical distance for high cycle fatigue predictions of Ti-6Al-4V. The experimental data were used in combination with finite element analyses to determine a ‘critical distance’ for all of the considered geometries. It was determined from the stress distribution surrounding the notch in combination with fatigue limit stress data from un-notched specimens. However, it was not possible to define a unique synthesis parameter for the fatigue assessment of all of the specimen geometries. In [7] existing multiaxial fatigue models are examined in order to determine their suitability for estimating the fatigue damage in Ti-6Al-4V under

combined modes. Both equivalent stress-based models and critical plane approaches were discussed but only one equivalent stress model and two critical plane models showed promising results for the range of loadings and material considered. Another newsworthy paper is presented by [8], in which a predictive model for the fatigue crack propagation in metal alloys in laboratory air is proposed. The model was applied to different alloys, such as Ti-6Al-4V with very promising results.

In [9] a study on the fatigue behaviour of notch sensitivity of Ti-6Al-4V is presented. Notch sensitivity data was compared with those of steels. The results indicated that the notched material presented a different sensitivity when the specimens were subjected to high cycle fatigue (HCF) or low cycle fatigue (LCF) tests. The notch sensitivity of this alloy was shown generally to be much lower than steels with comparable ultimate strength values. The fatigue behaviour of notched Ti-6Al.4V in air and corrosive environment has been investigated in [10]. Axial fatigue tests ( $R=0.1$ ) in air and recirculated 3.5 wt.% NaCl solution were carried out, considering smooth and V-notched specimens.

Considering the specific Grade 2, an interesting work is presented in [11], in which the effect of thermal exposure on the room temperature tensile properties of Grade 2 titanium was studied. It was showed that at high temperature the ductility of samples exposed in air is dramatically reduced and a protective atmosphere is required during heat treatment.

After this brief literature review it is possible to conclude that different phenomena related to different titanium alloys have been investigated, and some other recent papers that deal with different aspects of titanium and its alloys are available in literature [12–19]. However, when dealing with high temperature fatigue of notch components made of titanium, the number of papers is reduced drastically, and moreover, no papers are available for the specific titanium alloy considered in this work (Grade 2), which among the traditional applications at room temperature, it could be used at moderate high temperatures. With the aim to fill this lack, since the significant industrial relevance of the considered material, this study is carried out to investigate the high temperature fatigue behaviour of notched specimens made of titanium Grade 2. Semicircular and V-notched specimens are considered. They have been tested at room temperature and 500°C in laboratory air. At the best of author knowledge, a complete set of data from V-notches and semicircular notches at high

temperature made of titanium Grade 2 is not available in literature. The aim of this experimental study is to present a set of new results from high-temperature fatigue tests in the high-cycle regime and to give a useful tool to design against fatigue, considering a temperature which, having regard to the properties of titanium Grades 2, can be considered as a limit temperature. Indeed, it is well known that sometimes, in the final applications, component can be intentionally or unintentionally pushed to the limit.

The tests have been performed under uniaxial tension and load-controlled conditions. At last, a final synthesis of the results is carried out by means of the Strain Energy Density approach in order to propose an easy and fast tool to design against fatigue, regardless of the specimen geometries.

## **3.2 Material properties and experimental procedures**

### **3.2.1 Titanium Grade 2 and specimen geometries**

Different titanium grades are available for industrial application, among them the first four are the commercially pure classified. In order to keep production costs as low as possible, “Commercially Pure” (CP) titanium has acceptable mechanical properties and has been used for numerous applications. The titanium under investigation in the present section is an unalloyed Grade 2, which is called the “workhorse” of the CP titanium industry, thanks to its varied usability and wide availability. It shares many of the same qualities as Grade 1 titanium, but it is slightly stronger, while both are equally corrosion resistant. Grade 2 possesses good weldability, strength, ductility and formability. This makes Grade 2 titanium bars and sheet are the prime choice for many fields of applications. In general, CP Titanium Grade 2 may be considered in any application where formability and corrosion resistance are important, and strength requirements are moderate. Some examples of aerospace applications have included airframe skins in "warm" areas, ductwork, brackets, galley equipment and pipes, where also high temperature needs to be handled. The Grade 2 Ti has also been widely used in marine and chemical applications such as condensers, evaporators, reaction vessels for chemical processing, tubing and tube headers in desalinization plants.

**Table 1:** Mechanical properties of the CP titanium Grade 2 under investigation

	$\sigma_y$ (0.2%) (MPa)	$\sigma_R$ (MPa)	E (GPa)
Room Temp.	350	544	103
500°C	175	227	75

**Table 2:** Chemical composition of the titanium Grade 2 under investigation

	Fe (%)	O (%)	N (%)	H (%)	C (%)	Ti (%)
Max	0.3	0.25	0.03	0.015	0.08	balance
Specimen	0.060	0.140	0.004	0.003	0.016	99.78

Other uses have included items such as jigs, baskets, cathodes and starter-sheet blanks for the electroplating industry. It is well known that sometimes, in the final applications, component can be intentionally or unintentionally pushed to the limit (e.g. hot-rolling of metal), for this reason it is very interesting to study the behaviour of this material at a temperature moderately higher than the common use.

Regarding the specimens considered here, they are provided in annealed condition. The mechanical properties obtained through tensile tests, at room and 500°C, are reported in Table 1: the Young modulus is affected by a moderate variation, being at room temperature equal to 103 GPa and at high temperature equal to 75 GPa, that corresponds to a reduction of 27%. Substantial differences, instead, are registered for the tensile properties:  $\sigma_y$  decreases from 350 MPa (room temp.) to 175 MPa (500°C),  $\sigma_R$  from 544 MPa (room temp.) to 227 MPa (500°C) as might be expected.

As stated previously, Grade 2 is considered CP titanium but for the sake of completeness a chemical analysis has been carried out on the specimens under investigation. The results are given in Table 2 and show a percentage of titanium of 99.78%, while all the impurities have a percentage that is below the acceptable maximum limit for Grade 2.

Two specimen geometries were considered:

- Plates weakened by lateral symmetric V-notches, with a net cross section of 30 mm × 3 mm and a total length of 350 mm (see Figure 1). The notches were characterized by a depth,  $a$ , equal to 10 mm, an opening angle,  $2\alpha$ , equal

to  $90^\circ$  and a notch tip radius  $\rho=0.75$  mm. This geometry results in a theoretical stress concentration factor  $K_{t,n}=5.38$  (on the net area).

- Plates weakened by lateral symmetric semicircular notches, with a net cross section of  $30 \text{ mm} \times 3 \text{ mm}$ . The notches were characterized by a radius  $\rho=10$  mm. The stress concentration factor,  $K_{t,n}$  (on the net area), is 1.86. The geometry is shown in detail in Figure 2.

The specimens were designed to avoid an increase of temperature near the grippers of the test instrument, for this reason the total length of the specimens is equal to 350 mm, which is higher than the length usually adopted at room temperature.

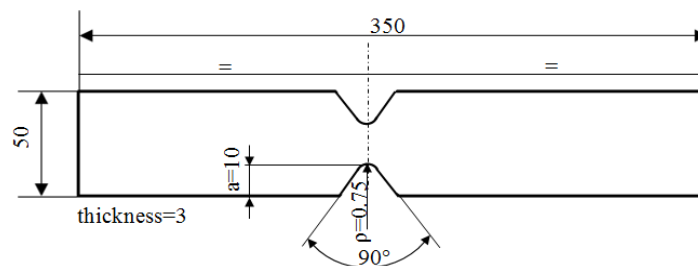


**Fig. 1:** V-notched specimen geometry, dimensions in mm

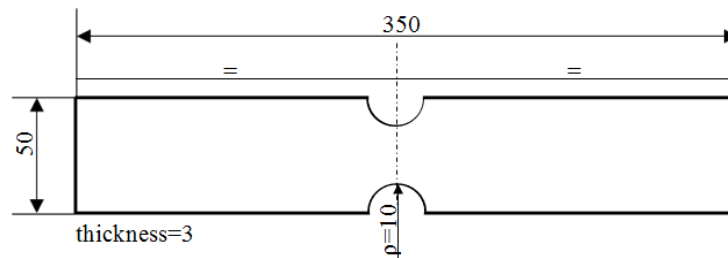


**Fig. 2:** Semicircular notched specimen geometry, dimensions in mm

### 3.2.2 Fatigue testing equipment and procedures

The fatigue tests were conducted on a servo-hydraulic MTS 810 test system with a load cell capacity of 250 kN. The system is provided with a MTS Model 653 High Temperature Furnace, as shown in Figure 3. It is ideal for a wide variety of high-temperature tests, including tension, compression, bending and fatigue testing of different materials, metallic and not. It has a center-split design that enables easy access to both grippers and specimens. The furnace includes the MTS digital PID Temperature Control System and is configured for two heating zones which can be

independently temperature-controlled through high precision thermocouples. The zone at constant temperature is 80 mm length. The heating elements are made of silicon carbide. An insulation plate situated between the upper and lower elements helps to ensure reliable zone separation and pre-cut insulation reduces heat loss. This furnace is particularly well-suited for applications that require a lower thermal gradient on a fatigue (or tensile) specimen. The nominal temperature for this furnace ranges from 100°C to 1400°C and the control point stability is about  $\pm 1^\circ\text{C}$ . Since the wedge grips are affected by the heat of the furnace, they are equipped with a cooling system that keeps the temperature low enough in order to not provoke any damage to the test-instruments.

The concerned load-controlled fatigue tests were carried out at room temperature and 500°C: the specimen was first heated to reach the desired temperature and after a short waiting period (10 minutes) necessary to assure a uniform temperature, the test was started. The temperature was maintained constant until specimen failure thank to the aforementioned PID temperature control system. The uniaxial tensile fatigue tests were carried out over a range of cyclic stresses at the constant frequency of 10 Hz; the nominal load ratio R was kept constant and equal to 0.1. Overall, four fatigue curves were obtained by testing more than 60 specimens.

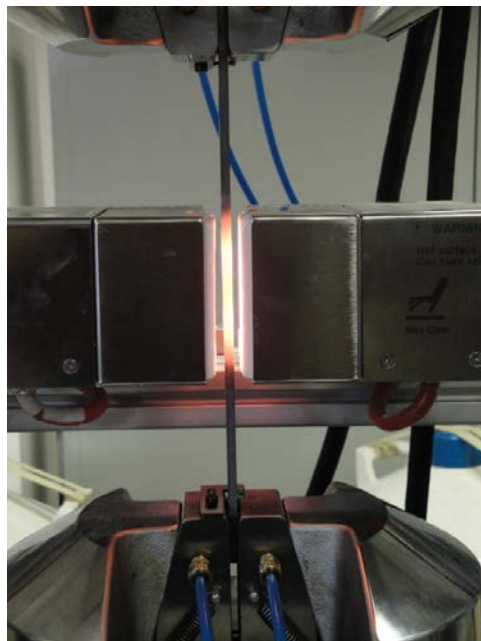


**Fig. 3:** High temperature test and furnace

### 3.3 Fatigue tests results and discussion

#### 3.3.1 Fatigue curves

The fatigue data were statistically re-analysed by using a log-normal distribution and are plotted in terms of nominal stress range referred to the net area in Figures 4, 5, 6 and 7. The run-out specimens (marked by tilted arrows) were excluded from the statistical analysis. A vertical line is drawn in correspondence of two million cycles where the mean value of the stress range is given to make the comparison easier. Details about inverse slope  $k$  and the scatter index  $T_\sigma$  are provided in the figures. Moreover the mean Wöhler curve (probability of survival  $P_s = 50\%$ ) and the Haibach scatter band referred to 10% and 90% of survival probabilities (for confidence level equal to 95%) are reported.

More specifically, Figures 4 shows the fatigue data of the semicircular notches tested at room temperature. The scatter index  $T_\sigma$  is very narrow being 1.21. The stress range at two million cycles reaches a value of 142.00 MPa and an inverse slope  $k=5.00$ . Figures 5 instead shows the fatigue data of the semicircular notches tested at high temperature (500°C). The scatter index  $T_\sigma$  is very narrow being 1.33. The stress range at two million cycles reaches a value of 80.60 MPa and an inverse slope  $k=4.80$ . Comparing room temperature data of semicircular notches with the high temperature ones, it is evident the effect of the high temperature on the fatigue strength: the stress range at two million cycles decreases from 142.00 MPa to 80.60 MPa that is 44% of reduction, while the inverse slope  $k$  has a little variation (5.00 VS 4.80).

Figures 6 depicts data from V-notched specimens tested at room temperature. Also in this case, the scatter index is very narrow being equal to 1.27. The inverse slope  $k$  is equal to 3.63 and the stress range at two million cycles to 57.00 MPa. It should be noted that the plateau is moved to the left, approximately to one million cycles where the stress range assumes a value equal to 69.00 MPa. This could be a more correct value to be assumed as fatigue strength in design against fatigue. In order to maintain a uniformity of the results presentation and for the sake of completeness, both stress range values are reported in the figure.

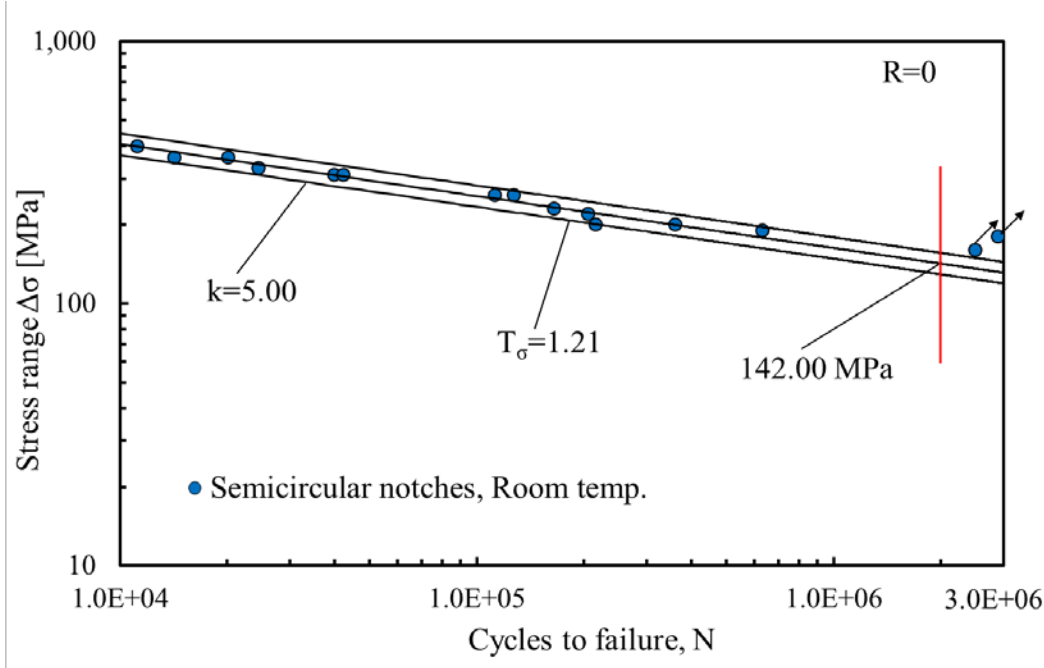


Fig. 4: Fatigue data of the semicircular notches tested at room temperature

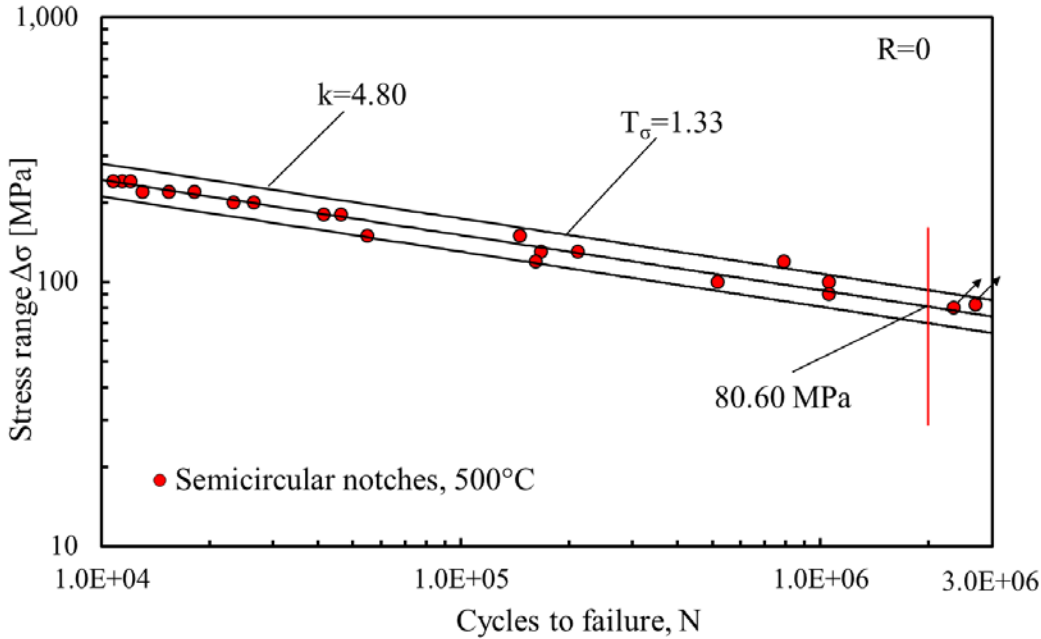
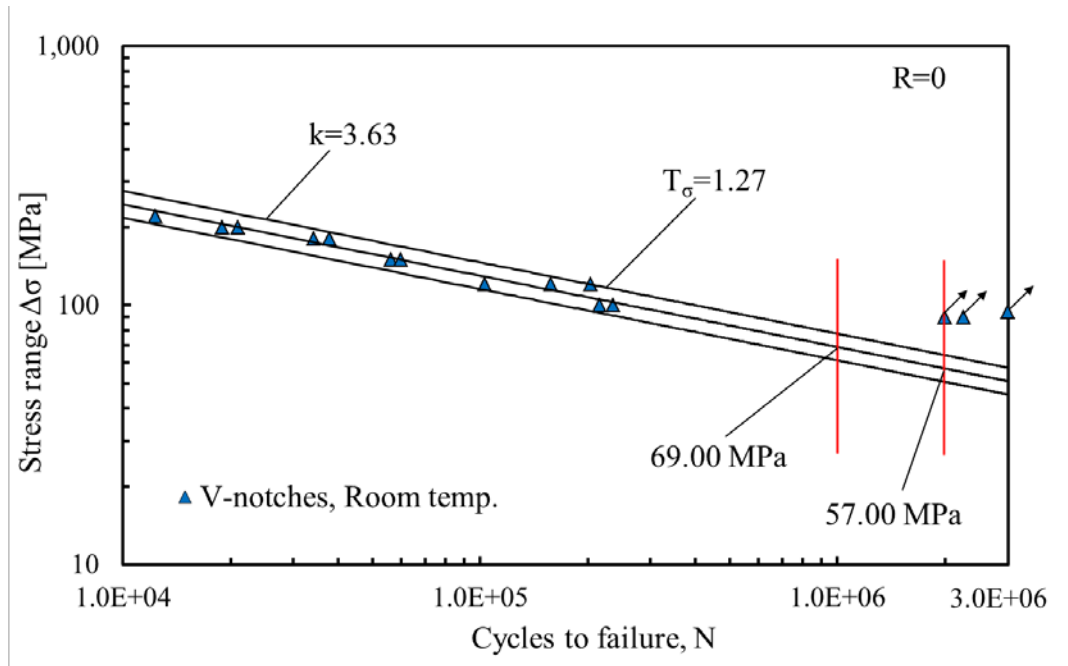
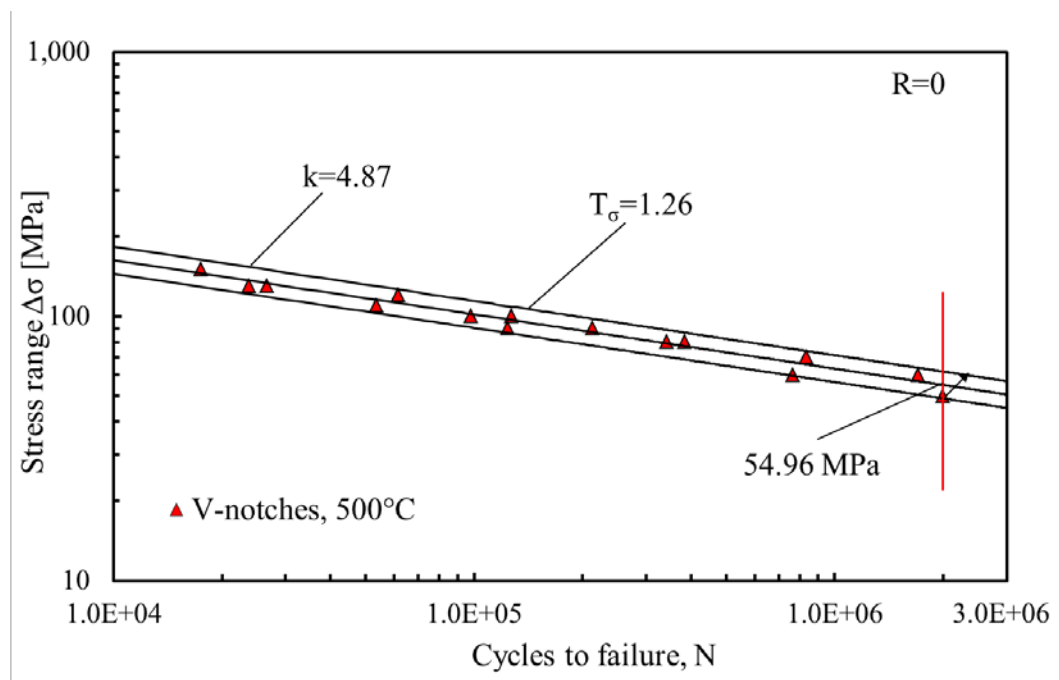


Fig. 5: Fatigue data of the semicircular notches tested at 500 °C





**Fig. 6:** Fatigue data of the V-notches tested at room temperature



**Fig. 7:** Fatigue data of the V-notches tested at 500 °C

Figure 7, instead, shows the fatigue data from V-notched specimens tested at 500 °C. The scatter index  $T_\sigma$  is very narrow being 1.26. The stress range at two million cycles reaches a value of 54.96 MPa and an inverse slope  $k=4.87$ . Comparing room temperature data of notched specimens with the high temperature ones, it is evident

that despite a variation of the inverse slope  $k$ , 3.63 at room temperature and 4.87 at high temperature, no variation is registered for the fatigue strength at two million cycles. In fact, the room temperature fatigue strength at two million cycles of the V-notches is 57.00 MPa, to be compared with the 500°C one that is 54.96 MPa. As stated above, instead, the semicircular notches present a reduction of 44% for the same temperature range. It can be observed that the presence of the V-notch with a small tip radii leads to a brittle behaviour also at high temperature and it seems to be the typical behaviour characterizing fatigue life at room and high temperature until a critical temperature is reached. Above this critical temperature, the fatigue properties decrease drastically. This trend was also found by [20] recently, for a ductile cast iron. On the basis of the experimental evidence, it is possible to conclude that the room temperature fatigue curve can be used as a design tool against fatigue up to 500 °C, since no relevant differences on fatigue behavior have been detected as stated previously.

Another important consideration is that even if the V-notches present lower fatigue strength at two million cycles at room and high temperature, they are less sensitive to the high temperature effects than the semicircular notches. The significance of this conclusion is remarkable, especially from an industrial viewpoint: in case of unexpected temperature variation, notched components with small tip radii made of titanium Grade 2 have a very good reliability and their fatigue properties are affected only marginally, at least up to 500 °C.

#### 3.3.2 Microstructural analyses

Figure 8 compares micrographs of the specimens tested at room temperature and 500 °C. The samples were obtained by cutting the specimens near the failure zone, and the micrographs were conducted on the transversal sectional surface of the specimens (normal to the load direction). The surfaces were prepared at first with a coarse mechanical polishing, and subsequently finalized with a chemical polishing. The samples were immersed in a solution made of 1 part of HF and 1 part of HNO<sub>3</sub> and agitated vigorously. When polishing actions became violent, the sample were treated for about 10s. This method was preferred respect to the complete-mechanical polishing because it could be difficult to obtain a suitable surface with a fine mechanical polishing without affecting the microstructure that tends to deform and smear.

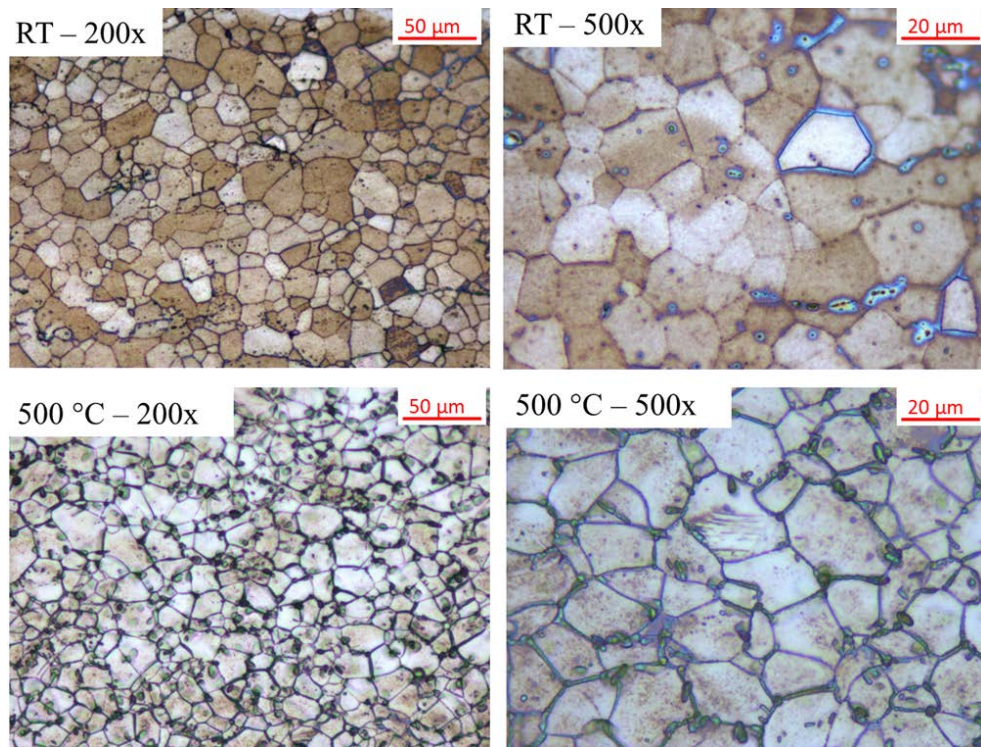


**Fig. 8:** Micrographs of specimens tested at room temperature (RT) and 500 °C at different magnification values

The microstructure is in general homogeneous, exhibiting a equiaxed grain structure. Comparing the micrographs of room-temperature tested specimen and 500 °C one, it is clear that no differences are registered in the microstructure. Even though the long-time exposure at high temperature, grain growth is not occurred. This assertion is supported by a grain size analysis that was conducted on the surfaces represented in Fig. 8, which as stated previously depicts the transversal sectional surface of specimens, obtained by cutting them near the failure zone. The mean grain size diameter is approximately 13.5 μm in both cases. However, the specimen tested at 500 °C presents an higher number of voids (especially at the grain boundaries) respect to the room temperature specimen. These voids may be due to the presence of initial creep phenomena during the test or to the large deformation that occurs before the specimen break. More analyses should be devoted to clarify this point and to investigate the fatigue-creep interaction in order to understand at which temperature creep is the dominant phenomena.

### 3.4 A synthesis in terms of linear elastic SED averaged over a control volume

The averaged Strain Energy Density (SED) criterion states that failure occurs when the mean value of the SED over a given control volume is equal to a critical value  $W_c$ . Under plane stress or plane strain condition the volume becomes an area as depicted in Fig. 9. Such a method has been extensively used in literature, and its power, especially when dealing with fatigue of welded joints and notched components, has been proofed by many studies. A review of the method has been recently presented [21,22]. In the aforementioned review the analytical frame and the main applications of the averaged SED approach are revisited in detail.

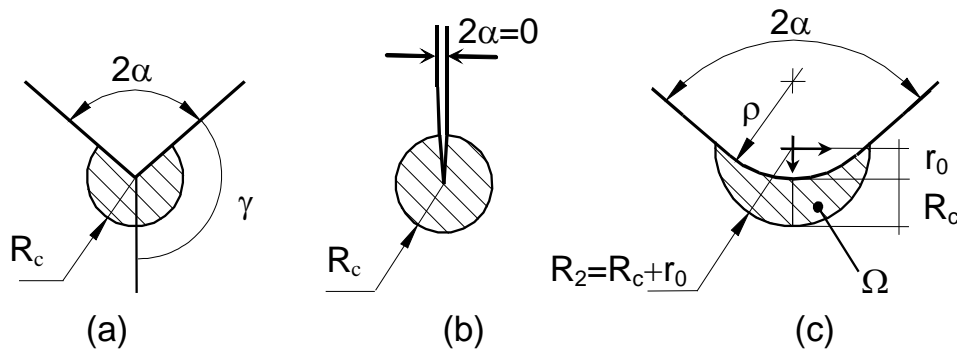


**Fig. 9:** Critical volume (area) for sharp V-notch (a), crack (b) and blunt V-notch (c) under mode I loading. Distance  $r_0 = \rho \times (\pi - 2\alpha) / (2\pi - 2\alpha)$

This review refers to more than 80 energy-based articles published over the last 50 years and has conducted the authors to formulate such a criterion for different materials and loading modes also under static loading. In addition, a comparison among some recent energy- and stress-based criteria for the fracture assessment of sharp V-notched components under Mode I loading (including the SED) has been presented in [23].

To underlined the potentialities of the method, it must be reported that, among the previous cited works, the SED has been used to handle very different cases and phenomena, such as the computation of notch stress intensity factors of flat plates with periodic sharp notches or three dimensional finite element mixed fracture mode under anti-plane loading of a crack [22].

In order to reanalyze the fatigue data in terms of SED, the main point is the determination of the critical radius  $R_c$  that defines the control volume over which the

SED is averaged. As widely described in the references given above, it depends on plain specimen fatigue limit and on the threshold behavior  $\Delta K_{th}$  in the case of high cycle fatigue loads. Under mode I loading condition, the critical radius can be estimated through the following equation [24,25]:

$$R_c = \frac{(1 + \nu)(5 - 8\nu)}{4\pi} \left( \frac{\Delta K_{th}}{\Delta \sigma_0} \right)^2 \quad (1)$$

where  $\nu$  is the Poisson's ratio,  $\Delta K_{th}$  is the threshold stress intensity factor range and  $\Delta \sigma_0$  the plain specimen fatigue limit (in terms of stress range).

### 3.4.1 Room temperature data by means of SED approach

At room temperature, the Poisson's ratio is equal to 0.3, while common titanium handbooks give a value of  $6 \text{ MPa}\cdot\text{m}^{0.5}$  and  $180 \text{ MPa}$  for  $\Delta K_{th}$  and  $\Delta \sigma_0$ , respectively [2,26,27]. Considering these values and Eq. (1), one obtains an  $R_c=0.3 \text{ mm}$ . The obtained critical radius is very similar to that obtained by [28] in which, thanks to the SED approach, different welded joint geometries made of steel have been summarized in a single scatterband.

Once determined the critical radius, in order to evaluate the strain energy density range two ways are available: through finite element analysis or by the following expression regarding blunt notches [29]:

$$\overline{\Delta W} = c_w F(2\alpha) \times H(2\alpha, \frac{R_c}{\rho}) \times \frac{K_{t,n}^2 \Delta \sigma_n^2}{E} \quad (2)$$

Where  $\Delta \sigma_n$  is the applied stress range,  $K_{t,n}$  is the theoretical stress concentration factor (both referred to the net sectional area),  $E$  is the Young's modulus.  $F(2\alpha)$  depends on the notch opening angle and is equal to 0.705 for  $2\alpha=90^\circ$  (V-notches) and 0.785 for  $2\alpha=0$  (semicircular notches). Finally  $H$  depends both on the notch angle and the critical radius-notch tip radius ratio. It is equal approximately to 0.5364 for semicircular notches and 0.3019 for V-notches. At last,  $c_w$  is the weighing parameter that takes into account the different loading ratio and it is equal to 1.0 for  $R=0$  and 0.5 for  $R=-1$ . Indeed, as a result of the reduction of the effective SED, the fatigue strength range for  $R=-1$  should theoretically increase according to a factor  $\sqrt{2}$  with respect to the  $R=0$  case [30]. The authors found a very good agreement in the obtained SED values between FEM analyses and analytical results (discrepancy

less than 2%, also using a very coarse mesh) that, in order to not be redundant, are omitted.

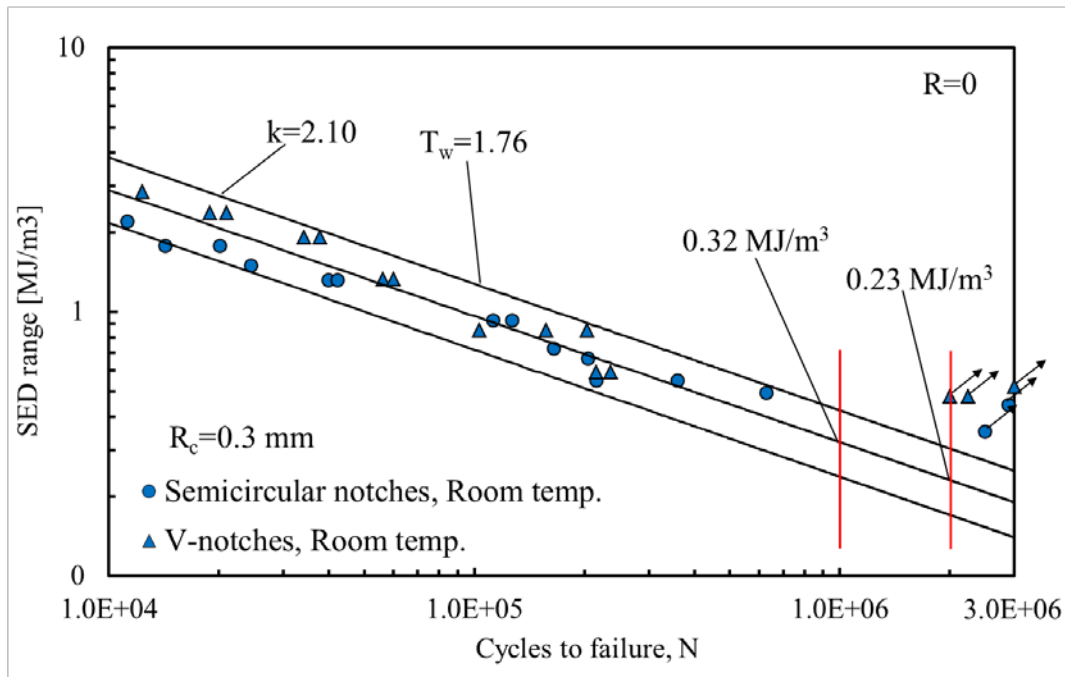


**Fig. 10:** Synthesis by mean of the SED averaged over a control volume of the room temperature fatigue data, regardless of the specimen geometries

In Figure 10 the synthesis of the room temperature fatigue data by means of the strain energy density averaged over a control volume of the room temperature fatigue data is presented. All the room temperature fatigue data, regardless of the specimen geometry (semicircular and V-notches) have been summarized in a single scatterband. The inverse slope  $k$  is equal to 2.10 and the scatter index related to the two curves with probabilities of survival  $P_S=10\%$  and  $90\%$ , has been found equal to 1.76, that returns a scatter index  $T_\sigma=1.33$  when reconverted to an equivalent local stress range. It should be noted that the plateau is moved to the left, approximately to one million cycles where the SED range assumes a value equal to  $0.32\text{MJ/m}^3$ . For the sake of completeness, SED range values referred to one million cycles and two million cycles are reported in the figure both.

### 3.4.2 High temperature data by means of SED approach

Considering now the high temperature fatigue data, at the best of the author knowledge the threshold stress intensity range  $\Delta K_{th}$  is not available at the considered

temperature (500 °C). For this reason, as done in the previous §Chapter 2 for a copper beryllium alloy [31], the critical radius has been estimated by equating the values of the critical SED range at  $2 \times 10^6$  cycles as determined from the V-notched and semicircular notches through FEM analyses. The radius of the control volume has been varied to match the SED values in both cases. The material has been assumed isotropic and linear elastic. The Young's modulus at 500 °C is equal 75000 MPa and the Poisson's ratio  $\nu=0.3$ . The idea of using, under mode I loading, the linear elastic SED also in case of small scale yielding conditions was motivated in some previous works [32,33]. Under plane strain conditions, the value of the energy concentration due to the notch is constant and independent of the constitutive law. When small scale yielding conditions are satisfied this immediately results in the constancy of the strain energy averaged over the control volume. These important considerations are in well agreement with results by other researchers investigating the fatigue behaviour of Inconel 718 at room temperature up to 500°C [34,35]. Chen et al., in fact, arrived to the final conclusion that Linear Notch Mechanics is applicable not only at room temperature but also at elevated temperature, as long as the small-scale yielding condition is satisfied.

After several analysis, a critical control radius equal to 0.6 mm has been found to be a good solution. This value has been used also in [31] to summarize fatigue data of copper beryllium alloy. The synthesis by mean of the strain energy density averaged over a control volume of the high temperature fatigue data is presented in Figure 11. Regardless of the specimen geometry (semicircular and V-notches) all fatigue results have been summarized in a single scatterband. The inverse slope  $k$  is equal to 2.45 and the scatter index related to the two curves with probabilities of survival  $P_S=10\%$  and 90%, has been found to be equal to 1.73, that returns a scatter index  $T_\sigma=1.32$  when reconverted to an equivalent local stress range, that is a very good result.

The advantages of the SED are clear: it is possible to summarize in a single scatter band all the fatigue data, regardless of the specimen geometry and as a function of the temperature.

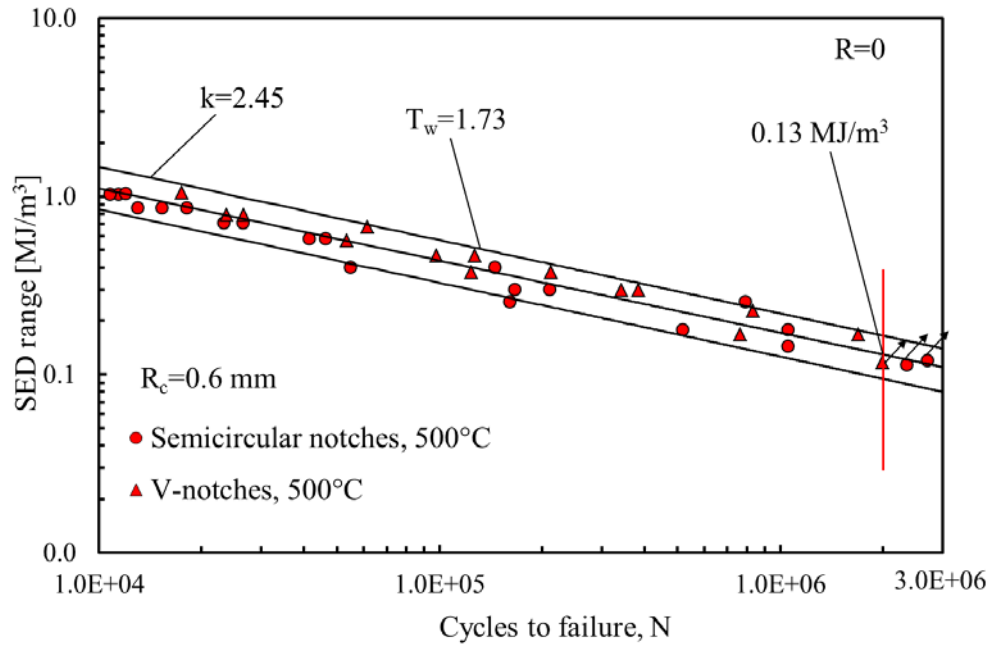


**Fig. 11:** Synthesis by mean of the SED averaged over a control volume of the fatigue data tested at 500 °C, regardless of the specimen geometries

From an industrial viewpoint, where different components of different geometries are continuously redesigned, this method directly results in a fast and easy way to design against fatigue, maintained a reasonable and narrow scatter. The fatigue curves in terms of SED presented in this work are related to room temperature and 500 °C only; an open point is to accomplish additional tests at different temperatures (below 500 °C) in order to determine the limit temperature below which the room temperature SED fatigue curve can be used for design against fatigue, regardless of the effective temperature. This point is clearly treated in [36] where the fatigue data from room temperature up to 500 °C of 40CrMoV13.9 steel has been summarized in a single scatter band, regardless of the specimen geometries, load ratio, and of effective temperature.

Further developments should be devoted to define analytically the proposed critical radius, and to investigate the influence of creep, that occurs for component long time exposure at temperature also lower than 500 °C.



### 3.5 Conclusions

Fatigue tests and metallographic analyses were carried out on specimens made of titanium Grade 2 for high temperature applications, in order to investigate the fatigue strength of this material at high temperature, more precisely at room temperature and 500°C. The work has been motivated by the fact that, at the best of author's knowledge, only a limited number of works dealing with high-temperature fatigue are available in the literature and no results seem to be available from notched components made of this material and tested at high temperatures.

Two specimen geometries were considered: plates weakened by lateral symmetric V-notches, and plates weakened by lateral symmetric semicircular notches. Furthermore, a statistical analysis of fatigue data was carried out for both geometries. The data obtained were first summarized in the fatigue curves and later re-analyzed in terms of the local energy density.

For the room temperature data, the critical radius of the volume over which the SED is averaged has been analytically determined, since all the needed parameters are largely available in literature and handbooks.

For the high temperature data, instead, the threshold stress intensity range  $\Delta K_{th}$  is not available at the considered temperature (500 °C). For this reason the critical radius has been estimated by equating the values of the critical SED range at  $2 \times 10^6$  cycles as determined from the V-notched and semicircular notches through FEM analyses. The radius of the control volume has been varied to match the SED values in both cases.

The following conclusions can be drawn:

- Titanium Grade 2 presents a good fatigue behavior at room and 500 °C.
- The microstructure is in general homogeneous, exhibiting equiaxed grain. Even though the long-time exposure at high temperature, grain degradation or growth is not occurred.
- The specimens tested at 500 °C present an higher number of voids (especially at the grain boundaries) respect to the room temperature specimen.
- The semicircular notches are subjected to a stress range at two million cycles equal to 142.00 MPa and to 80.60 MPa at room temperature and 500 °C, respectively. Considering instead the V-notches, they are subjected to a stress

range at two million cycles equal to 57.00 MPa and 54.96 MPa at room and 500 °C respectively. However, all the fatigue curves present a very narrow scatterband in terms of stress range.

- Even if the V-notches present a lower number of cycle for the same load with respect to the semicircular notches, they are less sensitive than semicircular notches to the high temperature effects thanks to the presence of small tip radius. In fact, considering in both cases two million cycles, the reduction of the stress range due to the high temperature is negligible, being less than 6%, while for the semicircular specimens is 44%. From an industrial viewpoint, in case of unexpected temperature variation, notched components with small tip radii made of titanium Grade 2 have a very good reliability and their fatigue properties are affected only marginally, at least up to 500 °C.
- For the V-notches, on the basis of the experimental evidence, the room temperature fatigue curve can be used as a design tool against fatigue up to 500 °C, since no relevant differences on fatigue behavior have been detected. In fact, the fatigue curves appear to be comparable.
- The fatigue data from tests carried out at room temperature have been summarized in terms of mean SED over a control volume with  $R_c=0.3$  mm, regardless of the specimen geometries and with a very narrow scatter index equal to 1.76 in terms of local energy, that becomes 1.33 when reconverted to an equivalent local stress range.
- The fatigue data from tests carried out at 500 °C have been summarized in terms of mean SED over a control volume with  $R_c=0.6$  mm, regardless of the specimen geometries and with a very narrow scatter index equal to 1.73 in terms of energy, that becomes 1.32 when reconverted to an equivalent local stress range. This control radius has been already used by the same authors to accomplish a synthesis in terms of SED of a copper beryllium alloy.
- The advantages of the SED are clear: it is possible to summarize in a single scatter band all the fatigue data, regardless of the specimen geometry and as a function of the temperature. From an industrial viewpoint, where different components from different geometries are continuously redesigned, the result is a fast and easy way to design against fatigue, maintaining a reasonable and narrow scatter in fatigue assessment.

## References

- [1] C. Leyens, M. Peters, eds., Titanium and Titanium Alloys, Wiley-VCH Verlag GmbH & Co. KGaA, Weinheim, FRG, 2003.
- [2] M.J. Donachie, Titanium: a technical guide, 2nd Edition, 2nd ed., ASM International, 2000.
- [3] R.R. Boyer, An overview on the use of titanium in the aerospace industry, Mater. Sci. Eng. A. 213 (1996) 103–114.
- [4] H. Ghonem, Microstructure and fatigue crack growth mechanisms in high temperature titanium alloys, Int. J. Fatigue. 32 (2010) 1448–1460.
- [5] H. Kitahara, K. Uchikado, J. Makino, N. Iida, M. Tsushida, N. Tsuji, et al., Fatigue Crack Propagation Behavior in Commercial Purity Ti Severely Deformed by Accumulative Roll Bonding Process, Mater. Trans. 49 (2008) 64–68.
- [6] D. Lanning, T. Nicholas, a Palazotto, The effect of notch geometry on critical distance high cycle fatigue predictions, Int. J. Fatigue. 27 (2005) 1623–1627.
- [7] A.R. Kallmeyer, A. Krgo, P. Kurath, Evaluation of Multiaxial Fatigue Life Prediction Methodologies for Ti-6Al-4V, J. Eng. Mater. Technol. 124 (2002) 229.
- [8] D.. Ramsamooj, T.. Shugar, Model prediction of fatigue crack propagation in metal alloys in laboratory air, Int. J. Fatigue. 23 (2001) 287–300.
- [9] S. Hosseini, M.B. Limooei, Investigation of Fatigue Behaviour and Notch Sensitivity of Ti-6Al-4V, Appl. Mech. Mater. 80-81 (2011) 7–12.
- [10] S. Baragetti, S. Cavalleri, F. Tordini, Fatigue behavior of notched Ti-6Al-4V in air and corrosive environment, Procedia Eng. 10 (2011) 2435–2440.
- [11] R. Dobeson, N. Petrazoller, M. Dargusch, S. McDonald, Effect of thermal exposure on the room temperature tensile properties of Grade 2 titanium, Mater. Sci. Eng. A. 528 (2011) 3925–3929.
- [12] D. Eylon, S. Fujishiro, P.J. Postans, F.H. Froes, High-Temperature Titanium Alloys—A Review, JOM. 36 (2013) 55–62.
- [13] S. Lesterlin, C. Sarrazin-Baudoux, J. Petit, Effects of temperature and environment interactions on fatigue crack propagation in a Ti alloy, Scr. Mater. 34 (1996) 651–657.
- [14] A.H. Rosenberger, H. Ghonem, Influence of creep-fatigue interaction on high

- temperature fatigue crack growth behavior of Ti-1100, *Fatigue Fract. Engng. Mater. Struct.* 17 (1994) 397–410.
- [15] J. Kumar, K. Prasad, V. Kumar, High-temperature low cycle fatigue damage assessment in near alpha IMI-834 titanium alloy, *Fatigue Fract. Engng. Mater. Struct.* 34 (2011) 131–138.
- [16] Mohandas, Srinivas, Kutumbarao, Effect of post-weld heat treatment on fracture toughness and fatigue crack growth behaviour of electron beam welds of a titanium (alpha+beta) alloy, *Fatigue Fract. Engng. Mater. Struct.* 23 (2000) 33–38.
- [17] A.H. Rosenberger, H. Ghonem, High temperature elastic-plastic small crack growth behavior in a Nickel-base superalloy, *Fatigue Fract. Engng. Mater. Struct.* 17 (1994) 509–521.
- [18] W.J. Plumbridge, Damage production during high temperature-low cycle fatigue of a Titanium alloy (IMI829), *Fatigue Fract. Engng. Mater. Struct.* 10 (1987) 385–398.
- [19] J. Kumar, A. V. Rao, V. Kumar, Simulation of elevated temperature fatigue damage evolution using the finite element method for near alpha titanium alloy, *Fatigue Fract. Engng. Mater. Struct.* (2014).
- [20] P. Matteis, G. Scavino, a. Castello, D. Firrao, High Temperature Fatigue Properties of a Si-Mo Ductile Cast Iron, *Procedia Mater. Sci.* 3 (2014) 2154–2159.
- [21] F. Berto, P. Lazzarin, A review of the volume-based strain energy density approach applied to V-notches and welded structures, *Theor. Appl. Fract. Mech.* 52 (2009) 183–194.
- [22] F. Berto, P. Lazzarin, Recent developments in brittle and quasi-brittle failure assessment of engineering materials by means of local approaches, *Mater. Sci. Eng. R Reports.* 75 (2014) 1–48.
- [23] P. Lazzarin, A. Campagnolo, F. Berto, A comparison among some recent energy- and stress-based criteria for the fracture assessment of sharp V-notched components under Mode I loading, *Theor. Appl. Fract. Mech.* 71 (2014) 21–30.
- [24] M.H. El Haddad, T.H. Topper, K.N. Smith, Prediction of non propagating cracks, *Eng. Fract. Mech.* 11 (1979) 573–584.

- [25] G. Pluvinaige, J. Capelle, On characteristic lengths used in notch fracture mechanics, *Int. J. Fract.* 187 (2014) 187–197.
- [26] W.F. Brown, H. Mindlin, C.Y. Ho, *Aerospace Structural Metals Handbook. Volume IV.*, Cindas/Purdue university, 1998.
- [27] G. Welsch, R. Boyer, E.W. Collings, *Materials Properties Handbook: Titanium Alloys*, ASM International, 1993.
- [28] P. Livieri, P. Lazzarin, Fatigue strength of steel and aluminium welded joints based on generalised stress intensity factors and local strain energy values, *Int. J. Fract.* 133 (2005) 247–276.
- [29] P. Lazzarin, F. Berto, Some Expressions for the Strain Energy in a Finite Volume Surrounding the Root of Blunt V-notches, *Int. J. Fract.* 135 (2005) 161–185.
- [30] P. Lazzarin, C.M. Sonsino, R. Zambardi, A notch stress intensity approach to assess the multiaxial fatigue strength of welded tube-to-flange joints subjected to combined loadings, *Fatigue Fract. Engng. Mater. Struct.* 27 (2004) 127–140.
- [31] F. Berto, P. Lazzarin, P. Gallo, High-temperature fatigue strength of a copper-cobalt-beryllium alloy, *J. Strain Anal. Eng. Des.* 49 (2014) 244–256.
- [32] G. Glinka, Energy density approach to calculation of inelastic strain-stress near notches and cracks, *Eng. Fract. Mech.* 22 (1985) 485–508.
- [33] P. Lazzarin, R. Zambardi, The Equivalent Strain Energy Density approach reformulated and applied to sharp V-shaped notches under localized and generalized plasticity, *Fatigue Fract. Engng. Mater. Struct.* 25 (2002) 917–928.
- [34] Q. Chen, N. Kawagoishi, H. Nisitani, Evaluation of notched fatigue strength at elevated temperature by linear notch mechanics, *Int. J. Fatigue.* 21 (1999) 925–931.
- [35] N. Kawagoishi, Q. Chen, H. Nisitani, Fatigue strength of Inconel 718 at elevated temperatures, *Fatigue Fract. Engng. Mater. Struct.* 23 (2000) 209–216.
- [36] F. Berto, P. Gallo, P. Lazzarin, High temperature fatigue tests of un-notched and notched specimens made of 40CrMoV13.9 steel, *Mater. Des.* 63 (2014) 609–619.



## 4. High temperature fatigue of 40CrMoV13.9 steel and influence of surface roughness

*F. Berto, P. Gallo, P. Lazzarin, High temperature fatigue tests of un-notched and notched specimens made of 40CrMoV13.9 steel, Mater. Design 63 (2014) 609-619.*

*P. Gallo, F. Berto, Influence of surface roughness on high temperature fatigue strength and cracks initiation in 40CrMoV13.9 notched components, Theor. Appl. Fract. Mech. 80 (2015) 226-234.*

### Highlights

The present chapter addresses experimentally the high temperature fatigue of 40CrMoV13.9 steel and the effect of surface roughness on fatigue strength and cracks initiation at elevated temperature.

The 40CrMoV13.9 steel considered here is widely used in different engineering high temperature applications among which hot-rolling of metals, where, in order to assure a constant temperature, the rolls are provided with cooling channels. These are the most stressed zone of the rolls where cracks initiate systematically.

In order to completely characterize the high temperature behaviour of this steel, firstly uniaxial-tension load controlled fatigue tests have been conducted at different temperatures up to 650°C. Two geometries are considered: plain specimens and plates weakened by symmetric V-notches, with opening angle and tip radius being equal to 90° and 1 mm, respectively. Subsequently, with the aim to investigate the influence of the cooling channels roughness on the high temperature behaviour and the cracks initiation, uniaxial-tension load controlled fatigue tests have been conducted on plate with central hole at the service temperature of 650°C, varying the surface roughness.

After a brief review of the recent literature, the experimental procedure is described in detail and the new data from un-notched and notched specimens are summarized in terms of stress range, at the considered temperatures.

Finally, fatigue data from un-notched and notched specimens are re-analysed by means of the mean value of the Strain Energy Density (SED) extended at high temperature.





## 4.1 Introduction

Hot-rolling process is increasingly required for higher mechanical performances, fatigue strength and quality of laminated products. Different steels have been employed in a large variety of applications to combine static and fatigue properties with an excellent wear resistance at high temperature and in corrosive environments. The 40CrMoV13.9 steel is widely used in different engineering high temperature applications among which hot-rolling of metals.

Rolls for hot-rolling, despite different decisions made by different engineers in the design phase, have some basic characteristics, such as the presence of cooling channels with the aim to assure a uniform and controlled temperature during the in-service operations. On the basis of numerous direct feedbacks, the cooling channels are the most stressed zone of the rolls and cracks initiate systematically from this area. For these reasons, it becomes very interesting to deeply investigate this kind of steel, with the aim to completely characterize its fatigue behaviour at high temperature, considering for example notch effects and/or the influence of surface roughness on the crack initiation. These topics, especially if considering notched components at high temperature and high number of cycles are often ignored by the modern literature. However, it is possible to find some interesting works briefly reported hereafter.

Dealing with un-notched specimens, the fatigue behavior of different materials at high temperature has been investigated by some researchers such as [1–3]. In [1] an experimental investigation was conducted on 22Cr-20Ni-18Co-Fe alloy at elevated temperature using plain specimens. Fatigue tests were carried out at a constant temperature (871°C) while the strain ranged from 0.265 to 1.5 %. The fatigue lives varied from  $10^3$  to  $10^6$  cycles to failure. Cyclic deformation properties of the tested material were obtained from the tests and three fatigue models were applied discussing the advantages and drawbacks of each model. The fatigue properties and crack growth mechanism of a 2.25Cr–1Mo steel were investigated in [2]. The study was aimed to investigate the fatigue life up to  $10^7$  cycles of structural components used in hot and high-pressure environments. The tests were conducted on un-notched specimens in a temperature range varying between 20 and 500°C. The high-cycle fatigue life was found to be strongly influenced by the density and size of interior inclusions.

Dealing with 1.25Cr0.5Mo steel, high-temperature stress controlled tests were carried out at different loading conditions to investigate the fatigue–creep interaction behavior at high temperatures [3]. Four fatigue–creep failure maps were obtained showing that for stress amplitudes lower than the mean stress a close interaction between fatigue and creep occurred. This interaction provoked a visible reduction of the fatigue strength. The complex relationship between the fatigue life and the main influencing factors was explained by means of the strain rate at half-life, which was considered as the governing factor associated with the fatigue strength.

The increasing working temperature range and the growing necessity for greater efficiency and reliability of automotive exhaust system has been requiring the accurate investigation of the fatigue properties of heat resisting stainless steels at high temperature. Fully reversed axial fatigue tests were performed in [4] on smooth specimens of 18Cr–2Mo ferritic stainless steel (type 444) at room temperature, 673 K and 773 K in laboratory air, with the aim to investigate the effect of temperature on high cycle fatigue behavior. A notable influence of temperature on the fatigue strength was observed during the tests. The crack growth was found to be considerably faster at elevated temperatures than at room temperature and some fractographic analyses revealed brittle features in fracture surfaces near the crack initiation site, which were more pronounced and extensive at 773 K. An evident embrittlement occurred in the investigated temperature range and such embrittlement was found to be the main responsible for the observed decrease in the fatigue properties.

While results from un-notched materials are not so rare in the past and recent literature as just discussed, only few systematic investigations have been performed on notched specimens under fatigue loading at high temperature at medium-high cycle fatigue [5–7].

In [5,6], the notched fatigue strength of the nickel-base superalloy Inconel 718 was investigated under rotating bending loading at room temperature and 500°C in air. The linear notch mechanics was employed to assess the fatigue strength at elevated temperature being for that material the small-scale yielding conditions satisfied also at elevated temperature.

The effect of notch types and stress concentration factors on low cycle fatigue life and cracking of the DZ125 directionally solidified superalloy was experimentally

investigated by Shi et al. [8]. Single-edge notched specimens with V and U type geometries were tested at 850 °C with a stress ratio  $R = 0.01$ . The results revealed that the fatigue strength decreased with the elastic stress concentration factor,  $K_t$ , increasing from 1.76 to 4.35. The main conclusion of the paper was that  $K_t$  can be considered as a key parameter controlling the notch fatigue at least when the absolute dimensions of the tested notched specimens are similar.

Other authors has recently extended linear elastic approaches to assess high temperature fatigue such as Louks and Susmel [9] that investigated the accuracy of the linear-elastic Theory of Critical Distances (TCD) in estimating high-cycle fatigue strength of notched metallic materials experiencing elevated temperatures during in-service operations, with very good results.

The number of paper remains very poor if considering works on the influence of the surface roughness on the fatigue behavior at high temperature. However it is a very interesting topic from industrial viewpoint since the investigation of the cooling channels roughness on the high temperature behavior and the cracks initiation can lead to several advantages: first of all, it defines quantitatively the influence of the surface roughness on the fatigue performances, and therefore justifies the costs to obtain a high surface finish quality. This makes possible to evaluate in terms of cost-benefit analysis the choice of imposing a low surface roughness or, otherwise, high surface roughness.

An interesting work is presented by [10] on the sensitivity of surface crack initiation to surface roughness in LCF at 550 °C of AISI 404L and Cr-Mo-V steel, in a pure argon atmosphere, also under creep-fatigue interaction condition. The creep-fatigue interaction was obtained by the introduction of tensile hold time. Two different states of surface finish were obtained by mechanical polishing with emery papers of grade nos. 80 and 1200 respectively. For Cr-Mo-V steel specimens, the maximum value for the depth of the surface polished with emery paper nos. 80 and 1200 are about 8.0 and 0.4  $\mu\text{m}$  respectively. The result of the tests shown that for Cr-Mo-V steel the fatigue life of the specimen polished with emery paper no. 80 is significantly reduced (about 50%) compared with that of the specimen polished with emery paper no. 1200. The same trend was registered independent of the creep-fatigue interaction condition, which is a very important consideration. Since the surface roughness affects only the surfacial phenomena like crack initiation, they concluded that the

number of cycles for crack initiation was a large fraction of the fatigue life, both in the case of pure fatigue or fatigue-creep interaction. This is a very important conclusion because supports the significance to investigate the influence of the surface roughness on the crack initiation since this phase is the one that involves a large fraction of fatigue life. Moreover they observed that no grain boundary cavitation was detected during the tests and the fracture mode was observed to be transgranular. For such material, where transgranular crack initiation is faster in the specimen with a rough surface than in that with a smooth surface, the surface roughness has a strong influence on the creep-fatigue and pure fatigue life. The results were in agreement with a previous work by the same author [11] considering only Cr-Mo-V steel. In that work they tested cylindrical specimens made of Cr-Mo-V steel at 550 °C. Two different modes of surface roughness were obtained by mechanically polishing specimens with emery paper nos. 80 and 1200. They showed that a large fraction of the fatigue life is consumed in the crack initiation and that the effect of surface roughness on low-cycle fatigue life could be due to the reduction of the number of cycles for crack initiation.

In the above background, the present chapter deals with high temperature fatigue tests of 40CrMoV13.9. The tested material is characterized by four different heat treatments able to assure a high strength at room and elevated temperatures. The most important application is cold or hot rolling of metals. A complete set of data from notch specimens under torsion and combined tension and torsion loadings at room temperature has been recently provided by Berto and collaborators [12].

At the best of author's knowledge, a complete set of data from un-notched and notched specimens at high temperature, as a complete characterization on the influence of the surface roughness, is not available in the literature for 40CrMoV13.9. With the aim to fill this lack, the present paper experimentally investigate the high temperature fatigue of notched components of the considered alloy at different temperatures up to 650°C. Subsequently, with the aim to investigate the influence of the rolls cooling channels roughness on the high temperature behavior and the cracks initiation, fatigue tests have been conducted on plate with central hole at the service temperature of 650°C.

The final objective of this study is to present a set of new results from high-temperature fatigue tests on 40CrMoV13.9 un-notched and notched specimens in the

medium- and high-cycle regime ( $10^5$ – $10^6$  cycles). All the tests have been performed under uniaxial tension and load controlled conditions.

A final synthesis of the present results together with previous data from multiaxial tests (at room temperature) on the same material [12] is carried out by means of the Strain Energy Density (SED) approach, as recently made for Cu-Be alloys [13] and Titanium Grade 2 [14], at elevated temperature.

## 4.2 Material properties and specimens geometry

### 4.2.1 Material

The material investigated in the present study is 40CrMoV13.9 steel, usually employed for hot-rolling of metals where the material is subjected to a combination of mechanical and thermal loading conditions. Preliminary static tensile tests on a standard specimen were carried out to evaluate the elastic and strength properties at 650°C: Young's modulus  $E$  is equal to 135 GPa,  $\sigma_Y$  is equal to 520 MPa and  $\sigma_R$  to 610 MPa. The data-sheet reports the following mechanical properties at room temperature (25°C): elastic modulus  $E$  is equal to 206 GPa, tensile strength of about 1300 MPa and a yield strength of 1100 MPa with a percent elongation of 15%. The properties (at room temperature and 650°C) are also summarized in Table 1.

**Table 1:** Mechanical properties of 40CrMoV13.9

Temperature	$E$ (GPa)	$\sigma_R$ (GPa)	$\sigma_Y$ (MPa)	Elongation to fracture (%)	HRC
Room Temp.	206	1355	1127	15.2	52
650°C	135	610	520	23.5	35

The chemical composition of the material and the heat treatment schedule are given in Table 2 and Table 3, respectively. The material was first quenched at 920°C and subsequently tempered twice at 580°C and 590°C. A final stress relieving treatment at 570°C was carried out. The final microstructure was characterized by a high strength bainitic-martensitic structure. The microstructure of the specimens is shown in Fig. 1 at different magnification values. It is evident that the microstructure is homogenous along all the directions, also through the specimen thickness, due to the austenitizing and annealing processes.

**Table 2:** Chemical composition wt.%, balance Fe

C	Mn	Si	S	P	Cr	Ni	Mo	V	Al	W
0.38	0.5	0.27	0.006	0.003	3.05	0.24	1.04	0.24	0.013	0.005

**Table 3:** Thermal treatment of the considered material

Heat treatment	Heating ratio (°C/h)	Temperature (°C)	Holding (hours)	Cooling
1 Quenching	100	920 ± 10	3	water
2 Tempering 1	100	580 ± 10	5	air
3 Tempering 2	100	590 ± 10	5	air
4 Stress relieving	100	570 ± 10	3	air

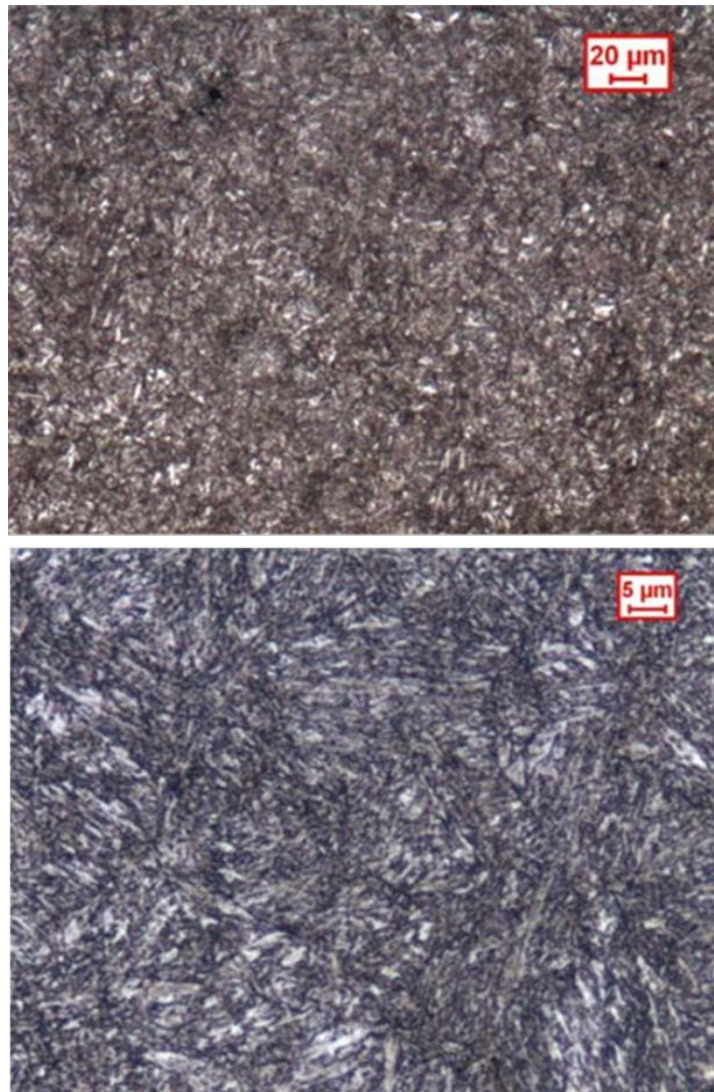


**Fig. 1:** Microstructure of the specimens at different magnification values

#### 4.2.2 Specimen geometry

Considering the high temperature fatigue tests and the investigation of the cracks growth, three specimen geometries were considered:

- Hourglass shaped (smooth) specimens with a theoretical stress concentration factor close to 1.0 (see Figure 2);
- Plates weakened by lateral symmetric V-notches, with a net cross section of 20 mm × 5 mm and a total length of 300 mm (Figure 3). The notches were characterized by a depth,  $a$ , equal to 5 mm, an opening angle,  $2\alpha$ , equal to  $90^\circ$  and a notch tip radius  $\rho=1$  mm. This geometry results in a theoretical stress concentration factor  $K_{t,n}=3.84$  (on the net transverse sectional area).
- Plates with a central hole (see Figure 4), with a cross section of 30 mm x 5 mm and a total length of 300 mm; the hole radius is 10 mm, which results in a theoretical stress concentration factor  $K_{t,n} = 2.3$  (on the net transverse area).

The specimens were designed to avoid an increase of temperature near the grippers and the length of 300 mm, which is higher than the length usually adopted at room temperature, was chosen for this reason. The diameter of the hole, instead, matches the real dimension of the rolls cooling channels.

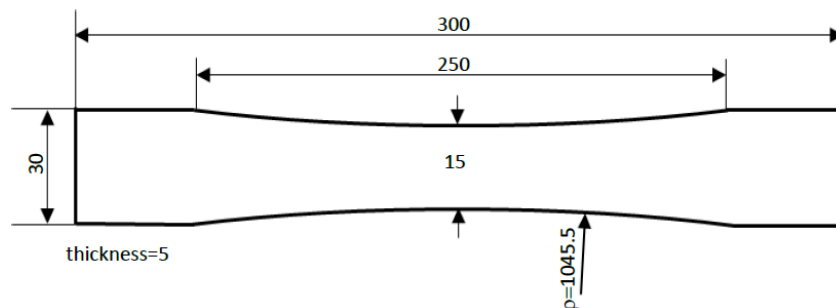


**Fig. 2:** Hour-glass shaped specimen geometry, dimensions in mm

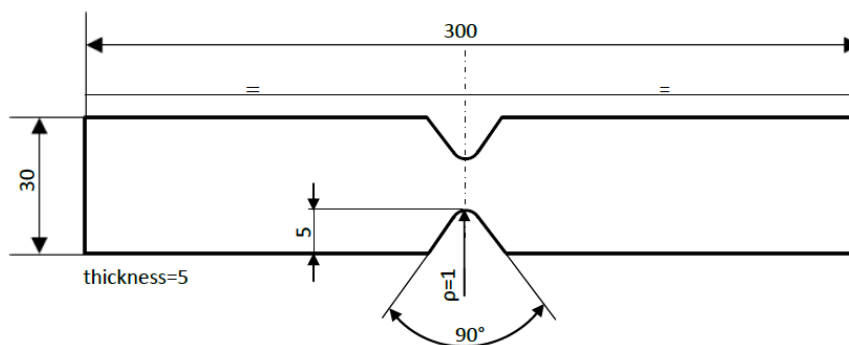


**Fig. 3:** Notched specimen geometry, dimensions in mm

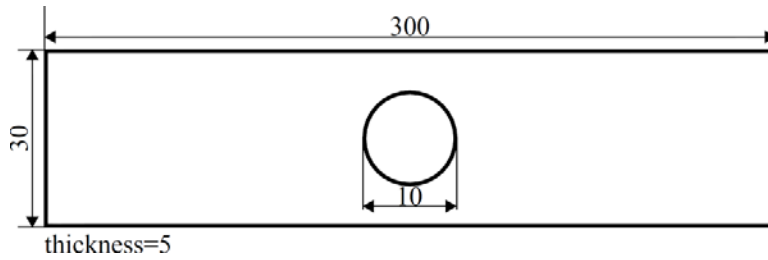


**Fig. 4:** Plates with central hole, dimensions in mm

### 4.3 Fatigue testing equipment and testing procedures

The fatigue tests are conducted on a servo-hydraulic MTS 810 test system with a load cell capacity of 250 kN. The system is provided with a MTS Model 653 High Temperature Furnace. It is ideal for a wide variety of high-temperature tests, including tension, compression, bending and fatigue testing of different materials, metallic and not. It has a center-split design that enables easy access to both grippers and specimens. The furnace includes the MTS digital PID Temperature Control System and is configured for two heating zones which can be independently temperature-controlled through high precision thermocouples.

In order to completely characterize the high temperature behavior of the considered alloy, firstly load-controlled fatigue tests were carried out at different temperatures. More precisely, the hour-glass shaped specimens were tested at room temperature, 360°C and 650°C; the V-notched specimens were tested at room temperature, 360°C, 500°C and 650°C. Overall, eight fatigue curves were obtained by testing more than 60 specimens. The specimen was heated to reach the desired temperature and after a short waiting period (10 minutes) necessary to assure a uniform temperature, the test was started. The temperature was maintained constant until specimen failures thank to the PID temperature control system. The uniaxial tensile fatigue tests were carried out over a range of cyclic stresses at the constant frequency of 5 Hz; the nominal load ratio  $R$  was kept constant and equal to 0.01.

Regarding, instead, the investigation on the influence of the surface roughness on the crack initiation, the plates with central hole were tested only at the service temperature of 650°C. The specimen was heated to reach the desired temperature, and after a short waiting period necessary to assure a uniform temperature, the test was started. Because of the available equipment, it was not possible to monitor continuously, in real time, the specimen hole. For this reason, an alternative



procedure has been adopted for the cracks detection: once reached a specific number of cycles, the test was temporarily stopped and the specimen checked through an optical microscope with the aim to detect any sign of cracks initiation. This operation was repeated until the crack was detected. The intervals, at which the tests were paused, were smaller as the number of cycles increasing (e.g. defining intervals 2500 N length, where necessary). After some calibration trials, a good reliable procedure was defined, especially for high number of cycles (i.e. for low loads) that are the most interesting for the final applications. The values of the stiffness, registered in real-time by the machine, also helped to define the procedure and the crack detection: the experimental evidences shown a significant drop of the stiffness as one or more cracks initiated. For this reason, that variable was very useful as a kind of warning that something was happened. Once detected stiffness variation, in fact, systematically after a few number of cycles (about 10000 to 30000 cycles) a crack appeared visible at the optical microscope. So the visual detection helped to define a good number of cycles range at which the crack initiated, while the stiffness variation defined a more accurate number of cycles within that range, a posteriori (analyzing the stored data), usually smaller than that of the optical detection.

The uniaxial tensile fatigue tests were carried out over a range of cyclic stresses at the constant frequency of 5 Hz while the nominal load ratio  $R$  was kept constant and equal to 0.01. The following values of the surface roughness, as the arithmetic average of the roughness profile, were considered for the plates with central hole:  $2\mu\text{m}$ ,  $1\mu\text{m}$ ,  $0.4\mu\text{m}$ ,  $0.15\mu\text{m}$ .

## 4.4. Results and discussion

### 4.4.1 Fatigue curves

The fatigue data were statistically re-analyzed by using a log-normal distribution and are plotted in terms of nominal stress ranges (referred to the net area) in Figures 5 and 6. More specifically, Figure 5 shows the fatigue data of the hourglass specimens, the Wöhler curve (mean curve,  $P_s = 50\%$ ), the Haibach scatter band referred to 10% and 90% probabilities of survival (for a confidence level equal to 95%) and the inverse slope  $k$  of the curves. Data from specimens tested at room temperature and at  $T=360^\circ\text{C}$  are found to belong to the same scatterband, with a value of the scatter index quite low,  $T_\sigma=1.29$ . The scatter of the specimens tested at  $T=650^\circ$ , instead, is

higher being  $T_\sigma=2.00$ , which show also a strong decrease of the fatigue strength combined with a strong variation of the slope. A vertical line is drawn in correspondence of one million cycles where the mean values of the stress range are given to make the comparison easier. At  $10^6$  cycles the stress range is equal to 675.14 MPa when  $T \leq 360^\circ\text{C}$ , while it is equal to 95.23 MPa at  $650^\circ\text{C}$ .

Fatigue data of the specimens weakened by lateral V-notches are shown in Figure 6 at different temperatures. The run-out specimens (marked by tilted arrow) were excluded from the statistical analysis. It is evident that up to  $500^\circ\text{C}$  there are no differences with respect to the room temperature, whereas a substantial decrease of fatigue strength can be observed at  $650^\circ\text{C}$ . The scatter-band related to the specimens tested at  $T=650^\circ\text{C}$  is compared with that summarizing data obtained for  $T \leq 500^\circ\text{C}$ . At one million cycles, the value of the stress referred to a probability of survival of 50% decreases from 213.12 to 74.32 MPa. The variation of the slope is also strong, it decreases from  $k=5.14$  to  $k=2.91$ . Conversely, the values of the scatter index are comparable.

For the sake of completeness, the results are also summarized in details in Table 4.

The drastic decrease of the fatigue properties observed at  $650^\circ\text{C}$  is linked to the specific heat treatments made on the material. The maximum temperature in the tempering treatment was equal to  $590^\circ\text{C}$  and the last stress relieving treatment was carried out at  $570^\circ\text{C}$ . Experimental data clearly document that under long time exposure at temperatures higher than  $570\text{-}590^\circ\text{C}$  all beneficial effects due to the heat treatments are lost.

By comparing the reduction of the fatigue strength exhibited at  $10^6$  cycles by the notched specimens tested at room temperature with respect to un-notched ones, one determines a fatigue strength reduction factor  $K_f$  equal to 3.17, which is a little lower than the theoretical stress concentration factor  $K_{t,n}=3.84$  obtained by means of a FE analysis (Ansys code) and in good agreement with the value provided by Peterson's handbook. This means that a notch root radius  $\rho=1$  mm involves the notch sensitivity index is less than 1.0. It is worth noticing that the fatigue strength reduction factor  $K_f$  at  $650^\circ\text{C}$  is equal to 1.48, which is remarkably lower than the value determined at room temperature. It is evident that the high temperature has strongly reduced the notch sensitivity of the steel.

**Table 4:** Results from fatigue tests at different temperatures. Stresses referred to the net area. HG stands for hour-glass shaped specimens while V stands for V-notched ones

Specimen - T (°C)	k	$T_\sigma$	$\sigma_{\max}(10^6 \text{ cycles})$		
			10% (MPa)	50% (MPa)	90% (MPa)
HG - room to 360°C	7.28	1.29	766	675	595
HG - 650°C	2.48	2.00	124	95	67
V - room to 500°C	5.14	1.48	259	213	174
V - 650°C	2.91	1.63	94	74	58

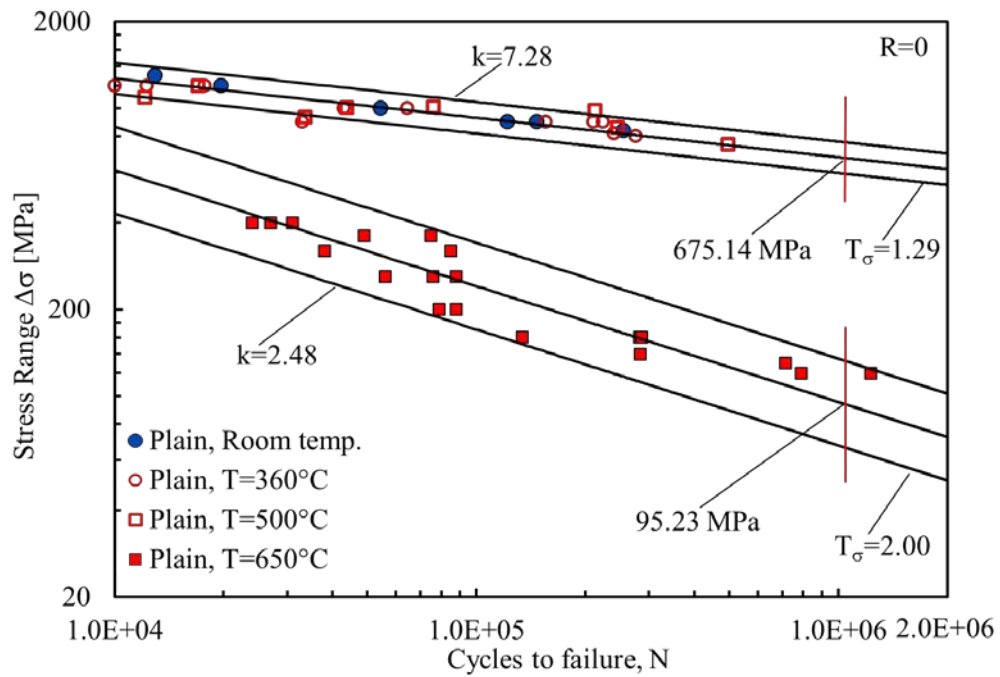


**Fig. 5:** Data from hourglass shaped specimens at different temperatures

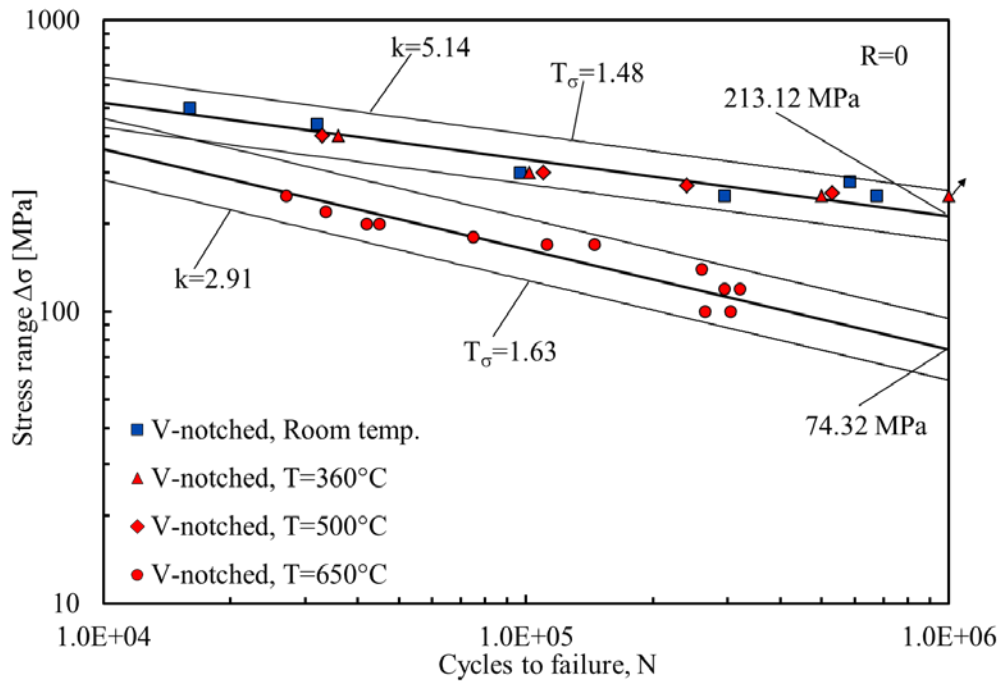


**Fig. 6:** Data from V-notched specimens at different temperatures

#### 4.4.2 Notch sensitivity

By comparing the reduction of the fatigue strength exhibited at  $10^6$  cycles by the notched specimens tested at room temperature with respect to un-notched ones, one determines a fatigue strength reduction factor  $K_f$  equal to  $675/213=3.17$  referred to  $10^6$  cycles (see Figures 5 and 6), which is a little lower than the theoretical stress concentration factor  $K_{t,n}=3.84$  obtained by means of a finite element analysis (Ansys code) and in good agreement with the value provided by Peterson's handbook. This means that a notch root radius  $\rho=1$  mm involves the notch sensitivity index is less than 1.0. It is worth noticing that the fatigue strength reduction factor  $K_f$  at  $650^\circ\text{C}$  is equal to  $95/74=1.28$  (see Figures 5 and 6), which is remarkably lower than the value determined at room temperature. It is evident that the high temperature has strongly reduced the notch sensitivity of the steel. On the basis of Figures 5 and 6 the fatigue strength reduction factor can be also evaluated at a specific number of cycles.

#### 4.4.3 Fracture surfaces by Scanning Electron Microscopy

The final geometrical configuration of some broken specimens was analyzed together to their fracture surfaces. Figure 7 compares plain specimens tested at room and elevated temperature ( $650^\circ\text{C}$ ), with comparable fatigue lives. It is evident that

the specimen tested at high temperature shows, as expected, a more ductile fracture if compared with the specimen tested at room temperature. It is also evident the visible necking on the net sectional area before the final failure. The fracture surfaces were also found to be different when analyzed by means of the Scanning Electron Microscope (SEM) at the same magnification value (see Figure 8). At high temperature some signs of transgranular fracture can be detected, as well as the formation of numerous micro-voids (Figure 8a). These micro-voids are big if compared to that of room temperature fracture surfaces (Figure 8b). At last, the fracture surface of plain specimens tested at high temperature is relatively clean, without any oxidation of the surface occurred during the tests. This remark is very important because the oxidation is a key phenomenon at elevated temperature; it can strongly influence both the crack initiation and its propagation, drastically reducing the fatigue strength of the material exposed to this event. The oxide film, in fact, is continually disrupted under repeated cyclic of strain/stress and the enhanced locally oxidized region acts as a notch to further concentrate local strains and stresses. However, if certain conditions are satisfied, e.g. high load frequency and short time exposure at high temperature, there would be insufficient time for chemical effects to act [15–18].

Creep of materials is classically associated with time-dependent plasticity under a constant stress at elevated temperatures, which for steels are typically greater than  $0.5 T_m$  (melting temperature) [15–17]. In the service conditions, the steel analyzed in the present paper is usually employed for hot rolling applications where the temperature ranges between 400 and 650°C, which is approximately equal to  $0.25-0.4 T_m$ . At this temperature, large deformations of the rolls as well as plasticity phenomena have to be avoided or minimized to guarantee a safe behavior of the roll (within the linear-elastic or small scale yielding conditions) and a satisfactory quality of the final laminated under the required lamination pressure. Under these conditions creep and fatigue interaction, as well as oxidation and ratchetting play a marginal role for the considered material. In particular, the time-dependent ratchetting is usually associated with creep and low cycle fatigue, as recently documented by Tong et al. [18] by utilizing different constitutive models.

Dealing with the fracture surfaces of V-notches, no significant plastic deformation was noted at failure in the vicinity of the notch tip at room temperature and at

elevated temperature. Figure 9 shows two specimens failed approximately at the same number of cycles. The fracture surfaces of the V-notched specimens were found very similar at different temperatures, almost flat in the crack initiation zone. This is most due to the presence of the V-notch, that leads to a brittle behavior of the material also at high temperatures.

This observation was also supported by the SEM micrographs, as shown in Figures 10 and 11. At room temperature and at  $T=650^{\circ}\text{C}$ , the fracture surfaces were found to be analogous near the notch tip where the crack initiation took place. No evident sign of micro-voids formation can be seen, nor evident signs of oxidation. At  $650^{\circ}\text{C}$ , two clear distinguishable zones of the fracture surfaces can be identified (see Figure 11): the bottom zone corresponds to the crack initiation and early propagation zone, the upper one corresponds to the final static failure. In this second zone, far away from the notch tip, small micro-voids similar (but smaller in diameter) to those detected on plain specimens (tested at high temperature) were observed.



**Fig. 7:** Fracture surface of plain specimen tested at  $650^{\circ}\text{C}$  (a) ( $\Delta\sigma=140$  MPa,  $N=284049$ ), and room temperature (b) ( $\Delta\sigma=900$ ,  $N=155000$ )

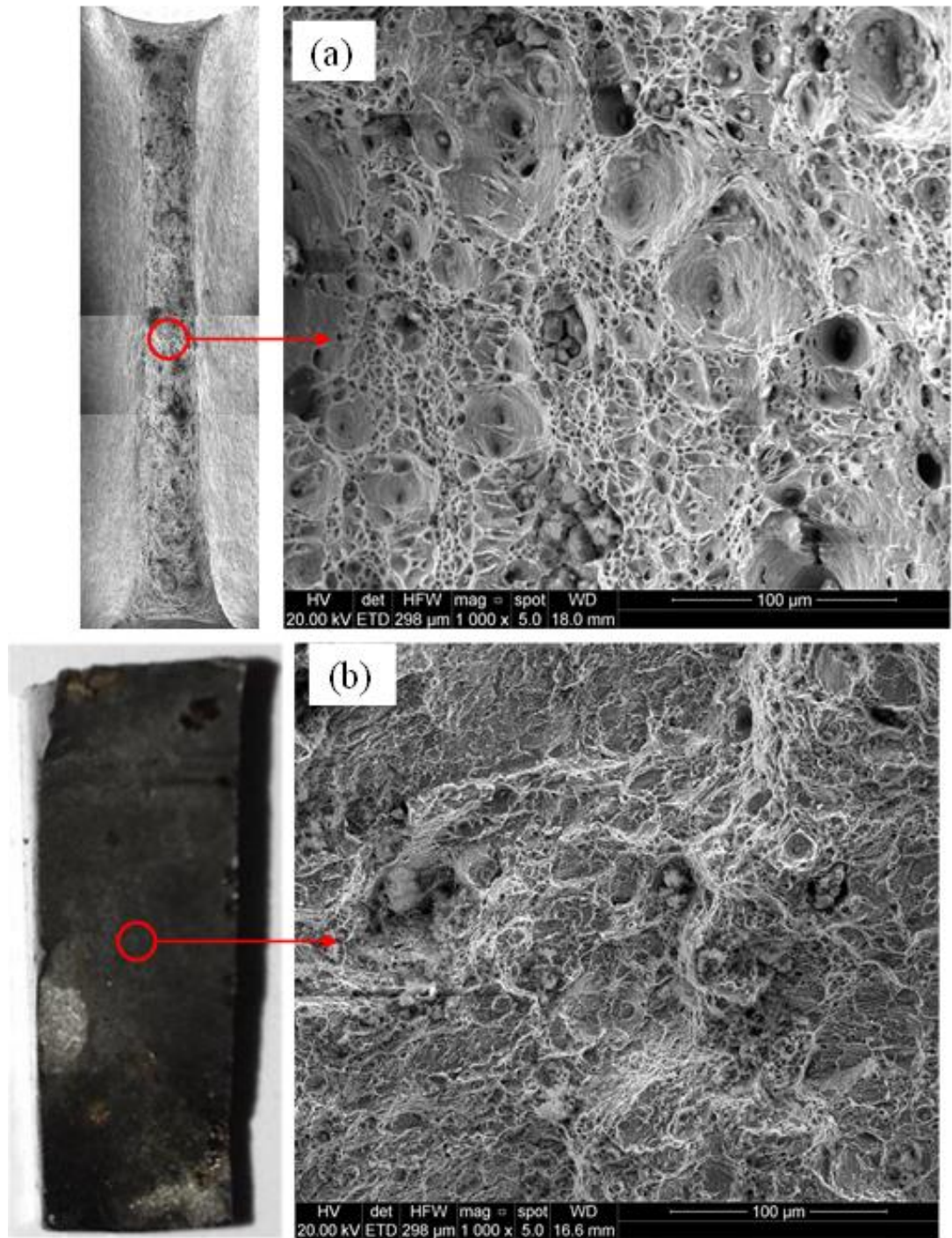


**Fig. 8:** Comparison between the fracture surface of plain specimen tested at 650°C (a) ( $\Delta\sigma=140$  MPa,  $N=284049$ ) and room temperature (b) ( $\Delta\sigma=900$ ,  $N=155000$ ), considering the same magnification value



**Fig. 9:** Fracture surfaces of the V-notched specimens tested at room temperature (a) ( $\Delta\sigma=250$  MPa,  $N=295000$ ) and high temperature (b) ( $\Delta\sigma=100$  MPa,  $N=304000$ )

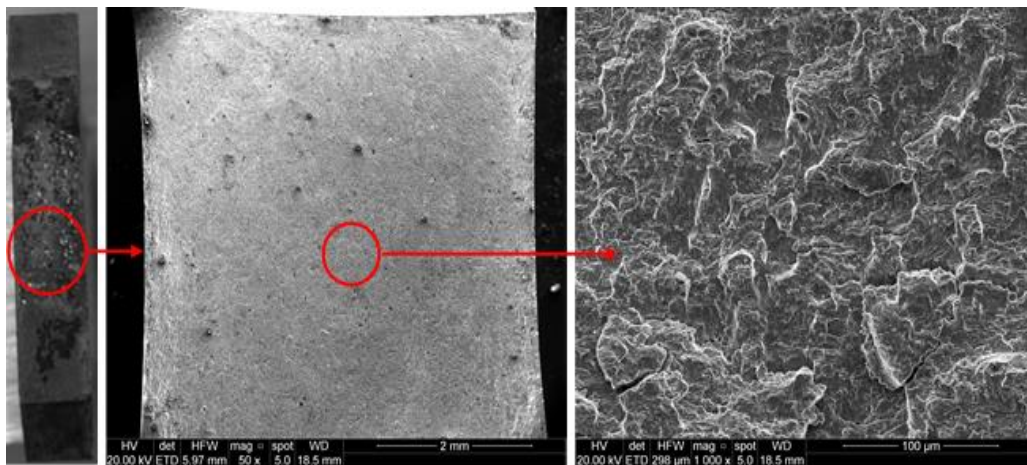


**Fig. 10:** Details of the fracture surface of a notched specimen tested at room temperature ( $\Delta\sigma=250$  MPa,  $N=295000$ )



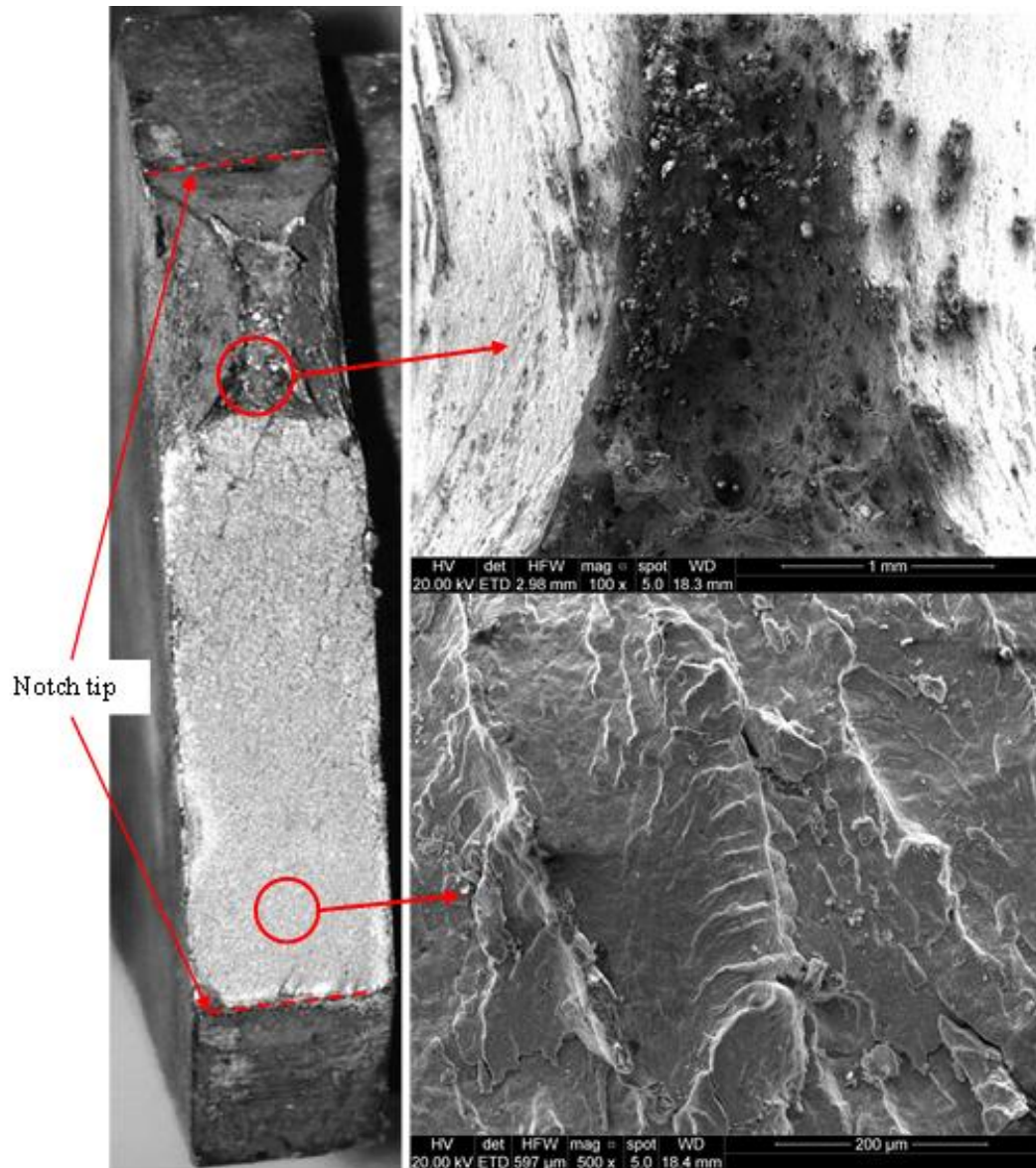


**Fig. 11:** Fracture surface of a notched specimen tested at 650°C at different magnification values ( $\Delta\sigma = 100$  MPa,  $N = 304000$ )

#### **4.4.4 Influence of surface roughness on high temperature fatigue and crack initiation**

The 40CrMoV13.9 steel is widely used in different engineering high temperature applications among which hot-rolling of metals, where, in order to assure a constant temperature, the rolls are provided with cooling channels. These are the most stressed zone of the rolls where cracks initiate systematically. The surface roughness is one of few parameters that can be set in the design stage. With the aim to investigate the influence of the cooling channels roughness on the high temperature

behaviour and the cracks initiation, uniaxial-tension load controlled fatigue tests have been conducted on plate with central hole at the service temperature of 650°C, as reported some sections above.

The understanding of the influence of this parameter on the component performances can lead to several advantages: first of all, it defines quantitatively the influence of the surface roughness on the fatigue performances, and therefore justifies the relative costs in order to obtain a high surface finish quality. This makes possible to evaluate in terms of cost-benefit analysis the choice of imposing a low surface roughness or, otherwise, high surface roughness.

The obtained Wöhler curves (mean curve,  $P_s = 50\%$ ) are summarized in Figure 12, in terms of stress range (referred to the net area). A vertical line is drawn in correspondence of two million cycles and one million cycles. The run-out specimens were not considered in the statistical analysis and are marked with a tilted arrow. From the figure it is clear how the roughness influences the fatigue strength. For poor roughness, the effects on the fatigue behaviour are negligible. In fact, there are no differences between the curves regarding  $R_a=2\mu\text{m}$  and  $R_a=1\mu\text{m}$ , especially if considering the stress range at one million cycles (that is the most interesting for the final application). When the quality of the surface finish is improved, we can see some enhancements on the fatigue behaviour. The more evident improvement is registered for the value of  $R_a=0.15\mu\text{m}$ . Comparing this value with that of the starting poor roughness, the stress range at one million cycles increases of 44%, that is a very remarkable result, in agreement with [11]. Similar results for other materials have been obtained recently by other authors such as Hussain et al. [19], Gao et al. [20]: from these works also emerged that a good surface finishing has a beneficial effect on the fatigue limit, even if the effects were not notable in comparison with those of the present paper and [11].

The decrement of the fatigue life of the specimens with rough surfaces at high temperature suggests this result is originated from the reduction in the number of cycles for crack initiation. It can be asserted that a large number of fraction of the high temperature fatigue life was spent in the crack initiation process in agreement with [10,11].

In order to better support the conclusions, an analysis on the crack initiation near the hole has been conducted. The plates with central hole were tested at 650°C and once

reached a specific number of cycles, the test was temporarily stopped and the specimen checked through an optical microscope with the aim to detect any sign of cracks initiation. Figure 13 depicts an example of the crack detection. The number of cycles to crack initiation and failure for a constant stress range as a function of the surface roughness is reported in Figure 14. The stress range is selected in order to analyse the high cycle fatigue life. Some considerations deserve to be spent on this figure: above all, it is clear the beneficial effect of the surface roughness on the fatigue behaviour, in fact for the same stress range of 240MPa, an  $R_a$  of  $2\mu\text{m}$  returns an  $N_i$  equal approximately to  $1\text{E}+05$  cycles, that becomes almost  $1\text{E}+06$  for an  $R_a=0.15\mu\text{m}$ , a very remarkable results; secondly, the number of cycles for crack initiation is very near to the number of cycles to failure, supporting the thesis that a large number of fraction of the fatigue life was spent for the crack initiation phase. The ratio between  $N_i$  and  $N$  is always greater than 0.8, for all of the surface roughness values. On the basis of the experimental evidences, a good surface finish quality can be justified by the resultant beneficial effects.

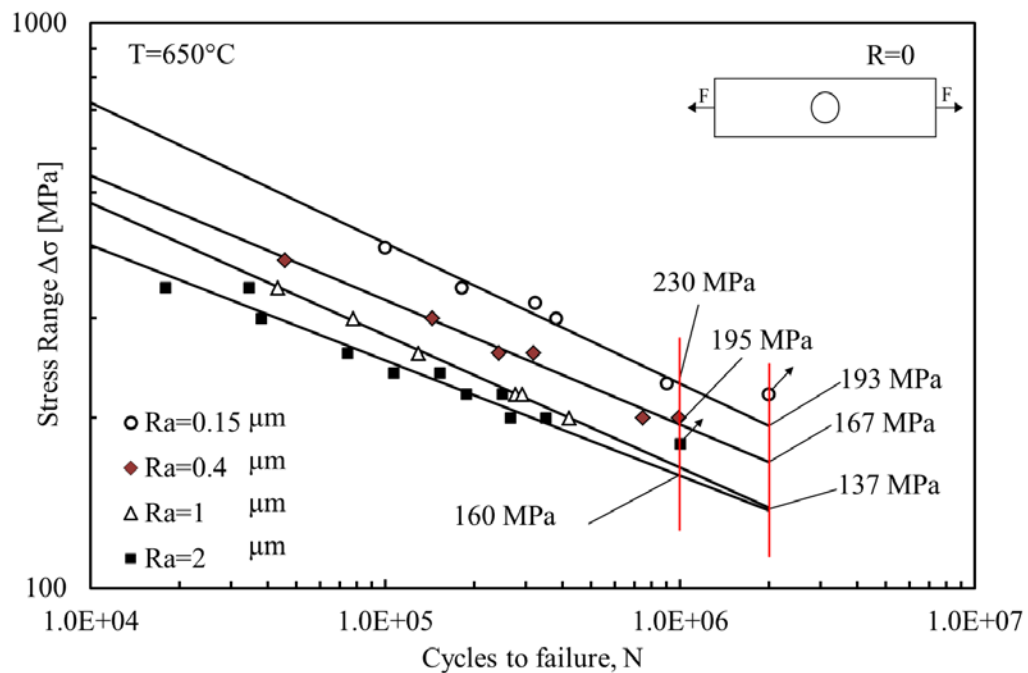


**Fig. 12:** Data from plate with central hole at  $650^\circ\text{C}$ , varying the surface roughness

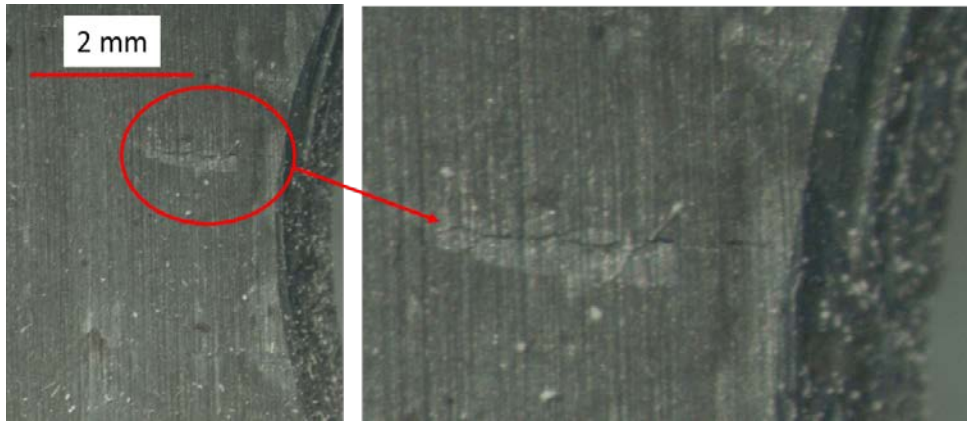


**Fig. 13:** Visual crack detection through optical microscope

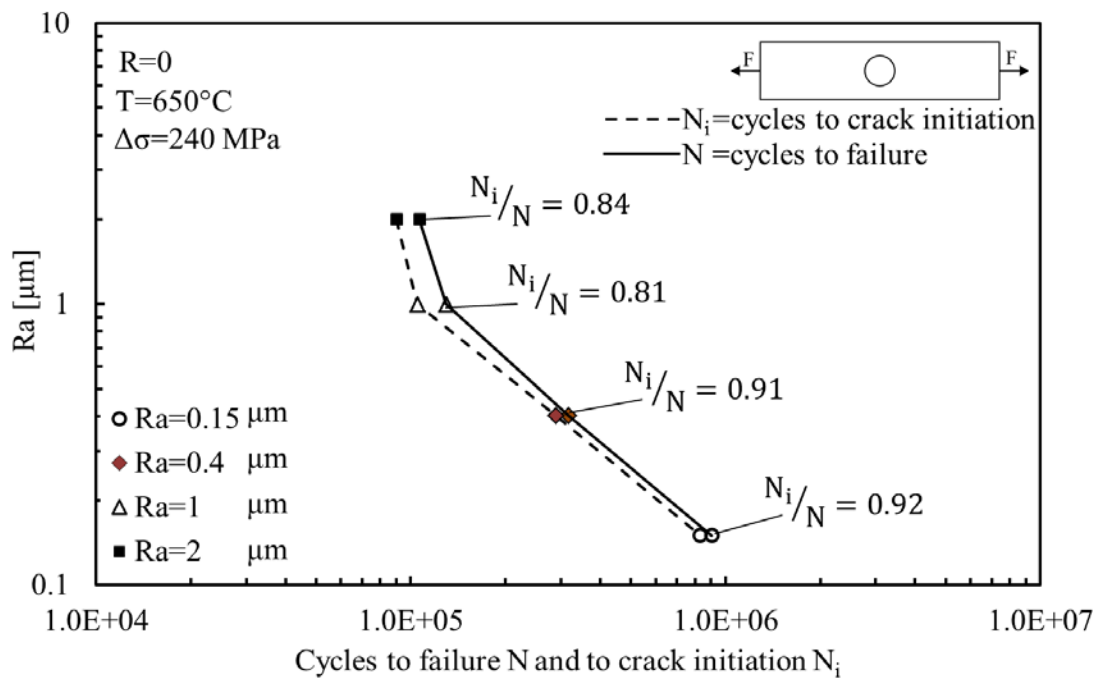


**Fig. 14:** Number of cycles to failure  $N$  and for crack initiation  $N_i$  for plate with central hole, as a function of the surface roughness

## 4.5 A synthesis in terms of linear elastic SED averaged over a control volume

### 4.5.1 Strain energy density as a design parameter

The averaged SED states that failure occurs when the mean value of the strain energy density averaged over a given control volume surrounding the sharp or blunt notch tip is equal to a critical value  $W_c$  [21,22]. Under plane stress or plane strain condition the volumes becomes an area as depicted in Figure 15, where the radius of the

control volume  $R_c$  does not depend on the notch geometry. The SED-based method has been extensively used in the last years dealing with high cycle fatigue of welded joints and notched components [23–27]. It has been also employed to assess fracture data from cracked and notched specimens tested under static conditions [28–31].

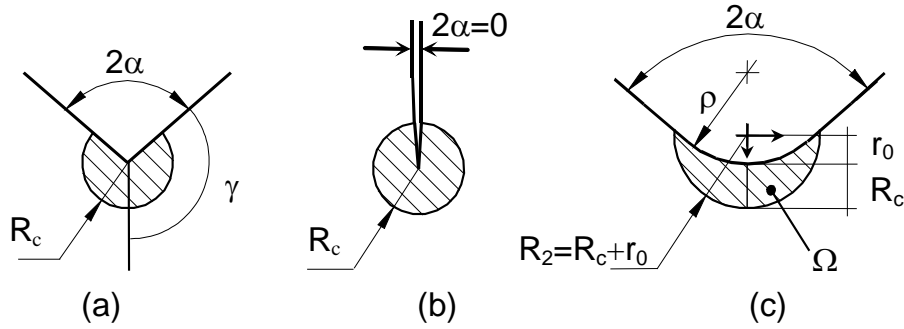


**Fig. 15:** Critical volume (area) for sharp V-notch (a), crack (b) and blunt V-notch (c) under mode I loading, distance  $r_0 = \rho \times (\pi - 2\alpha) / (2\pi - 2\alpha)$

A recent review of the method has been presented in [32], where the analytical frame and the main applications of the SED approach are documented in detail. Some links with Neuber’s concept of “Elementary control volume”, Sih’s factor  $S$  and Gillemot’s concept of “Specific absorbed energy” are underlined with about four hundred citations to papers published over the last fifty years.

Under mode I fatigue loading, the radius  $R_c$  of the control volume can be estimated as a function of the high cycle fatigue strength of plain specimens at a specific reference number of cycles,  $\Delta\sigma_{1A}$ , and the range of notch stress intensity factor,  $\Delta K_{1A}$ , both values typically referred to  $5 \times 10^6$  cycles [21]:

$$R_c = \left( \sqrt{2e_1} \times \frac{\Delta K_{1A}}{\Delta\sigma_{1A}} \right)^{\frac{1}{1-\lambda_1}} \quad (1)$$

Parameters  $e_1$  and  $\lambda_1$  depend on the V-notch angle, according to Williams’ solution. Equation (1) is valid also in the crack case, where the V-notch opening angle is zero. Under fatigue limit conditions, by introducing the threshold value of the stress intensity factor range for long cracks under Mode I conditions,  $\Delta K_{th}$ , and the plain specimen fatigue limit,  $\Delta\sigma_0$ , one obtains:

$$R_c = \frac{(1 + \nu)(5 - 8\nu)}{4\pi} \left( \frac{\Delta K_{th}}{\Delta \sigma_0} \right)^2 \quad (2)$$

Where  $\nu$  is the Poisson's ratio.

When  $\nu=0.3$ , Eq. (2) gives  $R_c=0.845a_0$ , where  $a_0 = (1/\pi)(\Delta K_{th} / \Delta \sigma_0)^2$  is the El Haddad-Smith-Topper parameter [33]. With reference to virtual plane stress conditions, (out-of-plane stress  $\sigma_z=0$  in thin plates), simple algebraic considerations give:

$$R_c = \frac{(5 - 3\nu)}{4\pi} \left( \frac{\Delta K_{th}}{\Delta \sigma_0} \right)^2 \quad (3)$$

Resulting in  $R_c=1.025a_0$  for  $\nu=0.3$ . Relationships (2) and (3) prove the link between the radius  $R_c$  employed in the SED approach and the El-Haddad-Smith-Topper parameter  $a_0$  under Mode I loading. For additional considerations on the characteristic length parameters used in local notch fracture criteria one should consult Ref. [34].

Dealing with blunt notches under fatigue loading the following expression can be used to evaluate the strain energy density range [22]:

$$\overline{\Delta W} = c_w F(2\alpha) \times H(2\alpha, \frac{R_c}{\rho}) \times \frac{K_{t,n}^2 \Delta \sigma_n^2}{E} \quad (4)$$

Here  $\Delta \sigma_n$  is the stress range,  $K_{t,n}$  is the theoretical stress concentration factor (both referred to the net sectional area),  $E$  is the Young's modulus.  $F(2\alpha)$  depends on the notch opening angle and is equal to 0.705 for  $2\alpha=90^\circ$ . Finally  $H$  depends both on the notch angle and the critical radius-notch tip radius ratio.

In order to unify in a common diagram the fatigue results from both  $R=-1$  and  $R=0$ , the weighting parameter  $c_w$  has to be applied, according to the simple rule reported in Ref. [23]. This rule states, in particular,  $c_w=1.0$  for  $R=0$  and  $c_w=0.5$  for  $R=-1$ . As a result of the reduction of the effective SED, the fatigue strength range for  $R=-1$  should theoretically increase according to a factor  $\sqrt{2}$  with respect to the  $R=0$  case.

#### 4.5.2 A synthesis in terms of linear elastic SED of room and high temperature data

The new high temperature data from un-notched and V-notched specimens made of 40CrMoV13.9 are summarized in this section by using the SED approach. On the basis of the experimental evidences of the present work, the synthesis in terms of SED has been carried out up to 500°C considering the same critical radius used in Ref. [35] for multiaxial fatigue data. In fact, as visible from Figures 5 and 6, no reduction in the fatigue strength has been detected until 500°C both for un-notched and notched specimens.

In the medium and high cycle fatigue regime the critical SED range for un-notched specimens can be simply evaluated by using the following expression:

$$\Delta \bar{W} = \frac{c_w}{2E} \Delta \sigma_n^2 \quad (5)$$

In Eq. (5)  $\Delta \sigma_n$  is the nominal stress range referred to the net sectional area. As already said, the weighting parameter  $c_w$  has to be applied to take into account different values of the nominal load ratio [23]. Being the actual tests referred to  $R=0.01$ ,  $c_w$  is equal to 1.0. Since Eq. (5) is applied at different temperatures, the Young's modulus has to be updated as a function of the temperature.

$E$  is equal to 206 GPa at room temperature and 135 GPa at 650°C. The datasheet also provided the values of the Young modulus for the other temperatures: at 360°C the Young's modulus  $E$  results to be 165 GPa and at 500°C it is equal to 150 GPa. These values have been obtained experimentally by the manufacturer, with the assistance of an external laboratory. It is possible to see that the Young modulus shows a linear trend as function of the temperature, which has been found also by other authors [36].

For the notched specimens Eq. (6) can be directly applied. For the specific case of  $2\alpha=90^\circ$  and  $R_c/\rho=0.05$ , parameters  $F$  and  $H$  are equal to 0.7049 and 0.5627, respectively [22]. The stress concentration factor referred to the net area is equal to 3.84.

$$\Delta \bar{W} = c_w F(2\alpha) \times H\left(2\alpha, \frac{R_c}{\rho}\right) \times \frac{K_{t,n}^2 \Delta \sigma_n^2}{E} \quad (6)$$

Here  $\Delta\sigma_n$  is the stress range,  $K_{t,n}$  is the theoretical stress concentration factor (both referred to the net sectional area),  $E$  is the Young's modulus.  $F(2\alpha)$  depends on the notch opening angle and is equal to 0.705 for  $2\alpha=90^\circ$ . Finally  $H$  depends both on the notch angle and the critical radius-notch tip radius ratio.

By using Equations (5) and (6) the new data from the tests carried out at room temperature up to  $500^\circ\text{C}$  can be summarized in Figure 16 in a single narrow scatterband, characterized by an inverse slope  $k$  equal to 5.31 and a scatter index  $T_w$  equal to 2.25. Moreover, the new data belong to the same scatter-band of multiaxial room-temperature fatigue data taken from literature [35] and regarding the same material. Thanks to the SED approach it has been possible to summarize in a single scatterband all the fatigue data, independently of the specimen geometry, of the temperature (up to  $500^\circ\text{C}$ ) and, considering the multiaxial data reported in [35], also of the loading condition.

Dealing with data carried out at  $650^\circ\text{C}$ , the fatigue strength of un-notched and notched specimens has been found strongly lower than the corresponding data from tests carried out at  $T<500^\circ\text{C}$ . For this specific temperature ( $T=650^\circ$ ), which is important in practical industrial applications, in particular for hot rolling of aluminum alloys, an empirical formula has been proposed for notched specimens by modifying Eq. (6). This allows us to take into account the notch sensitivity of this material at temperatures higher than  $500^\circ\text{C}$ :

$$\overline{\Delta W} = c_w Q(T) L(f/f_0) F(2\alpha) \times H(2\alpha, \frac{R_c}{\rho}) \times \frac{K_{t,n}^2 \Delta\sigma_n^2}{E} \quad (7)$$

$Q(T)$  is the notch sensitivity function at a specific temperature  $T$ . This function has to be set (as a function of the temperature  $T$ ) by equating at high cycle fatigue ( $10^6$  cycles) the SED value from plain specimens and those from notched specimens;  $f$  is the test frequency of notched specimens at high temperature and  $f_0$  the test frequency of unnotched specimens at the same temperature.  $L$  is a function related to the sensitivity of the material to the load frequency and depends on the ratio  $f/f_0$ . Function  $L$  is required to be equal to 1.0 if  $f=f_0$ , a condition respected in all tests of the present analysis. The critical radius  $R_c$  is kept constant and equal to that obtained at room temperature ( $R_c=0.05$  mm). Dealing with our specific case  $Q(T=650^\circ\text{C})=$



0.18. Equation (7) can be re-written by substituting the numerical value of each function:

$$\overline{\Delta W} = 1.0 \times 0.18 \times 1.0 \times 0.7049 \times 0.5627 \frac{K_{t,n}^2 \Delta \sigma_n^2}{E} = 0.07139 \frac{K_{t,n}^2 \Delta \sigma_n^2}{E} \quad (8)$$

Where, as said above,  $K_{t,n}=3.84$ .

Considering Eq. (7) applied to notched specimens and Eq. (5) applied to plain specimens, the SED master curve for 40CrMoV13.9 at 650°C has been obtained. The fatigue data from tests at 650°C are plotted in terms of averaged strain energy density range over a control volume in Figure 16, considering the critical radius previously derived at room temperature. It is possible to observe that the scatter band is quite narrow, with the scatter index being  $T_w = 2.56$  that results in  $T_\sigma=1.60$  in terms of equivalent local stress range. The inverse slope of the scatterband is equal to 1.43. Thanks to the SED approach it is possible to summarise in a single scatterband all the fatigue data at the same temperature, regardless of the specimen geometry.

Future developments will be devoted to set the proposed empirical equation to other geometries and temperatures. The idea is to further increase the temperature, in order to study the interactions between fatigue and creep. Another open point is the behaviour of the same steel under different loading conditions, for example in prevalent mode II or in combined mode I and mode III loading conditions. Another important aspect worth investigating is the constraint effect through the plate thickness. It can play a fundamental role in fracture and fatigue assessment.

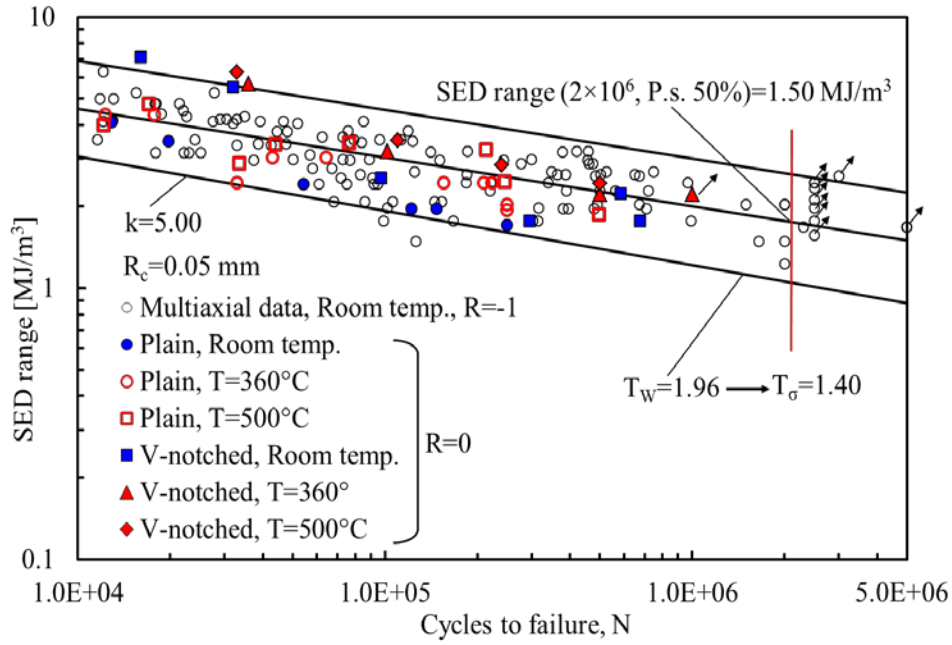


**Fig. 16:** Synthesis by means of local SED of new fatigue data up to 500°C and room temperature multiaxial fatigue data taken from [35]

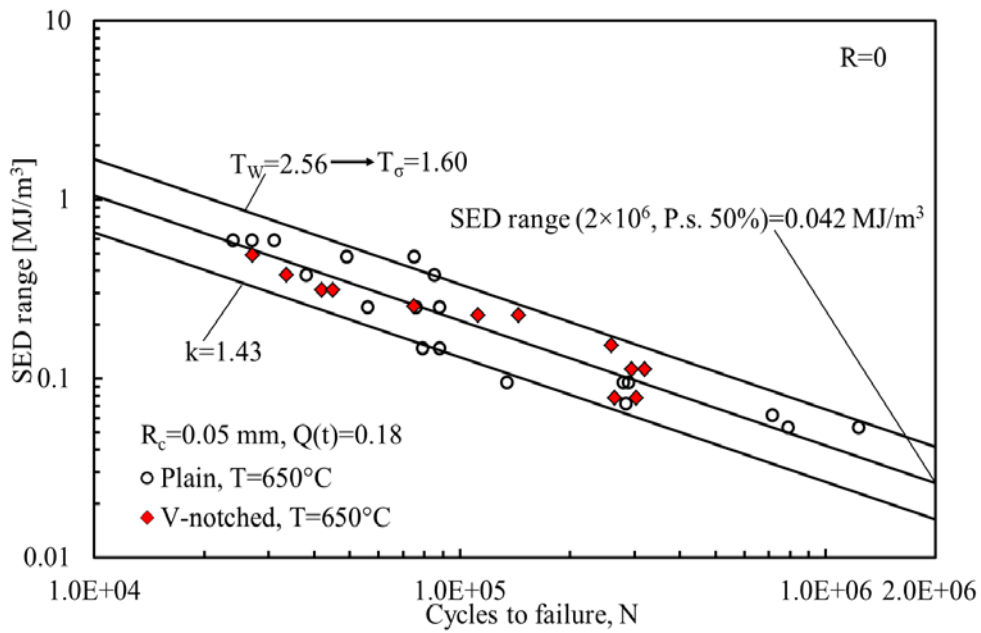


**Fig. 17:** Synthesis by means of local SED of new fatigue data at 650°C of plain and V-notched specimens

## 4.6 Conclusions

The present chapter addresses experimentally the high temperature fatigue of 40CrMoV13.9 steel and the effect of surface roughness on fatigue strength and cracks initiation. In order to completely characterize the high temperature behaviour of this steel, firstly uniaxial-tension load controlled fatigue tests have been conducted at different temperatures up to 650°C. Two geometries are considered in this phase: plain specimens and plates weakened by symmetric V-notches, with opening angle and tip radius being equal to 90 degrees and 1 mm, respectively. Subsequently, with the aim to investigate the influence of the roughness on the high temperature behaviour and the cracks initiation, uniaxial-tension load controlled fatigue tests have been conducted on plate with central hole at the service temperature of 650°C. This geometry simulates the cooling channels of rolls for hot-rolling of metals, which are the most stressed zone of the rolls. The understanding of the influence of the surface finish on the component performances can lead to several advantages from industrial viewpoint. Moreover, the work has been motivated by the fact that, at the best of authors' knowledge, only a limited number of works dealing with high-temperature fatigue are available in the literature and no results seem to be available from notched components made of this steel tested at elevated temperatures.

Finally, fatigue data from un-notched and notched specimens are re-analysed by means of the mean value of the Strain Energy Density (SED) extended at high temperature.

The main results can be summarized as follows:

- The tested alloy exhibits good high temperature fatigue behaviour up to 500°. Until that temperature, no reduction in the fatigue strength with respect to the room temperature has been detected for plain and V-notched specimens. Above 500°C, instead, a significant reduction in fatigue strength is shown.
- At 650°C the notch sensitivity of the present steel seems to be quite low. The inverse slope  $k$  is also very similar. It is equal to 2.48 for hourglass shaped specimens and 2.91 for plates weakened by lateral notches.
- The strong reduction of the fatigue properties of the present material at 650°C can be attributed to the specific thermal treatments performed on it. In fact the material was first quenched at 920°C and subsequently tempered at about 580°C twice. A final stress relieving treatment at 570°C was carried out. The tempered

temperature and final stress relieving temperatures were lower than 650°C. It seems that for a long time exposure at temperatures higher than 570-590°C the beneficial effects due to these specific treatments were lost.

- All new data from tests carried at room temperature up to 500°C are summarized in terms of mean SED over a control volume with  $R_c=0.05$  mm. A sound agreement in terms of SED has been found between the present results and those recently obtained from a large bulk of multiaxial tests performed at room temperature on the same material.
- A quite narrow scatter band characterized by a limited value of the scatter index has been obtained by summarizing together new data and old multiaxial data taken by [35] up to 500°C.
- A specific master curve based on SED has been proposed for the considered steel tested at  $T=650^\circ\text{C}$  in Fig 17. The scatter band makes possible to summarize together data from plain and notched specimens. Dealing with notched specimens an empirical expression has been also proposed for the SED calculation. The equation can be directly employed for practical applications of 40CrMoV13.9 steel at 650°C.
- The roughness influences the fatigue strength. When the quality of the surface finish is improved, we can see some enhancements on the fatigue behaviour. The more evident improvement is registered for the value of  $R_a=0.15\mu\text{m}$ . Comparing this value with that of the starting poor roughness, the stress range at one million cycles increases of 44%. These results are well supported by Fig. 12.
- The ratio between  $N_i$  (number of cycles to crack initiation) and  $N$  (number of cycles to failure) is always greater than 0.8, for all of the surface roughness values (see Fig. 14), proving that a large fraction of the fatigue life is spent for crack initiation phase.

## References

- [1] T.H. Krukemyer, A. Fatemi, R.W. Swindeman, Fatigue Behavior of a 22Cr-20Ni-18Co-Fe Alloy at Elevated Temperatures, *J. Eng. Mater. Technol.* 116 (1994) 54.
- [2] H. Kobayashi, a Todoroki, T. Oomura, T. Sano, T. Takehana, Ultra-high-cycle fatigue properties and fracture mechanism of modified 2.25Cr-1Mo steel at elevated temperatures, *Int. J. Fatigue.* 28 (2006) 1633–1639.
- [3] Z. Fan, X. Chen, L. Chen, J. Jiang, Fatigue–creep behavior of 1.25Cr0.5Mo steel at high temperature and its life prediction, *Int. J. Fatigue.* 29 (2007) 1174–1183.
- [4] Y. Uematsu, M. Akita, M. Nakajima, K. Tokaji, Effect of temperature on high cycle fatigue behaviour in 18Cr–2Mo ferritic stainless steel, *Int. J. Fatigue.* 30 (2008) 642–648.
- [5] Q. Chen, N. Kawagoishi, H. Nisitani, Evaluation of notched fatigue strength at elevated temperature by linear notch mechanics, *Int. J. Fatigue.* 21 (1999) 925–931.
- [6] N. Kawagoishi, Q. Chen, H. Nisitani, Fatigue strength of Inconel 718 at elevated temperatures, *Fatigue Fract. Engng. Mater. Struct.* 23 (2000) 209–216.
- [7] F. Berto, P. Gallo, P. Lazzarin, High Temperature Fatigue Tests of a Cu-Be Alloy and Synthesis in Terms of Linear Elastic Strain Energy Density, *Key Eng. Mater.* 627 (2015) 77–80.
- [8] D.Q. Shi, X.A. Hu, J.K. Wang, H.C. Yu, X.G. Yang, J. Huang, Effect of notch on fatigue behaviour of a directionally solidified superalloy at high temperature, *Fatigue Fract. Engng. Mater. Struct.* 36 (2013) 1288–1297.
- [9] R. Louks, L. Susmel, The linear-elastic Theory of Critical Distances to estimate high-cycle fatigue strength of notched metallic materials at elevated temperatures, *Fatigue Fract. Engng. Mater. Struct.* 38 (2015) 629–640.
- [10] J.J. Kim, S.W. Nam, J.H. Ryu, The sensitivity of surface crack initiation to surface roughness in low-cycle fatigue at high temperature, *Mater. Sci. Eng. A.* 130 (1990) L7–L10.
- [11] J. Ryu, S. Nam, Effect of surface roughness on low-cycle fatigue life of Cr-Mo-V steel at 550 °C, *Int. J. Fatigue.* 11 (1989) 433–436.

- [12] F. Berto, A. Campagnolo, P. Lazzarin, Fatigue strength of severely notched specimens made of Ti-6Al-4V under multiaxial loading, *Fatigue Fract. Engng. Mater. Struct.* 38 (2015) 503–517.
- [13] F. Berto, P. Lazzarin, P. Gallo, High-temperature fatigue strength of a copper-cobalt-beryllium alloy, *J. Strain Anal. Eng. Des.* 49 (2014) 244–256.
- [14] P. Gallo, F. Berto, P. Lazzarin, High temperature fatigue tests of notched specimens made of titanium Grade 2, *Theor. Appl. Fract. Mech.* 76 (2015) 27–34.
- [15] M.E. Kassner, *Fundamentals of Creep in Metals and Alloys*, 2nd ed., Elsevier Ltd, 2009.
- [16] L. F. Coffin Jr, Fatigue at high temperature-Prediction and interpretation, *Proc. Inst. Mech. Eng.* 188 (1974) 109–127.
- [17] S.S. Manson, G.R. Halford, *Fatigue & Durability of Metals at High Temperatures*, ASM Intern, Ohio, 2009.
- [18] J. Tong, L.G. Zhao, B. Lin, Ratchetting strain as a driving force for fatigue crack growth, *Int. J. Fatigue.* 46 (2013) 49–57.
- [19] K. Hussain, D.S. Wilkinson, J.D. Embury, Effect of surface finish on high temperature fatigue of a nickel based super alloy, *Int. J. Fatigue.* 31 (2009) 743–750.
- [20] Y.K. Gao, X. Bin Li, Q.X. Yang, M. Yao, Influence of surface integrity on fatigue strength of 40CrNi2Si2MoVA steel, *Mater. Lett.* 61 (2007) 466–469.
- [21] P. Lazzarin, R. Zambardi, A finite-volume-energy based approach to predict the static and fatigue behavior of components with sharp V-shaped notches, *Int. J. Fract.* 112 (2001) 275–298.
- [22] P. Lazzarin, F. Berto, Some Expressions for the Strain Energy in a Finite Volume Surrounding the Root of Blunt V-notches, *Int. J. Fract.* 135 (2005) 161–185.
- [23] P. Lazzarin, C.M. Sonsino, R. Zambardi, A notch stress intensity approach to assess the multiaxial fatigue strength of welded tube-to-flange joints subjected to combined loadings, *Fatigue Fract. Engng. Mater. Struct.* 27 (2004) 127–140.
- [24] D. Radaj, F. Berto, P. Lazzarin, Local fatigue strength parameters for welded joints based on strain energy density with inclusion of small-size notches, *Eng.*

- Fract. Mech. 76 (2009) 1109–1130.
- [25] D. Radaj, P. Lazzarin, F. Berto, Fatigue assessment of welded joints under slit-parallel loading based on strain energy density or notch rounding, *Int. J. Fatigue*. 31 (2009) 1490–1504.
- [26] F. Berto, D. Croccolo, R. Cuppini, Fatigue strength of a fork-pin equivalent coupling in terms of the local strain energy density, *Mater. Des.* 29 (2008) 1780–1792.
- [27] F. Berto, P. Lazzarin, Fatigue strength of structural components under multi-axial loading in terms of local energy density averaged on a control volume, *Int. J. Fatigue*. 33 (2011) 1055–1065.
- [28] P. Lazzarin, F. Berto, M. Elices, J. Gómez, Brittle failures from U- and V-notches in mode I and mixed, I + II, mode: a synthesis based on the strain energy density averaged on finite-size volumes, *Fatigue Fract. Engng. Mater. Struct.* 32 (2009) 671–684.
- [29] F. Berto, P. Lazzarin, C. Marangon, Brittle fracture of U-notched graphite plates under mixed mode loading, *Mater. Des.* 41 (2012) 421–432.
- [30] F. Berto, A. Campagnolo, M. Elices, P. Lazzarin, A synthesis of Polymethylmethacrylate data from U-notched specimens and V-notches with end holes by means of local energy, *Mater. Des.* 49 (2013) 826–833.
- [31] F. Berto, P. Lazzarin, A review of the volume-based strain energy density approach applied to V-notches and welded structures, *Theor. Appl. Fract. Mech.* 52 (2009) 183–194.
- [32] F. Berto, P. Lazzarin, Recent developments in brittle and quasi-brittle failure assessment of engineering materials by means of local approaches, *Mater. Sci. Eng. R Reports*. 75 (2014) 1–48.
- [33] M.H. El Haddad, T.H. Topper, K.N. Smith, Prediction of non propagating cracks, *Eng. Fract. Mech.* 11 (1979) 573–584.
- [34] G. Pluvinage, J. Capelle, On characteristic lengths used in notch fracture mechanics, *Int. J. Fract.* 187 (2014) 187–197.
- [35] F. Berto, P. Lazzarin, C. Marangon, Fatigue strength of notched specimens made of 40CrMoV13.9 under multiaxial loading, *Mater. Des.* 54 (2014) 57–66.
- [36] B.A. Latella, S.R. Humphries, Young's modulus of a 2.25Cr–1Mo steel at

*References*

elevated temperature, *Scr. Mater.* 51 (2004) 635–639.



# **5. High temperature fatigue assessment by local Strain Energy Density of C45, Inconel 718 and DZ125 superalloy**

*P. Gallo, F. Berto, Advanced Materials for Applications at High Temperature: Fatigue Assessment by Means of Local Strain Energy Density, Advanced Engineering Materials. In Press, DOI: 10.1002/adem.201500547*

## **Highlights**

The present chapter presents the accuracy of Strain Energy Density (SED) averaged over a control volume approach when applied to high temperature fatigue data from notched components. A large bulk of high temperature fatigue data, taken from literature and regarding notched components made of different advanced materials, is reanalysed by means of the SED approach. In detail: C45 carbon steel at 250°C, Inconel 718 at 500°C and directionally solidified superalloy DZ125 at 850°C are considered. This validation allowed proving that the proposed approach can be a reliable design method in practical applications when dealing with high temperature. The main advantage of SED averaged over a control volume is that different geometries can be summarised in a single narrow scatter band. From an industrial viewpoint, where different components are continuously redesigned, the use of a geometry independent parameter (and fatigue curve) leads to a considerable advantage in terms of time and cost.



## **5.1 Introduction**

The interest on fatigue assessment of steels and different alloys at high temperature has increased continuously in the last years. The applications in which fatigue phenomenon is affected by high temperature are of considerable interest and involve different industrial sectors such as transportation, energy and metal-manufacturing (e.g. jet engine components, nuclear power plant, pressure vessel, hot rolling of metal). To provide as optimum performance as possible in these high demanding conditions, it is necessary to be aware of the application and of proper tools to perform the fatigue assessment at high temperature.

The state of the art regarding high temperature fatigue of advanced materials employed in such high demanding conditions, suggests that problem has been addressed mainly in terms of strain, focusing the attention on the plastic part of the cyclic deformation. However, it must be pointed out that real components present a complex shape, and in some applications they must be designed for high number of cycles fatigue regime. From these last considerations, it emerges the importance to investigate the high cycles fatigue regime and notch effect at elevated temperatures. As recently underlined by [1], the high-temperature notch fatigue problem has been mainly investigated considering only low and medium fatigue regime. On the contrary, little research work has been carried out in order to formalise and validate appropriate design methods suitable for designing against high-cycles fatigue of notched metallic components experiencing high temperature during in-service operations.

Just to name few works, Hamada et al. [2] discussed the effects of non-proportional loading on low cycle fatigue (LCF) lives for Type 304 stainless steel at 923 K. In fact, high temperature applications sometimes involve multiaxial damage rather than uniaxial. Fifteen proportional and non-proportional strain paths at a strain rate of 0.1%/s were employed. They concluded that non-proportional straining drastically decreased low cycle fatigue lives of the considered steel. A parameter  $\alpha$  quantifying the amount of additional hardening at high temperature was proposed. However, only low cycle fatigue was considered.

An interesting work was presented by Prasad et al. [3]. Low cycle fatigue deformation behaviour of forged turbine disc of IN 718 superalloy of different sections, and thus geometries, was studied under asymmetrical waveforms (slow-fast

and fast-slow) at 650°C. The superalloy exhibited dynamic strain aging by showing serration during the lower strain rate plastic region of the hysteresis loop under asymmetrical waveforms. Irrespective of different sections, the superalloy showed a marginally reduction of fatigue life under slow-fast waveform as compared to fast-slow waveform, because of the LCF damage accumulation.

Numerous experimental as well as theoretical investigations have been conducted also to quantify the effect of stress/strain concentration on the fatigue behaviour of different advanced materials experiencing high temperature in service [4–7], considering also single-crystal components [8,9].

Because of the lack of literature on high cycle fatigue behaviour of notched components at high temperature, the present author, in the last years, have devoted some efforts in experimental testing of different materials (of industrial relevance) at high temperature. Moreover, the Strain Energy Density (SED) approach, successfully applied at room temperature in the past, has been extended to high temperature considering the obtained data, as well documented in the previous chapters of the present thesis.

Some authors have gone further on this topic, investigating the interactive creep-fatigue crack growth, obtaining very good results [10].

Kawagoishi and co-workers [11,12] investigated the strength of nickel-base superalloy Inconel 718 under rotating banding loading at room temperature and 500°C in air. The applicability of linear notch mechanics to the evaluation of notched fatigue strength at elevated temperature was assessed in terms of the fatigue limit for crack initiation and that for crack growth. The effect of temperature on the fatigue strength and notch sensitivity of Inconel 718 was examined. They showed that linear notch mechanics is applicable not only at room temperature but also at elevated temperature, as long as the small-scale yielding condition is satisfied.

Shi et al. [13], investigated the effect of notch on fatigue behaviour of a directionally solidified superalloy DZ125 at 850°C. Single-edge notched specimens with V and U type geometries were tested, with a stress ratio  $R=0.1$ . It was underlined that for the same applied nominal stress, the fatigue resistance decreased with  $K_t$  increasing from 1.76 to 4.35. Moreover, the impact of U-type and V-type notch on the fatigue behaviour was close. It has been proposed that  $K_t$  can be regarded as a key parameter to dominate the notch fatigue when absolute dimensions of notched specimens are

similar. Different fatigue curves were obtained, as well as a deep analysis of ratcheting effect, crack initiation and failure mechanics at high temperature.

Recently, Louks and Susmel [14] investigated the accuracy of Theory of Critical Distances (TCD) in estimating high-cycle fatigue strength of notched metallic materials experiencing elevated temperatures during in-service operations. They checked the accuracy of TCD against a number of experimental results generated, under uniaxial loading, by testing at 250°C notched specimens made of carbon steel C45, as well as considering many data taken from literature. It has been proved that the TCD can be used as a fatigue assessment parameter at high temperature.

The aim of this chapter is to present a further validation of the application of the SED approach as a reliable tool for high-cycle fatigue assessment of notched components, at high temperature. Different data taken from the literature have been considered and re-analysed by means of the strain energy density averaged over a control volume. In detail, C45 carbon steel tested at 250°C [14], Inconel 718 tested at 500°C [11,12] and directionally solidified superalloy DZ125 at 850°C [13] have been considered.

This validation allowed proving that the proposed approach can be a reliable design parameter in practical applications when dealing with high temperature fatigue. The main advantage of the SED averaged over a control volume is that different geometries can be summarised in a single narrow scatter band, regardless of the notch radius and opening angle. From an industrial viewpoint, where components are usually redesigned, the use of a parameter (and fatigue curve) that is not dependent on the geometrical shape leads to a considerable advantage in terms of time and costs.

## **5.2 Fundamentals of the Strain Energy Density averaged over a control volume**

The averaged Strain Energy Density (SED) method, that has been formalized by Lazzarin and co-workers for sharp [15] and blunt notches [16], derived from Neuber's concept of elementary volume, and local mode I concept proposed by Erdogan and Sih [17]. When dealing with fracture assessment of cracked and notched components, a clear distinction should be done between large and small bodies [18–20].

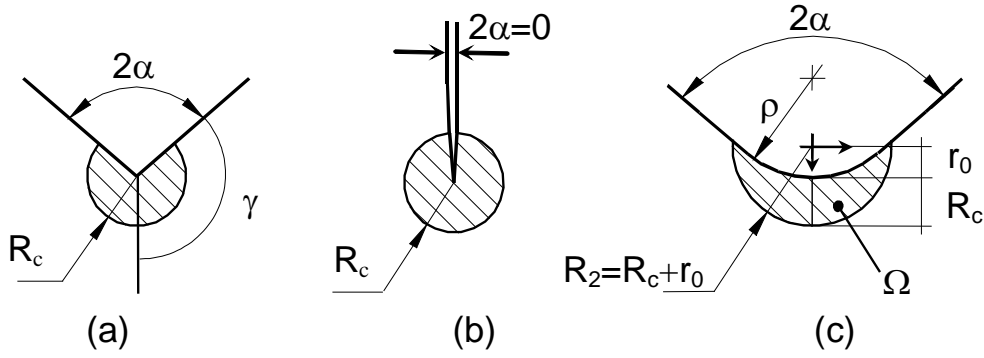


**Fig. 1:** Critical volume (area) for sharp V-notch (a), crack (b) and blunt V-notch (c) under mode I loading, distance  $r_0 = \rho \times (\pi - 2\alpha) / (2\pi - 2\alpha)$

In fact, the design rules applied to large bodies, assume that local inhomogeneities can be averaged because of the large volume surface ratio involved. In small bodies, instead, the high ratio within surface and volume makes not negligible the local discontinuities and an adoption of multiscale scheme is needed [18,19]. The averaged SED method, under the hypothesis of large bodies, combines the concept of energy criterion with the advantages tied to the definition of a material-dependent structural volume. The fundamental basis and late developments of the strain energy density approach have been summarized in some recent contributions [21–23]. In those works, the analytical frame and the main applications of the averaged SED approach are revisited in detail. Such a method has been extensively used in the literature and its predictive capability, especially when dealing with fatigue of notched components, has been largely proofed. This approach is based on the idea that under tensile stresses, failure occurs when the strain energy density averaged over a given control volume,  $\bar{W}$ , reaches the critical energy value  $W_c$  (that depends on the selected material). In plane problems, the control volume becomes a circle or a circular sector with a radius  $R_c$ . Figure 1 shows example of control areas. In the case of blunt notches, the area assumes a crescent shape. Considering the mixed-mode loading, the control area is no longer centred with respect to the notch bisector, but rotated and centred on the point where the maximum principal stress reaches its maximum value.

Under plane strain conditions,  $R_c$  for static loading can be easily evaluated by using the following equation as a function of the fracture toughness and the ultimate tensile stress [24]:

$$R_c = \frac{(1+\nu)(5-8\nu)}{4\pi} \left( \frac{K_{IC}}{\sigma_t} \right)^2 \quad (1)$$

In case of fatigue loading,  $R_c$  depends on smooth specimen fatigue limit  $\Delta\sigma_0$  and on the threshold behaviour  $\Delta K_{th}$  for metallic materials:

$$R_c = \frac{(1+\nu)(5-8\nu)}{4\pi} \left( \frac{\Delta K_{th}}{\Delta\sigma_0} \right)^2 \quad (2)$$

When  $\nu=0.3$ , Equation (2) gives  $R_c=0.845a_0$ , where  $a_0 = (1/\pi)(\Delta K_{th} / \Delta\sigma_0)^2$  is the El Haddad-Smith-Topper parameter [25].

With reference to plane stress conditions, simple algebraic considerations give for static and fatigue loading, respectively:

$$R_c = \frac{(5-3\nu)}{4\pi} \left( \frac{K_{IC}}{\sigma_t} \right)^2 \quad (3)$$

$$R_c = \frac{(5-3\nu)}{4\pi} \left( \frac{\Delta K_{th}}{\Delta\sigma_0} \right)^2 \quad (4)$$

Resulting in  $R_c=1.025a_0$  for  $\nu=0.3$ .

If the material behaviour is ideally brittle, then the critical energy value  $W_c$  can be evaluated by using the conventional ultimate tensile strength  $\sigma_t$  for static cases and the fatigue strength  $\Delta\sigma_0$  for fatigue loading:

$$W_c = c_w \frac{\sigma_t^2}{2E} \quad (5)$$

$$\Delta W_c = c_w \frac{\Delta\sigma_0^2}{2E} \quad (6)$$

The parameter  $c_w$  is introduced to take into account the possible influence of the nominal load ratio on the variation of the deviatoric energy given to the material in one cycle, according to the simple rule reported in literature [26]. It is derived analytically, by simple considerations on the evaluation of the strain energy density range that is nothing but the area under the  $\sigma$ - $\varepsilon$  curve. In other words, the parameter  $c_w$  represents the ratio within  $\Delta W$  in case of generic R and  $\Delta W(R=0)$ , which is assumed as a reference value. It was derived in particular  $c_w=1.0$  for  $R=0$  and  $c_w=0.5$  for  $R=-1$ . In fact, as a result of the reduction of the effective SED, the fatigue strength range for  $R=-1$  should theoretically increase according to a factor  $\sqrt{2}$  with

respect to the case  $R=0$ . More details regarding this parameter can be found in the given references.

Dealing with blunt notches under fatigue loading, the following expression can be used to evaluate the strain energy density range [16]:

$$\overline{\Delta W} = c_w F(2\alpha) \times H\left(2\alpha, \frac{R_c}{\rho}\right) \times \frac{K_{t,n}^2 \Delta \sigma_n^2}{E} \quad (7)$$

Here  $\Delta \sigma_n$  is the stress range,  $K_{t,n}$  is the theoretical stress concentration factor (both referred to the net sectional area),  $E$  is the Young's modulus.  $F$  is a function that depends on the notch opening angle. Finally  $H$  depends on the notch angle and on the critical radius-notch tip radius ratio. Values of the function  $H$  and  $F$  for numerous Poisson's ratios and opening angles are given in literature [16]. The coefficient  $c_w$  takes into account the different loading ratio, as already explained before.

Once defined the control volume, the SED can be easily evaluated through a finite element analysis. As opposed to the evaluation of the NSIFs that needs very refined meshes and high computational effort, the mean value of the elastic SED on the control volume can be determined with high accuracy by using very coarse meshes [27]. The SED, in fact, can be derived directly from the nodal displacements, that are accurately evaluated also when coarse mesh is employed. Other important advantages can be achieved by using the SED approach. The most relevant are:

- It permits consideration of the scale effect which is fully included in the NSIF approach;
- It permits consideration on the contribution of different modes;
- It permits consideration of the cycle nominal load ratio;
- It overcomes the problem tied to the different NSIF units of measure in the case of different notch opening angles;
- It directly takes into account the T-stress for thin structures;
- It directly includes the loading effects thanks to the analytical parameter  $c_w$  cited previously;
- It directly includes three-dimensional effect and out-of-plane singularities.

Under the hypothesis that all the material inhomogeneities can be averaged, the SED approach showed to be a powerful tool both for static and fatigue strength assessment of notched and welded structures.



### 5.3 Validation of Strain Energy Approach applied to high temperature fatigue

Louks and Susmel [14] presented some results from high temperature fatigue tests conducted on C45 notched specimens. The aim was to check the accuracy of linear-elastic TCD in estimating high-cycle fatigue strength of notches metals, when experiencing in service high temperature. Plain and notched samples of C45 were considered and tested under uniaxial loading at 250°C. The load ratio,  $R$ , was set equal to 0.1 and the load frequency to 15 Hz. C45 is a very common and conventional structural steel that presents lower mechanical properties with respect to high-performance alloys employed in high temperature applications. However, there are situations of practical interest (e.g. vehicle engines, engine beds) where conventional structural steels experience medium/high temperatures. For C45 steel, the fatigue damage reaches its maximum value at a temperature in the range of 200-250 °C [28], which is the motivation to choose 250°C as the testing temperature. The geometries are shown in detail in Figure 2. Plain, Blunt U-Notches, Sharp U-Notches and Sharp V-Notches were considered. Table 1 reports all the values of the tested geometries.

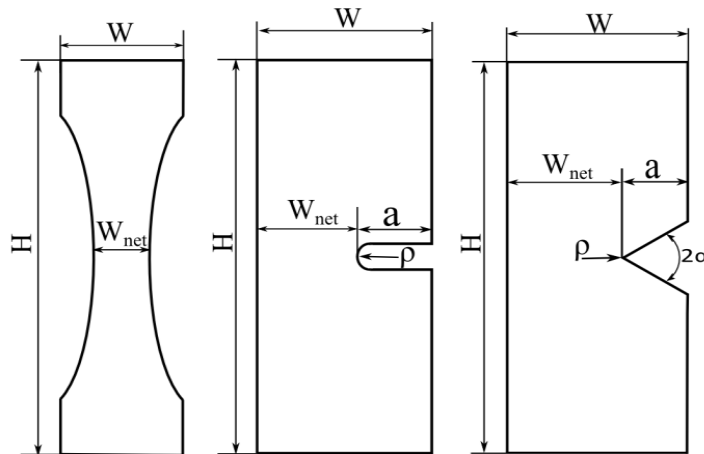


**Fig. 2:** Specimens geometry details

**Table 1:** Details of the geometry considered by Louks and Susmel [14]

Specimens	$K_{t\ net}$	$\rho$	$a$	$2\alpha$	$W$	$W_{net}$	$H$
-----------	--------------	--------	-----	-----------	-----	-----------	-----

	[mm]	[mm]	[°]	[mm]	[mm]	[mm]
Plain	1.0	-	-	25	5	160
Blunt U-notch	6.9	3.00	12	0	25	13
Sharp U-notch	10.0	1.00	12	0	25	13
Sharp V-notch	26.5	0.15	12	45	25	13

The strain energy density of the plain specimens has been evaluated through Equation (6). At 250°C, C45 steel presents a Young's modulus  $E=190$  GPa. The evaluation of the control radius for the notched geometries, instead, has been evaluated analytically following the existing link within the theory of the critical distance and the SED approach. Lazzarin and Bertó [29] showed that the critical radius can be also expressed as function of  $a_0=(1/\pi)(\Delta K_{th}/\Delta\sigma_0)^2$  that is the El Haddad-Smith-Topper parameter [25]. Considering a value of the Poisson's ratio  $\nu=0.3$  and following Equation (4), one obtains the final relationship:

$$R_c = \frac{0.845}{\pi} \left( \frac{\Delta K_{th}}{\Delta\sigma_0} \right)^2 = 0.845a_0 \quad (8)$$

To perform the high-cycle fatigue assessment of notched components, TCD makes use of the range of an effective stress which is calculated by taking into account a suitable material length scale parameter. This material characteristic length, called  $L$ , is a material property and defined as follows [30–32]:

$$L = \frac{1}{\pi} \left( \frac{\Delta K_{th}}{\Delta\sigma_0} \right)^2 \quad (9)$$

From Equations (8) and (9), the critical radius can be easily expressed as a function of  $L$ :

$$R_c = 0.845a_0 = 0.845L \quad (10)$$

Louks and Susmel [14] evaluated the value of the material characteristic length of the considered C45 steel, that has been found to be 0.252 mm. This value, according to Equation (10), returns a critical radius  $R_c=0.21$  mm. This critical radius has been adopted here to reanalyse the same data at high temperature in terms of strain energy density averaged over a control volume. Briefly recalling the considered geometry (see Table 1 and Figure 2): plain specimens, blunt U-notches, sharp U-notches and sharp V-notches. The obtained curve in terms of SED averaged over a control volume is given in Fig. 3. The fatigue data were statistically re-analysed by using a lognormal distribution and are plotted in terms of SED range referred to the net area.

The run-out specimens (marked by tilted arrows) were excluded from the statistical analysis. A vertical line is drawn in correspondence of five hundred thousand cycles where the mean value of the SED range is given to make the comparison easier. Details about inverse slope  $k$  and the scatter index  $T_w$  are provided in the figure.

It is evident that, thanks to SED approach, all the fatigue data, regardless of the specimen geometries, can be summarized in the same narrow scatter band. The value of the scatter index  $T_w$  is equal to 3.00 in terms of energy, and becomes  $T_\sigma=1.73$  if reconverted in terms of local stress range.

Shi [13] provided fatigue test results conducted at 850°C, considering flat specimens with a single lateral notch made of Directionally Solidified (DS) superalloy DZ125. It is a DS Ni-base superalloy used for turbine blade and vanes. It was characterized by the following elastic constants at 850°C:  $E_1(L)=91$  GPa,  $E_2(T)=117$  GPa.

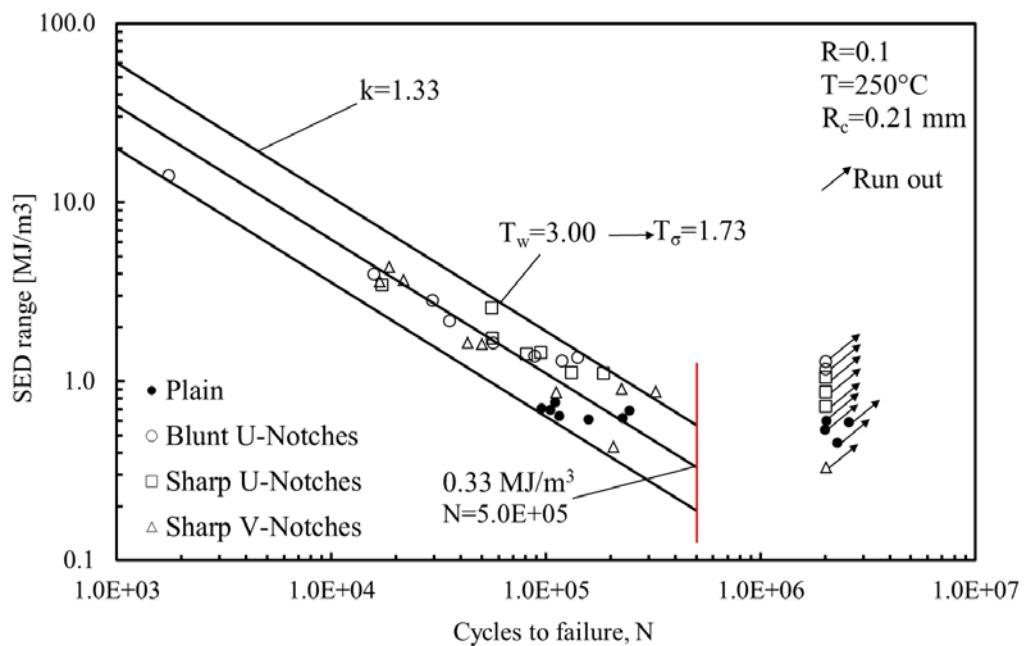


**Fig. 3:** Synthesis by means of local SED of the C45 steel fatigue data

The loading direction was parallel to the direction of solidification and the load ratio  $R$  was kept constant and equal to 0.1. The specimens were tested in air. U-notches and V-notches were considered, with different notch tip radii and opening angles:

- U-notched geometry with root radius of 0.4 mm and 0.2 mm, called U3 and U4 respectively;

- V-notched geometry with opening angle equal to 120° and tip radius of 0.3 mm, called V1;
- V-notched geometry with opening angle equal to 60° and tip radius of 0.2 mm called V2.

The detailed geometrical specifications are reported in Table 2. Refer to Figure 2 for the identification of the parameters.

**Table 2:** Details of the geometry considered by Shi [13]

Notch type	$K_{t,net}$	$\rho$ [mm]	$a$ [mm]	$2\alpha$ [°]	$W$ [mm]	$W_{net}$ [mm]
U-notch U3	3.0	0.4	0.6	0	6	5.4
U-notch U4	4.4	0.2	0.5	0	6	5.5
V-notch V1	3.0	0.3	0.6	120	6	5.4
V-notch V2	4.3	0.2	0.5	60	6	5.5

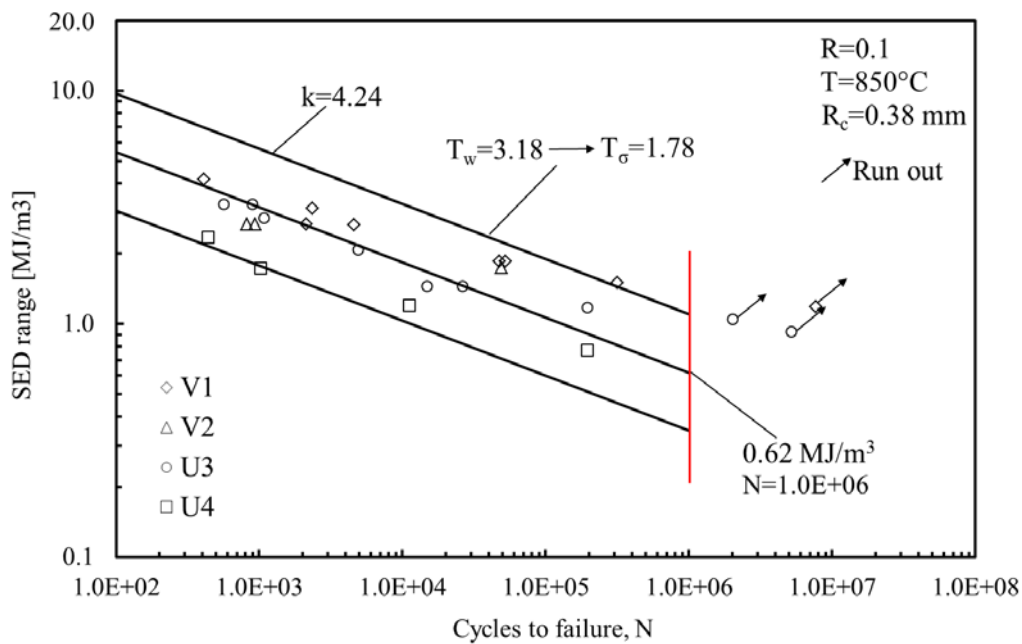


**Fig. 4:** Synthesis by means of local SED of the DS DZ125 superalloy fatigue data

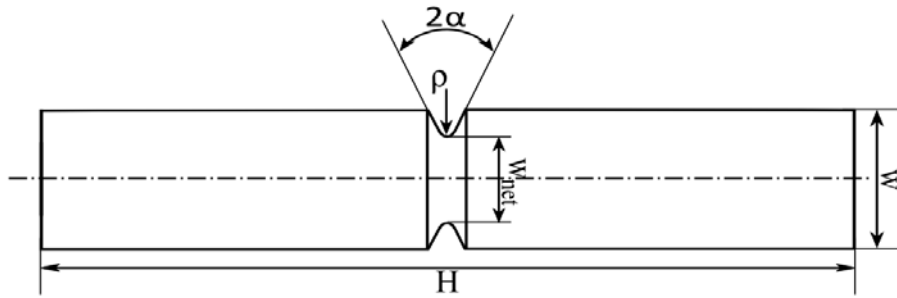


**Fig. 5:** Cylindrical specimen considered by Chen et al. [11]

The control radius has been determined through Equation (10). Considering a value of the material characteristic length  $L$  equal to 0.452 mm [14], a value of  $R_c=0.38$  mm was obtained. The fatigue data reanalysed in terms of SED averaged over a control volume are given in Figure 4. The same procedure presented before has been adopted for the statistical analysis: data were statistically re-analysed by using a lognormal distribution; the run-out specimens (marked by tilted arrows) were not considered and a vertical line is drawn in correspondence of one million cycles. Figure 4 shows that all the fatigue data, regardless of the specimen geometries, can be summarized in the same narrow scatter band. The value of the scatter index  $T_w$  is equal to 3.18 in terms of energy, and becomes  $T_\sigma=1.78$  if reconverted in terms of the local stress range.

Chen [11] investigated the high-cycle fatigue behaviour of V-notched and smooth cylindrical specimens of Inconel 718, which is a precipitation hardened nickel-base superalloy widely used in the critical components of jet and gas turbine engines. The samples were tested under rotating bending ( $R=-1$ ) at 500°C. The net diameter  $w_{net}$  of the samples was kept constant and equal to 8 mm, three different values of the notch root radius  $\rho$  were considered: 1 mm, 0.1 mm and 0.05 mm. The opening angle was kept constant and equal to 60°. By the way, only the fatigue curve of plain and V-notched geometry with a tip radius  $\rho$  of 0.05 mm was reported in detail. For this reason, only that geometry and the plain specimens were considered herein for the final synthesis based on SED. The details of the V-notched specimens considered in the present investigation are reported in Figure 5 and listed as follows: tip radius  $\rho=0.05$ , opening angle  $2\alpha=60^\circ$ ,  $w_{net}=8$  mm, gross diameter  $w=9$  mm and total length  $H=80$  mm. The plain cylindrical specimens presented a net section of 8 mm.

In order to reanalyse the data by means of the strain energy, it is necessary to evaluate the critical radius as already done for the previous considered advanced materials. Also in this case, as already explained before, the critical radius can be expressed as a function of the material characteristic length  $L=0.154$  mm determined by Louks and Susmel [14].  $R_c$  results to be equal to 0.13 mm. Considering the equations given above for the SED evaluation, it must be pointed out that the weighting parameter  $c_w$  [26] must be equal to 0.5 since the fatigue tests were carried out under rotating bending condition and then the load ratio  $R$  was equal to -1.

The fatigue data reanalysed in terms of the SED averaged over a control volume are presented in Fig. 6. The same procedure presented before was employed for the statistical analysis. All the details about the scatter index, the inverse slope  $k$  and other information related to the re-analysis are provided in the figure. It appears evident that both plain and notched specimens have been summarized in the same narrow scatter band characterized by a scatter index equal to 2.83 in terms of local energy and 1.68 if reconverted in terms of the stress range. The obtained scatter is not so far from the value obtained for the other series considered here and those previously analysed in literature [33,34].

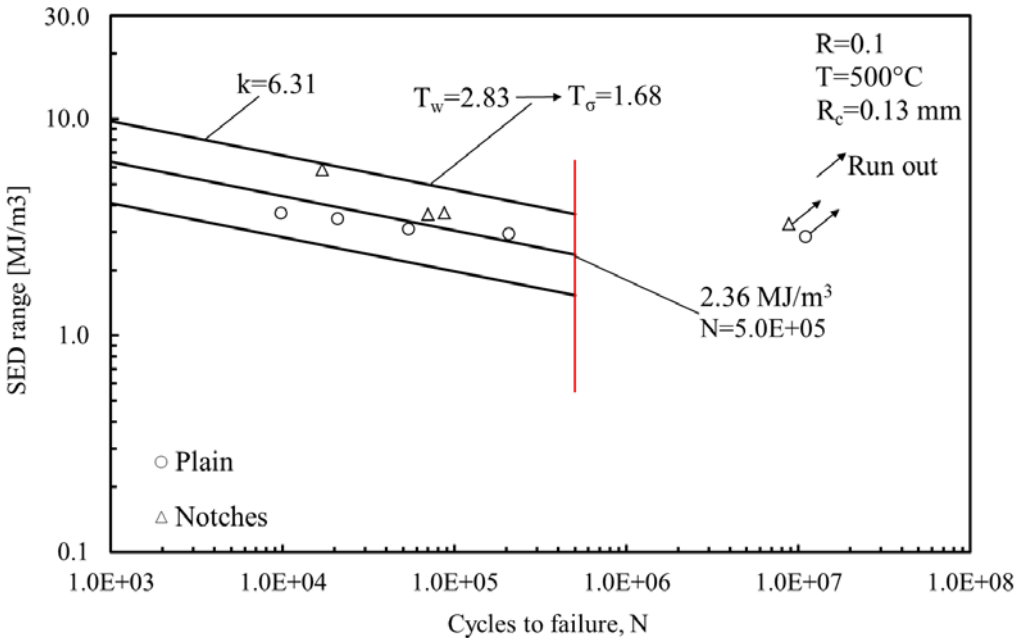


**Fig. 6:** Synthesis by means of local SED of the Inconel 718 fatigue data

## **5.4 Discussion**

High performance applications mostly required advanced and innovative materials, because of the high strength at high temperature and corrosive resistance possessed by them. Most researchers focused on creep and low cycle fatigue at high temperature but neglecting high cycle fatigue that is very important in many applications. Meanwhile, the design criteria and fatigue assessment methods for this kind of application have become more and more complicated, especially when dealing with low-cycle fatigue. Because of the lack of literature on high cycle fatigue of advanced materials at elevated temperature and the lack of simple reliable methods, some authors suggested to extend, if possible, linear notch mechanics also at high temperature, as asserted in the references given in the introduction. Following this idea, the present paper presented a synthesis by means of the Strain Energy Density averaged over a control volume of high temperature fatigue data taken from the literature, regarding advanced materials (DZ125, Inconel 718) and C45 steel.

The SED method has been successfully applied in the past and recent literature to room temperature fatigue data of notched components and welded joints [16,22], and some attempts to extend the method also to high temperature has been done by the present authors considering different advanced materials as documented in the present thesis. The main idea is that the linear elastic approach can be applied not only at room temperature but also at elevated temperature, as long as the small-scale yielding condition is satisfied, as suggested by Nisitani and collaborators [11].

In the results presented here, all the fatigue data taken from literature have been successfully summarised in terms of the SED, and this validation exercise strongly support the idea that, also at high temperature, some linear approaches can be applied neglecting non-linearities. In fact, as suggested by Lazzarin and Zambardi [35], the linear-elastic energy equals the elasto-plastic one when they are averaged over the entire fatigue process zone. The advantage of the energy approach, moreover, becomes evident if comparing the SED data with the original high temperature fatigue data expressed in terms of stress range: regardless of the specimen geometry, all the results collapse in a single curve, maintaining a narrow scatter-band. The obtained curves presented here can be used as master curves to design against fatigue for the considered materials at elevated temperature. From an industrial view point where different components are redesigned several times, the SED approach can lead

to an easy and fast way to design against fatigue. Recently, other similar results have been obtained considering thermo-mechanical tests by other authors, employing a nonlocal invariant area-averaging method to collapse all experimental data in a single trend [36].

Another interesting aspect is that the SED can be easily evaluated through the given formulas or through a linear elastic finite element analysis with very coarse mesh [22]. Moreover, it can be linked to different well established method such as Theory of Critical Distances (as shown in the present paper) but also to J-Integral [37–40].

The results are very promising and the extension of the method also to multiaxial fatigue at high temperature or under thermomechanical fatigue has been seriously considered.

## 5.5 Conclusion

The present chapter presented a further validation of the accuracy of the Strain Energy Density (SED) averaged over a control volume approach when applied to high temperature fatigue data of notched components. A large bulk of high temperature fatigue data taken from literature, regarding notched components of C45 carbon steel at 250°C, Inconel 718 at 500°C and directionally solidified superalloy DZ125 at 850°C have been considered. This validation test allowed proving that the proposed approach can be a reliable design parameter in some practical applications when dealing with high temperature of notched components. The main conclusions can be summarized as follows:

- The Strain Energy Density averaged over a control volume has been extended successfully to high temperature applications;
- The method permitted to summarise in a single narrow scatter band all the fatigue data, regardless of the specimen geometry;
- All the considered fatigue data, taken from the literature, have been re-analysed successfully by means of SED approach, giving master curves for the considered advanced materials that can be used as an easy and fast tool to design against fatigue;
- At high temperature, until small scale yielding condition is satisfied, the linear notch mechanics and linear elastic approaches can be extended to high temperature high cycles fatigue;



## References

- [1] F. Berto, P. Gallo, P. Lazzarin, High temperature fatigue tests of un-notched and notched specimens made of 40CrMoV13.9 steel, *Mater. Des.* 63 (2014) 609–619.
- [2] N. Hamada, M. Sakane, T. Itoh, H. Kanayama, High temperature nonproportional low cycle fatigue using fifteen loading paths, *Theor. Appl. Fract. Mech.* 73 (2014) 136–143.
- [3] K. Prasad, R. Sarkar, P. Ghosal, V. Kumar, M. Sundararaman, High temperature low cycle fatigue deformation behaviour of forged IN 718 superalloy turbine disc, *Mater. Sci. Eng. A.* 568 (2013) 239–245.
- [4] T. Hasebe, M. Sakane, M. Ohnami, High Temperature Low Cycle Fatigue and Cyclic Constitutive Relation of MAR-M247 Directionally Solidified Superalloy, *J. Eng. Mater. Technol.* 114 (1992) 162.
- [5] T. Inoue, M. Sakane, Y. Fukuda, T. Igari, M. Miyahara, M. Okazaki, Fatigue-creep life prediction for a notched specimen of steel at 600°C, *Nucl. Eng. Des.* 150 (1994) 141–149.
- [6] P. Hurley, M. Whittaker, S. Williams, W. Evans, Prediction of fatigue initiation lives in notched Ti 6246 specimens, *Int. J. Fatigue.* 30 (2008) 623–634.
- [7] M. Whittaker, W. Evans, P. Hurley, D. Flynn, Prediction of notched specimen behaviour at ambient and high temperatures in Ti6246, *Int. J. Fatigue.* 29 (2007) 1716–1725.
- [8] D. Leidermark, J. Moverare, M. Segersäll, K. Simonsson, S. Sjöström, S. Johansson, Evaluation of fatigue crack initiation in a notched single-crystal superalloy component, *Procedia Eng.* 10 (2011) 619–624.
- [9] M. Filippini, Notched fatigue strength of single crystals at high temperature, *Procedia Eng.* 10 (2011) 3787–3792.
- [10] K.K. Tang, S.H. Li, Interactive creep-fatigue crack growth of 2024-T3 Al sheets: selective transitional functions, *Fatigue Fract. Eng. Mater. Struct.* 38 (2015) 597–609.
- [11] Q. Chen, N. Kawagoishi, H. Nisitani, Evaluation of notched fatigue strength at elevated temperature by linear notch mechanics, *Int. J. Fatigue.* 21 (1999) 925–931.

- [12] N. Kawagoishi, Q. Chen, H. Nisitani, Fatigue strength of Inconel 718 at elevated temperatures, *Fatigue Fract. Eng. Mater. Struct.* 23 (2000) 209–216.
- [13] D.Q. Shi, X.A. Hu, J.K. Wang, H.C. Yu, X.G. Yang, J. Huang, Effect of notch on fatigue behaviour of a directionally solidified superalloy at high temperature, *Fatigue Fract. Eng. Mater. Struct.* 36 (2013) 1288–1297.
- [14] R. Louks, L. Susmel, The linear-elastic Theory of Critical Distances to estimate high-cycle fatigue strength of notched metallic materials at elevated temperatures, *Fatigue Fract. Eng. Mater. Struct.* 38 (2015) 629–640.
- [15] P. Lazzarin, R. Zambardi, A finite-volume-energy based approach to predict the static and fatigue behavior of components with sharp V-shaped notches, *Int. J. Fract.* 112 (2001) 275–298.
- [16] P. Lazzarin, F. Berto, Some Expressions for the Strain Energy in a Finite Volume Surrounding the Root of Blunt V-notches, *Int. J. Fract.* 135 (2005) 161–185.
- [17] F. Erdogan, G.C. Sih, On the Crack Extension in Plates Under Plane Loading and Transverse Shear, *J. Basic Eng.* 85 (1963) 519.
- [18] G.C. Sih, Crack tip mechanics based on progressive damage of arrow: Hierarchy of singularities and multiscale segments, *Theor. Appl. Fract. Mech.* 51 (2009) 11–32.
- [19] X.S. Tang, T.T. Wei, Microscopic inhomogeneity coupled with macroscopic homogeneity: A localized zone of energy density for fatigue crack growth, *Int. J. Fatigue.* 70 (2015) 270–277.
- [20] G.C. Sih, K.K. Tang, Short crack data derived from the fatigue data of 2024-T3 Al with long cracks: Material, load and geometry effects locked-in by transitional functions, *Theor. Appl. Fract. Mech.* 71 (2014) 2–13.
- [21] F. Berto, P. Lazzarin, Recent developments in brittle and quasi-brittle failure assessment of engineering materials by means of local approaches, *Mater. Sci. Eng. R Reports.* 75 (2014) 1–48.
- [22] F. Berto, P. Lazzarin, A review of the volume-based strain energy density approach applied to V-notches and welded structures, *Theor. Appl. Fract. Mech.* 52 (2009) 183–194.
- [23] F. Berto, A. Campagnolo, P. Gallo, Brittle Failure of Graphite Weakened by V-Notches: A Review of Some Recent Results Under Different Loading

- Modes, *Strength Mater.* 47 (2015) 488–506. doi:10.1007/s11223-015-9682-7.
- [24] Z. Yosibash, A. Bussiba, I. Gilad, Failure criteria for brittle elastic materials, *Int. J. Fract.* 125 (2004) 307–333.
- [25] M.H. El Haddad, T.H. Topper, K.N. Smith, Prediction of non propagating cracks, *Eng. Fract. Mech.* 11 (1979) 573–584.
- [26] P. Lazzarin, C.M. Sonsino, R. Zambardi, A notch stress intensity approach to assess the multiaxial fatigue strength of welded tube-to-flange joints subjected to combined loadings, *Fatigue Fract. Eng. Mater. Struct.* 27 (2004) 127–140.
- [27] P. Lazzarin, F. Berto, F.J. Gómez, M. Zappalorto, Some advantages derived from the use of the strain energy density over a control volume in fatigue strength assessments of welded joints, *Int. J. Fatigue.* 30 (2008) 1345–1357.
- [28] H.-J. Christ, C.K. Wamukwamba, H. Mughrabi, The effect of mean stress on the high-temperature fatigue behaviour of SAE 1045 steel, *Mater. Sci. Eng. A.* 234-236 (1997) 382–385.
- [29] P. Lazzarin, F. Berto, From Neuber's Elementary Volume to Kitagawa and Atzori's Diagrams: An Interpretation Based on Local Energy, *Int. J. Fract.* 135 (2005) L33–L38.
- [30] K. Tanaka, Engineering formulae for fatigue strength reduction due to crack-like notches, *Int. J. Fract.* 22 (1983) 39–46.
- [31] D. Taylor, Geometrical effects in fatigue: a unifying theoretical model, *Int. J. Fatigue.* 21 (1999) 413–420.
- [32] M.H. El Haddad, K.N. Smith, T.H. Topper, Fatigue Crack Propagation of Short Cracks, *J. Eng. Mater. Technol.* 101 (1979) 42.
- [33] P. Livieri, P. Lazzarin, Fatigue strength of steel and aluminium welded joints based on generalised stress intensity factors and local strain energy values, *Int. J. Fract.* 133 (2005) 247–276.
- [34] P. Lazzarin, P. Livieri, F. Berto, M. Zappalorto, Local strain energy density and fatigue strength of welded joints under uniaxial and multiaxial loading, *Eng. Fract. Mech.* 75 (2008) 1875–1889.
- [35] P. Lazzarin, R. Zambardi, The Equivalent Strain Energy Density approach reformulated and applied to sharp V-shaped notches under localized and generalized plasticity, *Fatigue Fract. Eng. Mater. Struct.* 25 (2002) 917–928.
- [36] P. Fernandez-Zelaia, R.W. Neu, Influence of notch severity on

- thermomechanical fatigue life of a directionally solidified Ni-base superalloy, *Fatigue Fract. Eng. Mater. Struct.* 37 (2014) 854–865.
- [37] P. Lazzarin, M. Zappalorto, F. Berto, Averaged strain energy density and  $J$ -integral for U- and blunt V-shaped notches under torsion, *Int. J. Fract.* 188 (2014) 173–186.
- [38] D. Radaj, State-of-the-art review on the local strain energy density concept and its relation to the  $J$ -integral and peak stress method, *Fatigue Fract. Eng. Mater. Struct.* 38 (2015) 2–28.
- [39] Z. He, A. Kotousov, F. Berto, Effect of vertex singularities on stress intensities near plate free surfaces, *Fatigue Fract. Eng. Mater. Struct.* 38 (2015) 860–869.
- [40] P. Gallo, F. Berto, Some considerations on the  $J$ -Integral under elastic-plastic conditions for materials obeying a Ramberg-Osgood law, *Phys. Mesomech.* 18 (2015) 298–306.

## 6. Estimation of strains and stresses at blunt V-notches under creeping condition

*P. Gallo, F. Berto, G. Glinka, Generalized approach to estimation of strains and stresses at blunt V notches under non-localized creep, Fatigue Fract. Engng. Mater. Struct. In Press, DOI: 10.1111/ffe.12374*

### Highlights

Geometrical discontinuities such as notches need to be carefully analyzed by engineers because of the stress concentration generated by them. Notches become even more important when the component is subjected, in service, to very severe conditions, such as the high temperature fatigue and imposed visco-plastic behavior such as creep. The knowledge of strains and stresses in such stress concentration zones is essential for efficient and safe design process.

The aim of this chapter is to present an improvement and extension of the existing notch tip creep stress-strain analysis method developed by Nuñez and Glinka, validated for U-notches only, to a wide variety of blunt V-notches.

The key in getting the extension to blunt V-notches is the substitution of the Creager-Paris equations with the more generalized Lazzarin-Tovo solution allowing a unified approach to the evaluation of linear elastic stress fields in the neighborhoods of both cracks and notches.

Numerous examples have been analyzed up to date and the stress fields obtained according to the proposed method were compared with appropriate finite element data resulting in a very good agreement.

In view of the promising results discussed below, a possible further extension to sharp V-notches and cracks introducing the concept of the strain energy density will be presented in the next §Chapter 7.



## 6.1 Introduction

Analysis and design of mechanical engineering objects means the application of acceptable engineering procedures. Such procedures are used to verify the integrity and/or functionality of the entire object and its components. Because of technological progress demanding service conditions, engineering components are becoming more complex geometry-wise including various geometrical discontinuities (e.g. notches) that generate localized high stress concentration zones [1–4]. Therefore geometrical discontinuities in a component are regions which have to be carefully considered by the engineers. They become even more important when, in operating conditions, the component is subjected to very demanding conditions such as high temperature fatigue [5,6]. This situation is currently very important when considering the aerospace and automotive industry.

The high temperature environment induces time and temperature dependent deformations resulting in a nonlinear stress-strain response such as creep (viscoplasticity). When the creep phenomena are localized or concentrated in a small region near the notch root, they can be considered as localized-creep cases. However, creep strains (although low) can also occur away from the notch tip, resulting in a non-localized creep. Non-localized (or gross) creep condition refers to situations in which the far stress field also experiences some creep and this may contribute to more intense creeping around the notch tip. This situation is not so rare in components working at high temperature. Numerous components in different applications are subjected to non-localized creep, such as power plant, gas turbine and nuclear pressure vessel industry. Gas turbine blades and disks are particularly subjected to creep phenomenon. Considering power plant, between start-up and shut-down there is a period of on-load running. The material at the surface of the stress concentrating feature may be at constant strain during this period, and stress relaxation will take place by creep. In many other cases, pressure or centrifugal stresses may also be present, resulting in general creep deformation [7]. If these components are subjected to high temperature during constant load situation, non-localized creep must be considered.

To the best of the authors' knowledge only a limited number of solutions concerning localized time-dependent creep-plasticity problems are available in literature. Chaudonneret and Culie (1985) proposed an extension of Neuber's theory [9] in

order to evaluate instantaneous viscoplastic notch-root behaviour under arbitrary type of loading (i.e. creeping around notches). Several examples were presented and compared with results of numerical viscoelastic computations. However, the procedure has shown to be computationally intense. Kubo and Ohji [10] extended the concept of small-scale creep to notch problems, to develop a method for predicting the stress and strain behavior at notches under plane-strain axi-symmetric conditions. It must be underlined that, in spite of good results obtained, their method was limited to strictly localized creep, neglecting the creep effect far from the notch tip. In the work of Moftakhar et al. [11], another method for predicting localized time-dependent creep stresses and strains was presented. That method was based on strain energy density considerations: it was assumed that under steady load the total strain energy density at the notch tip does not change in time even if creep is taking place around the notch tip. Therefore the strain energy density at the notch tip can be obtained from the linear elastic solution even if the creep phenomenon is in reality taking place around the notch tip. The solution method has been derived in a general form so that it may be applied to multiaxial notch tip stress states. Creep strains at the notch tip based on the strain energy equivalence have shown good agreement when compared with appropriate finite element data. The computation time for calculating notch tip stresses and strains in the latest case was shorter than that one required for the finite element analysis. In the work by Härkegård and Sørbo [12], a differential form of Neuber's rule, originally proposed by Chaudonneret and Culie [8], has been re-formulated with the purpose to analyze a generic visco-plastic notch problems. It was shown that the stress-strain history at the notch root in a viscoplastic body can be determined directly from the elastic stress-strain response, provided that far-field visco-plastic strains could be neglected. Predictions were in good agreement with results of detailed finite element analyses.

Recently, Zhu et al. [13] presented singular fields near sharp V-notch for power law creep material under plane strain condition. The theoretical solution, based on the C-integral, and the iterative method were compared with numerical simulation. Under steady state condition, the absolute singular order only depends on the creep exponent and the V-notch angle, and becomes larger with the decrease of the exponent and the angle. But for the transient, the order corresponds to the time either.



Nuñez and Glinka have recently presented in one of their papers [14] a solution for non-localized creep strains and stresses at the notch root, based on the linear-elastic stress state, the constitutive law and the material creep model. The method was derived by using the Neuber total strain energy density rule [9]. This approach yielded very good results when applied to U-notches ( $2\alpha=0$  and  $\rho\neq 0$ ). The aim of this chapter is to introduce an extension of the method proposed by Nuñez and Glinka [14] to blunt V-notches. The base of the extension to blunt V-notches is the substitution of the Creager-Paris equations [15] with the more general Lazzarin-Tovo equations [16] allowing a unified evaluation of linear elastic stress fields in the neighbourhood of both cracks and notches.

The new methodology extended for V-notches, preceded by a brief introduction of the original Nuñez and Glinka [14] method and Lazzarin-Tovo's equations [16], is discussed below. The new approach has been illustrated with a number of examples showing good agreement with a set validation data obtained from detailed FE analyses. The proposed method permits a fast evaluation of the stresses and strains at notches under non-localized creeping condition, without the use of complex and time-consuming FE non-linear analyses. The obtained stresses and strains can be used as input parameters for life prediction creep models based on local approaches. Some comments on the extension of the method to sharp V-notches and cracks based on the average strain energy density concept, as well as on the applicability of linear elastic approaches under creeping conditions, are discussed at the end.

## **6.2 Nuñez and Glinka method for the evaluation of stresses and strains under non-localized creep**

The method presented in the paper by Nuñez and Glinka [14] is based on the Neuber [9] concept and it was applied to stress-strain analysis of notched bodies with U-notches experiencing non-localized creep deformation. As stated in the introduction, the non-localized creep condition refers to a situation in which the creep takes place not only locally around the notch tip, but the far field is experiencing some creep as well. This phenomenon can be interpreted as an additional amount of energy to be added at the notch tip because of the constraint loss imposed. It will be discussed in

detail later in this section. This contribution representing the non-localized effect is introduced into the original Neuber's rule for time dependent problems.

In general, the extension of Neuber's rule to time dependent plane stress problems can be summarized as follows:

$$\Omega = \sigma_{22}^e \varepsilon_{22}^e = \sigma_{22}^0 \varepsilon_{22}^0 = \sigma_{22}^t \varepsilon_{22}^t \quad (1)$$

where  $\sigma_{ij}^e$  are the hypothetical stress components obtained from the linear elastic analysis and  $\varepsilon_{ij}^e$  are the corresponding elastic strain components,  $\sigma_{ij}^0$  and  $\varepsilon_{ij}^0$  are the actual elastic-plastic stress and strain components,  $\sigma_{22}^t$  and  $\varepsilon_{22}^t$  are the respective time dependent notch tip stress and strain components. Equation (1) holds when inelastic deformations occur locally, including creep relaxation. This is due to the invariance of the total strain energy density at the notch tip ( $\Omega = \sigma_{ij}^e \varepsilon_{ij}^e$ ) discussed by Moftakhar et al. [11].

In case of non-localized creep, far field creep contribution has to be considered and Eq. (1) assumed the following form:

$$\sigma_{22}^0 \varepsilon_{22}^0 + K_{\Omega} \sigma_{22}^f \varepsilon_{22}^{cf} = \sigma_{22}^t \varepsilon_{22}^t \quad (2)$$

Where  $\sigma_{22}^f \varepsilon_{22}^{cf}$  represents the total strain energy density due to local and far field creep.

The far field stress in the case of a body subjected to pure axial load is assumed to be equal to the elastic stress found at a distance of three times the notch radius. In the case of pure bending load, instead, the far field stress is defined as one-half of the nominal simple bending stress. The distance from the coordinate system origin at which the far field contribution is evaluated is called  $d$ .

The  $K_{\Omega}$  parameter [11] is the strain energy concentration factor defined as the ratio of the total strain energy density at the notch tip obtained from the linear elastic analysis to the total strain energy density at the distance  $d$  in the far field, also obtained from the linear elastic solution. This parameter takes into account the energy contribution at the notch tip due to the gross creeping condition. In fact, as briefly mentioned at the beginning of the present section, the non-localized creep can be interpreted as an additional amount of energy to be added at the notch tip, because

of the constraint loss imposed. It can be assumed that the total strain energy density changes occurring in the far field produce identical but magnified effects at the notch tip. For this reason, the total strain energy density concentration factor is introduced in order to magnify in the appropriate way the energy at the notch tip. The introduction of this parameter and of the far field stress and strain contribution in the Neuber's time dependent formulation is the main difference within the non-localized and localized creep formulation, that, instead, can be easily derived directly by extending the Neuber's rule [14].

Due to the complexity of differential equations derived analytically for the notch stress-strain creep problem, Moftakhar et al. [11] proposed a special time integration method necessary for obtaining the numerical solution. Namely the integration time period was divided into a finite number of discrete steps,  $\Delta t_n$ , and then solutions were generated for subsequent time steps. Such an approach resulted in a set of equations formulated in-incremental form. The set of equations to be solved for each increment are [14]:

- The creep strain increment at the notch tip at step  $n$ :

$$\Delta \varepsilon_{22}^{c_n} = \Delta t_n \cdot \dot{\varepsilon}_{22}^c(\sigma; t) \quad (3)$$

This is the incremental form of the creep law used in the proposed procedure, where  $\dot{\varepsilon}_{22}^c(\sigma; t) = A\sigma^\alpha t^\beta$  is the Norton creep power law [17].

- The stress decrement at the notch tip occurred due to creep at the step  $n$ :

$$\Delta \sigma_{22}^{f_n} = \frac{(K_\Omega C_p) \sigma_{22}^{f_0} \Delta \varepsilon_{22}^{c_n} - \sigma_{22}^{f_{n-1}} \Delta \varepsilon_{22}^{c_n}}{\frac{2}{E} \sigma_{22}^{f_{n-1}} + \varepsilon^{p_0} + \varepsilon_{22}^{c_n}} \quad (4)$$

with the introduction of the Glinka plastic zone correction factor  $C_p$  [18]. The correction factor  $C_p$  is a function of the plastic zone size  $r_p$  and the plastic zone increment  $\Delta r_p$ . It compensates for the stress redistribution occurring at the notch tip due to the plastic yielding;  $K_\Omega$  is the strain energy concentration factor [11] discussed previously;  $\sigma_{22}^{f_0}$  is the far field stress at the time  $t = 0$  (assumed to be constant during the hold time);  $\sigma_{22}^{f_{n-1}}$  is the stress at the notch tip at time  $t$  for the

step  $n-1$ ;  $\Delta\varepsilon_{22}^{cf_n}$  is the incremental far field creep strain while  $\varepsilon^{p0}$  and  $\varepsilon_{22}^{c_n}$  are the plastic strains at the time  $t=0$  and the creep strain at the notch tip at the step  $n$ , respectively. It must be underlined that the time-depending strain can be considered as the composition of the elastic, initial plastic and the creep strain contribution. In the last equation, the effect of the non-localized creep becomes evident and is represented by the contribution of the far field in terms of  $(K_{\Omega}C_p)\sigma_{22}^{f0}\Delta\varepsilon_{22}^{cf_n}$ . Neglecting this term one obtains the localized creep formulation.

- Increment of the total strain:

$$\Delta\varepsilon_{22}^{t_n} = \Delta\varepsilon_{22}^{c_n} - \frac{\Delta\sigma_{22}^{t_n}}{E} \quad (5)$$

Defined as the difference between the creep strain increment at the step  $n$  and the elastic strain (replaced by stress according to the Hooke law) at the time  $t$  for the step  $n$ .

The general stepwise procedure to generate the solution is:

1. Determine the notch tip stress,  $\sigma_{22}^e$ , and strain,  $\varepsilon_{22}^e$ , using the linear-elastic analysis.
2. Determine the elastic-plastic stress,  $\sigma_{22}^0$ , and strain,  $\varepsilon_{22}^0$ , using the Neuber rule [9] or other methods (e.g. ESED [19], finite element analysis).
3. Begin the creep analysis by calculating the increment of creep strain,  $\Delta\varepsilon_{22}^{c_n}$ , from Eq. (3), for a given time increment  $\Delta t_n$ . The selected creep hardening rule has to be followed.
4. Determine the decrement of stress,  $\Delta\sigma_{22}^{t_n}$ , from Eq. (4), due to the previously determined increment of creep strain,  $\Delta\varepsilon_{22}^{c_n}$ .
5. For a given time increment  $\Delta t_n$ , determine from Eq. (5) the increment of the total strain at the notch tip,  $\Delta\varepsilon_{22}^{t_n}$ .
6. Repeat steps from 3 to 5 over the required time period.

The method can be easily programmed and yields to good results for various creep data and creep hardening models, especially for notched components under constant load.

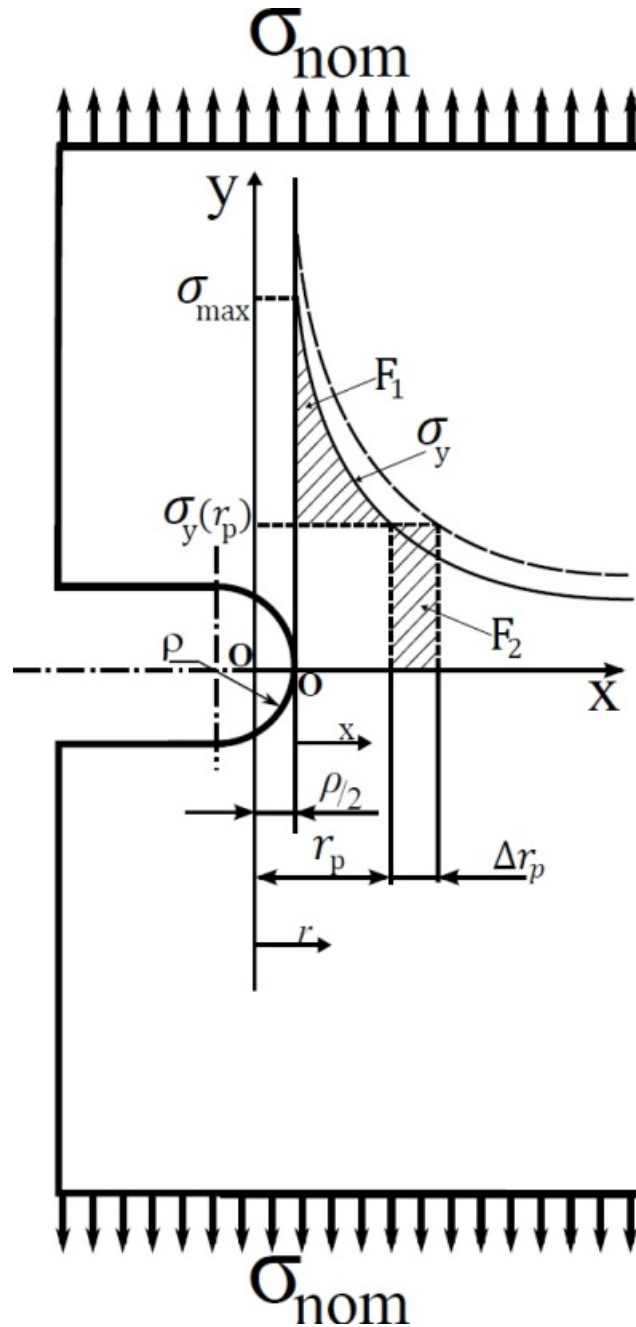


**Fig. 1:** Coordinate system and symbols used for the elastic stress field redistribution for U-shaped notches

However, the method can be also extended to variable loading processes. More details concerning the theoretical formulation and the description of the solution algorithm are available in the given references [14].

Regarding the applicability of the method, the main points are the definition of the plastic zone correction factor  $C_p$ , that is a function of plastic zone size  $r_p$  and plastic zone increment  $\Delta r_p$ . Once assumed the Creager-Paris stress distribution [15], for  $\theta=0$  in Cartesian coordinates:

$$\begin{Bmatrix} \sigma_x \\ \sigma_y \end{Bmatrix} = \frac{K_I}{\sqrt{2\pi r}} \begin{bmatrix} 1 - \frac{\rho}{2r} \\ 1 + \frac{\rho}{2r} \end{bmatrix} \quad (6)$$

$$\sigma_z = 0 \quad (\text{plane stress})$$

$$\sigma_z = \nu(\sigma_x + \sigma_y) \quad (\text{plane strain})$$

The origin of the coordinate system is centred at a distance from the notch tip equal to  $\rho/2$ , where  $\rho$  is the notch tip radius, as shown in Fig.1. Imposing  $r = \rho/2$ , one obtains the peak stress  $\sigma_{max}$  and a good approximation of the stress concentration factor  $K_t$ :

$$\sigma_{max} = \frac{2K_I}{\sqrt{\pi\rho}} \quad (7)$$

$$K_t = \frac{\sigma_{max}}{\sigma_{nom}} = \frac{2K_I}{\sigma_{nom}\sqrt{\pi\rho}} \quad (8)$$

$$K_I = \frac{K_t\sigma_{nom}\sqrt{\pi\rho}}{2} \quad (9)$$

Substituting Eq. (9) into Eqs. (6), one obtains the stress distribution as a function of the stress concentration factor  $K_t$  and the notch tip radius  $\rho$ :

$$\begin{cases} \sigma_x \\ \sigma_y \end{cases} = \frac{K_t \sigma_{nom}}{2\sqrt{2}} \begin{bmatrix} \left(\frac{\rho}{r}\right)^{1/2} - \frac{1}{2}\left(\frac{\rho}{r}\right)^{3/2} \\ \left(\frac{\rho}{r}\right)^{1/2} + \frac{1}{2}\left(\frac{\rho}{r}\right)^{3/2} \end{bmatrix} \quad (10)$$

It is suggested using a stress concentration factor  $K_t$  obtained independently from Eq.(8), in order to improve the solution of Eqs.(10).

Referring to Fig.1, considering the Mises Yield Criterion [20] that is:

$$\sigma_{ys} = \sqrt{\sigma_x^2 - \sigma_x \sigma_y + \sigma_y^2} \quad (11)$$

and introducing Eqs. (10) into Eq. (11), it is possible to obtain a first approximation of  $r_p$  solving numerically the following Equation:

$$\sigma_{ys} = \frac{K_t \sigma_{nom}}{2\sqrt{2}} \left[ \frac{\rho}{r_p} + \frac{3}{4} \left( \frac{\rho}{r_p} \right)^3 \right]^{1/2} \quad (12)$$

Once  $r_p$  is known, the force  $F_I$  (depicted in Fig. 1) can be evaluated by means of the following integral:

$$F_I = \int_{\rho/2}^{r_p} \sigma_y dr - \sigma_y(r_p) \cdot \left( r_p - \frac{1}{2}\rho \right) \quad (13)$$

Where  $\sigma_y(r_p)$  is the stress evaluated at a distance  $r = r_p$ , through Eqs. (10).

Due to the plastic yielding at the notch tip, the force  $F_I$  cannot be evaluated directly in the plastic zone define by  $r_p$ . But in order to satisfy the equilibrium conditions,  $F_I$  has to be carried through by the material beyond the plastic zone  $r_p$ . For this reason, stress redistribution occurs, increasing the plastic zone by the increment  $\Delta r_p$ .

It should be specified that the stress  $\sigma_y(r_p)$  is assuming to be constant inside the plastic zone, that means elastic-perfectly plastic behaviour of the material has been

assumed. Therefore the correction factor may slightly overestimate the effect of stress redistribution.

Because  $F_1 = F_2 = \sigma_y(r_p) \cdot \Delta r_p$  (all the variables are depicted in Fig.1), the plastic zone increment  $\Delta r_p$  can be expressed as the ratio between  $F_I$  and  $\sigma_y$  evaluated at a distance equal to the previously calculated  $r_p$ . By simple substitutions one obtains the following explicit form of plastic increment for tension load case [18]:

$$\Delta r_p = \frac{F_1}{\sigma_y(r_p)} = \rho \frac{\left[ 2(r_p / \rho)^{1/2} - (\rho / r_p)^{1/2} \right]}{\left[ (\rho / r_p)^{1/2} + 1/2(\rho / r_p)^{3/2} \right]} - \rho \left( \frac{r_p}{\rho} - \frac{1}{2} \right) \quad (14)$$

At last, the correction factor for the energy density  $C_p$  at the notch tip can be written as follows, for tension load case:

$$C_p = 1 + \frac{\Delta r_p}{r_p} = 1 + \left( \frac{\rho}{r_p} \right) \left\{ \frac{\left[ 2(r_p / \rho)^{1/2} - (\rho / r_p)^{1/2} \right]}{\left[ (\rho / r_p)^{1/2} + 1/2(\rho / r_p)^{3/2} \right]} - \left( \frac{r_p}{\rho} - \frac{1}{2} \right) \right\} \quad (15)$$

It should be noted that the procedure to determine the plastic zone adjustment is analogous to that proposed by Irwin [21] for sharp notches and cracks.

More details and the bending load case are exhaustively treated by Glinka et al. [18].

### 6.3 Extension of Nuñez-Glinka Method to blunt V-Notches

The key to extend the Nuñez-Glinka method also to blunt V-notches is the introduction of the Lazzarin-Tovo equations [16]. Lazzarin and Tovo proposed in the 1996 an unequivocal mathematical justified approach for notched and cracked components, with parallel or V-shaped edges. General expressions of the stress field were proposed, taking into account both the notch tip radius and opening angle variations. It must be pointed out that, the stress fields valid for sharp cracks [22], V-cracks [23], notch tip radii higher than zero [15] and parallel edges [24] can be derived from the general solution, imposing approximate values to the free parameters. The Lazzarin-Tovo equations, in the presence of a traction loading,



along the bisector, can be expressed as follows, as a function of the maximum stress (see Fig. 2):

$$\begin{cases} \sigma_\theta \\ \sigma_r \end{cases} = \frac{\sigma_{max}}{4} \left( \frac{r}{r_0} \right)^{\lambda_1 - 1} \begin{bmatrix} (1 + \lambda_1) + \chi_1(1 - \lambda_1) + \left( \frac{r}{r_0} \right)^{\mu_1 - \lambda_1} [(3 - \lambda_1) - \chi_1(1 - \lambda_1)] \\ (3 - \lambda_1) - \chi_1(1 - \lambda_1) - \left( \frac{r}{r_0} \right)^{\mu_1 - \lambda_1} [(3 - \lambda_1) - \chi_1(1 - \lambda_1)] \end{bmatrix} \quad (16)$$

Where  $\sigma_{max}$  can be expressed as a function of stress concentration factor  $K_t$  and the applied load  $\sigma_{nom}$ ,

$$\sigma_{max} = K_t \sigma_{nom} \quad (17)$$

The notch radius,  $\rho$ , and the origin of the coordinate system,  $r_0$ , are related by the following equation:

$$\rho = \frac{q \cdot r_0}{q - 1} \quad (18)$$

where  $q = \frac{2\pi - 2\alpha}{\pi}$ .

When  $q=2$  (and so  $\alpha=0$ ) the origin of the coordinate system is centred at a distance  $r_0 = \rho/2$  behind the notch tip, and the Lazzarin-Tovo equations immediately return the Creager-Paris equations [15]. Moreover, when  $r = r_0$  one determines the stress concentration factor  $K_t$ , and the elastic peak stress  $\sigma_{max}$ . In Table 1, the values of the parameters introduced previously are reported for the main opening angles under mode I loading.

The main steps to extend the method to blunt V-Notches can be summarised as follows:

- Assumption of Lazzarin-Tovo equations to describe the stress distribution ahead the notch tip instead of Creager-Paris equations;

- Calculation of the origin of the coordinate system,  $r_0$ , as a function of the opening angle and notch radius, as described by Eq. (18);
- Re-definition of the plastic zone correction factor  $C_p$  that is a function of plastic zone size  $r_p$  and plastic zone increment  $\Delta r_p$ ;

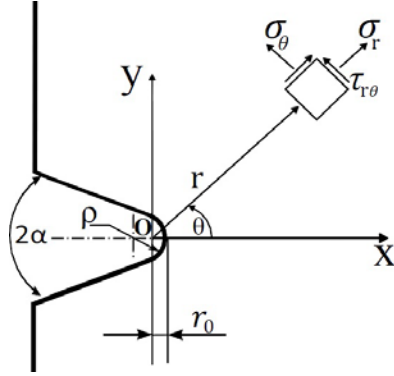


**Fig. 2:** Coordinate system and symbols used for the stress field components in Lazzarin-Tovo equations

**Table 1.** Reference values for (mode I and mode II) power of the stress at the free surface

$2\alpha$ [°]	$\lambda_1$	$\mu_1$	$\chi_1$
0	0.5	-0.5	1
30	0.5014	-0.4057	1.0707
60	0.5122	-0.4057	1.3123
90	0.5448	-0.3449	1.8414
120	0.6157	-0.2678	3.0027
135	0.6736	-0.2198	4.1530

The definition of the parameters  $C_p$ ,  $r_p$  and  $\Delta r_p$  is not so different as clearly reported by Glinka [18], except for the assumption of different stress distribution equations. In fact, once assuming the Lazzarin-Tovo equations, these variables are redefined automatically as briefly reported hereafter. Referring to Fig. 3, considering the Mises Yield Criterion in polar coordinates that is:

$$\sigma_{ys} = \sqrt{\sigma_r^2 - \sigma_r\sigma_\theta + \sigma_\theta^2} \quad (19)$$

and introducing Eqs. (16) into Eq. (19), it is possible to obtain a first approximation of  $r_p$  that can be solved numerically.

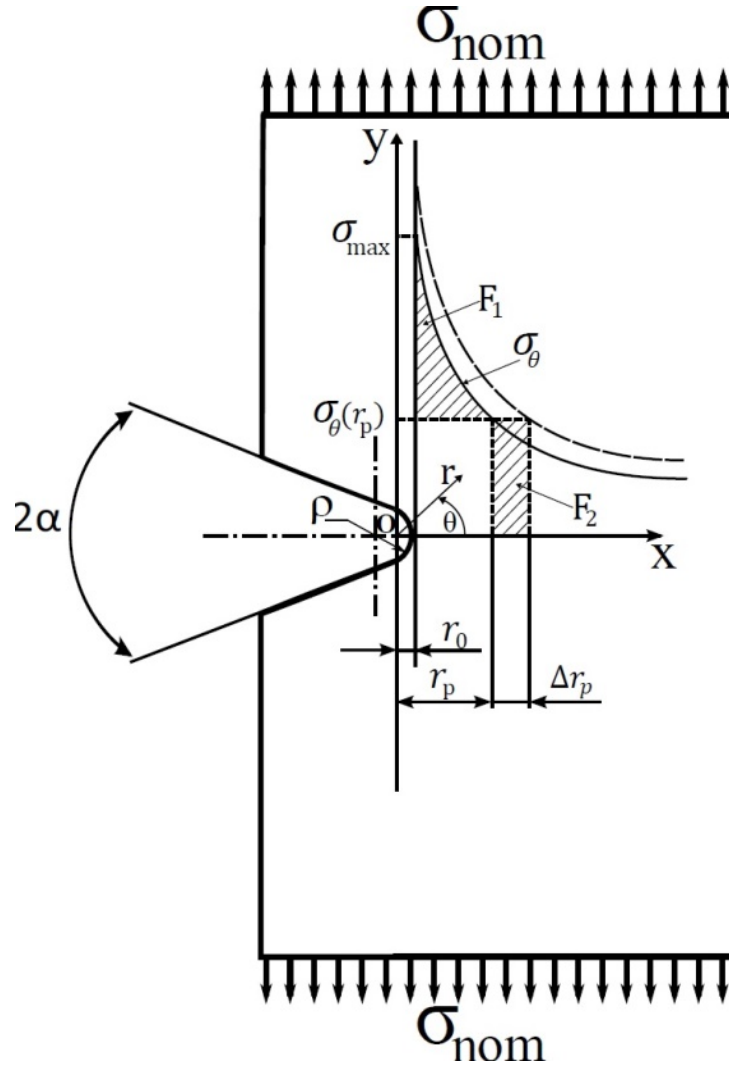


**Fig. 3:** Coordinate system and symbols used for the elastic stress field redistribution for blunt V-notches

Once  $r_p$  is known,  $F_1$  can be evaluated by means of the following integral:

$$\begin{aligned}
 F_1 &= \int_{r_0}^{r_p} \sigma_{\theta} dr - \sigma_{\theta}(r_p) \cdot (r_p - r_0) = \\
 &= \frac{K_t \sigma_{nom}}{4} \left\{ (r_0 - r_p) \left( \frac{r_p}{r_0} \right)^{\lambda_1 - 1} \left[ (\lambda_1 - 1) + \chi_1 (1 - \lambda_1) \left[ 1 - \left( \frac{r_p}{r_0} \right)^{\mu_1 - \lambda_1} \right] + (3 - \lambda_1) \left( \frac{r_p}{r_0} \right)^{\mu_1 - \lambda_1} \right] + \right. \\
 &\quad \left. \left[ (\lambda_1 + 1) + \chi_1 (1 - \lambda_1) \right] \left[ r_0 - r_p \left( \frac{r_p}{r_0} \right)^{\lambda_1 - 1} \right] + \left[ \chi_1 (1 - \lambda_1) - (3 - \lambda_1) \right] \left[ r_0 - r_p \left( \frac{r_p}{r_0} \right)^{\mu_1 - 1} \right] \right\} \quad (20) \\
 &\quad \left. \begin{matrix} \lambda_1 & \mu_1 \end{matrix} \right\}
 \end{aligned}$$

Where  $\sigma_\theta(r_p)$  is:

$$\sigma_\theta(r_p) = \frac{K_t \sigma_{nom}}{4} \left(\frac{r_p}{r_0}\right)^{\lambda_1-1} \left[ (1+\lambda_1) + \chi_1(1-\lambda_1) + \left(\frac{r_p}{r_0}\right)^{\mu_1-\lambda_1} [(3-\lambda_1) - \chi_1(1-\lambda_1)] \right] \quad (21)$$

The stress  $\sigma_y(r_p)$  is still be considered to be constant inside the plastic zone (elastic-perfectly plastic behavior) as commented also in the previous §Section 6.2. It must be underlined that, unlike what proposed by Glinka [18], in this case the lower integration limit is  $r_0$ , that depends on the opening angle and notch tip radius.

As already explained in §Section 6.2, due to the plastic yielding at the notch tip, in order to satisfy the equilibrium conditions,  $F_I$  has to be carried through by the material beyond the plastic zone  $r_p$  and a stress redistribution occurs, increasing the plastic zone by the increment  $\Delta r_p$ .

Since  $F_1 = F_2 = \sigma_\theta(r_p) \cdot \Delta r_p$ , the plastic zone increment can be expressed as the ratio between  $F_I$  and  $\sigma_\theta$  evaluated (through Lazzarin-Tovo equations) at a distance equal to the previously calculated  $r_p$ :

$$\Delta r_p = \frac{F_I}{\sigma_\theta(r_p)} \quad (22)$$

Substituting in Eq. (22) the formula given in Eq. (20) for  $F_I$ , and the explicit form of  $\sigma_\theta$  represented by Eq. (21), one obtains the expression for the evaluation of  $\Delta r_p$ :

$$\Delta r_p = \left\{ \left(\frac{r_p}{r_0}\right)^{1-\lambda_1} \left[ (r_0 - r_p) \left(\frac{r_p}{r_0}\right)^{\lambda_1-1} \left[ (\lambda_1 + 1) + \chi_1(1-\lambda_1) \left[ 1 - \left(\frac{r_p}{r_0}\right)^{\mu_1-\lambda_1} \right] + (3-\lambda_1) \left(\frac{r_p}{r_0}\right)^{\mu_1-\lambda_1} \right] \right. \right. \right. \\ \left. \left. \left. - \frac{[(\lambda_1 + 1) + \chi_1(1-\lambda_1)] \left[ r_0 - r_p \left(\frac{r_p}{r_0}\right)^{\lambda_1-1} \right]}{\lambda_1} + \frac{[\chi_1(1-\lambda_1) - (3-\lambda_1)] \left[ r_0 - r_p \left(\frac{r_p}{r_0}\right)^{\mu_1-1} \right]}{\mu_1} \right] \right\} \right\} \quad (23)$$

$$1 / \left\{ (\lambda_1 + 1) + \chi_1(1-\lambda_1) \left[ 1 - \left(\frac{r_p}{r_0}\right)^{\mu_1-\lambda_1} \right] + (3-\lambda_1) \left(\frac{r_p}{r_0}\right)^{\mu_1-\lambda_1} \right\}$$

At last, the plastic zone correction factor  $C_p$ , [18] is defined as:

$$\begin{aligned}
 C_p &= 1 + \frac{\Delta r_p}{r_p} = \\
 &= 1 + \left\{ \left( \frac{r_p}{r_0} \right)^{1-\lambda_1} \left[ (r_0 - r_p) \left( \frac{r_p}{r_0} \right)^{\lambda_1-1} \left[ (\lambda_1 + 1) + \chi_1 (1 - \lambda_1) \left[ 1 - \left( \frac{r_p}{r_0} \right)^{\mu_1 - \lambda_1} \right] + (3 - \lambda_1) \left( \frac{r_p}{r_0} \right)^{\mu_1 - \lambda_1} \right] + \right. \right. \\
 &\quad \left. \left. - \frac{[(\lambda_1 + 1) + \chi_1 (1 - \lambda_1)] \left[ r_0 - r_p \left( \frac{r_p}{r_0} \right)^{\lambda_1 - 1} \right]}{\lambda_1} + \frac{[\chi_1 (1 - \lambda_1) - (3 - \lambda_1)] \left[ r_0 - r_p \left( \frac{r_p}{r_0} \right)^{\mu_1 - 1} \right]}{\mu_1} \right] \right\} \cdot \quad (24) \\
 &1 / \left\{ r_p \left[ (\lambda_1 + 1) + \chi_1 (1 - \lambda_1) \left[ 1 - \left( \frac{r_p}{r_0} \right)^{\mu_1 - \lambda_1} + (3 - \lambda_1) \left( \frac{r_p}{r_0} \right)^{\mu_1 - \lambda_1} \right] \right] \right\}
 \end{aligned}$$

At this point, the general stepwise procedure to be followed to generate a solution is identical to that proposed by Nuñez and Glinka [14] and briefly reported in the §Section 6.2.

### 6.3.1 Examples of Nuñez-Glinka method applied to U-notches: considerations and comparison between numerical and FEM analysis

The Nuñez-Glinka method has been applied to an hypothetical plate weakened by lateral symmetric U-notches, under Mode I loading. The notch tip radius  $\rho$  and the notch depth  $a$  has been varied. Three values of the notch depth,  $a$ , has been considered: 10, 15 and 20 mm. Notch tip radius assumed for every notch depth three values: 0.01, 1 and 6 mm. Figure 4 depicts the considered geometry. The plate has a constant height,  $H$ , equal to 192 mm and a width,  $W$ , equal to 100 mm. The numerical results have been obtained thanks to the implementation of the method and its equations in the MATLAB<sup>®</sup> software. In order to conduct the analysis, it is necessary to define quantitatively the distance  $d$  (from the coordinate system origin) representing the “far field” at which the elastic contribution is evaluated. Glinka et al. [14] proposed a value of three times the notch radius in case of a body subjected to pure axial loading. However, this solution has been found to generate good results only when the notch tip radius is approximately bigger than 2 mm.

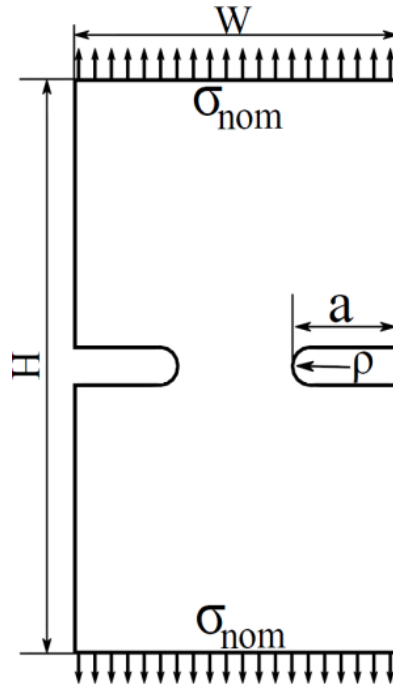


**Fig. 4:** Plates weakened by lateral symmetric V-notches

Since for smaller tip radius the generated  $d$  is too small, the distance at which the elastic contribution is evaluated has to be larger than three times the notch radius, in order to be in the elastic field. The correct values have been determined through a finite element linear elastic analysis applying the desired load, and are reported in Table 2 where  $d$  expresses the distance measured from the origin of the coordinates system, while  $x(\rho)$  expresses the distance measured from the notch tip as a function of the notch radius.

At the same time, a finite element analysis has been carried out through ANSYS code. The plate has been modelled with a Solid 8 node 183, and the plane stress condition is assumed.

The material elastic ( $E$ ,  $\nu$ ,  $\sigma_{ys}$ ) and creep ( $n$ ,  $B$ ) properties are reported in Table 3. The creep law has been modelled as follows:

$$\dot{\epsilon} = B \cdot \sigma^n \quad (25)$$

Equation (25) is very similar to that proposed by Nuñez-Glinka [14] by imposing the parameter  $\beta=0$ :

$$\dot{\epsilon} = A\sigma^\alpha t^\beta \quad (26)$$

**Table 2:** Distance  $d$  (measured from the origin of the coordinates system) at which the elastic contribution is evaluated;  $x$  is the distance from the notch tip

$\rho$ (mm)	$x(\rho)$ (mm)	$d$ (mm)
0.01	/	20
1	$18*\rho$	18.5
6	$3*\rho$	21

**Table 3:** Mechanical properties.  $E$  is the Young's modulus,  $\nu$  the Poisson's ratio,  $\sigma_{ys}$  the yield stress,  $n$  and  $B$  the creep exponent and the creep constant, respectively.

$E$ (MPa)	$\nu$	$\sigma_{ys}$ (MPa)	$n$	$B$ (MPa <sup>-n</sup> /h)
191000	0.3	275.8	5	1.8

A uniform load equal to 345 MPa has been applied. In order to simulate the creep relaxation, the load has been applied in different load steps: in the first one, the load has been applied instantaneously, approximately in  $t = 10^{-5}$  h; subsequently, in a second load step, it has been maintained constant for the desired time  $t$ . At regular intervals during the relaxation process, the stresses and strains were stored.

The obtained results are summarized in Figs. 5 to 7, listed as a function of the notch depth  $a$  for the sake of clarity. The results suggest a very good agreement between the numerical FEM values and the theoretical solution proposed in the present paper. The stresses of all of the considered geometries have been predicted correctly, also when considering the small tip radius of 0.01 mm. Furthermore the strains present a good agreement. For the sake of brevity, the tip radius case of 0.01 mm and the strains of all of the cases are omitted here.

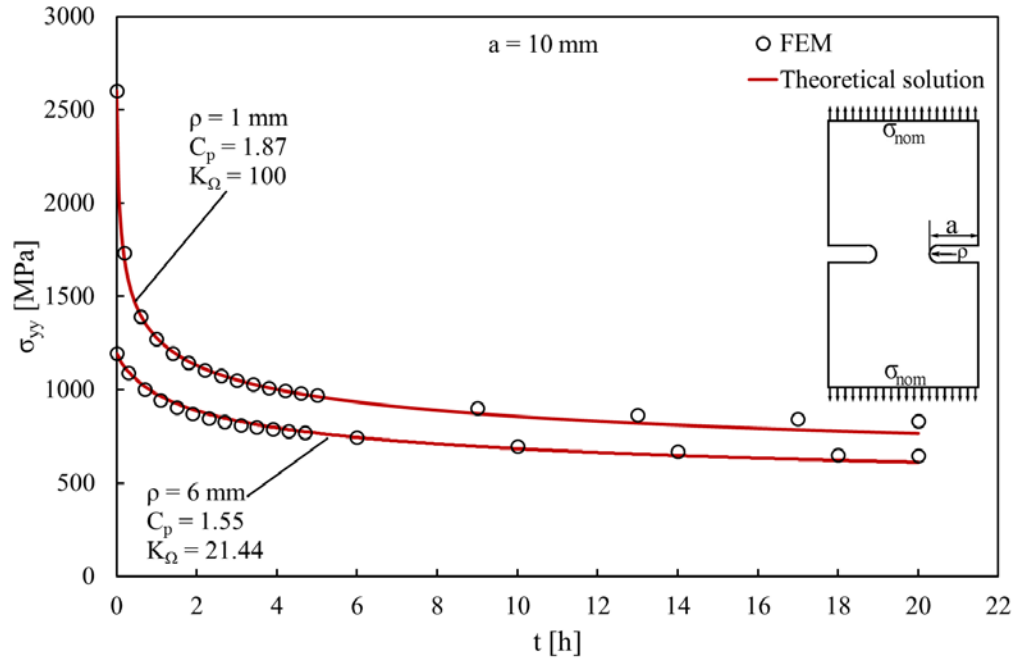


**Fig. 5:** Comparison between theoretical and FEM evolution of stresses as a function of time for U-notch geometry,  $a=10$  mm

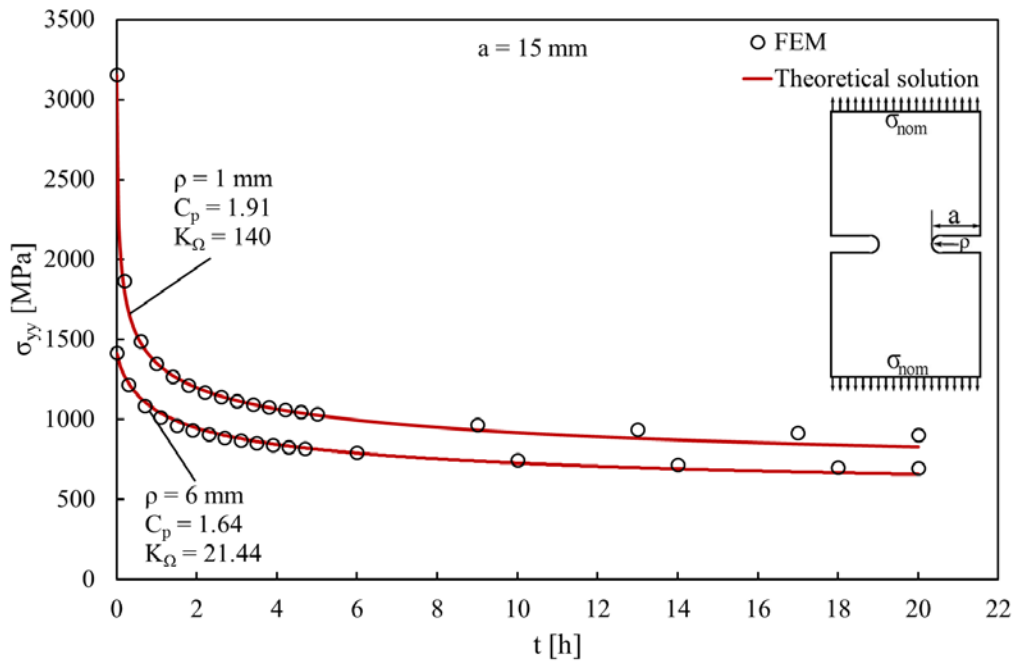


**Fig. 6:** Comparison between theoretical and FEM evolution of stresses as a function of time for U-notch geometry,  $a=15$  mm



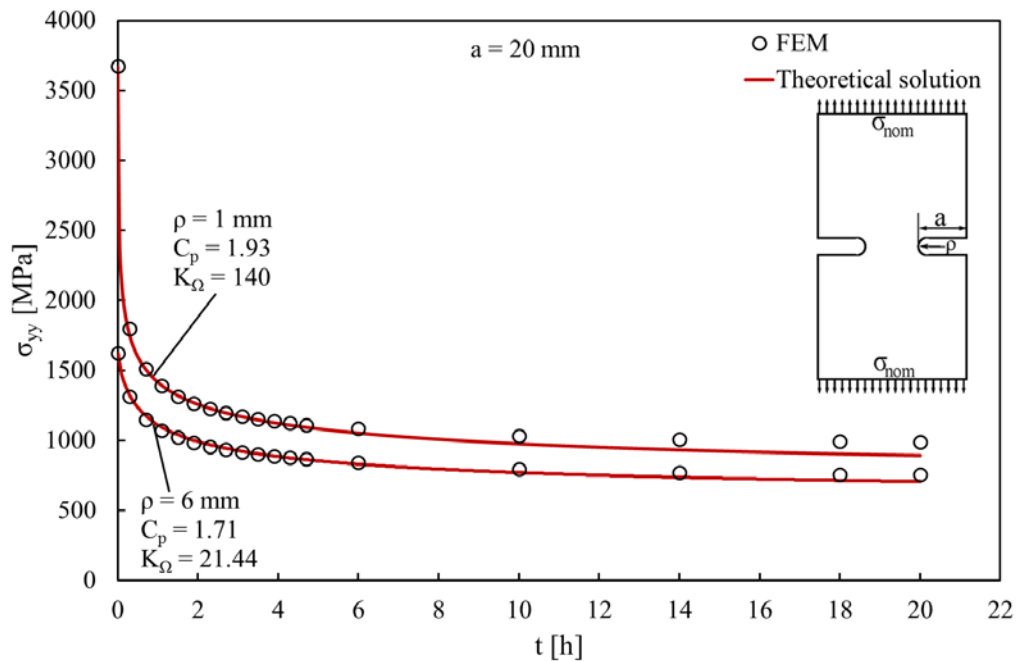


**Fig. 7:** Comparison between theoretical and FEM evolution of stresses as a function of time for U-notch geometry,  $a=20$  mm

#### 6.4 Examples of the new method applied to blunt V-notches: considerations and comparison between numerical and FE analysis

The proposed new method, based on the Lazzarin-Tovo equations [16], has been applied to an hypothetical plate weakened by lateral symmetric V-notches, under Mode I loading. The notch tip radius  $\rho$  and the opening angle  $2\alpha$  have been varied, while for the notch depth  $a$ , a constant value equal to 10 mm has been assumed.

Three values of the opening angle  $2\alpha$  have been considered:  $60^\circ$ ,  $120^\circ$  and  $135^\circ$ . The notch tip radius assumes for every opening angle three values: 0.5, 1 and 6 mm. Figure 8 depicts the considered geometry. The plate has a constant height,  $H$ , equal to 192 mm and a width,  $W$ , equal to 100 mm.

The numerical results have been obtained thanks to the implementation of the new developed method and its equations in the MATLAB<sup>®</sup> software. As discussed earlier, for small tip radius the distance at which the elastic contribution is evaluated has to be larger than three times the notch radius, in order to be in the elastic field. All these values have been determined through a finite element linear elastic analysis applying 345 MPa of nominal stress, and are reported in Table 4 where  $r$  expresses

the distance measured from the origin of the coordinates system (the so called  $d$  in the original formulation), while  $x(\rho)$  expresses the distance measured from the notch tip as a function of the notch radius.

A finite element analysis, has been carried out through ANSYS code following the modelling setting summarized in the previous §Section 6.3.1. The material elastic ( $E$ ,  $\nu$ ,  $\sigma_{ys}$ ) and creep ( $n$ ,  $B$ ) properties are reported in Table 3. The creep law has been modelled as reported in Eq. (25). The procedures to simulate the creep relaxation are the same presented previously: a load has been applied instantaneously in a first load step and subsequently, in a second load step, it has been maintained constant for the desired time  $t$ .

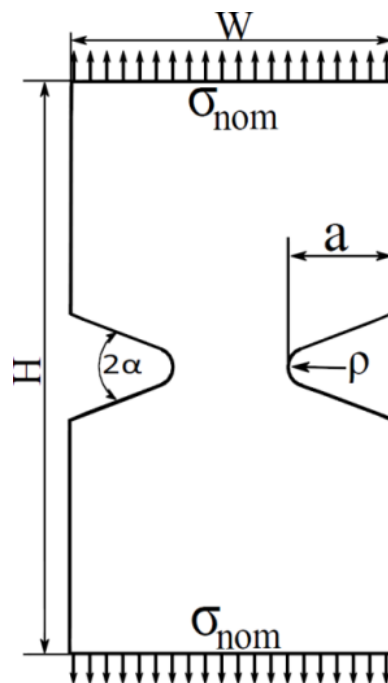


**Fig. 8:** Plates weakened by lateral symmetric V-notches

**Table 4:** Distance  $r$  (measured from the origin of the coordinates system) at which the elastic contribution is evaluated;  $x$  is the distance from the notch tip

$\rho$ [mm]	$x(\rho)$	$r$ [mm]		
		$2\alpha=60^\circ$	$2\alpha=135^\circ$	$2\alpha=120^\circ$
0.5	$40*\rho$	20.2	20.125	20.1
1	$18*\rho$	18.4	18.25	18.2
2	$9*\rho$	18.8	18.5	18.4
6	$3*\rho$	20.4	19.5	19.2

The obtained results are summarized in the Fig. 9 to 20 (page 118-124), ordered as a function of the notch opening angle  $2\alpha$  for the sake of clarity.

For the sake of brevity, only few examples are reported, showing the best and worse results. In details, Figs. 9 to 17 depict the stress relaxation for different opening angles and notch tip radii, while Figs. 18 to 20 give examples of the strain evolution considering an opening angle of  $120^\circ$  and notch radius equal to 0.5 mm, 1 mm and 6 mm, respectively. All the other cases present the same trend and are here omitted in order to not be redundant with the number of figures.

The theoretical results are in good agreement with the numerical FE values. All the stresses and strains as a function of time have been predicted with acceptable and quite limited errors.

However from the analyses emerges a repetitive behavior: regardless of the opening angle, the stresses of the notch radius of 0.5 mm are slightly overestimated, while the stresses of the notch radius of 6 mm are slightly underestimated. The best solution is shown for the notch radius equal to 1 mm. Moreover it is evident that the stresses present, after the relaxation phase, a plateau reached after almost the same time that is approximately 5 h, regardless of the specimen geometries. This means that the relaxation is most governed, as expected, by the creep-law, while the geometries only act on the values reached by stress and strain. Once the properties of the material is known or assumed, only one geometry must be analyzed, since the trend of stress and strain and the plateau are almost the same regardless of the specimen geometries. Considering the examples of the strain prediction depict in Fig. 18, 19, and 20, from the analyses it emerges a repetitive behavior, as previous stated for the stress evolution: the best solution is obtained for the notch radius of 0.5 mm, while the error increases as the notch-radius becomes bigger, with an overestimation of the strain values by the theoretical solution. The discrepancy within numerical and predicted solution can be considered acceptable for all the geometries with the exception of the last case where a notch tip radius of 6 mm is considered. For this configuration, the strain is clearly overestimated by 20%. This error is most likely due to different approximations introduced in the theoretical formulation, such as the assumption of the elastic-perfectly plastic behavior of the material inside the plastic zone and the employment of the Irwin's method to estimate the plastic radius. Among them, enhancement in the estimation of the plastic zone can lead to the major

improvements of the strain results. However, other researchers have found bigger discrepancy within finite element results and theoretical prediction when dealing with notches strains under creep condition. Just to name one example, Hatanaka et al. [25] studied the high temperature creep damage caused by voids generated at grain boundary. In that paper, notched components of 2.25%Cr-1% Mo steel, of which microstructure was prepared to be characteristic of the heat-affected zone in the welded joint by heat treatments, was creep-tested at 630°C. The stress/deformation state around the notch was calculated using finite element method. The strains obtained from experiment and FEM calculation were not in good agreement, showing a very high error. However, all the parameters related to the stress state (and also the minimum creep strain rate) were in good agreement comparing numerical/theoretical and experimental results.

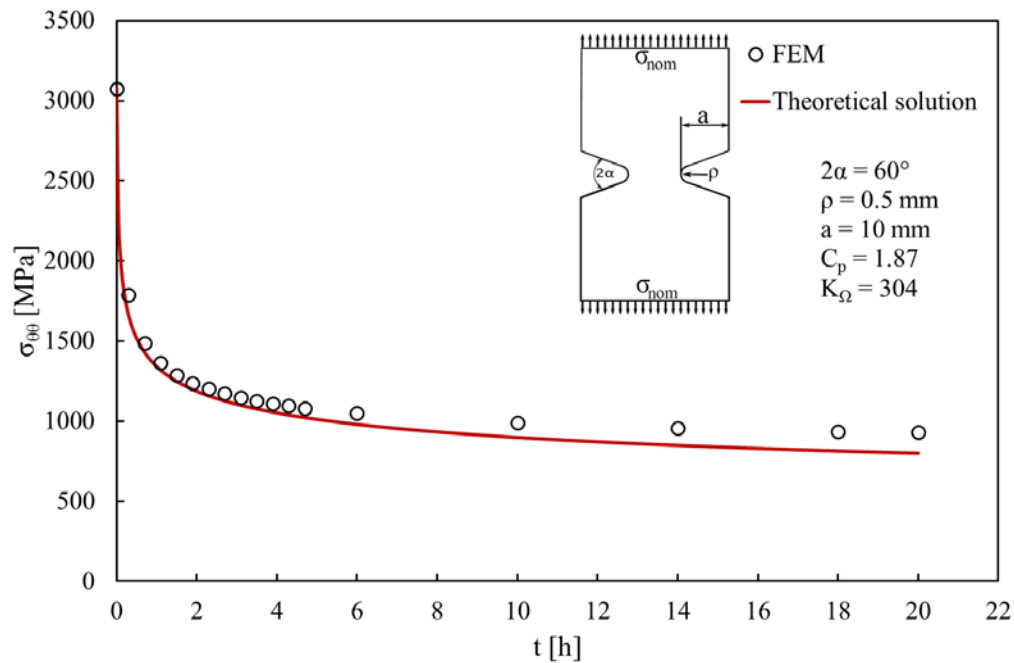


**Fig. 9:** Comparison between theoretical and FEM evolution of stresses as a function of time for V-notch geometry

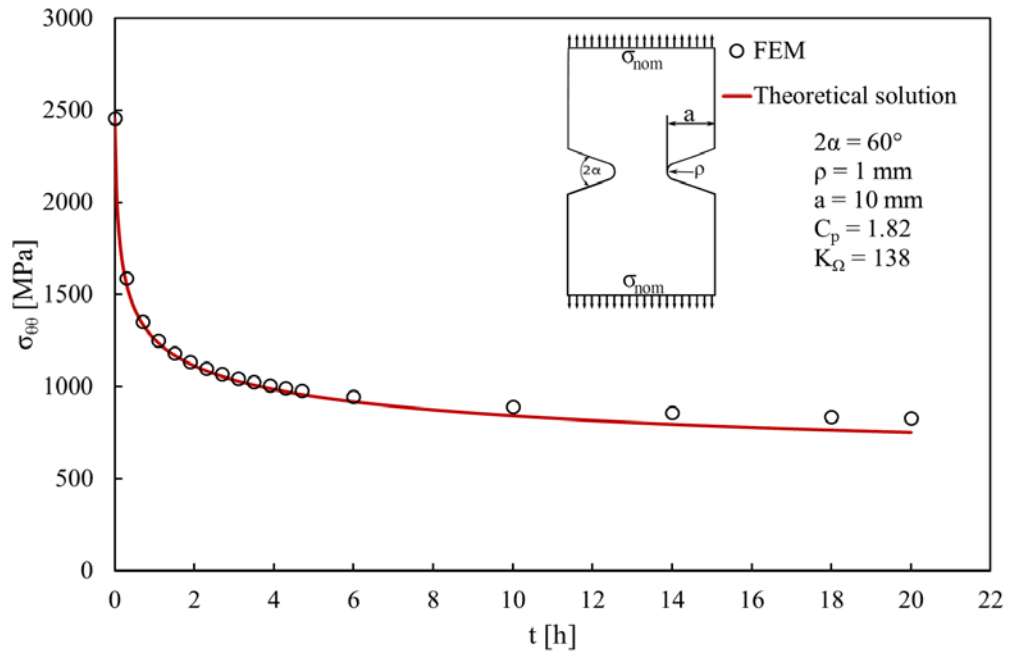


**Fig. 10:** Comparison between theoretical and FEM evolution of stresses as a function of time for V-notch geometry

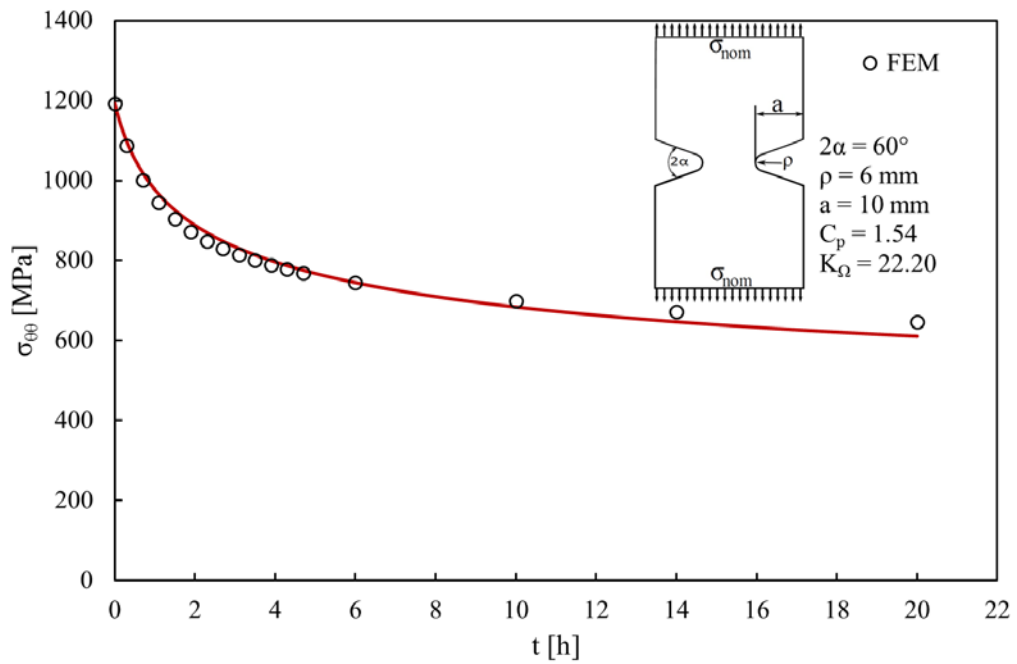


**Fig. 11:** Comparison between theoretical and FEM evolution of stresses as a function of time for V-notch geometry

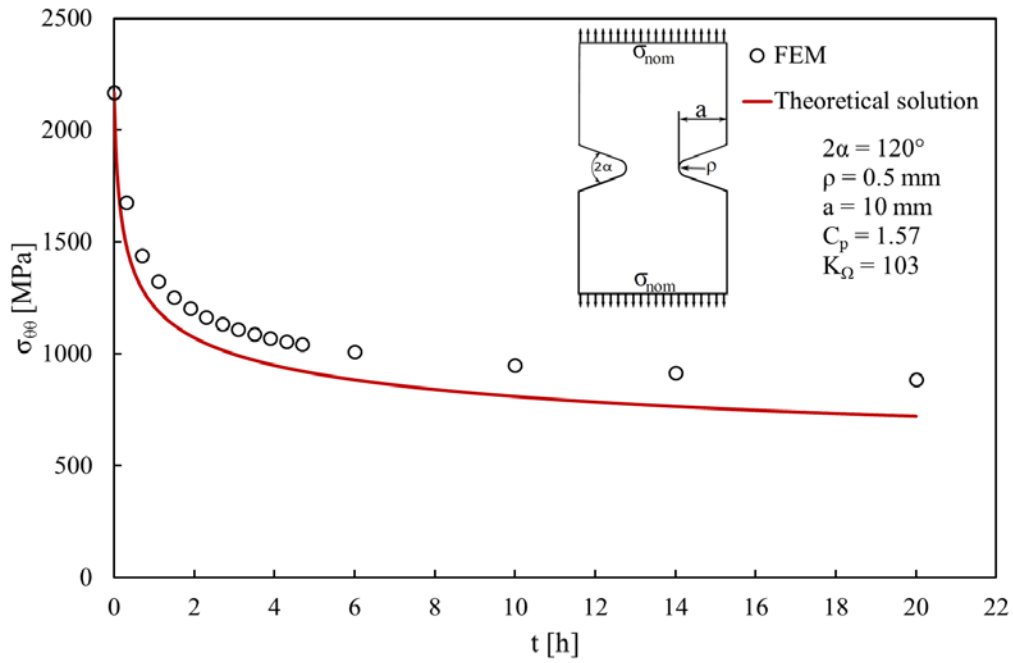


**Fig. 12:** Comparison between theoretical and FEM evolution of stresses as a function of time for V-notch geometry

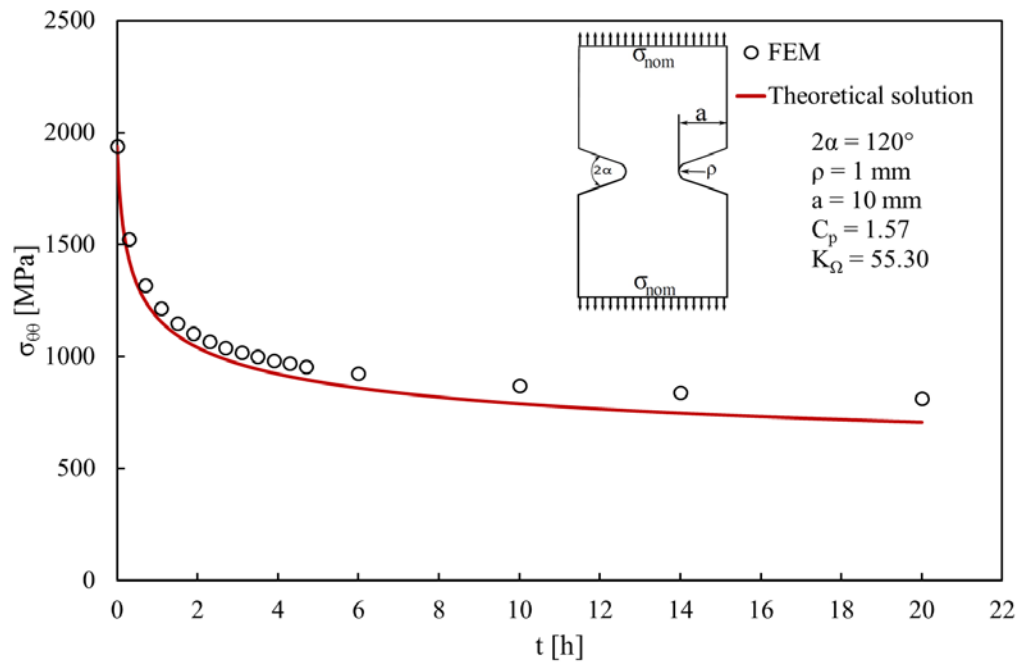


**Fig. 13:** Comparison between theoretical and FEM evolution of stresses as a function of time for V-notch geometry

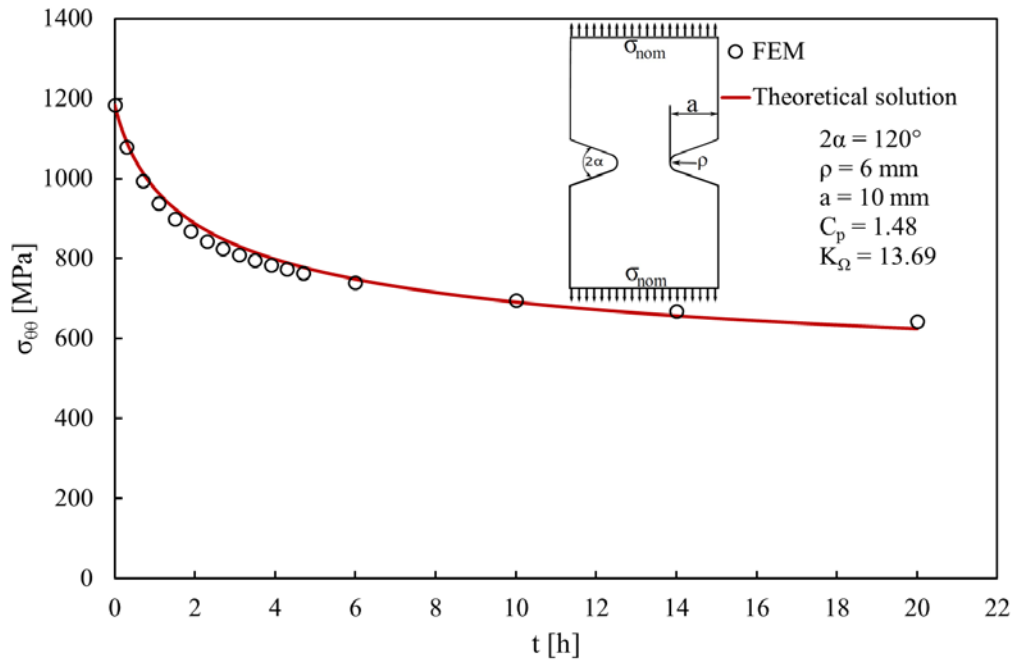


**Fig. 14:** Comparison between theoretical and FEM evolution of stresses as a function of time for V-notch geometry

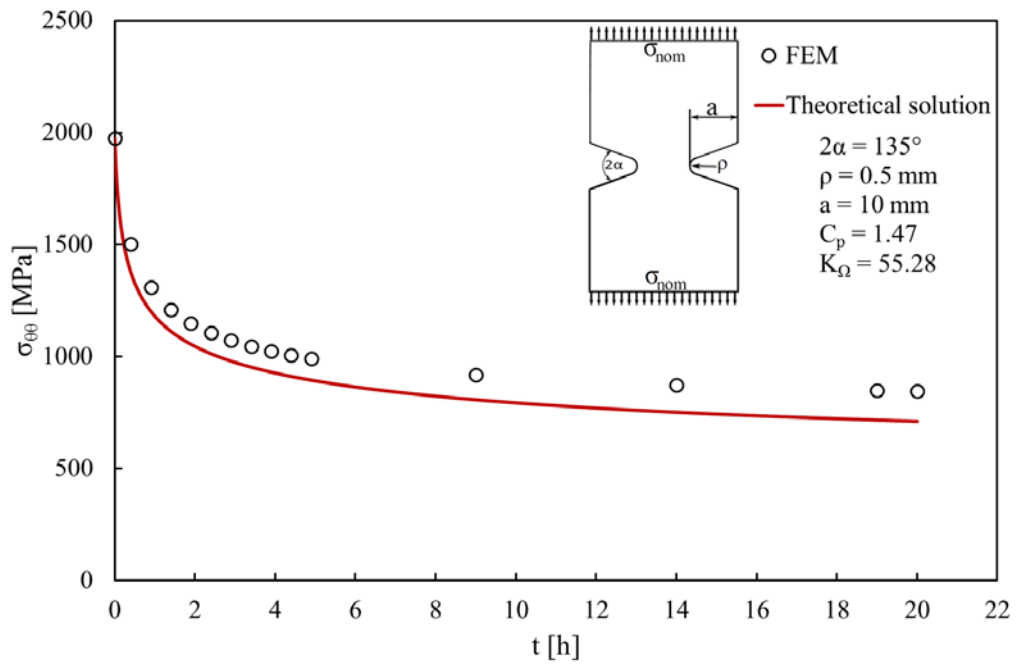


**Fig. 15:** Comparison between theoretical and FEM evolution of stresses as a function of time for V-notch geometry

6.4 Examples of the new method applied to blunt V-notches: considerations and comparison between numerical and FE analysis

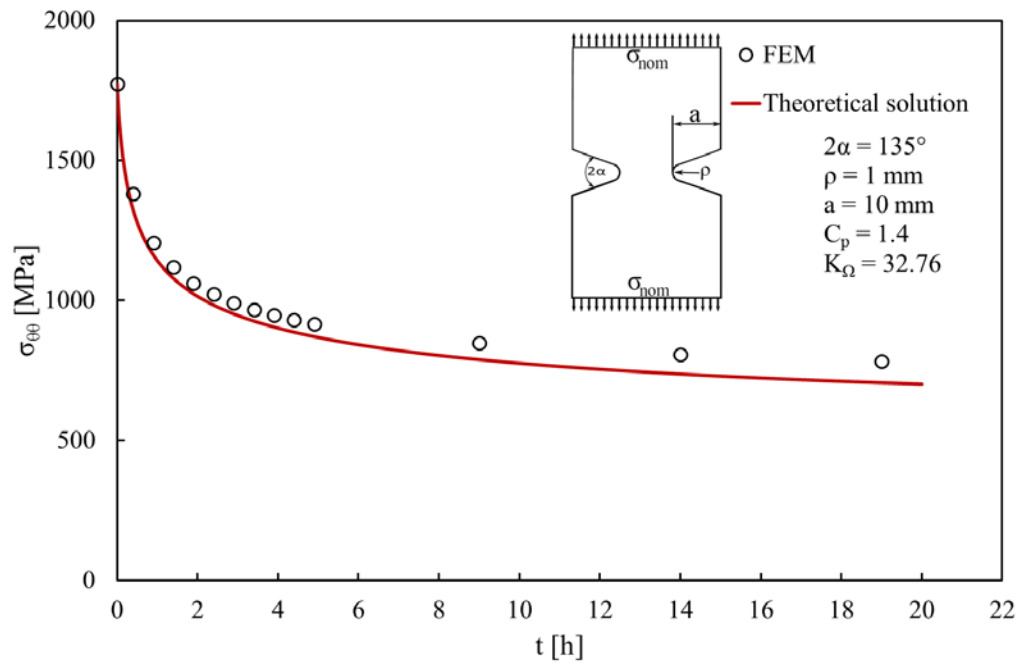


**Fig. 16:** Comparison between theoretical and FEM evolution of stresses as a function of time for V-notch geometry

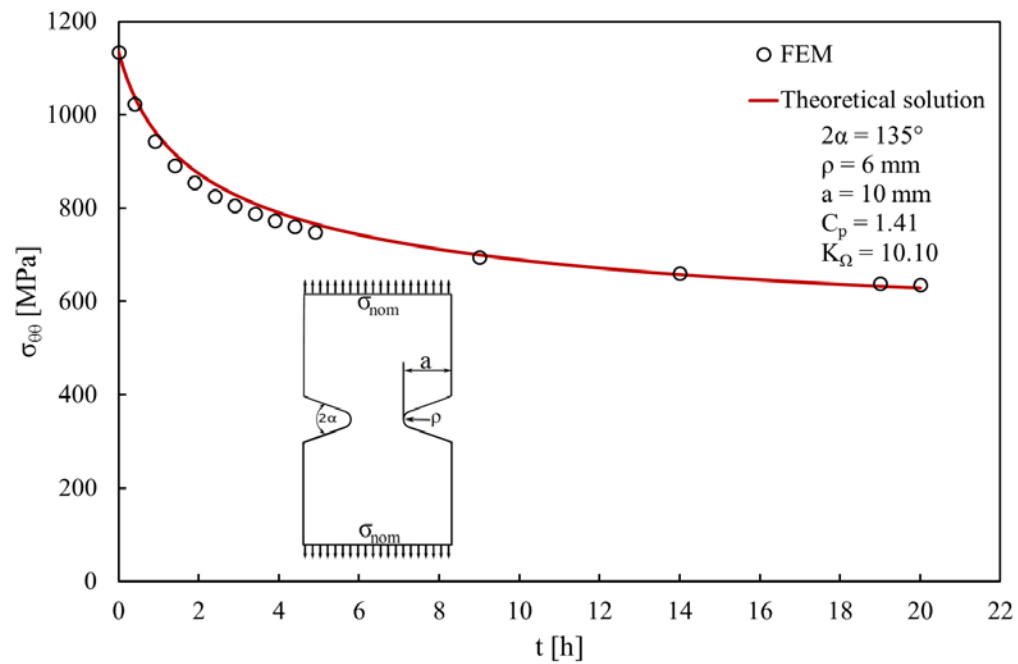


**Fig. 17:** Comparison between theoretical and FEM evolution of stresses as a function of time for V-notch geometry



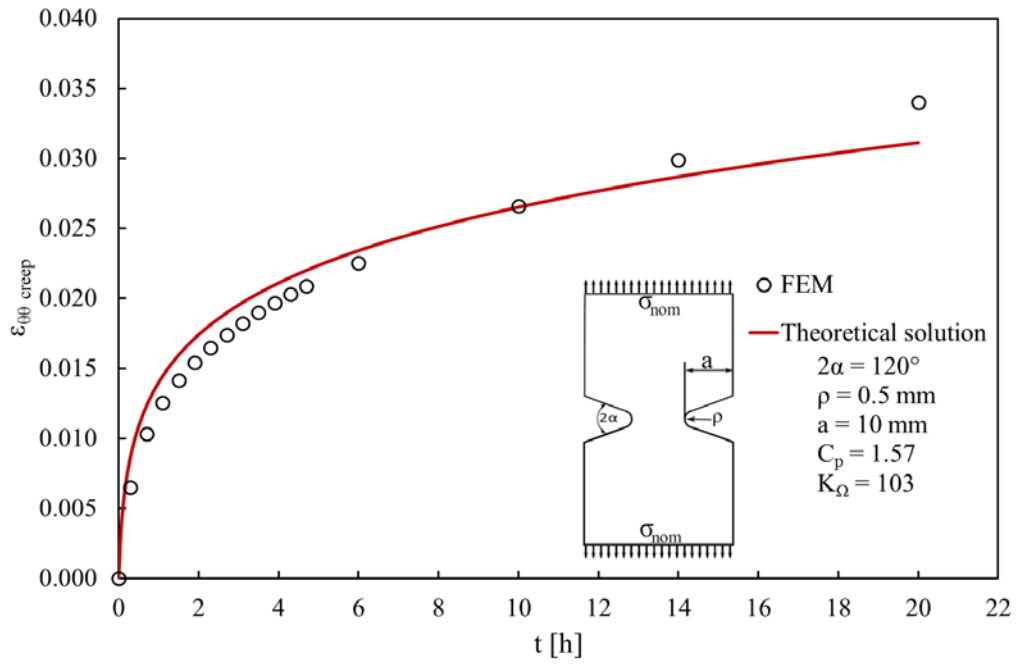


**Fig. 18:** Comparison between theoretical and FEM evolution of strains as a function of time for V-notch geometry

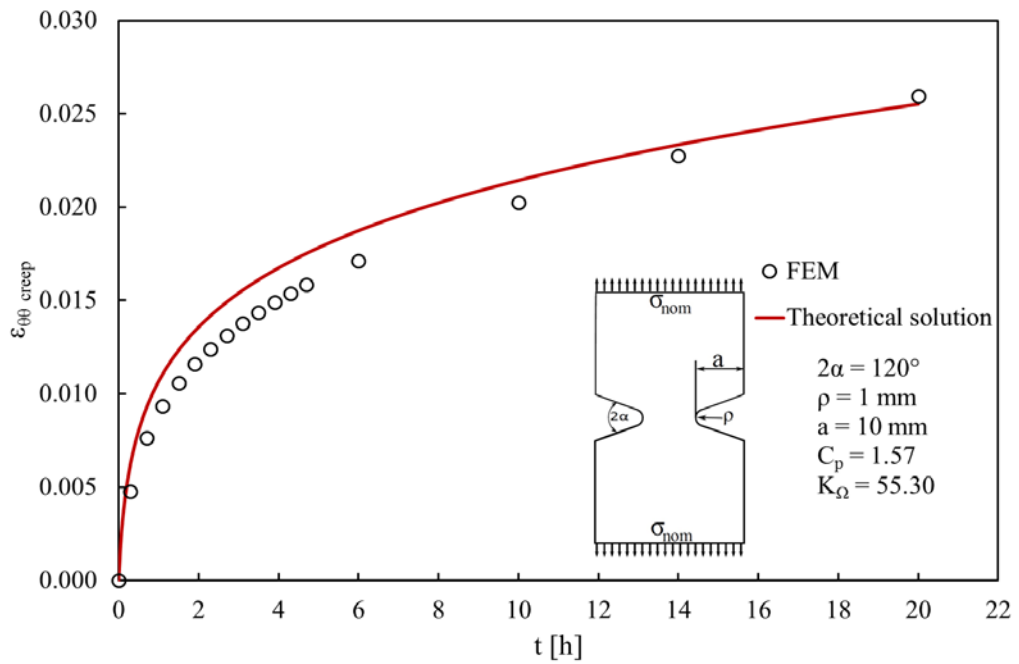


**Fig. 19:** Comparison between theoretical and FEM evolution of strains as a function of time for V-notch geometry

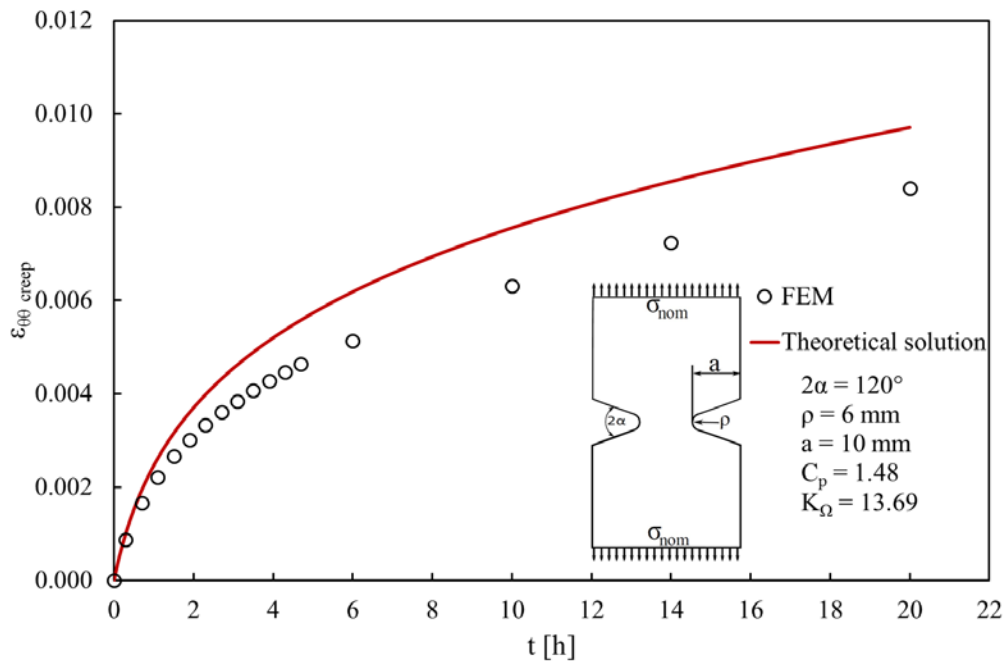


**Fig. 20:** Comparison between theoretical and FEM evolution of strains as a function of time for V-notch geometry

## 6.5 Discussion

The main advantage of the proposed method is that it permits a fast evaluation of the stresses and strains at notches under non-localized creeping condition, without the use of complex and time-consuming FE non-linear analyses. In fact, even if the theoretical formulation seems to be complex, once implemented the equations numerically in any commercial software, the evaluation of stress and strain is really fast and easy. The obtained stresses and strains can be used as input parameters for creep life prediction models for components subjected to mode I loading and in general on creep models based on local approaches. Moreover, the method has good potentialities to be extended to multiaxial fatigue.

It is clear that stress and strain are evaluated under non-localized creep only at the notch tip and not at some points ahead of the notch tip. The local values of stress and strain are useful when local approaches have been selected as the tool for life assessment or design. This is true not only in case of creep but, for example, also for fatigue life assessment. As well known, local approaches based on stresses and strains failed when the stress fields tends toward infinity (such as for crack or sharp

notches). In these cases, the evaluation of stress and strain at some points ahead of the notch tip may be a possible way to address the problem.

Different methods are available in literature dealing with this matter, for example the theory of critical distances, or based energy approaches such as Strain Energy Density. These methods, even if defined for linear-elastic conditions, have shown recently some good potentialities also under non-linear conditions as briefly reported below.

The strain energy method has been recently proposed by the authors as the characterizing parameter for high temperature fatigue of different materials [26–32] with very good results in fatigue assessment. This parameter could be useful also to characterize creeping conditions if combined with the present model, giving the possibility to include in the analysis also sharp V-notches and cracks. In these geometries, a localized approach in terms of stress/strain is no longer suitable because of the stress concentration effect, but a strain energy density averaged over a control volume based method [33,34] could lead to a very good solution, overcoming the problem that, at the notch tip, the stress tends toward infinity.

Theory of Critical Distances (TCD) [35–38] have been recently applied also at high temperature showing a good capability in the fatigue strength assessment under non-linear condition.

At the light of these recent and promising findings, further investigations on creep, fatigue at high temperature and their interactions is surely necessary.

Moreover, the estimation of the strain should be improved considering a better formulation of the plastic zone than the one proposed by Irwin and used here.

## **6.6 Conclusions**

The present chapter proposed an extension of the method presented by Nuñez and Glinka [14]. The method was proposed originally for the estimation of stress and strain at U-notches tip under non-localized creep. Non-localized (or gross) creep condition refers to situations in which the far stress field also experiences some creep and this may contribute to more intense creeping around the notch tip. In the present paper, the original work has been extended to blunt V-notches. The key to getting the extension to blunt V-notches is the substitution of the Creager-Paris equations [15] with the more general Lazzarin-Tovo equations [16].

The results have shown a good agreement between numerical and theoretical values. Thanks to the extension to blunt V-notches, all geometries can be easily treated with the aim of the numerical method developed.

The main results are:

- The solution proposed by Nuñez and Glinka presents good results for U-shaped notches. However, for small tip radii, the distance  $d$  at which the far field contribution is evaluated has to be larger than three times the notch radius, in order to be in the elastic field;
- The distance  $d$  at which the far field contribution is evaluated can be considered as a function of the geometry of the notch tip;
- From the analyses emerges a repetitive trend of the strain evolution: regardless of the opening angle, the best solution is obtained for the notch radius of 0.5 mm, while the error increases as the notch-radius becomes bigger, with an overestimation by the theoretical solution of the strain values. However, even if a few cases are not in good agreement with the finite element method analysis (error less than 20%), it does not affect the reliability of the procedure as shown also by other authors;
- The error found in some cases for the strains estimation is most likely due to different approximations introduced in the theoretical formulation, such as the assumption of the elastic-perfectly plastic behavior of the material inside the plastic zone and the employment of the Irwin's method to estimate the plastic radius;
- The original solution proposed by Glinka cannot be directly extended to sharp V-notches. In fact, since the method is Neuber's rule based, in case of sharp notches the peak stress tends toward infinity;
- Introducing the Lazzarin-Tovo equations, the method has been extended beyond the validity of the Creager-Paris equation, to blunt V-notches. All the results shown a very good agreement within the numerical and F.E.M. stresses;
- It is evident that the stresses present, after the relaxation phase, a plateau reached after almost the same time that is approximately 5 h, regardless of the specimen geometries. This means that the relaxation is most governed, as

expected, by the creep-law, while the geometries only act on the values reached by stress and strain. Once the properties of the material is known or assumed, only one geometry must be analyzed, since the trend of stress and strain and the plateau are almost the same regardless of the specimen geometries. Moreover, if in addition the peak stress is known for every geometries (thanks to  $K_t$ ), all the trends can be easily reconstructed starting from a single analysis;

- The Creager-Paris equation can be derived from Lazzarin-Tovo equations. For this reason, the solution proposed in the present paper for blunt V-notches can be considered as a general solution for different notch geometries (also U-notches);
- Neglecting the far field contribution, it can be easily derived the localized creep formulation.

## References

- [1] F. Berto, A. Campagnolo, P. Gallo, Brittle Failure of Graphite Weakened by V-Notches: A Review of Some Recent Results Under Different Loading Modes, *Strength Mater.* 47 (2015) 488–506.
- [2] Z. He, A. Kotousov, F. Berto, Effect of vertex singularities on stress intensities near plate free surfaces, *Fatigue Fract. Eng. Mater. Struct.* 38 (2015) 860–869.
- [3] F. Berto, A. Campagnolo, P. Lazzarin, Fatigue strength of severely notched specimens made of Ti-6Al-4V under multiaxial loading, *Fatigue Fract. Eng. Mater. Struct.* 38 (2015) 503–517.
- [4] G.C. Sih, Redemption of the formalism of segmented linearity: multiscaling of non-equilibrium and non-homogeneity applied to fatigue crack growth, *Fatigue Fract. Eng. Mater. Struct.* 38 (2015) 621–628.
- [5] K.K. Tang, S.H. Li, Interactive creep-fatigue crack growth of 2024-T3 Al sheets: selective transitional functions, *Fatigue Fract. Eng. Mater. Struct.* 38 (2015) 597–609.
- [6] F.K. Zhuang, S.T. Tu, G.Y. Zhou, Q.Q. Wang, A small cantilever beam test for determination of creep properties of materials, *Fatigue Fract. Eng. Mater. Struct.* 38 (2015) 257–267.
- [7] R.P. Skelton, *Fatigue at high temperature*, Applied Science Publishers, 1983.
- [8] M. Chaudonneret, J.P. Culie, Adaptation of Neuber's theory to stress concentration in viscoplasticity, *Rech. Aerosp. English Ed.* 4 (1985) 33–40.
- [9] H. Neuber, Theory of Stress Concentration for Shear-Strained Prismatical Bodies With Arbitrary Nonlinear Stress-Strain Law, *J. Appl. Mech.* 28 (1961) 544.
- [10] S. Kubo, K. Ohji, Development of simple methods for predicting plane-strain and axi-symmetric stress relaxation at notches in elastic-creep bodies, in: *Proc. Int. Conf. Creep, JSME, Tokyo, Japan, 1986*: pp. 417–422.
- [11] A.A. Moftakhar, G. Glinka, D. Scarth, D. Kawa, Multiaxial stress-strain creep analysis for notches, in: *ASTM Spec. Tech. Publ.*, ASTM, 1994: pp. 230–243.
- [12] G. Härkegård, S. Sørnbø, Applicability of Neuber's Rule to the Analysis of Stress and Strain Concentration Under Creep Conditions, *J. Eng. Mater. Technol.* 120 (1998) 224–229.

- [13] H. Zhu, J. Xu, M. Feng, Singular fields near a sharp V-notch for power law creep material, *Int. J. Fract.* 168 (2011) 159–166.
- [14] J.. Nuñez, G. Glinka, Analysis of non-localized creep induced strains and stresses in notches, *Eng. Fract. Mech.* 71 (2004) 1791–1803.
- [15] M. Creager, P. Paris, Elastic field equations for blunt cracks with reference to stress corrosion cracking, *Int. J. Fract. Mech.* 3 (1967) 247–252.
- [16] P. Lazzarin, R. Tovo, A unified approach to the evaluation of linear elastic stress fields in the neighborhood of cracks and notches, *Int. J. Fract.* 78 (1996) 3–19.
- [17] F.H. Norton, *The creep of steel at high temperatures*, McGraw-Hill, New York, 1929.
- [18] G. Glinka, Calculation of inelastic notch-tip strain-stress histories under cyclic loading, *Eng. Fract. Mech.* 22 (1985) 839–854.
- [19] K. Molski, G. Glinka, A method of elastic-plastic stress and strain calculation at a notch root, *Mater. Sci. Eng.* 50 (1981) 93–100.
- [20] R. Von Mises, *Mechanik der festen Körper im plastisch- deformablen Zustand*, *J. Math. Phys.* 1 (1913) 582–592.
- [21] G.R. Irwin, *Linear fracture mechanics, fracture transition, and fracture control*, *Eng. Fract. Mech.* 1 (1968) 241–257.
- [22] G.R. Irwin, Analysis of stresses and strains near the end of cracking traversing a plate, *J. Appl. Mech.* 24 (1957) 361–364.
- [23] M.L. Williams, *Stress Singularities Resulting From Various Boundary Conditions*, *J. Appl. Mech.* 19 (1952) 526–528.
- [24] G. Glinka, A. Newport, Universal features of elastic notch-tip stress fields, *Int. J. Fatigue.* 9 (1987) 143–150.
- [25] K. Hatanaka, A.N. Yahya, I. Nonaka, H. Umaki, Initiation of High Temperature Creep Voids in Notched Components., *JSME Int. J. Ser. A.* 42 (1999) 280–287.
- [26] P. Gallo, F. Berto, P. Lazzarin, High temperature fatigue tests of notched specimens made of titanium Grade 2, *Theor. Appl. Fract. Mech.* 76 (2015) 27–34.
- [27] F. Berto, P. Gallo, P. Lazzarin, High temperature fatigue tests of un-notched and notched specimens made of 40CrMoV13.9 steel, *Mater. Des.* 63 (2014)

- 609–619.
- [28] F. Berto, P. Lazzarin, P. Gallo, High-temperature fatigue strength of a copper-cobalt-beryllium alloy, *J. Strain Anal. Eng. Des.* 49 (2014) 244–256.
- [29] P. Gallo, F. Berto, P. Lazzarin, P. Luisetto, High Temperature Fatigue Tests of Cu-be and 40CrMoV13.9 Alloys, *Procedia Mater. Sci.* 3 (2014) 27–32.
- [30] F. Berto, P. Gallo, Extension of linear elastic strain energy density approach to high temperature fatigue and a synthesis of Cu-Be alloy experimental tests, *Eng. Solid Mech.* 3 (2015) 111–116.
- [31] F. Berto, P. Gallo, P. Lazzarin, High Temperature Fatigue Tests of a Cu-Be Alloy and Synthesis in Terms of Linear Elastic Strain Energy Density, *Key Eng. Mater.* 627 (2015) 77–80.
- [32] P. Gallo, F. Berto, Influence of surface roughness on high temperature fatigue strength and cracks initiation in 40CrMoV13.9 notched components, *Theor. Appl. Fract. Mech.* 80 (2015) 226–234.
- [33] F. Berto, P. Lazzarin, Recent developments in brittle and quasi-brittle failure assessment of engineering materials by means of local approaches, *Mater. Sci. Eng. R Reports.* 75 (2014) 1–48.
- [34] F. Berto, P. Lazzarin, C.H. Wang, Three-dimensional linear elastic distributions of stress and strain energy density ahead of V-shaped notches in plates of arbitrary thickness, *Int. J. Fract.* 127 (2004) 265–282.
- [35] D. Taylor, Geometrical effects in fatigue: a unifying theoretical model, *Int. J. Fatigue.* 21 (1999) 413–420.
- [36] Taylor, Wang, The validation of some methods of notch fatigue analysis, *Fatigue Fract. Eng. Mater. Struct.* 23 (2000) 387–394..
- [37] L. Susmel, D. Taylor, Fatigue design in the presence of stress concentrations, *J. Strain Anal. Eng. Des.* 38 (2003) 443–452.
- [38] L. Susmel, D. Taylor, Two methods for predicting the multiaxial fatigue limits of sharp notches, *Fatigue Fract. Eng. Mater. Struct.* 26 (2003) 821–833.



# 7. Strain Energy Density under creeping conditions: preliminary analysis and considerations

*P. Gallo, F. Berto, G. Glinka, Some considerations on blunt and sharp V-notches subjected to creep loading. Under Review.*

## Highlights

Geometrical discontinuities, such as notches, need to be carefully analysed because of the stress concentration generated by them. Notches become even more important in components subjected, in service, to high temperature fatigue or imposed viscoplastic behaviour such as creep.

From the state of the art on that topic, it emerges that tools to manage creep of notched components are still missing. In the previous §Chapter 6, the candidate presented the implementation of a numerical method useful for the evaluation of stresses and strains at U and blunt V-notches, based on the Lazzarin-Tovo equations and the method developed by Nuñez and Glinka. The knowledge of stresses and strains, indeed, can be used as input parameters for creep models based on local approaches. Unfortunately, when dealing with cracks and sharp notches, a localized approach in terms of stress/strain is no longer suitable, while a Strain Energy Density (SED) averaged over a control volume, combined with the developed model can lead to good results. In this chapter, past and recent contributions regarding sharp-V notches under creeping condition and energy approaches are summarized. Subsequently, preliminary analysis on the estimation of the strain energy density under creeping condition is presented for sharp V-notches. A critical analysis of the results is also made, discussing the open points and the problems that must be overcome in the near future for a successful extension of the SED method to creep.



## **7.1 Introduction**

When dealing with high temperature applications, time and temperature dependent deformations are involved, resulting in a nonlinear stress-strain response of the material such as creep (visco-plasticity). Creep can be localized or concentrated in a small region near the notch root (localized-creep) or creep strains can occur far away from the notch tip (non-localized or gross creep). Gross creep condition refers to situations in which the far stress field also experiences creep behaviour and this may contribute to more intense creeping ahead of the notch tip. This situation is not so rare in components working at high temperature, such as power plant, gas turbine and nuclear pressure vessels. Gas turbine blades and disks for example are very sensitive to creep phenomenon. Considering power plant, between start-up and shut-down there is a period of on-load running. The material at the surface of the stress concentrating feature may be at constant strain during this period, and stress relaxation takes place due to creep [1]. Usually, when the components are subjected to high temperature and constant load, non-localized creep can be considered.

Dealing with V-notches under linear elastic conditions, extensive works have been proposed by different authors and some pioneering works can be briefly re-called. Williams [2] firstly proposed an investigation on the stress singularities in plates subjected to tensile loading, varying the boundary conditions, and exploring the asymptotic nature of the stress field. Later, Gross and Mendelson [3] interpreted the intensity of the linear elastic stress fields in terms of stress intensity factor of mode I and II loading. From the definitions given by Gross and Mendelson, in the last decade, Lazzarin and collaborators presented different investigations for the estimation of stresses and strains in the proximity of V-notches [4–6].

To the best of authors' knowledge, only limited works concerning the evaluation of stress and strain at the V-notch tip under creeping condition are available in literature. The number of papers reduces drastically if non-localized creep formulation and based on energy approaches are considered, although some authors, in the past, have tried to propose some solutions.

Li et al. [7] studied the dominance of the asymptotic crack tip fields through a finite element solution for near tip stress and strain field in elastic-power law creeping solids. Full range within small scale and extensive creep was analysed. The results were found to be in good agreement with the results obtained by other authors and

showed that, in the transient regime, under small scale creep, HRR theory is applicable over a region that is about one fifth the extent of the creep zone. Moreover, finite deformation effects were found to dominate over a size scale of the order of the crack tip opening as is the case for rate independent solids.

A differential form of Neuber's rule has been formulated for a generic viscoplastic notch problem in [8]. It has been shown that the stress-strain history at the root of a notch in a viscoplastic body can be determined directly from the elastic regime if viscoplastic strains can be neglected. The results obtained were in good agreement with finite element analyses considering nominal creep conditions and stress relaxation under a constant nominal strain. A very interesting consideration was also drawn: stress and strain concentration factors were found to approach stationary values after long-time loading.

In [9], application of the domain boundary element method was evaluated in case of creep analysis of two-dimensional viscoplastic structures containing V-notches, under plane stress condition. Stress and strain distributions are obtained for tensile specimens with a single edge notch and the combined creep-plasticity constitutive Hart's model was employed. The formulation assumed small-strain and small-rotation. However, when the temperature of service increases, the small-strain hypothesis could not be satisfied and a power law mode near V-notch cannot be neglected.

More recently, Zhu et al. [10] presented the singular field near a sharp V-notch for power law creep material. The paper was very interesting because it considered sharp notches. Plain strain condition was applied. In order to obtain the singular order in steady state, C-integral method and iterative scheme were adopted. In the transient stage, instead, due to the effect of time parameters, the solution from finite element analysis was discussed. It was underlined that under steady-state condition, the degree of singularity depends on creep exponent and V-notch angle. However the work does not present the evolution of stresses and strains as a function of time but focused on the singular order variation with time.

Some authors, in the past, proposed based on energy approaches as creep characterizing method for different aims e.g. crack propagation and damage assessment.

In the pioneering work by Landes and Begley [11],  $C^*$  parameter was suggested to assess the creep crack growth at high temperature (920 K) of some superalloy. From the analytical viewpoint,  $C^*$  derived from the  $\dot{J}$  was introduced by other authors [12]. In particular, crack growth rates were correlated with the  $C^*$  parameter that is an energy rate line integral. However, the  $C^*$  was found to be able to characterize the crack tip stress and strain rate fields provided that elastic and transient creep effects were negligible. Under such conditions, the results showed that crack growth rate correlated with  $C^*$  integral, while other parameters (e.g.  $K$ , nominal stress), failed to adequately characterize the crack growth rate. Despite some limitations, this work gave an interesting fracture mechanics interpretation of creep phenomenon.

The use of  $C^*$  parameter for the prediction of creep crack propagation rates was also considered by other authors. In [13], a new method for estimating  $C^*$  was presented. Experimental results from creep crack growth tests, conducted on 1CrMoV steel using both compact tension and single edge notch bend specimen, indicated that good correlation with  $C^*$  was obtained once the effects of stress redistribution become negligible.

An energy-based fatigue and creep-fatigue damage parameter was also derived by Leis [14], assuming the hypothesis that damage is dependent on the internal total octahedral strain energy. This general parameter was valid for isothermal mechanical cycling and inherently accounted for multiaxiality and mean stress for both non-viscous and viscous deformation response, including hold times. The results were compared with experimental fatigue and creep-fatigue life data for the corresponding conditions. It was shown that those specific forms of the general parameter affected a high degree of data consolidation.

$C^*$  was considered also by Saxena [15] for the characterization of creep-crack-growth behaviour in 304 stainless steel. An experimental program was conducted, considering several temperatures. Crack growth rates obtained from center crack tension and compact type specimens were correlated by the energy rate line integral,  $C^*$ . From the experimental data it emerged that microstructure and temperature did not affect the relationship within crack growth rate and  $C^*$ .

Recently, a new energy-based fatigue damage parameter in life prediction of high temperature structural materials was proposed by Lee and collaborators [16]. The method was based on plastic strain energy density (PSED). The work was mainly

focused on low-cycle fatigue at high temperature (accounting also for creep and other high temperature effects) of 316L austenitic stainless steel and 429EM ferritic stainless steel. The advantage of the method was the possibility to predict low cycle fatigue at high temperature with only tensile test data. High cycle fatigue instead was not considered.

A very interesting solution, based on the strain energy density method was proposed in [17]. The method predicted the creep-fatigue damage in high temperature components. It was assumed that, on macroscopic level, the energy dissipated in the material may be taken as a measure of the creep damage induced in the material and hence the creep damage is directly proportional to absorbed internal energy density. Comparing the results of the energy density model and the measured creep-fatigue lives, good results have been found.

Zhu and collaborators [18] proposed a new model for life prediction of turbine disk alloys (GH4133). The method was based on plastic strain energy density. Moreover, a generalized energy-based fatigue-creep damage parameter was developed to account for creep and mean strain/stress effects in the low cycle fatigue regime as well as cyclic hardening. The results showed a better prediction of fatigue behaviour than common methods.

Despite the fact that some based on energy approaches are available to manage creep and fatigue-creep regime, they are most focus on low cycle fatigue, taking into account non-linear behaviour. Moreover, notches behaviour under non-localized creep is completely neglected, especially in those geometries where a local approaches based on local stresses and strains are no longer suitable.

If one considers the non-localized creep, Nuñez and Glinka have recently presented a solution for non-localized creep strains and stresses at the notch root, briefly presented in the previous chapter (see §Section 6.2) [19]. This approach yielded very good results when applied to U-notches ( $2\alpha=0$  and  $\rho\neq 0$ ) and the undersigned has extended that method to a larger variety of geometries, including blunt V-notches (see §Chapter 6) [20]. The base of the extension to blunt V-notches was the assumption of the more general Lazzarin-Tovo equations [21] in the estimation of the elastic contribution.

Dealing with V-notches, stresses tend to infinity near the notch tip and they are no longer suitable as input parameters for life prediction creep models based on local

stress/strain approaches. The energy in a small volume of material surrounding the notch tip, instead, has obviously a finite value, regardless of the stresses and strains behaviour. For these reasons, the approach deserves to be investigated also when dealing with creep problem.

In this background, the present chapter proposes some preliminary analyses and considerations on the mean Strain Energy Density (SED) [22–24] approach to design and characterize notch components under creep conditions. Several investigations on the SED approach extended to situation in which non-linear effects occur have been already carried out by the candidate and well documented in the present thesis.

The chapter is organized as follows: first, the numerical estimation of the strain energy density is presented considering sharp V-notches; later a critical analysis of the results is reported, discussing the open points and the problems that must be overcome in the near future for a successful extension of the SED method to creep.

## **7.2 Evaluation of Strain Energy Density under creep conditions**

The averaged Strain Energy Density (SED) method, that has been formalized by Lazzarin and co-workers derived from Neuber's concept of elementary volume, and local mode I concept proposed by Erdogan and Sih [25]. It has been already introduced in several parts of the present thesis, e.g. §Section 5.2 among all, and the reader can refer to numerous references for more details [23,24,26].

As already discussed in the introduction, stresses tend toward infinity in case of singularity occurring at cracks or sharp notches. In these situations, approaches based on local stress and strain are no longer suitable for design assessment, also if creeping conditions are taking place. At first glance, it derives that also the method proposed in the §Chapter 6 for evaluation of stress and strain under non-localized creep [20], cannot be directly applied to V-sharp notched components. On the other hand, the strain energy density averaged over a control volume could lead to overcome the problem that, at the notch tip, stresses tend toward infinity. In fact, despite this fact, the energy in a small volume of material surrounding the notch tip has obviously a finite value and such a value is thought as the main parameters controlling the failure. For these reasons, the approach deserves to be investigated also when dealing with creep problem.

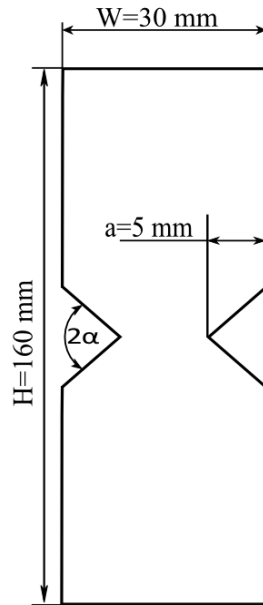


**Fig. 1:** Plates weakened by lateral symmetric sharp V-notches: geometric details

**Table 1:** Mechanical elastic properties and creep properties

E [MPa]	v	n	B [MPa <sup>-n</sup> /s]
2000	0.3	3	2.80E-12
2000	0.3	5	2.80E-10
2000	0.3	7	2.80E-08

To reach this goal, some finite element (FE) non-linear analyses have been conducted on a plate weakened by lateral symmetric V-notches under creep conditions. The considered geometry is depicted in Fig. 1. The following opening angles  $2\alpha$  have been considered:  $60^\circ$ ,  $90^\circ$ ,  $120^\circ$ ,  $135^\circ$ ,  $160^\circ$ . In detail: simulations have been carried out through ANSYS® code; the plate has been modelled with a Solid 8 node 183 and a uniform pressure as a function of the creep parameters has been applied. In order to simulate the creep relaxation, the load has been applied in two steps: in the first one, the load has been applied instantaneously, approximately in  $t = 10^{-5}$  h; subsequently, in a second load step, it has been maintained constant for the desired time  $t$ . At regular intervals during the relaxation process, the SED is evaluated over a tentative control volume corresponding to the zone of material near the notch tip where stresses are affected by the local creep. The considered mechanical properties are reported in Table 1 and are in agreement with those used in Ref. [10].



The SED is plotted in Figures 2-4 as a function of the normalized time  $\tau$  defined as follows in [10]:

$$\tau = \frac{B\sigma_g^n t}{\sigma_g/E} \tag{11}$$

For all of the considered geometries and creep exponents, the mean SED presented a time-dependent trend. It assumes the elastic value at time  $\tau=0$ , and decreases until the achievement of a plateau value, in agreement with Ref. [8] where the plateau has been reached in terms of stress and strain concentration factors. The time needed to reach the limit value depends on the creep exponent: the higher the value of  $n$ , the lower value of plateau time  $\tau$ . Moreover, the mean SED decreases with increasing the opening angle  $2\alpha$ .

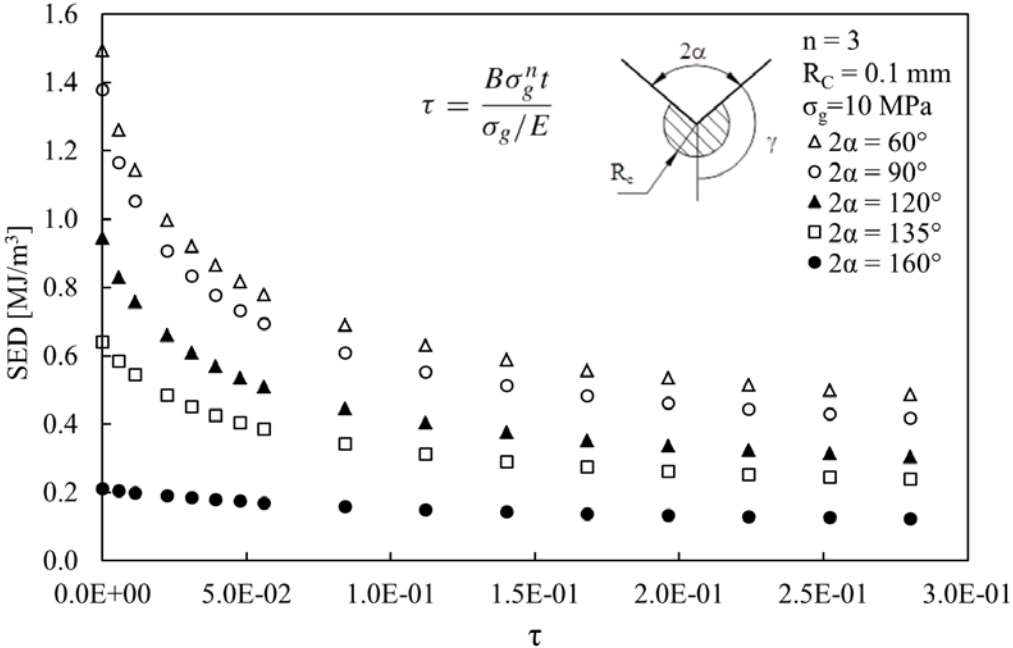


**Fig. 2:** Evolution of mean SED against adimensional parameter  $\tau$  for V-notches, considering different opening angles; creep exponent  $n=3$

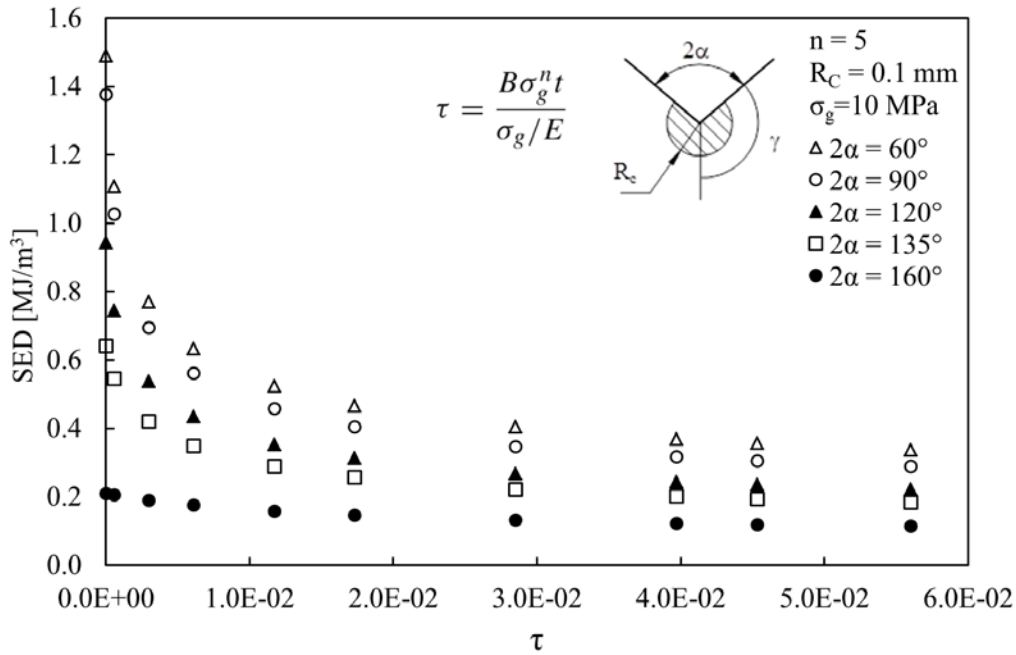


**Fig. 3:** Evolution of mean SED against adimensional parameter  $\tau$ , considering different opening angles; creep exponent  $n=5$

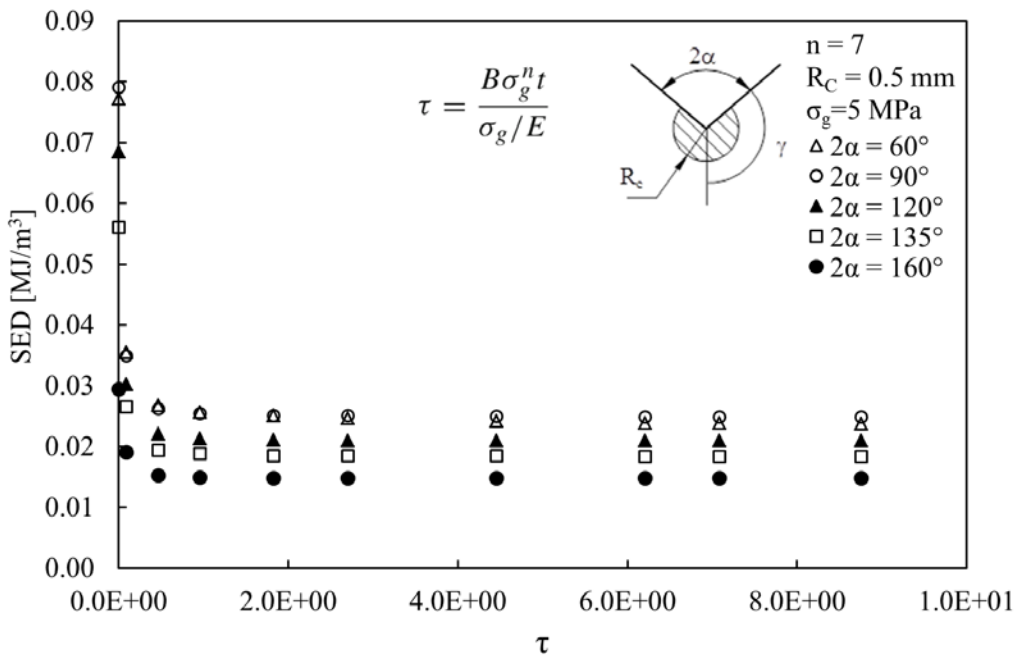


**Fig. 4:** Evolution of mean SED against adimensional parameter  $\tau$ , considering different opening angles; creep exponent  $n=7$

### 7.3 Effect of mesh refinement on the SED evaluation under creeping condition

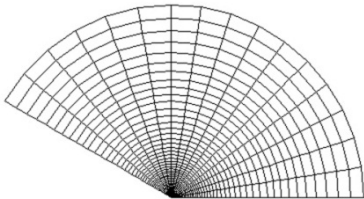
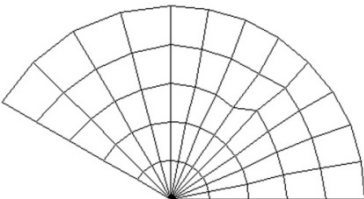
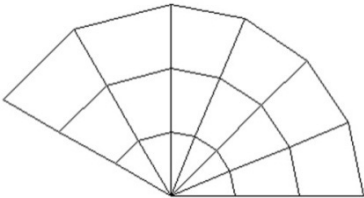
Once defined the control volume, the SED can be easily evaluated through a finite element analysis. As opposed to the evaluation of the NSIFs that needs very refined meshes and high computational efforts, the mean value of the elastic SED on the control volume can be determined with high accuracy by using very coarse meshes [27]. The SED, in fact, can be derived directly from the nodal displacements, that are accurately evaluated also when coarse meshes are employed. This comes from simple considerations on how the SED is evaluated in FE codes that does not involve any calculations regarding stress and strain. This advantage has been well proved by some works on the topic in the past [27,28], and has been here verified for the first time under creeping condition in the present work.

To analyze the effect of the mesh refinement on the SED values, under creeping condition, finite element analyses have been conducted considering sharp V-notches under creeping condition. The geometry is reported in Fig. 1. Different mesh refinement degrees have been employed and the value of the SED against time has been stored at regular intervals. The analyses have been repeated considering three values of the creep exponent  $n$  and a large number of different notch geometries varying the opening angle. For sake of brevity, only the results regarding  $n=5$  and opening angle  $2\alpha=60^\circ$  and  $120^\circ$  have been reported and are summarized in Tables 2 and 3 in the next pages, for three degrees of mesh refinement. The number of elements in the critical volume, the time, the mean SED value and a picture of the volume are reported in the tables. From the results it emerges that the mean SED is slightly influenced by the mesh refinement, with a percentage difference always lower than 12%. It must be pointed out that the results are overestimated, and never underestimated, being anyway in safe condition. The same results have been obtained considering other creep properties and notch opening angles, but are here omitted for sake of conciseness.

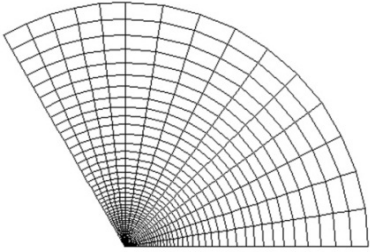
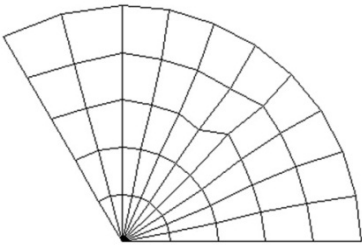
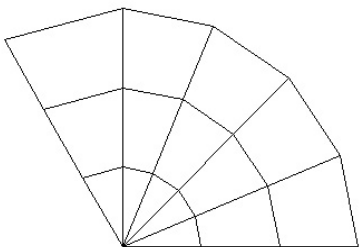
It is clear that, also under non-linear analyses condition such as creep, the evaluated SED still remains unaffected by the mesh refinement. In view of an industrial application of the SED for design against creep of sharp geometries, this is an evident and relevant advantage: the main problems affected non-linear FE analyses are their computational effort and time consumption that become bigger with the

increase of mesh refinement. The possibility to employ a very coarse mesh returns a fast, easy and low computational power non-linear analysis, without any affection to the final results that still is reliable and anyway, in the worst scenario, safely overestimated. Another important consideration: as soon as the SED is known, local quantities (such as NSIFs) can be easily determined through expressions linking the SED to different parameters.

**Table 2:** Mean value of SED under creeping condition for different mesh refinement degrees,  $2\alpha=60^\circ$ ,  $n=5$

$R_C = 0.1 \text{ mm}$	Number FE $R_C$	t [s]	$\bar{W}$ [MJ/m <sup>3</sup> ]	$\Delta\%$
<b>Reference mesh</b>				
	1400	0	1.490	-
		10	0.338	-
		100	0.241	-
<b>Coarse mesh 1</b>				
	60	0	1.497	+0.5
		10	0.346	+2.4
		100	0.245	+1.7
<b>Coarse mesh 2</b>				
	18	0	1.499	+0.6
		10	0.349	+3.3
		100	0.249	+3.3

**Table 3:** Mean value of SED under creeping condition for different mesh refinement degrees,  $2\alpha=120^\circ$ ,  $n=5$ 

$R_C = 0.1 \text{ mm}$	Number FE $R_C$	t [s]	$\bar{W}$ [MJ/m <sup>3</sup> ]	$\Delta\%$
<b>Reference mesh</b>				
	1352	0	0.945	-
		1	0.435	-
		10	0.223	-
		100	0.157	-
<b>Coarse mesh 1</b>				
	50	0	0.950	+0.5
		10	0.226	+1.3
		100	0.157	0
<b>Coarse mesh 2</b>				
	15	0	0.953	+0.8
		10	0.227	+1.8
		100	0.158	0

#### 7.4. Discussion of the results: SED as a creep characterizing parameter

The main advantage of the method proposed in §Chapter 6 [20] is that it permits a fast evaluation of the stresses and strains at notches under creep conditions, without the use of complex and time-consuming FE non-linear analyses. It is valid for U-notches and blunt V-notches. Moreover, the localized creep formulation can be easily derived neglecting the contribution of the far field. Once the method is implemented in any system providing machine aid for the mechanical symbolic processes

encountered in analysis, the obtained stresses and strains can be used as input parameters for creep life prediction models for components subjected to mode I loading and in general on creep models based on local approaches.

Although Lazzarin and Tovo equations employed in the proposed method are valid also in case of sharp V-notches, the values of stress and strain are no longer suitable as characteristic parameters governing failure. As well known, in fact, these local approaches failed when the stress fields tends toward infinity (such as for crack or sharp notches), and the development of alternative solutions becomes crucial.

The evaluation of stress and strain at some points ahead of the notch tip may be a possible way to address the problem. Different methods are available in literature dealing with this matter, for example the theory of critical distances [29–31], or based on energy local approaches. These methods, even if applied in linear-elastic conditions, have shown recently some good potentialities also under non-linear conditions. In fact it has been proposed by the candidate as characterizing parameter for high temperature fatigue of different materials with very good results in fatigue assessment as shown in different chapters. This parameter could be useful also to characterize creeping conditions if combined with the present model, giving the possibility to include in the analysis also cracks and sharp V-notches. However, some points remain open:

-order singularity variation with time: when considering creeping conditions, the singularity order does not assume a constant value, but varies with time. This phenomenon has been observed by different authors [10], and it still is under investigation also by the present authors.

-evolution against time from elastic to elastic-plastic or fully plastic state of the system, especially when dealing with high temperature. Considerations on how to manage this matter must be drawn, in order to modify the proposed model appropriately.

Because of the promising results showed in the preliminary analyses, the author still devoting effort to overcome the problems cited previously and to combine successfully the proposed model for the prediction of stresses and strain with the SED averaged over a control volume, in order to give a useful and more general tool when dealing with notches subjected to creep, regardless of the specimen geometries.

## 7.5. Conclusions

The present chapter deals with the extension of the Strain Energy Density to components subjected, in operating conditions, to non-localized creep. The SED estimation is made possible through the implementation of a numerical method able to predict creep notch tip stress and strain evolution against time. The method, firstly developed by Nuñez and Glinka [19], has been recently extended to a large variety of geometries [20] thanks to the Lazzarin-Tovo equations, as well documented in §Chapter 6. The knowledge of stresses and strains, indeed, can be used as input parameters for creep models based on local approaches. However, when dealing with sharp notches and cracks, a localized approach in terms of stress/strain is no longer suitable, while a strain energy density averaged over a control volume base method still be applicable.

Some preliminary analyses on averaged SED applied to sharp V-notches are really encouraging for future development, provided that some open points have been addressed.

The following concluding remarks can be drawn:

- From the state of the art, despite some attempts made by different authors, it emerges that a lot of effort must be dedicated in the near future to develop reliable tools to design against creep when notched geometries are considered;
- It is clear that, in case of singularity (such as sharp V-notches and cracks) the local stresses and strains cannot be employed anymore, because their values tend toward infinity;
- From the last conclusion, it emerges the necessity to develop and propose new approaches that can overcome that problem, and the SED averaged over a finite volume, combined with the model proposed in §Chapter 6, seems to be an appropriate tool;
- Some preliminary analyses on the SED under creeping condition has been conducted, highlighting a strong time dependence;
- The trend of the SED, although varies with time, tends to a plateau value after a certain time  $t$ , function of the creep exponent  $n$ ; the opening angles, instead, as already shown by other authors in the past for linear elastic condition, influences the absolute values of the SED;

- The main advantage of the averaged SED, that is its mesh in-dependence, seems to be preserved also under non-linear/creep condition;
- Because of the promising results, more effort must be dedicated to the development of this approach for design against creep; the main problem to be overcome analytically are how to manage the singularity order variation with time and the evolution during time from an elastic to elastic-plastic behaviour and then from elastic to elastic-plastic SED.



## References

- [1] R.P. Skelton, *Fatigue at high temperature*, Applied Science Publishers, 1983.
- [2] M.L. Williams, Stress Singularities Resulting From Various Boundary Conditions, *J. Appl. Mech.* 19 (1952) 526–528.
- [3] B. Gross, A. Mendelson, Plane elastostatic analysis of V-notched plates, *Int. J. Fract. Mech.* 8 (1972) 267–276.
- [4] P. Lazzarin, R. Zambardi, P. Livieri, Plastic notch stress intensity factors for large V-shaped notches under mixed load conditions, *Int. J. Fract.* 107 (2001) 361–377.
- [5] R. Afshar, F. Berto, P. Lazzarin, L.P. Pook, Analytical expressions for the notch stress intensity factors of periodic V-notches under tension by using the strain energy density approach, *J. Strain Anal. Eng. Des.* 48 (2013) 291–305.
- [6] F. Berto, P. Lazzarin, D. Radaj, Fictitious notch rounding concept applied to V-notches with root hole subjected to in-plane mixed mode loading, *Eng. Fract. Mech.* 128 (2014) 171–188.
- [7] F. Li, A. Needleman, C. Shih, Characterization of near tip stress and deformation fields in creeping solids, *Int. J. Fract.* 186 (1988) 163–186.
- [8] G. Härkegård, S. Sørbo, Applicability of Neuber's Rule to the Analysis of Stress and Strain Concentration Under Creep Conditions, *J. Eng. Mater. Technol.* 120 (1998) 224–229.
- [9] C.P. Provdakis, Creep analysis of V-notched metallic plates: boundary element method, *Theor. Appl. Fract. Mech.* 32 (1999) 1–7.
- [10] H. Zhu, J. Xu, M. Feng, Singular fields near a sharp V-notch for power law creep material, *Int. J. Fract.* 168 (2011) 159–166.
- [11] J. Landes, J. Begley, A Fracture Mechanics Approach to Creep Crack Growth, in: *Mech. Crack Growth*, ASTM International, 100 Barr Harbor Drive, PO Box C700, West Conshohocken, PA 19428-2959, 1976: pp. 128–148.
- [12] K. Nikbin, G. Webster, C. Turner, Relevance of Nonlinear Fracture Mechanics to Creep Cracking, in: *Cracks Fract.*, ASTM International, 100 Barr Harbor Drive, PO Box C700, West Conshohocken, PA 19428-2959, 1976: pp. 47–62.
- [13] M.P. Harper, E.G. Ellison, The use of the  $C^*$  parameter in predicting creep crack propagation rates, *J. Strain Anal. Eng. Des.* 12 (1977) 167–179.

- [14] B.N. Leis, An Energy-Based Fatigue and Creep-Fatigue Damage Parameter, *J. Press. Vessel Technol.* 99 (1977) 524.
- [15] A. Saxena, Evaluation of  $C^*$  for the Characterization of Creep-Crack-Growth Behavior in 304 Stainless Steel, in: *Fract. Mech.*, ASTM International, 100 Barr Harbor Drive, PO Box C700, West Conshohocken, PA 19428-2959, 1980: pp. 131–151.
- [16] K.-O. Lee, S.-G. Hong, S.-B. Lee, A new energy-based fatigue damage parameter in life prediction of high-temperature structural materials, *Mater. Sci. Eng. A.* 496 (2008) 471–477.
- [17] W.M. Payten, D.W. Dean, K.U. Snowden, A strain energy density method for the prediction of creep–fatigue damage in high temperature components, *Mater. Sci. Eng. A.* 527 (2010) 1920–1925.
- [18] S.-P. Zhu, H.-Z. Huang, L.-P. He, Y. Liu, Z. Wang, A generalized energy-based fatigue–creep damage parameter for life prediction of turbine disk alloys, *Eng. Fract. Mech.* 90 (2012) 89–100.
- [19] J.. Nuñez, G. Glinka, Analysis of non-localized creep induced strains and stresses in notches, *Eng. Fract. Mech.* 71 (2004) 1791–1803.
- [20] P. Gallo, F. Berto, G. Glinka, Generalized approach to estimation of strains and stresses at blunt V-notches under non-localized creep, *Fatigue Fract. Eng. Mater. Struct.* (2015) In Press. doi:10.1111/ffe.12374.
- [21] P. Lazzarin, R. Tovo, A unified approach to the evaluation of linear elastic stress fields in the neighborhood of cracks and notches, *Int. J. Fract.* 78 (1996) 3–19.
- [22] F. Berto, P. Lazzarin, Recent developments in brittle and quasi-brittle failure assessment of engineering materials by means of local approaches, *Mater. Sci. Eng. R Reports.* 75 (2014) 1–48.
- [23] P. Lazzarin, F. Berto, Control volumes and strain energy density under small and large scale yielding due to tension and torsion loading, *Fatigue Fract. Eng. Mater. Struct.* 31 (2008) 95–107.
- [24] F. Berto, P. Lazzarin, A review of the volume-based strain energy density approach applied to V-notches and welded structures, *Theor. Appl. Fract. Mech.* 52 (2009) 183–194.
- [25] F. Erdogan, G.C. Sih, On the Crack Extension in Plates Under Plane Loading

- and Transverse Shear, *J. Basic Eng.* 85 (1963) 519.
- [26] D. Radaj, State-of-the-art review on the local strain energy density concept and its relation to the  $J$ -integral and peak stress method, *Fatigue Fract. Eng. Mater. Struct.* 38 (2015) 2–28.
- [27] P. Lazzarin, F. Berto, F.J. Gómez, M. Zappalorto, Some advantages derived from the use of the strain energy density over a control volume in fatigue strength assessments of welded joints, *Int. J. Fatigue.* 30 (2008) 1345–1357.
- [28] P. Lazzarin, F. Berto, M. Zappalorto, Rapid calculations of notch stress intensity factors based on averaged strain energy density from coarse meshes: Theoretical bases and applications, *Int. J. Fatigue.* 32 (2010) 1559–1567.
- [29] L. Susmel, D. Taylor, Fatigue design in the presence of stress concentrations, *J. Strain Anal. Eng. Des.* 38 (2003) 443–452.
- [30] R. Louks, L. Susmel, The linear-elastic Theory of Critical Distances to estimate high-cycle fatigue strength of notched metallic materials at elevated temperatures, *Fatigue Fract. Eng. Mater. Struct.* 38 (2015) 629–640.
- [31] L. Susmel, D. Taylor, Two methods for predicting the multiaxial fatigue limits of sharp notches, *Fatigue Fract. Eng. Mater. Struct.* 26 (2003) 821–833.



## 8. Some considerations on the J-Integral under high temperature elastic-plastic conditions

*P. Gallo, F. Berto, Some considerations on the J-Integral under elastic-plastic conditions for materials obeying a Ramberg-Osgood law, Physical Mesomechanics 18 (4)(2015) 298-306.*

### Highlights

Among the approaches available for structural analysis, the J-Integral has received an excellent feedback as a fracture parameter under elastic-plastic conditions, that are often assumed to characterize high temperature behavior. In the literature, dealing with the crack case, it is proposed to evaluate the J-Integral as a sum of elastic and plastic contributions. However, some uncertainties arise when applying this method to a Ramberg-Osgood law, especially under large scale yielding conditions.

The aim of the present chapter is to discuss how the J-Integral evaluation can be performed for elastic-plastic cracked components, in view of possible assumption of this parameter for the development/improvement of energy methods for creep assessment of notches. Two different non-linear behaviors have been considered for the material: a Ramberg Osgood (RO) law and a Power Law (PL). Numerical and FE results from different approaches have been accurately compared, proving that the most appropriate way to evaluate the J-Integral for a material obeying RO law is to perform two FE analyses evaluating separately the elastic contribution (through a linear elastic analysis) and the plastic contribution (through a nonlinear analysis considering PL behavior).



## **8.1 Introduction**

Design of mechanical components requires the application of an acceptable procedure based on engineering principles. The procedure is applied to verify the integrity and/or functionality of components. Sometimes, for simple problems, the use of handbooks and simplified formulas could be sufficient. Unfortunately, more often the analysis relates to complex components and applications, and the use of more accurate methodology becomes essential.

Nowadays, it is very common for an engineer to design a component that, in operating conditions, is subjected to stress and strain well beyond the elastic limit of the material and has the ability to exhibit a nonlinear stress-strain response (material nonlinearity). Components subjected to plasticity, crushing, and cracking are good examples, but time-dependent effects such as visco-elasticity or visco-plasticity (creep) can be also mentioned. Due to advanced industrial applications in critical environments (e.g. very high temperature applications), the design procedure under linear elastic conditions is sometimes not applicable. This situation is not so rare, for example, considering the aerospace and automotive industries.

Among the local approaches [1–12] available for non-linear analyses, the contour J-Integral has received an excellent feedback as a fracture parameter characterizing nonlinear materials under different loading conditions, considering also thermo-mechanical fatigue and creep [13–15].

In 1968, Rice [16] provided the basis for extending fracture mechanics methodology well beyond the validity limits. It was originally proposed for near tip stresses characterization of notches and cracks under two-dimensional deformation field and consists in a path independent integral surrounding cracks or notches. The path independence is maintained only if the notch opening angle is equal to zero. Hutchinson [17] and Rice and Rosengren [18] also showed that J can characterize crack-tip stresses and strain in nonlinear materials, underlining the double form of the J-Integral: energy parameter and/or stress intensity parameter.

Under linear elastic conditions J-Integral can be easily correlated to mode I, II and III stress intensity factors as well as to the Strain Energy Density. For opening angles different from zero, because of the loss of the path independence, a direct correlation between J-Integral and NSIFs is far from easy. However, different attempts have been made recently to obtain closed form relationships for the linear elastic strain

energy density averaged over the control volume [7–11,19,20] and the J-Integral at the tip of notches under different loading conditions [1]. Moreover other attempts have been made in the past years for sharp and blunt notches [21–26].

Considering the crack case under linear elastic conditions, analytical formulas are available to evaluate the J-Integral as a function of the stress intensity factor, Young's modulus and Poisson's ratio. Under elastic-plastic conditions, instead, different approaches are available. In [27–29], extensive tables for calculating J for various geometries, crack lengths and for different nonlinear stress-strain curves are provided. However, in some cases, different parameters are not available in the handbooks or some geometries are not considered at all. In these cases the finite element analyses become fundamental for the evaluation of the J-Integral.

In this chapter a brief overview on J-Integral evaluation for cracked components obeying an elastic-plastic rule is presented. The influence of the chosen material law on the results in terms of stress field is investigated and a number of nonlinear FE analyses are provided to support the conclusions. In particular, Ramberg-Osgood law and Power Law have been considered for modelling the material behavior. The objectives of this work are to precisely define all parameters necessary for the calculation of J, to summarize the analytical equations available to evaluate these parameters and to present some practical guidelines for conducting the J-Integral evaluation for a cracked plate obeying a Ramberg-Osgood law by means of FE analyses. Three methods will be presented, underlining the main advantages and drawbacks. This chapter wants to give useful guidelines for an easy evaluation of the J-Integral in practical applications, when facing a Ramberg-Osgood material law, in view of assumption of this parameter for improvement and development of high temperature fatigue models. It is also aimed to clarify the use of the available handbook formulas and the FE analyses to quantify elasto-plastic J-Integral for a Ramberg-Osgood material law.

In details, a plate with a central crack will be considered, and the following objectives will be addressed step by step:

- to clarify the definition of all parameters necessary for the calculation of J-Integral;
- to make a short review of the different analytical equations available in the literature;



-to propose some simple guidelines that can suggest a correct way for the estimation of J for an elastic-plastic Ramberg-Osgood cracked material by FEM analyses.

Regarding the last point, three methods will be presented, underling the main advantages and drawbacks. The results are aimed to be a useful tool giving some practical guidelines for an easy evaluation of the J-Integral for engineers in their practical applications, when a Ramberg-Osgood material law is employed. The present investigation creates more clarity both in the case of using handbook formulas and FE analyses to quantify elastic-plastic J-Integral from a Ramberg-Osgood material law.

## 8.2 Material models

### 8.2.1 Geometry and mechanical properties

The geometry investigated is shown in Fig. 1. It consists in a plate with a central crack. The crack length  $2a$  is equal to 20 mm, while the plate is 200 mm width and 200 mm height. The mechanical properties instead are reported in Table 1: the Young's modulus  $E$  is equal to 206000 MPa, the strength coefficient  $K$  to 950 MPa and the hardening exponent  $n$  is 8.33. These properties characterized the AISI 1045 steel.

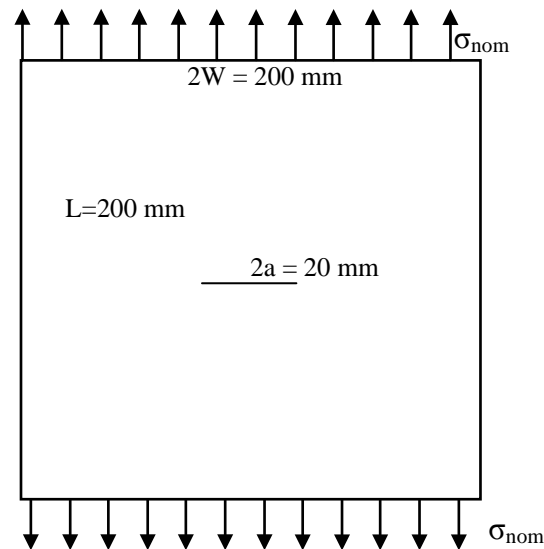


**Fig. 1:** Geometrical parameters

**Table 1:** Mechanical properties of AISI 1045

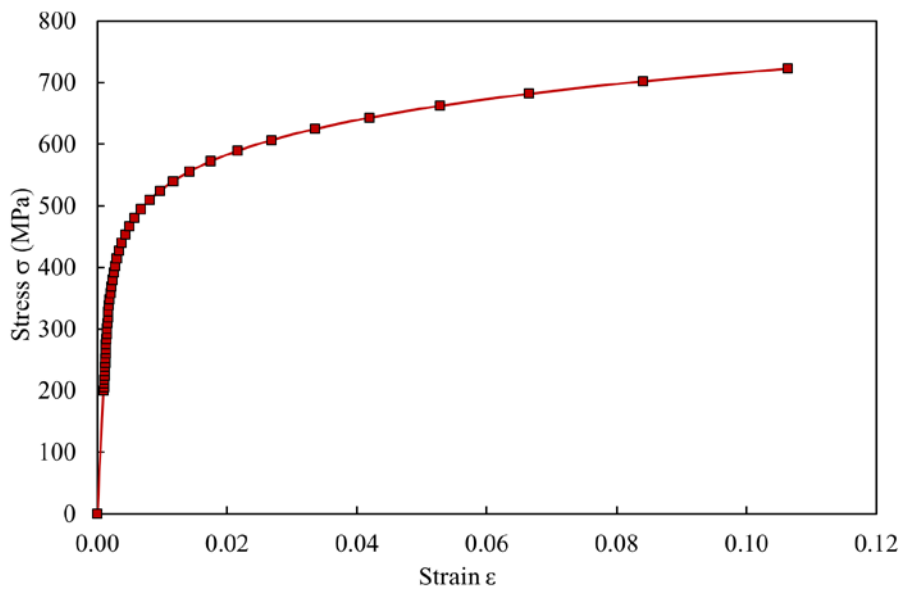
K (MPa)	n	E (MPa)	$\sigma_Y$ (MPa)
950	8.33	206000	450

### 8.2.2 Ramberg Osgood and power law

In 1943, Ramberg and Osgood [30] proposed the following simple formula for describing the non-linear relationship between stress and strain:

$$\varepsilon = \frac{\sigma}{E} + \left( \frac{\sigma}{K} \right)^n \quad (1)$$

The parameters K and n are constants and describe the hardening behavior of the material. The curve represented by the Ramberg-Osgood model depicts a continuous transition from the elastic to plastic behavior of the material. The adequacy of Eq. (1) was tested by Ramberg and Osgood by plotting on log-log graph the stress-deviation curves for the different materials taken from the literature [31], showing that the formula is adequate for aluminum alloy, carbon steel and chromium-nickel steel. The resulting Ramberg-Osgood curve, considering the mechanical properties of Table 1, is depicted in Fig. 2.

**Fig. 2:** Ramberg-Osgood curve

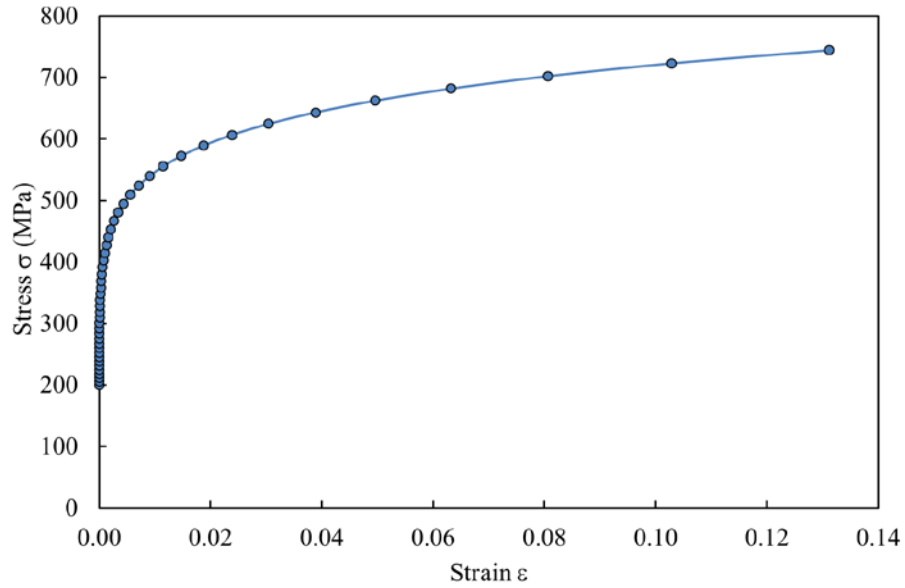


**Fig. 3:** Power law curve

Neglecting the elastic contribution of the Ramberg-Osgood law, one obtains the simple power law form reported below:

$$\varepsilon = \left( \frac{\sigma}{K} \right)^n \quad (2)$$

Assuming also in this case the mechanical properties previously proposed (Table 1), one obtains the power-law curve shown in Fig. 3. The elastic length of the RO law is clearly visible from the figure. For higher loads the two curves collapse into a single one.

### 8.3 J-Integral evaluation

#### 8.3.1 The J contour integral

When dealing with a Ramberg-Osgood law for the material, in the literature it is suggested an approximation of the elastic-plastic J that consists in an interpolation formula combining the linear elastic and the fully plastic conditions [27]:

$$J = J^e(a_e) + J^p(a, n) \quad (3)$$

Where:

- $J^e(a_e)$  is the elastic contribution based on an adjusted crack length  $a_e = a + \phi r_y$ , i.e. Irwin's effective crack length modified to account for strain hardening;

$$- r_y = \frac{1}{\beta\pi} \left[ \frac{n-1}{n+1} \right] \left( \frac{K_I}{\sigma_0} \right)^2;$$

$$- \phi = \frac{1}{1 + (P/P_0)^2};$$

-  $J^p(a,n)$  is the plastic contribution based on the material hardening exponent  $n$  and crack length;

For plane strain  $\beta = 6$ .

Under small-scale yielding, the plastic contribution is small compared with the elastic contribution and Eq. (3) reduces to the well-known elastic solution reported in [28]. On the other side, in the fully plastic range, the elastic contribution is negligible.

Equation (3) expresses the total  $J$  as a sum of the elastic and plastic contribution. Regarding the elastic contribution, the evaluation of  $J$  is very straightforward since it can be easily linked to various fracture mechanics parameters such as the stress intensity factor  $K$  that, in turn, can be evaluated through a finite element analysis [28]:

$$J^e = K_I^2 \left( \frac{1-\nu^2}{E} \right) \quad (4)$$

Considering the plastic contribution,  $J^p(a,n)$ , Kumar et al.[27] provide the following expression:

$$J^p = \alpha \varepsilon_0 \sigma_0 \frac{ba}{W} h_1 \left( \frac{P}{P_0} \right)^{n+1} \quad (5)$$

Expressed for the following power law constitutive model:

$$\frac{\varepsilon}{\varepsilon_0} = \alpha \left( \frac{\sigma}{\sigma_0} \right)^n \quad (6)$$

Where:

- $\sigma_0$  = reference stress value that is usually equal to the yield strength;
- $\varepsilon_0 = \sigma_0/E$  or in general  $f(\sigma_0)$ ;
- $\alpha$  = dimensionless constant;
- $n$  = hardening exponent;

- $h_1 = f(a/W, n)$  and it is provided by Anderson [28] for fully plastic J for a middle tension specimen in plane strain and plane stress;
- $P_0 = \text{reference load} = (2/\sqrt{3})2b\sigma_0$  (only for plane strain conditions);
- $P = \text{applied load referred to the gross area}$ ;
- $b, a$  and  $W$  are geometrical parameters, while  $B$  is the plate thickness (see Figure 1);

### 8.3.2 Parameters $\alpha$ , $P_0$ and $h_1$

When dealing with the estimation of  $J^P$ , different parameters of Eq. (5) need to be quantified by tables and/or figures available in the literature [27,28,32]. Two main difficulties can be pointed out: first, the considered geometries are limited; secondly, the parameters are defined only for the power law form expressed by Eq. (6), and so in terms of  $\sigma_0$  and  $\varepsilon_0$  while nowadays a power law expressed in terms of  $K$  and  $n$  as, shown in Eq. (2), is usually employed. For these reasons, some considerations deserve to be spent about the definition of parameters  $P_0$ ,  $h_1$  and  $\alpha$  when dealing with Eq. (2).

In the configuration under investigation, since the material constitutive model and its related  $\sigma$ - $\varepsilon$  curve are fully available, the dimensionless constant  $\alpha$  can be easily determined through a best fitting procedure, once defined the value of  $\sigma_0$  and  $\varepsilon_0$ . As suggested by Anderson's handbook [28] and other authors [27],  $\sigma_0$  can be assumed as the yield strength of the material, here called  $\sigma_Y$ . This assumption made possible to write  $\varepsilon_0$  as a function of the yield strength:

$$\varepsilon_0 = \frac{\sigma_0}{E} = \frac{\sigma_Y}{E} \quad (7)$$

An alternative procedure, avoiding the best fitting process, can be obtained by few simple considerations. Rearranging Eq. (6) and taking into account the relation expressed by Eq. (7), it is possible to express  $\alpha$  as follows:

$$\alpha = \frac{\varepsilon}{\varepsilon_0} \left( \frac{\sigma_0}{\sigma} \right)^n = \frac{\varepsilon E}{\sigma_0} \left( \frac{\sigma_0}{\sigma} \right)^n = \frac{\varepsilon E}{\sigma_Y} \left( \frac{\sigma_Y}{\sigma} \right)^n \quad (8)$$

Since Eqs.(2) and (6) represent the same material curve, with the same mechanical properties, the deformations can be defined also by the latter power law form. For

this reason, substituting Eq. (2) into Eq. (8) and rearranging the equation, it leads to the following formula of the dimensionless coefficient  $\alpha$  as a function of K and n:

$$\alpha = \left( \frac{1}{K} \right)^n E \sigma_y^{n-1} \quad (9)$$

Substituting the mechanical properties considered here, Equation (9) returns  $\alpha=0.9145$ .

Considerations deserve to be spent also on the definition of the limit load  $P_0$ . It is usually defined by a limit load solution for the geometry of interest, and normally corresponds to the load at which the net cross section yields. In general, it is defined as:

$$P_0 = \sigma_{y,nom\ ref} A_{net} \quad (10)$$

Where  $\sigma_{y,nom\ ref}$  is the stress at the limit condition. Considering now the von Mises equivalent stress for fully plastic and plane strain conditions and remembering the relations within stress components, one obtains:

$$\sigma_{eq} = \sqrt{\sigma_{y,nom}^2 + 0.5^2 \sigma_{y,nom}^2 - 0.5 \sigma_{y,nom}^2} = \sigma_{y,nom} \frac{\sqrt{3}}{2} \quad (11)$$

From the latter equation, it is possible to express  $\sigma_{y,nom}$  as a function of  $\sigma_{eq}$ :

$$\sigma_{y,nom} = \frac{2}{\sqrt{3}} \sigma_{eq} \quad (12)$$

Considering the definition of  $P_0$ , once reached the yield condition,  $\sigma_{eq}$  must equal  $\sigma_0$  :

$$\sigma_{y,nom\ ref} = \sigma_{y,nom}(\sigma_0) = \frac{2}{\sqrt{3}} \sigma_0 \quad (13)$$

Substituting Eq. (13) into Eq. (10) , the final expression for  $P_0$  can be obtained:

$$P_0 = \frac{2}{\sqrt{3}} \sigma_0 A_{net} \quad (14)$$

Parameter  $h_1$  is a function of  $a/W$  and  $n$ . It is catalogued for several values of  $a/W$  and  $n$  under plain strain and plain stress conditions [28]. However, in order to obtain the correct  $h_1$  for a not listed half-crack length plate width ratio and hardening exponent, an extrapolation/interpolation process based on the available curves is necessary: first, by interpolation, the value of  $h_1$  for a  $n=8.33$  is determined; subsequently, fixed the value of  $n=8.33$ , the value of  $h_1$  for the desired value of  $a/W$  is determined by extrapolation process. The equations obtained through interpolation/extrapolation techniques are those reported in the §Appendix (see p. 186) of the present chapter. The resulted value of the dimensionless parameter  $h_1$  for the considered geometry and mechanical properties is 4.456.

#### 8.4 Numerical analyses

The geometry shown in Fig. 1 was modeled in Ansys APDL. A Multilinear Isotropic Hardening (MISO) model was chosen. This model requires (like other non-linear models) the definition of the stress-strain curve point by point. As the model suggests, the resulting curve will be composed of many linear segments connecting the points defined. The MISO option can contain up to 20 different temperature curves, with up to 100 different stress-strain points allowed per curve. For this reason, the points have been opportunely distributed in order to have a better trend definition of the transition zone, near the yielding stress.

Only one quarter of the plate has been modelled, imposing Symmetry BC structural constraints. Element Plane 183 (Ansys V.14) with plane strain option is used. The applied nominal load is 360 MPa. As general rule, the generalized yielding condition is verified at least for a load equal to  $0.8 \sigma_Y$ , which is equal to 360 MPa for the considered material. A very refined mesh is modelled near the crack tip; with the smallest element size of  $1.0E-04$  mm.

The finite element analyses can be conducted following three methods that have been investigated in the present paper:

1. Under large scale yielding, it could be assumed that the elastic contribution of the Ramberg Osgood can be neglected. This assumption leads to the conclusion that the J-Integral of the Ramberg Osgood law has to be close to that obtained considering the simple power-law;

2. The J-Integral of Ramberg-Osgood law can be obtained by simply modelling the complete curve (elastic and plastic contribution) and carrying out a single non-linear analysis;
3. Superposition principle. The total J of the Ramberg-Osgood law can be obtained performing two finite element analyses: a linear elastic analysis, in order to determine the elastic J, and a non-linear analysis considering only the power law in order to determine the plastic contribution of J.

#### **8.4.1 Power-Law convergence problem**

The Power Law constitutive model has an infinity slope in the first portion of the curve, as shown in Fig. 3. The high slope may result in Ansys code solution convergence problems. In order to avoid this issue, a fictitious linear trend is imposed. This fictitious trend is shown in Fig.4 and compared with Ramberg Osgood linear portion in Fig.5. It is clear that the linear trend is very small and does not affect the final results. On the other hand, the improvement of the solution convergence is appreciated. To better support these last comments, Fig. 6 shows the influence of the length of the fictitious P.L. elastic portion on the stress distribution, for an applied constant load. Every curve in the picture depicts the stress distribution ahead the crack for different length of the fictitious linear trend. The first curve for example has the end of the linear elastic portion at 600 MPa. This means that the fictitious elastic portion starts from the value of zero and ends at 600 MPa, that is in turn where the plastic portion starts. If the final point of the elastic portion is under the value of 400 MPa, no differences emerge from the stress analysis. While for higher loads, the stress distribution is strongly influenced. In the present paper, the point of the elastic portion is settled at 200 MPa. In general it seems that, as a good rule, the ratio within the value of the end point of the fictitious linear portion and the yielding stress should be lower than 0.6.



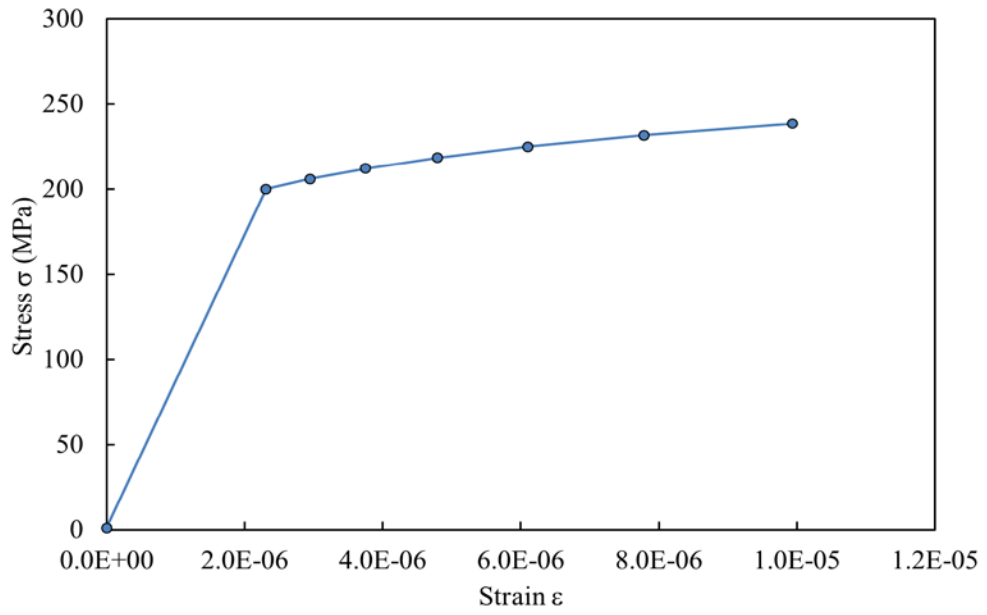


**Fig. 4:** Power law fictitious linear portion

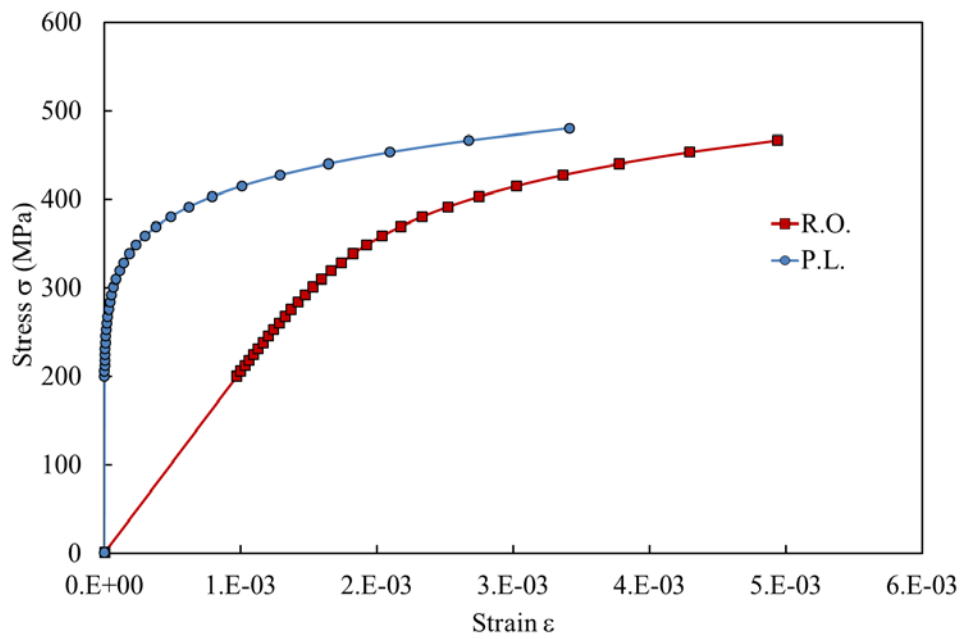


**Fig. 5:** Comparison within elastic portion of Ramberg-Osgood and power law

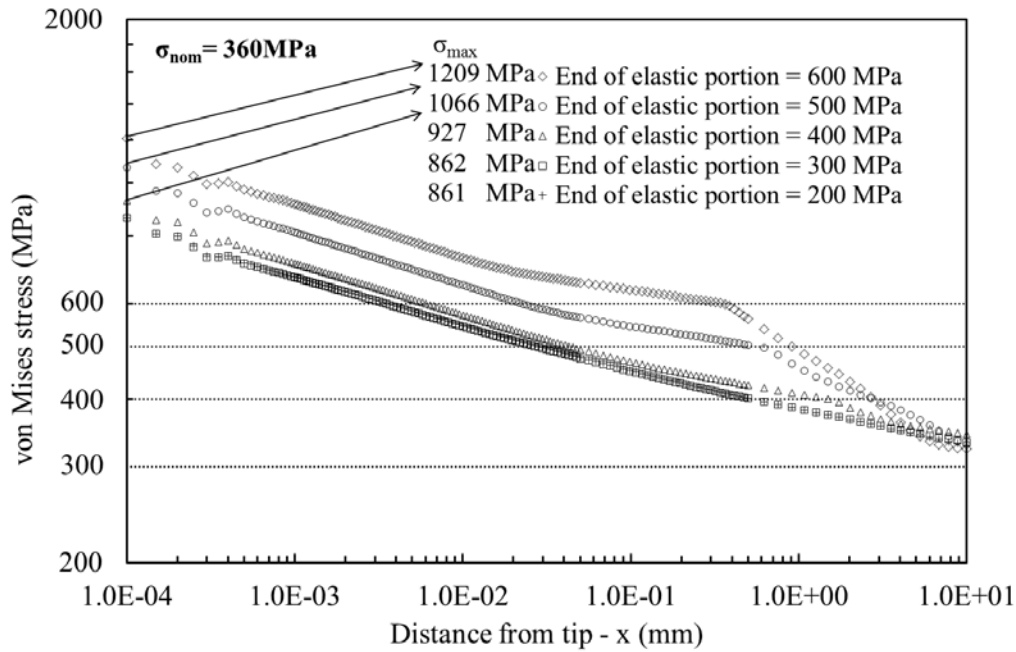


**Fig. 6:** Influence of the fictitious elastic portion on the stress distribution

## 8.5 Results

### 8.5.1 Assuming negligible elastic contribution of the Ramberg-Osgood law.

As stated previously, under fully plastic condition, assured by the applied load of 360 MPa, it could be assumed that the elastic contribution has a negligible value if compared with the plastic contribution. As general rule, in fact, the generalized yielding condition is verified at least for a load equal to  $0.8 \sigma_Y$ , which is equal to 360 MPa for the considered material. This assumption permits to approximate the total Ramberg Osgood  $J$  with that obtained considering a simple power law. With the aim to verify this simplification, a finite element analysis has been conducted assuming the power law material model. The results are compared with the analytical ones obtained through Eq. (3).

Table 2 reports the obtained results and shows an evident difference between the analytical and FEM results.  $J_{th}$  is the theoretical contour  $J$ -Integral obtained through Eq. (3) while  $J_{FEM}^p$  is the plastic  $J$  obtained by a FE analysis considering a pure power law: also with a very high applied load, the elastic contribution cannot be neglected.

**Table 2:** Comparison between J-Integral values, applied load=360 MPa

$J_{th}$ (kJ/m <sup>2</sup> )	$J_{FEM}^p$ (kJ/m <sup>2</sup> )
22.46	4.56

### 8.5.2 Unified assessment of elastic and plastic contribution

The J-Integral of Ramberg-Osgood law can be obtained by simply modelling the complete curve (elastic and plastic contribution) and carrying out a single non-linear analysis. In this case, the elastic contribution is no longer neglected, and no simplifications are introduced.

Table 3 reports the obtained results and shows a percentage difference between theoretical  $J_{th}$  and numerical value (considering a Ramberg Osgood material law)  $J_{R.O.FEM}$  equal to 10%.

**Table 3:** Comparison between J-Integral values, applied load=360 MPa

$J_{th}$ (kJ/m <sup>2</sup> )	$J_{R.O.FEM}$ (kJ/m <sup>2</sup> )	$\Delta J_{th - R.O.}$
22.46	24.68	10%

### 8.5.3 Evaluation of J through superposition principle

The total J of the Ramberg-Osgood law can be obtained performing two FEM analyses: a linear elastic analysis, in order to determine the elastic J, and a non-linear analysis considering only a pure power law in order to determine the plastic contribution of J. In other words, Dowling's approximation [33] is respected also through the FEM analyses, taking advantage of a superposition effect.

Table 4 reports the obtained results and shows a very good agreement between numerical and analytical values.

Where:  $J_{FEM}^e$  is the J obtained by FE linear elastic analysis;  $J_{FEM}^p$  is the plastic J obtained through a non-linear FE analysis and considering a pure power law material model;  $J_{FEM}$  is the arithmetic sum of the elastic and plastic  $J_{FEM}^e$  and  $J_{FEM}^p$ ;  $J_{th}$  is the expected total J contour integral, obtained through Eq. (3).

This procedure returns a very low value of percentage difference between the numerical and theoretical J-Integral. The best solution is to calculate the J-Integral for an elastic-plastic material implementing two analyses: one for the plastic

contribution, considering a power law, and a second one for the elastic contribution considering a pure elastic material, taking advantage of superposition principle.

**Table 4:** Comparison between J-Integral values, applied load=360 MPa

$J_{FEM}^e$ (kJ/m <sup>2</sup> )	$J_{FEM}^p$ (kJ/m <sup>2</sup> )	$J_{FEM}$ (kJ/m <sup>2</sup> )	$J_{th}$ (kJ/m <sup>2</sup> )	$\Delta J_{th - FEM}$ (kJ/m <sup>2</sup> )
18.38	4.56	22.94	22.46	2%

## 8.6 Conclusions

The J-Integral has received an excellent feedback as a fracture parameter under elastic-plastic conditions that are often assumed to characterize high temperature behavior. Considering a crack, the literature proposes to evaluate the J-Integral as a sum of elastic and plastic contribution. However, some uncertainties arise when applying this method to a Ramberg Osgood law, especially under large scale yielding.

The aim of this chapter was to discuss how the J-Integral evaluation can be carried out for elastic-plastic cracked components. Two different non-linear behaviors have been considered: Ramberg Osgood (RO) law and Power Law (PL). Theoretical and numerical results of different approaches have been compared. The following main results can be identified:

- In terms of J-Integral, the constitutive models return very different results. It seems that the elastic contribution of the Ramberg Osgood law cannot be neglected;
- The results support Dowling's approximation:  $J = J^e + J^p$  ;
- The Ramberg-Osgood material law could be considered as a sum of plastic and elastic contribution. Following this methodology, the calculation of the theoretical J-Integral for an elastic-plastic materials can be conducted by considering independently the elastic and plastic contribution, as it is shown by Eq. (3) and by the given references;
- Also under fully plasticity, the elastic contribution cannot be neglected by the analyses. The best procedure to determine the correct value of the total J-Integral for an elastic-plastic is to implement two non-linear analyses: one for the plastic contribution, considering a power law, and a second one for the

elastic contribution considering a pure elastic material. The sum of these values corresponds perfectly to the expected value of J-Integral.

- For the theoretical evaluation for J-Integral, interpolation/extrapolation procedure is proposed for the estimation of the dimensionless parameter  $h_1$ ;
- The parameter  $\alpha$  is given as a function of the mechanical properties  $K$ ,  $n$  and yielding stress, allowing an easy and fast evaluation based on the common mechanical properties of the Ramberg-Osgood and Power Law material.

## Appendix

Parameter  $h_1$  is a function of  $a/W$  and  $n$ . It is catalogued for several values of  $a/W$  and  $n$  under plain strain and plain stress conditions [28]. However, in order to obtain the correct  $h_1$  for half-crack length plate width ratio and hardening exponent not listed, an extrapolation/interpolation process based on the available curves is necessary: first, by interpolation, the value of  $h_1$  for a  $n=8.33$  is determined; subsequently, fixed the value of  $n=8.33$ , the value of  $h_1$  for the desired value of  $a/W$  is determined by extrapolation process.

Below, the employed formulas are reported:

$$y=h_1, x=n$$

$$a/W = 0.125$$

$$y = -1.8136E-06x^6 + 1.2447E-04x^5 - 3.4256E-03x^4 + 4.9069E-02x^3 - 3.9982E-01x^2 + 1.7118E+00x + 1.4433E+00$$

$$a/W = 0.25$$

$$y = 1.27735E-05x^5 - 7.53207E-04x^4 + 1.70327E-02x^3 - 1.85014E-01x^2 + 8.78505E-01x + 1.84269E+00$$

$$a/W = 0.375$$

$$y = -1.21519E-06x^6 + 8.51464E-05x^5 - 2.37417E-03x^4 + 3.35170E-02x^3 - 2.49108E-01x^2 + 8.05512E-01x + 1.75703E+00$$

$$a/W = 0.5$$

$$y = -1.39740E-06x^6 + 9.12734E-05x^5 - 2.33391E-03x^4 + 2.95003E-02x^3 - 1.87929E-01x^2 + 4.50323E-01x + 1.92481E+00$$

$$a/W = 0.625$$

$$y = -5.43849E-07x^6 + 3.38873E-05x^5 - 8.09214E-04x^4 + 9.13681E-03x^3 - 4.32795E-02x^2 - 9.46892E-02x + 2.25234E+00$$

$$a/W = 0.75$$

$$y = -2.70960E-08x^6 - 2.32908E-06x^5 + 2.05096E-04x^4 - 5.38089E-03x^3 + 6.84170E-02x^2 - 5.12603E-01x + 2.52013E+00$$

$$a/W = 0.875$$

$$y = -2.70960E-08x^6 - 2.32908E-06x^5 + 2.05096E-04x^4 - 5.38089E-03x^3 + 6.84170E-02x^2 - 5.12603E-01x + 2.52013E+00$$

NOTE: all the previous equations are valid only for interpolation process and not for extrapolation; the valid  $n$ -range is 1-20.

Fixed the desired value of  $n=8.33$ , the following equation is used to determine the desired value of  $h_1$  considering  $a/W=0.1$ :

$$y=h_1, x=a/W$$

$$y = 7.02819E+00x^2 - 1.15034E+01x + 5.63628E+00$$

## References

- [1] D. Radaj, State-of-the-art review on the local strain energy density concept and its relation to the  $J$ -integral and peak stress method, *Fatigue Fract. Engng. Mater. Struct.* 38 (2015) 2–28.
- [2] D. Radaj, State-of-the-art review on extended stress intensity factor concepts, *Fatigue Fract. Engng. Mater. Struct.* 37 (2014) 1–28.
- [3] G.C. Sih, Directional dissimilarity of transitional functions: Volume energy density factor, *Phys. Mesomech.* 16 (2013) 355–361.
- [4] G.C. Sih, D. Zacharopoulos, Tendency towards sphericity symmetry of pebbles: The rate change of volume with surface, *Phys. Mesomech.* 18 (2015) 100–104.
- [5] G.C. Sih, Short and long crack data for fatigue of 2024-T3 Al sheets: binariness of scale segmentation in space and time, *Fatigue Fract. Engng. Mater. Struct.* 37 (2014) 484–493.
- [6] F. Berto, A review on coupled modes in V-notched plates of finite thickness: A generalized approach to the problem, *Phys. Mesomech.* 16 (2013) 378–390.
- [7] P. Gallo, F. Berto, P. Lazzarin, High temperature fatigue tests of notched specimens made of titanium Grade 2, *Theor. Appl. Fract. Mech.* 76 (2015) 27–34.
- [8] P. Gallo, F. Berto, P. Lazzarin, P. Luisetto, High Temperature Fatigue Tests of Cu-be and 40CrMoV13.9 Alloys, *Procedia Mater. Sci.* 3 (2014) 27–32.
- [9] F. Berto, P. Lazzarin, P. Gallo, High-temperature fatigue strength of a copper-cobalt-beryllium alloy, *J. Strain Anal. Eng. Des.* 49 (2014) 244–256.
- [10] F. Berto, P. Gallo, P. Lazzarin, High temperature fatigue tests of un-notched and notched specimens made of 40CrMoV13.9 steel, *Mater. Des.* 63 (2014) 609–619.
- [11] F. Berto, P. Gallo, P. Lazzarin, High Temperature Fatigue Tests of a Cu-Be Alloy and Synthesis in Terms of Linear Elastic Strain Energy Density, *Key Eng. Mater.* 627 (2015) 77–80.
- [12] G.C. Sih, Redemption of the formalism of segmented linearity: multiscaling of non-equilibrium and non-homogeneity applied to fatigue crack growth, *Fatigue Fract. Engng. Mater. Struct.* 38 (2015) 621–628.
- [13] a. Iziumova, O. Plekhov, Calculation of the energy  $J$ -integral in plastic zone



- ahead of a crack tip by infrared scanning, *Fatigue Fract. Engng. Mater. Struct.* 37 (2014) 1330–1337.
- [14] L. Li, Y.H. Yang, Z. Xu, G. Chen, X. Chen, Fatigue crack growth law of API X80 pipeline steel under various stress ratios based on *J*-integral, *Fatigue Fract. Engng. Mater. Struct.* (2014) n/a–n/a.
- [15] Z. He, A. Kotousov, F. Berto, Effect of vertex singularities on stress intensities near plate free surfaces, *Fatigue Fract. Engng. Mater. Struct.* 38 (2015) 860–869.
- [16] J. Rice, A path independent integral and the approximate analysis of strain concentration by notches and cracks, *J. Appl. Mech.* 35 (1968) 379–386.
- [17] J. Hutchinson, Singular behaviour at the end of a tensile crack in a hardening material, *J. Mech. Phys. Solids.* 16 (1968) 13–31.
- [18] J.R. Rice, G.F. Rosengren, Plane strain deformation near a crack tip in a power-law hardening material, *J. Mech. Phys. Solids.* 16 (1968) 1–12.
- [19] F. Berto, A. Campagnolo, P. Lazzarin, Fatigue strength of severely notched specimens made of Ti-6Al-4V under multiaxial loading, *Fatigue Fract. Engng. Mater. Struct.* 38 (2015) 503–517.
- [20] A.R. Torabi, A. Campagnolo, F. Berto, Tensile fracture analysis of V-notches with end holes by means of the local energy, *Phys. Mesomech.* 18 (2015) 5–12.
- [21] F. Noori-Azghad, H. Khademizadeh, E. Barati, Some analytical and numerical expressions for evaluation of the critical *J*-integral in plates with blunt V-notches under Mode I loading, *J. Strain Anal. Eng. Des.* 49 (2013) 352–360.
- [22] F. Berto, P. Lazzarin, Y.G. Matvienko, *J*-integral evaluation for U- and V-blunt notches under Mode I loading and materials obeying a power hardening law, *Int. J. Fract.* 146 (2007) 33–51.
- [23] P. Livieri, A new path independent integral applied to notched components under mode I loadings, *Int. J. Fract.* 123 (2003) 107–125.
- [24] P. Lazzarin, R. Zambardi, P. Livieri, A *J*-integral-based approach to predict the fatigue strength of components weakened by sharp V-shaped notches, *Int. J. Comput. Appl. Technol.* 15 (2002) 202.
- [25] F. Berto, P. Lazzarin, C. Marangon, The effect of the boundary conditions on

- in-plane and out-of-plane stress field in three dimensional plates weakened by free-clamped V-notches, *Phys. Mesomech.* 15 (2012) 26–36.
- [26] H. Salavati, Y. Alizadeh, F. Berto, Effect of notch depth and radius on the critical fracture load of bainitic functionally graded steels under mixed mode I + II loading, *Phys. Mesomech.* 17 (2014) 178–189.
- [27] V. Kumar, M.D. German, C.F. Shih, *An Engineering Approaches for Elastic-Plastic Fracture Analysis*, Rep. EPRI/Electric Power Res. Inst. (1981).
- [28] T.L. Anderson, *Fracture Mechanics: Fundamentals and Applications*, Third Edition, III, Taylor & Francis, 2005.
- [29] A. Saxena, *Nonlinear fracture mechanics for engineers*, CRC Press, 1998.
- [30] W. Ramberg, W.R. Osgood, Description of stress-strain curves by three parameters, *Natl. Advis. Comm. Aeronaut.* (1943) Technical Note No. 902.
- [31] C.S. Atchison, J. Miller, Tensile and pack compressive tests of some sheets of aluminum alloy, 1025 carbon steel, and chromium-nickel steel, *Natl. Advis. Comm. Aeronaut.* (1942) Technical Note No. 840.
- [32] V. Kumar, M.D. German, W.W. Wilkening, W.R. Andrwes, H.G. DeLorenzi, D.F. Mewbray, *Advances in elastic-plastic fracture analysis*, Rep. EPRI/Electric Power Res. Inst. (1984).
- [33] N.E. Dowling, J.A. Begley, Fatigue crack growth during gross plasticity and the J-integral, *Astm Stp.* 590 (1976) 82–103.

## 9. Concluding remarks

The work reported in the present documents derives from intense research activity on a new topic, addressed for the first time by the research team of machine design. Different aspects of a wide and complex topic have been considered, and an excellent feedback was received from international and national conferences. The work has been also appreciated by different international experts on the topic, and led to several international fruitful collaborations and publications, as well as to solid bases for interesting future developments

Briefly summarized, the main purposes were:

- ❖ Obtainment of a new set of experimental high temperature fatigue data on different steels;
- ❖ Improvement of the understanding of high temperature fatigue behavior and creep of notched components;
- ❖ Evaluation of the applicability/extension of Strain Energy Density approach to high temperature and creep.

These goals were justified by the lack of recent literature on these topics.

In order to reach these aims, high temperature fatigue tests on notched components made of Cu-Be alloy, Titanium Grade 2 and 40CrMV13.9 have been conducted. Large variety of notches and temperatures has been considered. Moreover, investigation of crack initiation from notches at high temperature has been also addressed.

For all of the experimental results, extension of the Strain Energy Density to high temperature fatigue has been proposed with very good results, providing some master curves in terms of energy for high temperature design. These curves can be directly employed by engineering for practical applications. Moreover, to better support the extension of SED to high temperature, experimental data taken from literature have been re-analyzed with very good results.

Analysis of creep phenomenon regarding notched components has been conducted and a numerical method for the estimation of tip stresses and strains evolution in creeping notched components have been developed and verified with Finite Element analyses. The method is valid for U- and blunts V-notches, can be easily extended to

multiaxial fatigue and takes into account localized and non-localized creeping conditions. Moreover, some analyses regarding Strain Energy Density under creeping condition have been done and new interesting comments on creep-SED are presented. It becomes a time-dependent parameter, with the tendency to reach a plateau value. The mesh independence is maintained.

While for the high temperature fatigue, the SED shown a very good applicability following the simple rules reported herein, some points still are un-clear under creeping conditions:

- ❖ How to deal with the evolution of SED against time;
- ❖ How to deal with the evolution of the SED From an elastic to plastic field;
- ❖ How to deal with the time dependent eigenvalues.

A better definition of the SED under creeping conditions can be reached clarifying the points listed above. After this last step, with the aid of the present thesis, a unified SED approach for fatigue-creep interaction can be developed near future.

## List of publications

- P. Gallo, F. Berto, G. Glinka, Generalized approach to estimation of strains and stresses at blunt V-notches under non-localized creep, *Fatigue Fract. Engng. Mater. Struct.* In Press (2015) DOI: 10.1111/ffe.12374
- Gallo, F. Berto, *Advanced Materials for Applications at High Temperature: Fatigue Assessment by Means of Local Strain Energy Density*, *Advanced Engineering Materials*, In Press (2015) DOI: 10.1002/adem.201500547
- F. Berto, P. Gallo, P. Lazzarin, High temperature fatigue tests of un-notched and notched specimens made of 40CrMoV13.9 steel, *Mater. Design* 63 (2014) 609-619.
- Berto, P. Lazzarin, P. Gallo, High-temperature fatigue strength of a copper-cobalt-beryllium alloy, *J. Strain Analysis* 49(4) (2014) 244-256.
- P. Gallo, F. Berto, Influence of surface roughness on high temperature fatigue strength and cracks initiation in 40CrMoV13.9 notched components, *Theor. Appl. Fract. Mech.* 80 (2015) 226-234.
- P. Gallo, F. Berto, P. Lazzarin, High temperature fatigue tests of notched specimens made of titanium Grade 2, *Theor. Appl. Fract. Mech.* 76 (2015) 27-34.
- F. Berto, P. Gallo, Extension of linear elastic strain energy density approach to high temperature fatigue and a synthesis of Cu-Be alloy experimental tests, *Eng. Solid Mechanics* 3 (2015) 111-116.
- P. Gallo, F. Berto, Some considerations on the J-Integral under elastic-plastic conditions for materials obeying a Ramberg-Osgood law, *Physical Mesomechanics* 18 (4)(2015) 298-306.
- F. Berto, P. Gallo, P. Lazzarin, High Temperature Fatigue Tests of a Cu-Be Alloy and Synthesis in Terms of Linear Elastic Strain Energy Density, *Key Engineering Materials* Vol. 627 (2015) pp 77-80.
- P. Gallo, F. Berto, High temperature fatigue tests and crack growth in 40CrMoV13.9 notched components, *Fracture Structural Integrity* 34 (2015) 180-189.
- F. Berto, A. Campagnolo, P. Gallo, Brittle failure of graphite weakened by Vnotches: a review of some recent results under different loading modes, *Journal Strength of Materials* 47(3) (2015).
- P. Gallo, F. Berto, P. Lazzarin et al. High temperature fatigue tests of Cu-Be and 40CrMoV13.9 alloys, *Procedia Materials Science* 3 (2014) 27-32.

**Conferences:**

- P. Gallo, F. Berto, Some considerations on the J-Integral applied under elastic-plastic conditions. 4th International Conference of Engineering Against Failure (ICEAF IV) June 2015, Skiathos, Greece.
- P. Gallo, F. Berto, G. Glinka, Approccio generalizzato per la stima di deformazioni e tensioni in componenti intagliati soggetti a creep. 44th Convegno Nazionale AIAS (2015). Messina, Italy.
- P. Gallo, F. Berto, High temperature fatigue tests and crack growth in 40CrMoV13.9 notched components. The 5th International Conference on Crack Paths (CP 2015).
- P. Gallo, High temperature fatigue of notches components made of structural steel. ESIS TC-10 European Structural Integrity Society (2014).
- P. Gallo, F. Berto, P. Lazzarin, High temperature fatigue tests of Cu-Be and 40Cr- MoV13.9 alloys. 20th European Conference on Fracture (2014). Trondheim, Norway.
- P. Gallo, F. Berto, P. Lazzarin, Caratterizzazione a fatica ad elevata temperatura di provini intagliati in 40CrMoV13.9. 43th Convegno Nazionale AIAS (2014). Rimini, Italy.
- E. Sanjurjo, R. Pastorino, P. Gallo, M. A. Naya, Implementation Issues of an on Board Real-Time Multibody Model. The 3rd Joint International Conference on Multibody System Dynamics - The 7th Asian Conference on Multibody Dynamics (2014). Busan, Korea.
- F. Berto, P. Gallo, P. Lazzarin, P. Luisetto, Caratterizzazione a fatica ad elevate temperature di una lega di Cu-Co-Be in presenza di intagli. 42th Convegno Nazionale AIAS (2013). Salerno, Italy.

## Acknowledgments

Firstly, I would like to express my sincere gratitude to my advisor, Prof. Filippo Berto for the continuous support of my Ph.D study and related research, for his patience, immense knowledge and, especially for his friendship. His guidance helped me in all the time of research and writing of this thesis.

Besides my advisor, I would like to thank Prof. Paolo Lazzarin, for his guidance in the present research activity and special moments shared together. It was a mentor in my research activity and in everyday life. His contagious passion is unforgettable.

I thank all my labmates for the stimulating discussions, for the endless support and for all the fun we have had in the last three years. I wish them all the best and good luck for a successful career.

I would like to thank my family: my parents and to my sisters for supporting me spiritually throughout writing this thesis and in my life in general. They are my most precious thing.

Special thanks to my best friends Kris, Fabio, Mattia, Andrea, whom have been supported me and incited me to strive towards my goal in the last 15 years. They represent my second family.

I'm also really grateful to the *Fondazione Studi Universitari di Vicenza* who supported the research of the present work.